Computer Science & Information Technology 31

Natarajan Meghanathan
Jan Zizka (Eds)

Computer Science & Information Technology

The Sixth International Conference on Networks & Communications
(NeTCoM 2014)
Chennai, India, December 27 ~ 28 - 2014

AIRCC

Volume Editors

Natarajan Meghanathan,
Jackson State University, USA
E-mail: nmeghanathan@jsums.edu

Jan Zizka,
Mendel University in Brno, Czech Republic
E-mail: zizka.jan@gmail.com

ISSN: 2231 - 5403
ISBN: 978-1-921987-19-9
DOI : 10.5121/csit.2014.41301 - 10.5121/csit.2014.41316

Typesetting: Camera-ready by author, data conversion by NnN Net Solutions Private Ltd., Chennai, India

Preface

The Sixth International Conference on Networks & Communications (NeTCoM 2014) was held in Chennai, India, during December 27 ~ 28, 2014. International Conference on Computer Science and Information Technology (CSIT-2014), Sixth International Conference on Applications of Graph Theory in Wireless Ad hoc Networks & Sensor Networks (GRAPH-HOC 2014) and Second International Conference of Security, Privacy and Trust Management (SPTM 2014). The conferences attracted many local and international delegates, presenting a balanced mixture of intellect from the East and from the West.

The goal of this conference series is to bring together researchers and practitioners from academia and industry to focus on understanding computer science and information technology and to establish new collaborations in these areas. Authors are invited to contribute to the conference by submitting articles that illustrate research results, projects, survey work and industrial experiences describing significant advances in all areas of computer science and information technology.

The NeTCoM-2014, CSIT-2014, GRAPH-HOC-2014, SPTM-2014 Committees rigorously invited submissions for many months from researchers, scientists, engineers, students and practitioners related to the relevant themes and tracks of the workshop. This effort guaranteed submissions from an unparalleled number of internationally recognized top-level researchers. All the submissions underwent a strenuous peer review process which comprised expert reviewers. These reviewers were selected from a talented pool of Technical Committee members and external reviewers on the basis of their expertise. The papers were then reviewed based on their contributions, technical content, originality and clarity. The entire process, which includes the submission, review and acceptance processes, was done electronically. All these efforts undertaken by the Organizing and Technical Committees led to an exciting, rich and a high quality technical conference program, which featured high-impact presentations for all attendees to enjoy, appreciate and expand their expertise in the latest developments in computer network and communications research.

In closing, NeTCoM-2014, CSIT-2014, GRAPH-HOC-2014, SPTM-2014 brought together researchers, scientists, engineers, students and practitioners to exchange and share their experiences, new ideas and research results in all aspects of the main workshop themes and tracks, and to discuss the practical challenges encountered and the solutions adopted. The book is organized as a collection of papers from the NeTCoM-2014, CSIT-2014, GRAPH-HOC-2014, SPTM-2014.

We would like to thank the General and Program Chairs, organization staff, the members of the Technical Program Committees and external reviewers for their excellent and tireless work. We sincerely wish that all attendees benefited scientifically from the conference and wish them every success in their research. It is the humble wish of the conference organizers that the professional dialogue among the researchers, scientists, engineers, students and educators continues beyond the event and that the friendships and collaborations forged will linger and prosper for many years to come.

Natarajan Meghanathan
Jan Zizka

Organization

General Chair

Jagannathan Sarangapani	Missouri University of Science and Technology, USA
Natarajan Meghanathan	Jackson State University, USA

Program Committee Members

Abdel Salhi	University of Essex, United Kingdom
Abdulrahman Yarali	Murray state university, USA
Ahlem Drif	Computer science Department, Algeria
Ahmed Ezz Eldin Khaled	Cairo University, Egypt
Alexander Ferworn	Ryerson University, Canada
Ali Alawneh	Philadelphia University, Jordan
Alireza mahini	Islamic Azad University-Gorgan, Iran
Almir Pereira Guimaraes	Federal University of Alagoas, Brazil
Alvin Lim	Auburn University, USA
Antonio Ruiz-Martinez	University of Murcia, Spain
Asmaa Shaker Ashoor	Babylon University, Iraq
Bob Natale	MITRE, USA
Cathryn Peoples	University of Ulster, United Kingdom
Chih-Lin Hu	National Central University, Taiwan
Chin-Chih Chang	Chung Hua University,Taiwan
Christos Politis	Kingston University, UK
Cristina Ribeiro	University of Waterloo, Canada
Dac-Nhuong Le	Haiphong University, Vietnam
Daqiang Zhang	Nanjing Normal University, China
David C. Wyld	Southeastern Louisiana University, USA
Dhinaharan Nagamalai	Wireilla net solutions PTY ltd, Australia
Doina Bein	The Pennsylvania State University,USA
Ehsan Heidari	Islamic Azad University Doroud Branch, Iran
Emmanuel Jammeh	University of Plymouth, United Kingdom
Farshchi S.M.R	Seyyed Mohammd Reza Farshchi, Iran
Firdous Imam	Imam unversity Riyadh, Saudi Arabia
Gary Campbell	University College of the Caribbean, Jamaica
Ghaida Al-Suhail	Basrah Univirsity, Iraq
Hamadouche M	USDB, Algeria
Hamdouche Maamar	Université Saad Dahlab de Blida, Algeria
Hamza Aldabbas	De Montfort University, UK
Han Cong Vinh	Nguyen Tat Thanh University, Vietnam
Hangwei	Western Reserve University, USA
Hao-En Chueh	Yuanpei University, Taiwan, R.O.C.
Hazem Al-Najjar	Misurata university, Libya

Technically Sponsored by

Networks & Communications Community (NCC)

Computer Science & Information Technology Community (CSITC)

Digital Signal & Image Processing Community (DSIPC)

Organized By

Academy & Industry Research Collaboration Center (AIRCC)

TABLE OF CONTENTS

Sixth International Conference on Networks & Communications (NeTCoM 2014)

International Conference on Computer Science and Information Technology (CSIT-2014)

Sixth International Conference on Applications of Graph Theory in Wireless Ad hoc Networks & Sensor Networks (GRAPH-HOC 2014)

Second International Conference of Security, Privacy and Trust Management (SPTM 2014)

DEPLOYMENT-DRIVEN SECURITY CONFIGURATION FOR VIRTUAL NETWORKS

Ramaswamy Chandramouli

Computer Security Division, Information Technology Laboratory
National Institute of Standards & Technology
Gaithersburg, MD, USA
mouli@nist.gov

ABSTRACT

Virtualized Infrastructures are increasingly deployed in many data centers. One of the key components of this virtualized infrastructure is the virtual network – a software-defined communication fabric that links together the various Virtual Machines (VMs) to each other and to the physical host on which the VMs reside. Because of its key role in providing connectivity among VMs and the applications hosted on them, Virtual Networks have to be securely configured to provide the foundation for the overall security of the virtualized infrastructure in any deployment scenario. The objective of this paper is to illustrate a deployment-driven methodology for deriving a security configuration for Virtual Networks. The methodology outlines two typical deployment scenarios, identifies use cases and their associated security requirements, the security solutions to meet those requirements, the virtual network security configuration to implement each security solution and then analyzes the pros and cons of each security solution.

KEYWORDS

Virtualized Infrastructure, Virtual Machine, Virtual Network, Security Configuration, Software Defined Network

1. INTRODUCTION

Virtualized infrastructures are increasingly deployed in many data centers, driven by cost, efficiency, scalability and in some cases security considerations. The term virtualized infrastructure, in the context of this paper, includes the following: the physical host or server that is virtualized (called Virtualized Host), the Hypervisor software, the Virtual Machines (VMs) residing on a virtualized host, the software-defined virtual network that is configured inside a virtualized host, middleware and management tools specific to the virtualized environment, the hardware/software components relating to storage, the common networking components of the data center such as physical Network Interface Cards (physical NIC), switches (physical and virtual), routers, firewalls, load balancers, application delivery controllers etc.

One of the key components of this virtualized infrastructure is the virtual network [1] – a software-defined communication fabric that links together the various Virtual Machines (VMs) to each other and to the physical host on which the VMs reside. The VMs are instantiated and managed by a piece of software called "Hypervisor" which in turn is installed in many instances

Natarajan Meghanathan et al. (Eds) : NeTCoM, CSIT, GRAPH-HOC, SPTM - 2014
pp. 01–13, 2014. © CS & IT-CSCP 2014 DOI : 10.5121/csit.2014.41301

directly on a physical computing hardware. We will refer to the physical computing hardware on which the hypervisor is installed as Virtualized Host.

It is in fact the hypervisor that provides the API and the functional code necessary to define and configure a virtual network linking the various VMs with each other and to the virtualized host where they (Hypervisor and the VMs) all reside. Since the term "Virtual Network" in the context of networking as a whole is an overloaded term, it is good to clarify its semantics in the context of the virtualized infrastructure discussed in this paper. In our context, the term virtual network encompasses the two aspects: (a) Software-enabled NIC Virtualization and (b) Data path Virtualization. A brief explanation of these two aspects follows:

Software-enabled NIC Virtualization [2]: Here a physical Network Interface Card (pNIC) in a virtualized host is shared among many Virtual Operating Systems (OSs) (called Guest OS, Virtual Machines or Domains depending upon the product offering). This sharing is possible through a software-defined artifact called Virtual NIC (or vNIC), which is a software emulation of a physical NIC. Each vNIC is defined within a Virtual OS and the latter is therefore called the client of vNIC. Each vNIC may be assigned its own dedicated IP and MAC addresses. If the Virtual OSs (clients of vNIC) run a server software (e.g., Web Server, DNS Server or Firewall), they are also referred to as "Virtual Servers". The bridging of these vNICs or multiplexing of the traffic from different vNICs (and hence different VMs or Virtual Servers) for achieving the goal of sharing physical NICs is achieved using a software-defined switch called virtual switch (vSwitch in some product offerings) [3]. Links between vNICs and virtual switches are software-emulated links and so are the links between virtual switches and physical NICs (the later are also called uplinks).

Data path Virtualization [2]: The software-emulated links created by NIC virtualization above can be virtualized using a capability in the virtual switches. This type of link virtualization is different from virtualization of links found in physical channels (using multiplexing or creation of virtual circuit) where virtualization happens at the channel. In data path virtualization, virtualization of links happens at the network node level (i.e., virtual switch). These virtual switches (vSwitches) have the capability to define dynamic multiple port groups within it (just like ports in a physical switch). These port groups are tagged with what are known as Virtual LAN (VLAN) IDs [4]. These tags or labels are used by virtual switches to create multiple virtual links (data paths). Thus VLAN tags achieve two different objectives – to share the same infrastructure (e.g., the LAN infrastructure or communication channel) as well as creating data paths in the broadcast domain.

In Summary, the virtual network in the context of this paper is a "software-emulated network which generates traffic that is injected into the real world through a non-virtual/non-emulated physical NIC" [2] and has the following building blocks:

- Virtual Servers (Clients of vNICs)
- Virtual NICs (vNICs)
- Virtual Switches (vSwitch)
- Virtual Links and
- Physical NICs (pNICs).

In addition to the above components, we also include external physical switches/routers attached to virtualized hosts (more specifically to the physical NICs of the hosts) also under the umbrella of the "virtual network" since they play a role in configuration of the virtual network (e.g., inter-VLAN routing). Other components such as VLAN ID/Port Group (in the Virtual Switch), Software-defined firewalls & IDS/IPS installed as Virtual Security Appliance (VSA), Load Balancers etc (sometimes packaged as Virtual Appliances) are also included since they are artifacts used in a virtual network configuration as well.

Having settled on the semantics for the virtual network, let us turn our attention to the role of virtual networks in a virtualized infrastructure. While the hypervisor kernel provides the process-level isolation for the VMs, it is the virtual network that provides the connectivity between the VMs and the applications hosted on them. Hence, secure configuration of the virtual network forms the foundation for the security of the entire virtualized infrastructure. Two significant deployment scenarios for a large virtualized infrastructure are:

- Hosting Multi-tier applications (with extensive connectivity between components containing various application tiers) with a large user base, large volume of data or high volume of transactions or combination of all three

- Offering an Infrastructure as a Service (IaaS) public cloud service.

In this scenario, VMs belonging to different cloud service clients could be potentially co-residents in a single virtualized host of the infrastructure.

It must be emphasized that the two deployment scenarios stated above are not mutually exclusive. For example, a 3-tier application (consists of Web Server, Application Server & Database Server tiers) may be hosted on three different groups of VMs either by the enterprise itself (as part of its internal IT resources) or by a cloud service client (if the virtualized infrastructure is used for offering a public cloud service). In the former case, the virtualized infrastructure and all the VMs are owned by the enterprise while in the latter case, the ownership of the VMs is with the cloud service client while the virtualized infrastructure is owned by the cloud service provider.

The objective of this paper is to illustrate a methodology for obtaining a secure virtual network configuration based on deployment scenarios cited above. The methodology is based on identifying the typical set of use cases in the deployment scenarios. Section 2 lists the steps of the methodology and identifies the various use cases. Section 3 is the core material for this paper as it describes the steps of the methodology used to derive security configuration for a virtual network and also analyzes the pros and cons of the underlying security solution. Section 4 outlines the benefits of the methodology.

2. METHODOLOGY FOR DERIVING VIRTUAL NETWORK SECURITY CONFIGURATION

The methodology for deriving a virtual network security configuration has the following key steps:

- STEP 1: Identify the key use cases that result from the deployment scenarios stated in the previous section. We consider only use cases that have an impact on virtual network configuration parameters and identify those that are not within the scope of the methodology.

- STEP 2: For each chosen use case, identify the associated security requirements and a security solution that will meet the requirements.

- STEP 3: Identify and describe the virtual network security configuration operations that will implement the security solutions and also analyze the pros and cons of those security solutions.

2.1 Choice of Use Cases in Virtualized Infrastructure Deployments

As already mentioned, we consider here only those use cases that are relevant from the virtual network standpoint. Before identifying those use cases, we first provide here certain use cases that get a lot of attention in deployments involving virtualized infrastructures [5], but do not impact the virtual network configuration parameters. These use cases therefore are not considered within the scope of our methodology.

- Building a VM image, versioning of VM images, maintaining the integrity of the VM images both during storage and while using them for instantiating VM instances.
- Configuring the VM OS (or Guest OS)
- Configuring Endpoint (Virus & Malware) protection for VMs
- Providing Access Protection for accessing VMs from an external network
- Comprehensive Data Protection (Data in VM definition files and Application Data)

We now identify the typical set of use cases that may require virtual network configuration for their secure implementation. All these use cases by and large pertain to one or both of the two key components of the virtualized infrastructure: the Hypervisor and the VMs. They are:

- Managing the Hypervisor and the virtual network it spawns (e.g., VMs, Virtual Switches/Port Groups/VLANs etc) (MH)
- Providing Selective Isolation/Connectivity between various applications/VMs (VM-CO)

3. IMPACT OF USE CASE OPERATIONS ON VIRTUAL NETWORK SECURITY CONFIGURATION

In this section, we describe for each use case, the associated security requirements, the security solutions that will meet the security requirements and the virtual network security configuration operations that will implement each security solution and also analyze the pros and cons of each of the security solutions.

3.1 Management of the Hypervisor (MH)

The set of management commands sent to the hypervisor includes those that are needed for running a hypervisor as well those that are needed to create an application hosting environment (Provisioning VM instances & Creating a Virtual Network configuration to support them). Specifically these are the broad categories of commands sent to the hypervisor.

- Commands needed to set the hypervisor's functional parameters (e.g., the CPU scheduling algorithm it uses)

- The commands needed to define the topology of the virtual network (creation of virtual switches, ports within each virtual switch and connections between vNICs provided through virtual switches as well as connections from ports/virtual switches to physical NICs of the virtualized host)

- Commands relating to operations on VMs (e.g,, Start, Stop & Pause VMs, Migrate a VM from one Virtualized Host to another etc – these are sometimes called VM lifecycle operations)

In some hypervisor architectures, the functions relating to VM Management (VM Lifecycle operations) are offloaded to a dedicated, security hardened VM (sometimes called Management VM). Regardless of this architectural variation, all hypervisors have an interface (called management interface) for sending these management commands. The obvious security requirements (SR) considering the sensitive nature of the operations performed by the invocation of these commands are:

- MH-SR-1: The sources from which these commands originate must be restricted to some trusted sources

- MH-SR-2: The management commands must be sent securely - protecting their integrity and sometimes confidentiality.

- MH-SR-3: The communication channels (data paths) carrying these management commands must be logically isolated from channels carrying other types of traffic such as the data/application related traffic.

Out of the three security requirements stated above, MH-SR-1 is met by restricting the set of users who are authorized to invoke the hypervisor management commands to some trusted administrators and by restricting the origin of the command packets to designated administrative LANs within the enterprise [6]. For accomplishing this latter objective, a dedicated software-defined firewall may have to be installed exclusively for protecting the management interface. MH-SR-2 is met by establishing a secure communication protocol such as SSH with the management interface and sending the management commands digitally signed and/or encrypted [6]. Hence the only security requirement here that has to be met through a virtual network-based security solution is MH-SR-3. The security solution (SS) for obtaining an isolated communication channel exclusively dedicated to management commands (requirement MH-SR-3) is:

- SS-1: Use a dedicated virtual network segment for sending all management commands to the Hypervisor.

The virtual network security configuration operations to implement the above security solution are:

- VN-SC-OP-1: Dedicate a VLAN for carrying just the hypervisor management traffic. This is accomplished by creating a port of connection type console or kernel (depending upon the hypervisor) on a virtual switch of the hypervisor and assigning a VLAN ID to that port and associating the management interface (along with its IP address) with it. A dedicated VLAN on a kernel-type port is also the preferred configuration option for supporting VM Migration commands.

- VN-SC-OP-2: An added security assurance, in the pursuit of isolating management traffic from all other traffic into the hypervisor, can be obtained by having a virtual switch (vSwitch) just dedicated for defining the management VLAN with no other connections.

Analysis of the security solution: A dedicated virtual network segment is just one of the three security solutions for managing the hypervisor. It has to be augmented with administrator access control, interface-protecting firewall and a secure communication protocol.

3.2 Providing Selective Isolation/Connectivity between various applications/VMs (VM-CO)

In the previous section, the need for isolating the management traffic from the application traffic was addressed. There is also a need to provide selective isolation among traffic pertaining to different applications running in VMs. This need is closely aligned with the two deployment scenarios outlined in Section 1 as follows:

- Multi-tier Applications: The enterprise may run multiple multi-tier applications of different sensitivity levels in VMs based on the type of data processed or the functions/operations performed. In some instances, VMs need to be isolated based on the Line of Business (LOB) and/or functional departments.

- Multiple Tenants on a Host: VMs belonging to different cloud service clients must be logically isolated from one another to protect the integrity of data and applications hosted on them. In many instances, there may be the need to provide logical isolation among VMs belonging to the same cloud service client.

After isolating the VMs by the nature of the application (or LOB or Functional Department) or cloud service client, it may be found that some business processes require that applications in the VMs of one department/LOB may need to communicate or interact with applications in VMs of other departments/LOBs. These twin security requirements (Selective Isolation and Connectivity) are stated as follows:

- VM-SR-1: Traffic going into/emanating from VMs running sensitive applications must be isolated from traffic pertaining to non-sensitive applications. Traffic among VMs belonging to a Line of Business (LOB) or a functional department (e.g., Accounting, Engineering etc) or a cloud service client must be isolated from corresponding traffic from other LOBs, functional departments or cloud service clients respectively.

- VM-SR-2: Communication between VMs belonging to different logical groups (Application Profile, LOB or Functional Department) must be enabled in some instances but should be governed by a security policy.

The various security solutions that can meet the above requirements are:

- SS-2: Virtual Network Segmentation using VLAN IDs

- SS-3: Virtual Network Segmentation using VLAN IDs with Software Defined Network (SDN) support

- SS-4: Control of Network traffic using Firewalls installed as Virtual Security Appliances (VSA)

- SS-5: Control of Network traffic using Virtual Switches with SDN Support

A description of the above security solutions, the virtual network security configuration operations needed to implement each of the solutions and performance characteristics of each of these solutions are given below:

3.2.1 Virtual Network Segmentation using VLAN IDs

Isolation of traffic among VMs residing in a virtualized host (or in different hosts) is achieved by segmentation of the virtual network and connecting the VMs (or Virtual Network Interface Cards (vNICs)) to the corresponding port in the virtual switch tagged with the ID of that virtual network segment. A common technology used for this purpose is the Virtual Local Area Network or VLAN. Since the VMs in a virtualized host are connected to virtual switches, the ports in the virtual switches are tagged with VLAN IDs and the VMs designated for a particular VLAN segment are assigned (connected) to the corresponding virtual switch port. The necessary operations for achieving the requisite virtual network security configuration are:

- VN-SC-OP-3: Identify the set of VMs that belongs to a specific cloud service client (tenant) or Line of Business (LOB) or functional department and assign them to a new VLAN (VLAN ID). Also identify the set of virtualized hosts that are targets for hosting them.

- VN-SC-OP-4: Define a new VLAN using the interface that your LAN management software provides.

- VN-SC-OP-5: Define/Identity virtual switches on the target hosts (for identified VMs), define/identify ports on those virtual switches and associate the new VLAN ID with those switch ports. This type of ports is simply called VM portgroup in some hypervisors. Connect the identified VMs (or the vNIC) to those portgroups.

- VN-SC-OP-6: The previous operation has configured the virtual switches inside the virtualized hosts with the new VLAN. The same VLAN has to be configured on the external physical switches connected to those virtualized hosts. This requires four operations: (1) The new VLAN ID has to be added to the external switch's VLAN database; (2) At least one of the ports on that external switch must be enabled to support traffic carrying that VLAN ID; (3) The port enabled for that VLAN ID must be connected to the physical NIC of the virtualized host, and finally (4) that particular physical NIC should be connected as the uplink port for the virtual switch on which the new VLAN ID is defined.

This establishes a communication path from the vNIC of the VM to the virtual switch's port (to which the former is connected) and through its (the virtual switch) uplink port to the virtualized host's physical NIC and on to the external physical switch. One requirement needed for this configuration is that the port on the external switch on which VLAN is enabled should be configured as a trunk port (capable of receiving/forwarding traffic belonging to multiple VLANs). Firewall rules can then defined on this external switch to provide selective connectivity between different VLANs.

Analyzing the above security solution, we find the following limitations. They are [7]:

- There is a limit to the number of VLAN IDs that can be used (the figure is 4096)

- Configuring the virtual switches inside the virtualized hosts (where identified VMs are hosted) as well as physical switches connected to the virtualized hosts for one or more VLANs is a manual, time-consuming and error-prone process, part of which may have to be repeated if application profile of VMs change.

- To enforce restrictions on inter-VLAN communication, the enforcement point is a physical firewall or the physical switch. This requires routing all traffic originating from or coming into a VM to the physical NIC of the virtualized host and on to the trunk port of a external physical switch, thus increasing the latency of communication packets with consequent increase in application response times.

3.2.2 Virtual Network Segmentation using VLAN IDs with SDN support

Before looking at this security solution, it would be good to review the architectural concepts underlying SDN. SDN is an architectural concept that enables direct programmability of networks through open-source Standards-based APIs [8]. This capability is enabled by dividing the functionality of a network device such as a switch or router into two distinct layers – the data plane and control plane. The control plane is implemented by a software called SDN controller and defines how data flows (i.e., how network messages/packets are forwarded and routed) while the data plane performs the basic task of storing/forwarding packets based on entries in the forwarding table. The SDN controller is often centralized (so that it controls data forwarding functions of multiple data planes each associated with a network device) and communicates with data planes through a standardized API (e.g., OpenFlow [9]). The interface to the data plane (which in the SDN architecture is essentially is a network device with SDN support (such as a SDN switch) is also called "Southbound Interface". Similarly the SDN controller also can be implemented to have an open interface, called the "Northbound Interface". An architectural diagram of a SDN is given in Figure 1 below:

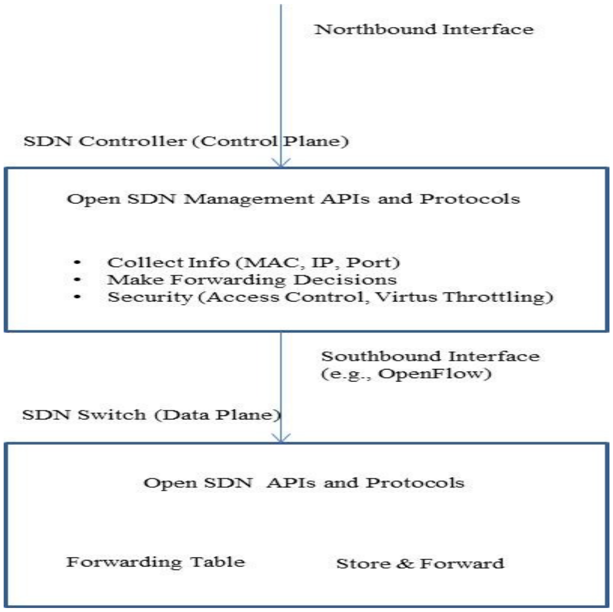
Northbound Interface
SDN Controller (Control Plane)
Open SDN Management APIs and Protocols
• Collect Info (MAC, IP, Port)
• Make Forwarding Decisions
• Security (Access Control, Virtus Throttling)
Southbound Interface
(e.g., OpenFlow)
SDN Switch (Data Plane)
Open SDN APIs and Protocols
Forwarding Table
Store & Forward

Figure 1. SDN High Level Architecture

The SDN architecture can be leveraged to automate the creation of VLANs for isolating traffic among VMs in the following way. First, the virtual switches that can be defined using the hypervisor APIs should be capable of supporting SDN capabilities. An example is the open vSwitch [10]. Secondly, there should be a SDN controller that can communicate with and control all SDN supported virtual switches. With this set up, the Northbound interface exposed by SDN controller can be used to send in commands to create the necessary VLANs (operation VN-SC-OP-4) as well as send in information regarding VMs and their locations (virtualized hosts and SDN virtual switches) pertaining to each VLAN. This information is used in the SDN controller to generate commands, that is sent through the Southbound Interface for: (a) creating the necessary port groups/VLAN tags on SDN supported switches and (b) connect the VMs to those switch ports (operation VN-SC-OP-5). Similarly the tasks involved in VN-SC-OP-6 can also be automated if the external physical switch is also a SDN switch.

This security solution presents the following advantages:

- Due to standardized interfaces and pre-programmed scripts, the creation of VLAN and enabling the connectivity of VMs to the designated VLAN are automated thereby reducing/eliminating the errors that could creep in manual configuration. The relevant interfaces are: (a) SDN controller interface (Northbound Interface) and (b) SDN supported virtual switch interface (Southbound Interface).

- Similarly, the VLAN reconfiguration necessitated by VM migrations or change in application profiles of VMs can also be automated using SDN interfaces.

- The VLAN ID limit of 4096 imposed by IEEE 802.1Q standard can be overcome by creating packet forwarding rules in SDN controller based on MAC addresses to be placed on virtual switches

3.2.3. Control of Network traffic using Firewalls installed as Virtual Security Appliances

In the virtualized infrastructure, network security using firewalls can be implemented in two ways: (a) installing a firewall in each of the VMs to be protected or (b) installing a firewall at the hypervisor-level to enforce traffic control rules for all VMs in that virtualized host. The latter solution uses the hypervisor's Virtual Machine Introspection (VMI) API. The configuration operations for this solution are:

VN-SC-OP-7: Install a firewall as a Virtual Security Appliance (VSA) inside a hardened VM. This appliance has the ability to enforce traffic restrictions on traffic going into any VM by virtue of its access to the hypervisor's VMI API. The packets for enforcement are fed into it by a hypervisor kernel module that forwards all or selected (based on a set of rules) packets coming into the vNIC of every VM in the virtualized host [11].

The performance characteristics of this security solution are:

- It does not consume the valuable CPU cycles in individual VMs which could otherwise be used for running the business applications.

- All policies needed for the firewall can be defined centrally in the Virtual Infrastructure Management server and then pushed in to the firewall VSA running in several virtualized hosts.

- Firewall VSAs are capable of supporting sophisticated logic for traffic control rules such as the ability to define security groups based on customized criteria.

3.2.4. Control of Network traffic using Virtual Switches with SDN Support

To implement this solution, the virtualized infrastructure should have a network with SDN capabilities as described in 3.2.2. In this solution, traffic control using firewall like rules which only allow packets based on the following values – *A specific protocol (TCP or UDP), from port, to port, A single IP address or range of IP addresses* can be implemented directly on virtual switches in a hypervisor instead of in a virtual security appliance (VSA) [12]. A set of VMs is associated with a Security Group. A traffic control rule can be associated with one or more Security Groups. A VM instance can also be associated with multiple Security Groups. Using these combinations, the set of traffic control rules applicable for a particular VM instance (say VM1) can be identified. Let us assume for simplicity that VM1 is associated with a single Security Group (SG1). An example of a traffic control rule (SG1-R1) associated with this Security Group SG1 is given in Table 1. This rule allows TCP traffic on port 6001 from any VM in the IP address range 10.10.2.1 to 10.10.2.4 into the VM instance VM1.

Let us also assume that the VM instance VM1 is launched with an IP address of 10.10.2.27. Let us also assume that VM instances within the IP range specified in Table 1 is connected to the same virtual switch as VM1. Hence to install incoming traffic control rules for VM instance VM1 on the virtual switch to which it is connected, the configuration operations are as follows:

- VN-SC-OP-8: The Virtualized Infrastructure Management server provides to the SDN controller through its Northbound interface the following information for VM instance VM1: VM1's IP address (10.10.2.27), the virtual switch (vS1) to which VM1 will be connected, the Security Groups associated with VM1 (SG1) and the associated traffic control rules (SG1-R1).

TABLE 1. Security Rule (SG1-R1) for Security Group (SG1)

Field	**Value**
Protocol	TCP
From Port	6001
To Port	6001
Source	10.10.2.1 – 10.10.2.4

- VN-SC-OP-9: Now the SDN controller has the task of connecting VM instance VM1 to virtual switch vS1 and to implement the security group rule (SG1-R1) on the switch vS1 (since the VM instance VM1 belongs to security group SG1). To accomplish the latter task, the SDN controller converts the SG1-R1 rule into the format of SDN-standard rule (e.g., an OpenFlow rule) and installs them on the virtual switch vS1 to which the VM instance VM1 is connected. This operation is repeated for every VM instance added to the Security Group SG1.When a new rule (SG1-R2) is added to the Security Group SG1, the virtualized management infrastructure server communicates this information to SDN controller. The SDN controller generates the list of VM instances belonging to the Security Group SG1 and installs the new rule on the virtual switch that hosts each instance. Similarly, if a rule is removed from SG1, the SDN controller will uninstall (delete) the corresponding traffic flow rules for each VM instance from their respective virtual switches.

We can clearly see the advantages of the traffic control implemented on virtual switches instead of in firewalls (installed as virtual security appliance) as follows:

- It avoids the unnecessary forwarding of all traffic destined for all VMs to the security VM hosting the virtual security appliance-based firewall.

- Thanks to programmable scripts within the SDN controller, the virtual network configuration operations required due to addition and deletion of rules or VMs to Security Groups can be completely automated.

4. BENEFITS & CONCLUSIONS

This paper has outlined a methodology for deriving security configuration of a virtual network in a virtualized infrastructure for two deployment scenarios. The security configurations are implementations of security solutions which meet the security requirements for use cases of the two deployment scenarios. We have also performed an analysis of those security solutions.

The artifacts generated by the methodology are summarized in Table 2 below. The methodology has the following two security assurance benefits:

- The first benefit is that, the use-case/security requirements/security solution/virtual network configuration trajectory adopted in the approach provides automatic traceability of the any configuration setting to a use case/security requirement. It thus implicitly provides a logical basis for versioning of a particular virtual network configuration. It also provides the validity for modifying, removing or enhancing a virtual network security configuration based on the following: (a) A use case has been dropped or modified (b) A new threat scenario has necessitated the need for additional security requirements for an existing use case.

- The second benefit is that, the analysis of the security solutions underlying a particular virtual network security configuration helps to ensure that the resulting configuration meets the security requirements/objectives, are appropriate for the virtualized infrastructure context and use the state of practice technology.

The role of virtual networks in ensuring the security of the overall virtualized infrastructures is likely to grow with adoption of technologies like: (a) Distributed virtual switches (as opposed to switches specific to a virtualized host), (b) More SDN capabilities for virtual switches, and (c) Attestations of boot integrity for VMs (in addition to hypervisor modules). Being a use-case driven methodology, it has the flexibility and scalability to be applied in these emerging virtualized infrastructure environments as well.

TABLE 2. SUMMARY OF VIRTUAL NETWORK SECURITY CONFIGURATION

Use Case	**Security Requirements**	**Security Solution & its Analysis**	**Virtual Network Security Configuration**
1. Management of the Hypervisor and the Virtual Network it spawns (MH)	(a)Restricting commands to trusted sources (b) Protecting the Integrity & Confidentiality of Commands (c) Restricting Management Traffic to dedicated channels	Dedicated Virtual Network Segment: (a) Not a stand- alone solution. Must be augmented with administrator access control, firewall and secure communication protocol	(a) Assign a VLAN ID on a Service Console or Kernel type port of a virtual switch and associate only the management interface with it. (b) Configure no other traffic on that virtual switch (dedicate that virtual switch for management traffic)
2. Selective Isolation/Connectivity between existing applications/VMs (VM-CO)	(a)Isolating Traffic among Logical VM Groups (LOB, Functional Department or Cloud Service Client) (b)Controlled Communication between logical VM Groups based on a security policy (which translates to a set of Traffic Control Rules)	Virtual Network Segmentation using VLAN IDs: (a)VLAN ID Limitation (b) Manual, Error-prone process (c) Communication latency as all traffic is routed to an external switch	(a)Select a new VLAN ID and associate it with a port on vSwitch (b) The new VLAN ID is added to the external switch's VLAN database and enabled on one of its ports (c) Define firewall rules on the switch for Inter-VLAN communication
		Virtual Network Segmentation using VLAN IDs with SDN support VLAN configuration and re-configuration can be totally automated	Same as the previous row except that all VLAN configuration operations can be performed by executing scripts using Northbound & Southbound interfaces of SDN

		Control of Network traffic using Firewalls installed as Virtual Security Appliances (a)Communication Traffic policy defined centrally and implemented uniformly in all virtualized hosts (b) Security Groups can be defined based on an customized criteria and used in firewall rules (c) All traffic coming into all VMs must be routed to the VM hosting the firewall VSA potentially affecting application response times	(a)Install a firewall as a Virtual Security Appliance (VSA) inside a hardened VM (b)Link it to a kernel module that forwards all packets destined for any VM
		Control of Network traffic using Virtual Switches with SDN Support: (a)Avoids unnecessary traffic generated due to the need to route all traffic to VM hosting the firewall (b) Automated propagation of changes to the security rule set to all affected VM instances	(a) For a given Security Group, the information about its constituent VMs , as well as Traffic control rules are sent to SDN controller through Northbound Interface (b) SDN controller installs the rules on virtual switches connected to those VM instances through its Southbound interface

REFERENCES

[1] Virtualization Overview [On-line] Available: http://www.vmware.com/pdf/virtualization.pdf [Retrieved: June 2014]

[2] A. Wang, M.Iyer, R.Dutta, G.Rouskas, and I. Baldine, "Network Virtualization: Technologies, Perspectives, and Frontiers," Journal of Lightwave Technology, Vol. 31, No. 4, Feb 15, 2013

[3] VMware Virtual Networking Concepts, [On-line]. Available: http://www.vmware.com/files/pdf/virtual_networking_concepts.pdf [Retrieved: June 2014]

[4] IEEE 802.1Q Virtual LANs (VLANs), [On-line]. Available: http://www.ieee802.org/1/pages/802.1Q.html [Retrieved: June 2014]

[5] R. Chandramouli, "Analysis of Protection Options for Virtualized Infrastructures in Infrastructure as a Service Cloud," Proceedings of the Fifth International Conference on Cloud Computing, Venice, Italy, May 2014.

[6] "Amazon Web Services: Overview of Security Processes," March 2013, http://aws.amazon.com/security/ [Retrieved: February, 2014]

[7] Q. Chen, et al, "On State of the Art in Virtual Machine Security", IEEE Southeastcon, 2012, pp. 1-6.

[8] Open Networking Foundation,[On-line]. Available: http://www.opennetworking.org [Retrieved: June 2014]

[9] OpenFlow, [On-line].Available: http://www.openflow.org [Retrieved: June 2014]

[10] Open vswitch, [On-line]. Available: http://openswitch.org [Retrieved July 2014]

[11] "The Technology Foundations of VMware vShield," [On-line] Available: http://www.vmware.com/files/pdf/techpaper/vShield-Tech-Foundations-WP.pdf [Retrieved: April, 2014]

[12] G. Stabler, et al, "Elastic IP and security groups implementation using OpenFlow," Proceeedings of the 6th International Workshop on Virtualization Technologies in Distributed Computing, Deft, Netherlands, 2012

.

INTENTIONAL BLANK

PERFORMANCE ANALYSIS OF RESOURCE SCHEDULING IN LTE FEMTOCELLS NETWORKS

Samia Dardouri[1] and Ridha Bouallegue[2]

[1]National Engineering School of Tunis, University of Tunis El Manar, Tunisia
samia_telecom@yahoo.fr
[2] Innov'COM Laboratory, Sup'Com, University of Carthage, Tunisia
ridha.bouallegue@ieee.org

ABSTRACT

3GPP has introduced LTE Femtocells to manipulate the traffic for indoor users and to minimize the charge on the Macro cells. A key mechanism in the LTE traffic handling is the packet scheduler which is in charge of allocating resources to active flows in both the frequency and time dimension. So several scheduling algorithms need to be analyzed for femtocells networks. In this paper we introduce a performance analysis of three distinct scheduling algorithms of mixed type of traffic flows in LTE femtocells networks. The particularly study is evaluated in terms of throughput, packet loss ratio, fairness index and spectral efficiency.

KEYWORDS

Femtocells, Macrocells, LTE, Resource Scheduling, Performance Analysis.

1. INTRODUCTION

Recently demands of users for wireless data communications in cellular networks are rapidly increasing as fascinating mobile devices and mobile applications. One of the important challenges for LTE systems is to ameliorate the indoor coverage and enhance high-data-rate services to the users in a performant way and at the same time to improve network capacity [1].

However, The LTE femtocells are referred to as Home evolved Node Bs (HeNBs) which is a femtocell base station and extensive evolved UMTS terrestrial radio access network (E-UTRAN) architecture are defined to support femtocells in the LTE system which is illustrated in Fig. 1 [2]. HeNB contains most functionalities of eNB and is linked to cellular core networks through the existing Internet access and HeNB gateway. The femtocell is a home base station which is meant to be deployed in homes or companies to rice the mobile network capacity or offer mobile network coverage where none exists [3],[4].

Therefore many searchers discuss reuse of wireless resources in macro and femtocell in order to enhance utilization of the limited wireless resources [2]. Radio resources in both time and frequency domains can be individually allowed to macro and femtocells. All of the scheduling algorithms are developed by considering the dynamics of the macrocell wireless networks.

Natarajan Meghanathan et al. (Eds) : NeTCoM, CSIT, GRAPH-HOC, SPTM - 2014
pp. 15–25, 2014. © CS & IT-CSCP 2014 DOI : 10.5121/csit.2014.41302

However femtocell networks are different from macrocell networks in terms of network coverage range number of simultaneous users served total transmission power and total available networks resources [5]. So several scheduling methods need to be developed for femtocell networks and before that the performance of suggested schedulers need to be analyzed such as those presented in [6], [7] and [8].

Furthermore resource allocation can be classified in the light of applications demands like that the performance of scheduling algorithms extremely relies on the type of mixed flows [9], [10]. In order to implement higher performance of system, it is important to select appropriate algorithms depending on flows applications. The flows can be mixture of Real-Time as well as Non-Real-Time flows due to the evaluation of basic services of LTE, including voice service, data service, and live video service [11], [12], [13].

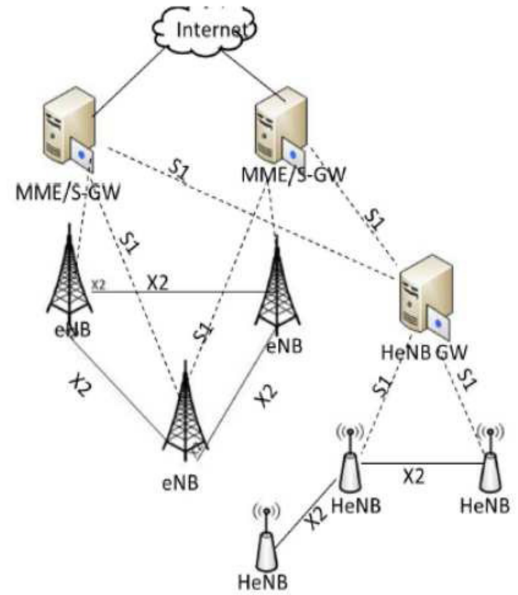

Fig. 1: Architecture of LTE Femtocell Networks.

In this work, we study several scheduling algorithms of different types of downlink traffic in LTE system. we apply a metrics which enables fast evaluation of performance metrics such as mean flow transfer times manifesting the effect of resource allocation techniques using LTE-Sim simulator [14]. This paper examines the radio resource scheduling in LTE femtocell wireless network and is organized as follows: Section II represents the radio resource allocation in LTE and presents scheduling algorithms with mathematical formula. Then Section III exposes the simulation results and performance analysis. Section IV is consecrated to the conclusion.

2. RADIO RESOURCES SCHEDULING

In an LTE system, the spectrum is separated into fixed sized chunks called Resource Blocks (RBs). One or more RBs can be affected to service an application request subject to the availability of the resource and network policies. Unless stated otherwise, the ensuing discussion is based on the assumption that the underlying system under consideration is LTE [15].

The radio resource scheduling in LTE is assigned in both time and frequency domain. The LTE air interface elements are given in Fig. 2. In time-domain the DL channels in air interface are separated into Frames of 10 ms each. Frame includes 10 Sub frames each of 1 ms. Each subframe interval is attributed to as Transmission Time Interval (TTI). Each subframe consists of 2 Slots of 0.5ms. In frequency domain the total available system bandwidth is separated into sub-channels of 180 kHz with each sub-channel including 12 successive equally spaced OFDM sub-carriers of 15 KHz each [16].

A time-frequency radio resource covering over 0.5 ms slots in the time domain and over 180KHz sub-channel in the frequency domain is named Resource Block (RB). The LTE effectuate in the bandwidth of 1.4 MHz up to 20 MHz with number of RBs ranging from 6 to 100 for bandwidths 1.4 MHz to 20 MHz respectively [2].

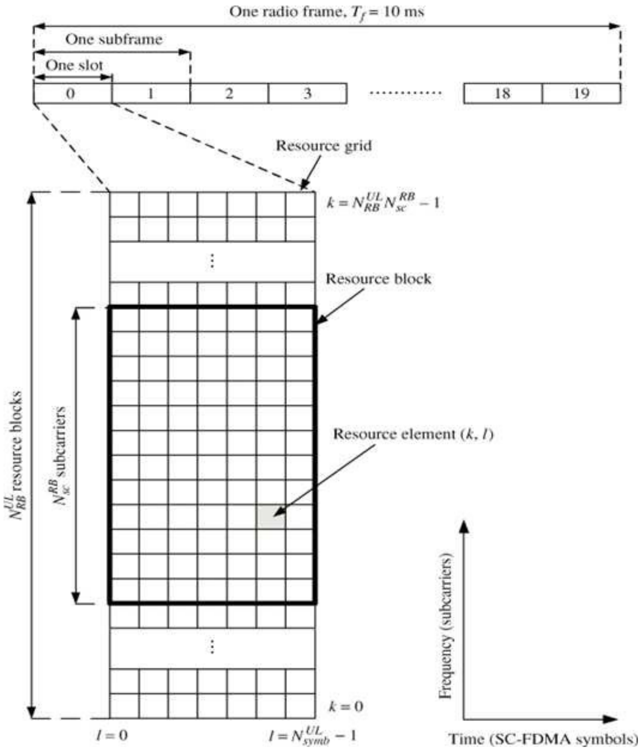

Fig. 2: The structure of the downlink resource grid.

In the following, the description of different scheduling algorithms were used in all simulation scenarios, these are: PF as well as Log-Rule and FLS.

2.1. Proportional Fair (PF)

The PF scheduling algorithm [16] provides a good trade-off between system throughput and fairness by selecting the user. For this algorithm, the metric is given by:

$$j = \max_i \frac{u_i(t)}{\bar{u}_i} \qquad (1)$$

Where $\bar{u}_i$ is the rate corresponding to the mean fading level of user *i and* $u_i(t)$: is the state of the channel of user i at time t.

2.2. Logarithmic rule (LOG rule)

The log rule has been presented in [7]. The log rule is explained as follows:

$$j = \max_i \log(1 + a_i q_i)\frac{u_i(t)}{\overline{u_i}} \qquad (2)$$

Where $u_i(t)$ and $\overline{u_\iota}$ are the same parameters already presented in PF scheduler. The value of qi represents the length queue. $a_i = 5/d_i$Where d_i is the maximal delay target of the i-th user's flows.

2.3. Frame Level Scheduler (FLS)

The FLS [8] is a two-level scheduling techniques with one upper level and lower level. Two different algorithms are implemented in these two levels. At the upper level, a discrete time linear control law is used every LTE frame (i.e.10 ms). It computes the total amount of data that real-time flows should transmit in the following frame in order to satisfy their delay constraints. When FLS finishes its task, the lowest layer scheduler works every TTI to assign resource scheduling using the PF schemas. PF considers the bandwidth requirements proposed by the FLS. Firstly, the lowest layer scheduler allocates RBs to those UEs that experience the best CQI (Channel Quality Indicator) and then the rest ones are considered. If any RBs left unattached, they would be allocated to best-effort flows.

3. Simulation Results And Performance Analysis

This section describes the simulations results to evaluate three schedulers performance and discusses the results obtained from experiments conducted using the LTE simulator developed in [14]. Before the discussion on the simulation results, the simulation scenario and the performance metrics are given. Then,We compare three previously proposed schedulers in terms of their achieved throughput, fairness index, Packet Loss Ratio and spectral efficiency in different number of users.

3.1. Simulation Scenario

In these simulations we designed a scenario including one macrocell and 56 buildings situated as in a urban scenario. The cell itself has one enodeB which transmits using an omnidirectional antenna in a 5 MHz bandwidth. Each UE uses at same time a video flow a VoIP flow and a best effort flow as shown in Figure 3. The video flow are based on realistic video trace files with a rate of 128 kbps was used. For VoIP a G.729 voice stream with a rate of 8.4 kbps was considered. The LTE propagation loss model is organized by four different models (shadowing, multipath, penetration loss and path loss):

- Path loss: PL = 128.1 + 37.6 log10(d) where d is the distance between the UE and the eNodeB in km.

- Multipath: Jakes model.

- Penetration loss: 10 dB.

- Shadowing: log-normal distribution, with mean 0 dB and standard deviation of 8 dB.

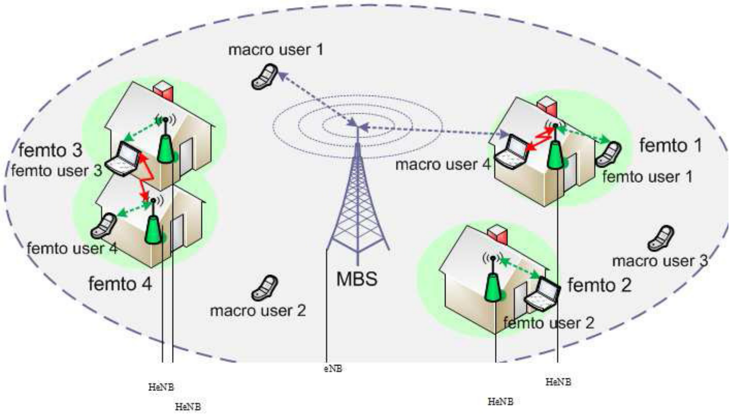

Fig. 3: LTE simulated scenario with video, VoIP and best effort flows.

3.2 Performance Metrics

When evaluating the Quality of service, several metrics are used in this work such as Average Throughput, packet loss Ratio, fairness index and spectral efficiency. Three metrics are used in this paper and are explained as follows:

- Average Throughput per user. This metric presents the average rate of successful message delivery over physical channel. It is elaborated by dividing the size of a transmitted packet by the time it selects to transfer the packets per each user. We chose this metric to examine the impact of throughput when the number users increase.

- Packet Loss Ratio (PLR). This metric try to measure the percentage of packets of data transmitting across a physical channel which fail to reach their destination. Also there exist packet losses caused by buffer overflows [19].

- Fairness Index. In order to acquire an index related to the fairness level we use the Jains fairness index method [20].

$$FI = \frac{(\sum_1^N x_i)^2}{N \sum_1^N x_i^2} \qquad (3)$$

Where x_i is the throughput assigned to user i among N competing flows.

3.3 Simulation Results

Now, we examine the effect of the femtocells unfolding in urban environments. For this, a typical urban Scenario without femtocells and urban Scenario with femtocells exposed are compared. From Fig.4. It is possible to observe that the PLR of best effort flows increase of all sheduling algorithms in case of adoption of femtocells. With reference to VoIP flows, we examined that they achieved smaller PLR without femtocells.

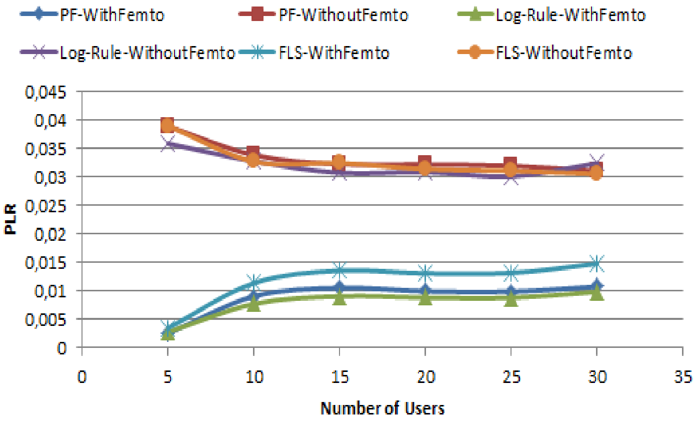

Fig. 4. Packet Loss Ratio of best effort flows

The VOIP flows experience has lower PLRs than Video flows are illustrated in Fig. 5. Initially, Fig. 6 shows that the PLR increased as the number of UEs in the cell increased, which is obviously due to the increased load on the network. The FLS scheduler is outperformed than LOG-Rule and FLS algorithms in terms of PLR, especially for video streaming. FLS has achieved the lowest PLR in video and VoIP flows.

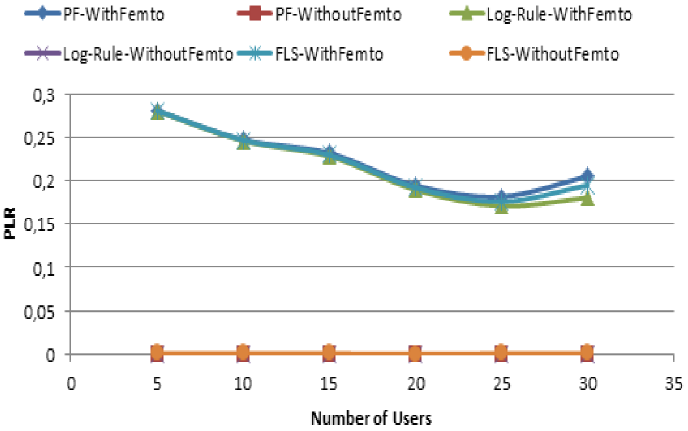

Fig. 5. Packet Loss Ratio of VoIP flows

Then we analysed the throughput obtained by different flows for the presented scheduling algorithms. In order to do that, we analysed the overall system throughput for each scenario considering the number of UEs in both the macrocells and femtocells scenario. In all the cases, it is figured that the PF Algorithm shows good throughput performance for best effort flows. This result is shown in Fig. 7.

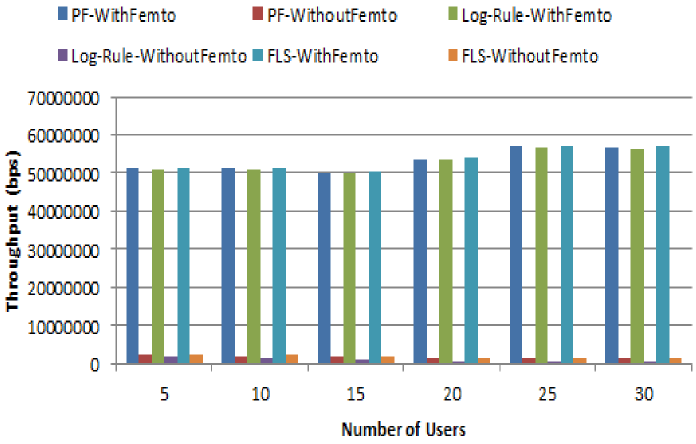

Fig. 6. Throughput of best effort flows.

Throughput, can also analysed by evaluating the performance of real time flows. The Fig.8 shows the throughput obtained by VoIP flow versus the number of UEs in the cell. We see that when number of users in the cell increases, the Log-Rule and FLS schedulers maintain a high throughput compared with the PF. Finally, it is important to remark that VoIP flows experience exactly smaller throughput than video ones is shown in Fig. 9. The performance of FLS scheduler is the greater. In such case we need to choose an algorithm having comparatively higher throughput especially in Real time flows.

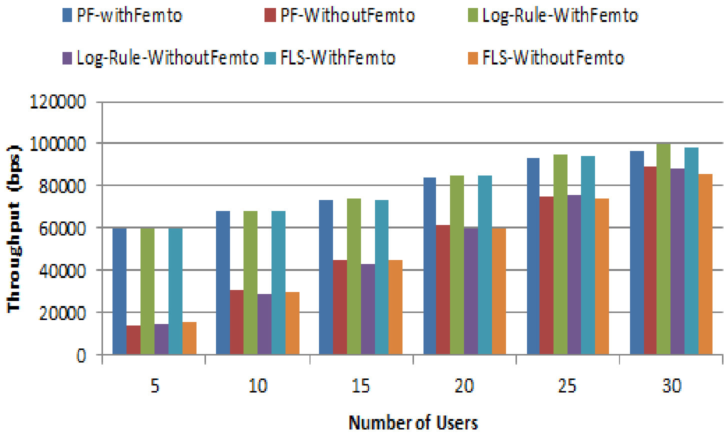

Fig. 7. Throughput of VoIP flows.

Resource scheduling techniques should optimally scale between fairness in order to ensure QOS. Although, Table 1 demonstrate that the FLS scheduling discipline can maintain a high level of fairness index in both femtocells and macrocells scenario. Table 2 presents the fairness index experienced by VOIP flows. It shows that the FLS scheduler degree of fairness performance is higher compared to PF and LOG-Rule scheduler in both femtocells and macrocells scenario.

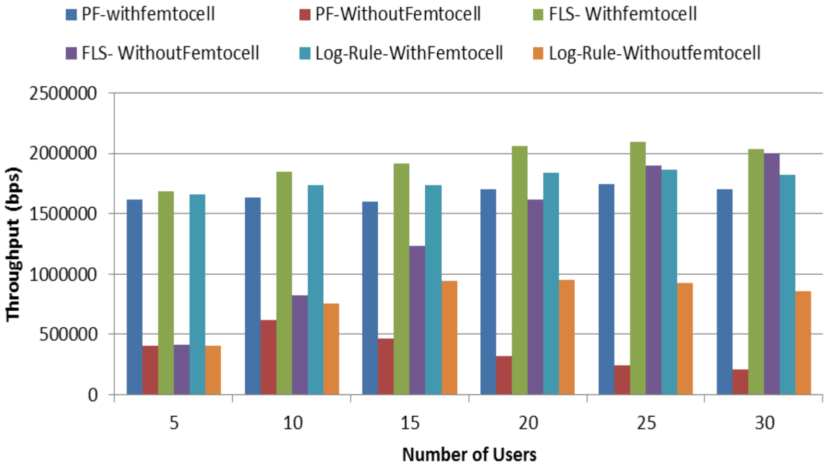

Fig. 8. Throughput of video flows.

Table 1: FAIRNESS INDEX VALUE OF VIDEO FLOWS.

Scenario	Without Femtocell			With Femtocell		
Number of users	**PF**	**FLS**	**LOG-Rule**	**PF**	**FLS**	**LOG-Rule**
5	0.28	0.35	0.34	0.39	0.4	0.39
10	0.10	0.26	0.19	0.26	0.3	0.29
15	0.10	0.26	0.17	0.1461	0.33	0.32
20	0.07	0.24	0.15	0.12	0.34	0.30
25	0.06	0.19	0.12	0.10	0.31	0.25
30	0.05	0.16	0.09	0.08	0.32	0.23

Table 2: FAIRNESS INDEX VALUE FOR VOIP FLOWS.

Scenario	Without Femtocell			With Femtocell		
Number of users	**PF**	**FLS**	**LOG-Rule**	**PF**	**FLS**	**LOG-Rule**
5	0.33	0.33	0.33	0.37	0.38	0.39
10	0.34	0.35	0.35	0.39	0.39	0.39
15	0.28	0.28	0.28	0.32	0.31	0.32
20	0.29	0.30	0.30	0.33	0.34	0.34
25	0.30	0.32	0.31	0.34	0.34	0.34
30	0.27	0.30	0.29	0.32	0.32	0.32

Finally, Table 3 shows that the FLS scheduling algorithm can maintain a high level of fairness index especially in scenario with Femtocells.

Table 3: FAIRNESS INDEX VALUE OF BEST EFFORT FLOWS.

Scenario	Without Femtocell			With Femtocell		
Number of users	PF	FLS	LOG-Rule	PF	FLS	LOG-Rule
5	0.2	0.2	0.2	0.2	0.2	0.2
10	0.18	0.17	0.18	0.25	0.24	0.25
15	0.18	0.18	0.18	0.26	0.25	0.26
20	0.16	0.16	0.16	0.23	0.20	0.23
25	0.17	0.17	0.17	0.25	0.22	0.25
30	0.14	0.14	0.14	0.24	0.19	0.24

Finally, Fig.10 shows that the total cell spectral efficiency increases as long as the number of users increases. It can notice that the use of femtocells increases spectral efficiency in LTE systems.

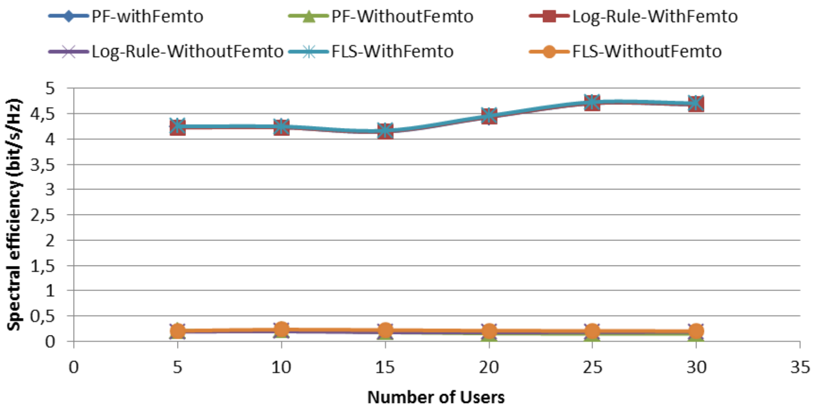

Fig. 9: Spectral efficiency

3. CONCLUSIONS

In this paper, we studied the resource allocation problem in LTE femtocells networks. Using the LTE-SIM simulator, the study compares the performance of scheduling schemas such as average system throughput, PLR, and fairness via video and VoIP traffic in femtocells scenario. Our simulation shows FLS performs better than both PF and Log-Rule with respect to throughput satisfaction rate. For RT Traffic, PF shows the highest PLR value, the lowest attained throughput and a high delay when the cell is charged; thus this algorithm could be suitable for non-real-time flows but is inappropriate to manipulate real time multimedia services.

We found that FLS always reaches the lowest PLR in all used scenarios, among all those schemas that try to ensure attached delay but at the cost of reducing resources for best effort flows. Adoption of femtocells can increase the Overall system throughput.

Upcoming work will examine also the more challenging problem of scheduling such as the uplink direction using multicells scenario.

ACKNOWLEDGEMENTS

This work was sustained in part by Laboratory InnovCOM of Higher School of Telecommunication of Tunis, and National Engineering School of Tunis.

REFERENCES

[1] Nazmus Saquib, Ekram Hossain, Long Bao Le, and Dong In Kim , Interference management in OFDMA femtocell networks: issues and approaches. H Wireless Communications, IEEE (Volume:19 , Issue: 3) , June 2012.

[2] 3GPP Technical Specication Group Radio Access Networks, 3G Home NodeB Study Item Technical Report (Release 8).

[3] Barbieri. A, Damnjanovic. A, Tingfang Ji, Montojo. J, Yongbin Wei, Malladi. D,Osok Song, Horn. G, LTE Femtocells: System Design and Performance Analysis, in Selected Areas in Communications, IEEE Journal on Volume:30 , Issue: 3, April 2012.

[4] Roberg, Kristoffer, Simulation of scheduling algorithms for femtocells in an LTE environment, MSc Thesis, 2010.

[5] S. Bae et. al., ”Femtocell interference analysis based on the development of system-level LTE simulator,” EURASIP Journal on Wireless Communications and Networking 2012, 2012:287.

[6] Yaser Barayan and Ivica Kostanic, Performance Evaluation of Proportional Fairness Scheduling in LTE, in Proceedings of the World Congress on Engineering and Computer Science 2013 Vol II WCECS 2013, 23-25 October, 2013.

[7] American Mathematical Society, Providence, RI, USA.B. Sadiq; S.J. Baek and G; de Veciana. Delay-optimal opportunistic scheduling and approximations: The log rule. In IEEE/ACM Transactions on Networking,Vol. 19(2), pages 405418, April 2011.

[8] Giuseppe Piro, Luigi Alfredo Grieco, Gennaro Boggia, Rossella Fortuna, and Pietro Camarda”, Two-level downlink scheduling for real-time multimedia services in LTE networks”, IEEE Trans. Multimedia, Volume:13 , Issue: 5, 2011.

[9] Sevindik, V. , Bayat, O. ; Weitzen, J.A., Radio Resource Management and Packet Scheduling in Femtocell Networks, in Modeling and Optimization in Mobile, Ad Hoc and Wireless Networks (WiOpt), 2011.

[10] Bilal Sadiq, Ritesh Madan and Ashwin Sampath, ”Downlink Scheduling for Multiclass Trac in LTE,” EURASIP Journal on Wireless Communications and Networking, ID 510617, pp. 18, 2009.

[11] Marshoud, H. Otrok, H. ; Barada, H. ; Estrada, R. ; Jarray, A. ; Dziong, Z., Resource Allocation in Macrocell-Femtocell Network Using Genetic Algorithm, in Wireless and Mobile Computing, Networking and Communications (WiMob), 2012.

[12] Sathya, V. Gudivada, H.V. ; Narayanam, H. ; Krishna, B.M. ; Tamma, B.R., Enhanced Distributed Resource Allocation and Interference Management in LTE Femtocell Networks,in Wireless and Mobile Computing, Networking and Communications (WiMob), 2013.

[13] D. Singh and Preeti, ”Performance Analysis of QOS-aware Resource Scheduling Strategies in LTE Femtocell Networks,” International Journal of Engineering Trends and Technology (IJETT), vol. 4. no. 7, pp. 2977- 2983, Jul 2013.

[14] Francesco Capozzi1, Giuseppe Piro, Luigi A Grieco, Gennaro Boggia and Pietro Camarda, On accurate simulations of LTE femtocells using an open source simulator, in EURASIP Journal on Wireless Communications and Networking, doi:10.1186/1687-1499-2012-328, 2012.

[15] Parag Kulkarni, Woon Hau Chin, and Tim Farnham. Radio resource management considerations for lte femtocells. ACM SIGCOMM Computer Communication, Volume 40 Issue 1, January 2010.

[16] S. M. Chadchan. C. B. Akki, A Fair Downlink Scheduling Algorithm for 3GPP LTE Networks, in International Journal of Computer Network and Information Security(IJCNIS), Vol. 5, No. 6, 2013.

[17] Francesco Capozzi, Giuseppe Piro, Luigi Alfredo Grieco, Gennaro Boggia, and Pietro Camarda,” Downlink Packet Scheduling in LTE Cellular Networks: Key Design Issues and a Survey”, IEEE Commun. Surveys and Tutorials, 2012.

[18] Roke Manor Research,”LTE MAC Scheduler Radio Resource Scheduling”, 2011.

[19] Iturralde Ruiz, Performances des Réseaux LTE, MSc Thesis, 2012.

[20] R. Jain; D. Chiu and W. Hawe. A quantitative measure of fairness and discrimination for resource allocation in shared computer systems. In Digital Equip. Corp., Littleton, MA, DEC Rep - DEC-TR-301, September 1984.

AUTHORS

DARDOURI Samia

Received the B.S. degree in 2009 from National Engineering School of Gabes, Tunisia, and M.S. degree in 2012 from National Engineering School of Tunis. Currently he is a Ph.D student at the School of Engineering of Tunis. He is a researcher associate with Laboratory at Higher School of Communications (SupCom), University of Carthage, Tunisia. Her Research interests focus on scheduling algorithms and radio resource allocation in LTE systems.

PR. RIDHA BOUALLEGUE

Received the Ph.D degrees in electronic engineering from the National Engineering School of Tunis. In Mars 2003, he received the Hd.R degrees in multiuser detection in wireless communications. From September 1990 He was a graduate Professor in the higher school of communications of Tunis (SUP'COM), he has taught courses in communications and electronics. From 2005 to 2008, he was the Director of the National engineering school of Sousse. In 2006, he was a member of the national committee of science technology. Since 2005, he was the laboratory research in telecommunication Director's at SUP'COM. From 2005, he served as a member of the scientific committee of validation of thesis and Hd.R in the higher engineering school of Tunis. His recent research interests focus on mobile and wireless communications, OFDM, OFDMA, Long Term Evolution (LTE) Systems. He's interested also in spacetime processing for wireless systems and CDMA systems.

INTENTIONAL BLANK

MC CDMA PERFORMANCE ON SINGLE RELAY COOPERATIVE SYSTEM BY DIVERSITY TECHNIQUE IN RAYLEIGH FADING CHANNEL

Gelar Budiman[1], Ali Muayyadi[2] and Rina Pudji Astuti[3]

[1]Electrical Engineering Faculty, Telkom University, Bandung, Indonesia
gelarbudiman@telkomuniversity.ac.id
[2]Electrical Engineering Faculty, Telkom University, Bandung, Indonesia
alimuayyadi@telkomuniversity.ac.id
[3]Electrical Engineering Faculty, Telkom University, Bandung, Indonesia
rinapudjiastuti@telkomuniversity.ac.id

ABSTRACT

Wireless communication now has been focus to increase data rate and high performance. The multi carrier on multi-hop communication system using relay's diversity technique which is supported by a reliable coding is a system that may give high performance.

This research is developing a model of multi carrier CDMA on multi hop communication system with diversity technique which is using Alamouti codes in Rayleigh fading channel. By Alamouti research, Space Time Block Code (STBC) for MIMO system can perform high quality signal at the receiver in the Rayleigh fading channel and the noisy system. In this research, MIMO by STBC is applied to single antenna system (Distributed-STBC/DSTBC) with multi carrier CDMA on multi hop wireless communication system (relay diversity) which is able to reduce the complexity of the system but the system performance even can be maintained and improved.

MC CDMA on multi hop wireless communication system with 2 hops is performing much better than Single Input Single Output (SISO) system (1 hop system). Power needed for 1 hop system to have the same quality as 2 hops system to reach BER 10^{-3} is 12 dB. And multi hop system needs orthogonal symbol to send from relay than original symbol to reach better performance. 12.5 dB power up is needed for multi hop system which sent same symbol as transmitter than relay system which sent orthogonal symbol.

KEYWORDS

Alamouti, MIMO, multi carier, CDMA, MC CDMA, STBC, Distributed-STBC/DSTBC, diversity, Rayleigh fading, multi-hop system, SISO, relay's diversity

1. INTRODUCTION

Wireless communication system development nowadays focused to support the services with high data rate for some the contents of multimedia such as sound, images, data and video. Moreover, the transmitted data is expected to have the better quality with a low bit error rate. To provide the interactive multimedia services, it needs a large bandwidth. However, the available bandwidth is

Natarajan Meghanathan et al. (Eds) : NeTCoM, CSIT, GRAPH-HOC, SPTM - 2014
pp. 27–39, 2014. © CS & IT-CSCP 2014 DOI : 10.5121/csit.2014.41303

limited, and the wireless communication system has more complex channel characteristic than wireline.

To improve the performance of the wireless system, there should be improvement of coding scheme in the transmitter and receiver. One of them is to apply the code block in multi antenna systems, known as Multiple Input Multiple Output (MIMO). One of MIMO transmission techniques often used is Space Time Block Code (STBC) found by Siavash M. Alamouti [1]. STBC is a such technique that relies on code orthogonality, so the correlation between the antennas would be very small and has an impact to perform better quality than the system without using STBC [1].

The application of STBC was not only good for the multi-antenna system or MIMO, but also the application of STBC in the cooperative communications with multi hop can improve the system transmission performance significantly even with single-antenna [2]. The application of STBC cooperative communications is called the Distributed-STBC (DSTBC). In this research, DSTBC applied to cooperative communication with single antenna on the Rayleigh fading channels and used 2 hops for the simulation.

2. BASIC THEORY

2.1. Basic Concept of Multi Input Multi Output System (MIMO)

MIMO system is a transmission system (Tx-Rx) where the number of antenna either transmitter or receiver consists of several antenna. Many coding scheme has been performed at MIMO system to get better received signal quality. Alamouti codes is one of the coding scheme to apply at MIMO system which perform good quality.

2.2. Diversity with *Space Time Block Code* (STBC)

Orthogonal space time block code is transmission scheme introduced by Alamouti. Alamouti has introduced coding scheme for 2x2 or 2x1 antenna which is shown at figure 2.1 [6].

$$\begin{array}{cc} & \begin{array}{cc} T_{x0} & \quad T_{x1} \end{array} \\ \begin{array}{c} t \\ t+1 \end{array} & \begin{bmatrix} S_0 & S_1 \\ -S_1^* & S_0^* \end{bmatrix} \end{array}$$

Figure 2.1: Orthogonal Space Time Block Code transmission scheme [1]

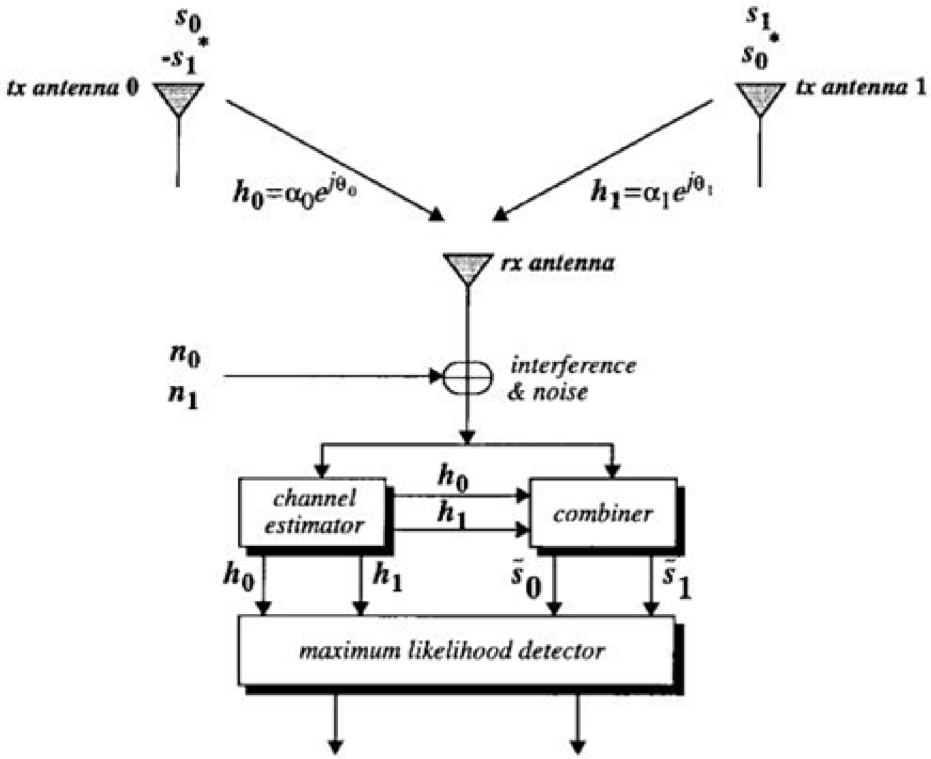

Figure 2.2 : MIMO scheme with 2 Tx Antenna and 1 Rx Antenna (2x1) [1]

The channel at time *t* is modelled by a complex multiplicative coefficient $\boldsymbol{h_0}(t)$ from 1st transmitter antenna and $\boldsymbol{h_1}(t)$ from 2nd transmitter antenna. Assuming that fading coefficients are constant across two consecutive symbols as [1]:

$$\begin{aligned} h_0(t) &= h_0(t+T) = h_0 = \alpha_0 e^{j\theta_0} \\ h_1(t) &= h_1(t+T) = h_1 = \alpha_1 e^{j\theta_1} \end{aligned} \tag{2.1}$$

According to figure 2.1 and figure 2.2, the equation of received signal is [1]:

$$\begin{aligned} r_0 &= r(t) = h_0 s_0 + h_1 s_1 + n_0 \\ r_1 &= r(t+T) = -h_0 s_1^* + h_1 s_0^* + n_1 \end{aligned} \tag{2.2}$$

$\boldsymbol{n_0}$ and $\boldsymbol{n_1}$ are complex random variable which representates interference and noise thermal. Combiner subsystem in figure 2 will decode received signal by maximum likelihood formula as [1]:

$$\begin{aligned} \tilde{s}_0 &= h_0^* r_0 + h_1 r_1^* \\ \tilde{s}_1 &= h_1^* r_0 - h_0 r_1^* \end{aligned} \tag{2.3}$$

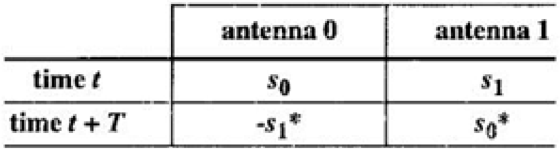

	antenna 0	antenna 1
time t	s_0	s_1
time $t + T$	$-s_1{}^*$	$s_0{}^*$

Figure 2.3 : Received Signal Notation In Scheme 2x1 [1]

Substituting equation 2.1 to 2.3 will make a result [1]:

$$\tilde{s}_0 = (\alpha_0^2 + \alpha_1^2)s_0 + h_0^* n_0 + h_1 n_1^*$$
$$\tilde{s}_1 = (\alpha_0^2 + \alpha_1^2)s_1 - h_0 n_1^* + h_1^* n_0 \quad (2.4)$$

2.3. Diversity by *Distributed Space Time Block Code* (DSTBC)

The application of STBC was not only good for the multi-antenna system or MIMO, but also for cooperative communications with multi hop system. It can improve the system transmission performance significantly even with single-antenna [2]. The application of STBC cooperative communication is called the Distributed-STBC (DSTBC). The system scenario is described as the situation displayed in figure 2.4.

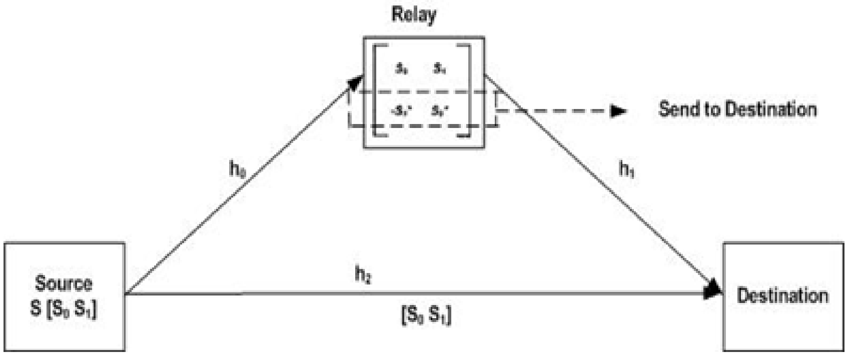

Figure 2.4 : Transmission scheme based of relay technique [3] [4]

According to figure 2.4, the equation of received signal is :

$$r_1 = -s_2^* h_1 + s_1 h_2$$
$$r_2 = s_1^* h_2 + s_2 h_3 \quad (2.5)$$

Combiner block in figure 2.4 makes two signals below which will be transmitted to *maximum likelihood* detector :

$$\tilde{s}_1 = r_1 h_3^* + h_2 r_2^*$$
$$\tilde{s}_2 = -h_2 r_1^* + h_3 r_2^* \quad (2.6)$$

2.4. Transmission Channel Decoding

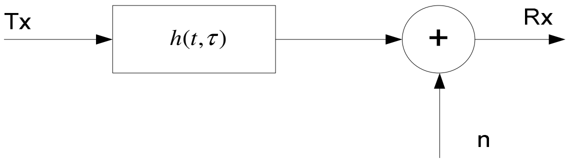

Figure 2.5 : General Channel Model [5]

A transmission channel generally can be defined:

$h(t,\tau)$ is time varying impulse response from multipath channel, mathematically it's defined as [5]:

$$h(t,\tau)=\sum_{i=0}^{N-1}\left\{a_i\left(t,\tau_i\left(t\right)\right)p\left(t,\tau_i\left(t\right)\right)\right\}$$
$$p\left(t,\tau_i\left(t\right)\right)=\mathrm{e}^{j2\pi f_c\tau_i(t)+\theta(t,\tau_i(t))\delta(t-\tau_i(t))} \qquad (2.7)$$

where:

- $a_i(t,\tau_i(t))$ is gain from *i*-th multipath component at time *t*.
- $2\pi f_c\tau_i(t)+\theta_i(t,\tau_i(t))$ is a term to representate phase shifting because of propagation at *i*-th multipath component.
- *N* is propagation path number.

Doppler shifting is expressed by equation [2]:

$$f_d=\frac{v}{\lambda}\cos\theta \qquad (2.8)$$

where :

v=relative movement velocity

$\lambda=$ wavelength of carrier

$\theta=$ angle between incoming signal direction and antenna movement direction

2.5 Multicarrier Modulation

Multicarrier modulation is defined as modulation technique in which there are several subcarrier or frequency to modulate the separate signal and every subcarrier is orthogonal each other. This mechanism is also called OFDM (*Orthogonal Frequency Division Multiplexing*). By this nature the signal in every subcarrier can be overlapped without Intercarrier Interference (ICI). This mechanism can save bandwitdh needs [9]. Spectrum illustration between conventional FDM and *multicarrier (*OFDM) is shown at figure 2.6.

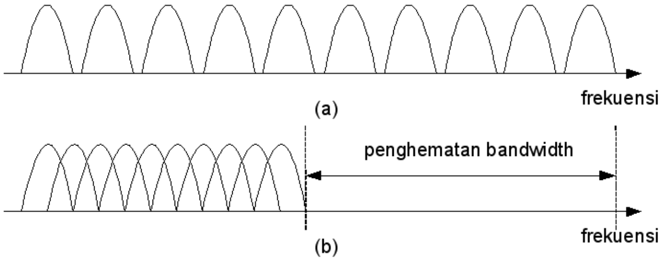

Figure 2.6 : Multi *Carrier* Spectrum (a) No Overlap (b) Orthogonally Overlap

Mathematically, group of signal φ_i, i = ± 0, ± 1, ±2, ….., akan ortogonal pada interval [a b], jika :

$$\int_a^b \varphi_l(t)\varphi_k^*(t)\,dt = \begin{cases} E_k, & jika\ l = k \\ 0, & jika\ l \neq k \end{cases} \qquad (2.9)$$

$$= E_k\delta(l-k)$$

E_k is constant resulting from integration and φ_k^*(t) is *conjugate complex* from signal $\delta(l-k)$ (delta *kronecker*) [10], which is defined as :

$$\delta(l-k) = \begin{cases} 1, & when\ l = k \\ 0, & when\ l \neq k \end{cases} \qquad (2.10)$$

Basis function *Discrete Fourier Transform* (DFT) or *Fast Fourier Transform* is : $\varphi_k(t) = e^{[j(2\pi kt)/T]}$, where k = 0, ± 1, ± 2, ± 3,…… forms group of orthogonal signal at interval (0, T) (*T* = signal periode) :

$$\int_0^T \phi_l(t)\varphi_k^*(t)\ dt = \int_0^T \exp\left[\frac{j(2\pi lt)}{T}\right]\exp\left[\frac{-j(2\pi kt)}{T}\right] dt$$
$$= \begin{cases} T, & jika\ l = k \\ 0, & jika\ l \neq k \end{cases} \qquad (2.11)$$

3. Cooperative System Based on One Relay Model (2 HOPS System)

3.1 Model System

The communication between the source and the user not only directly but also through the relay. So that, the received signal is the sum of the user that sent the signal directly (direct channel) and signal through the relay (the relay channel).

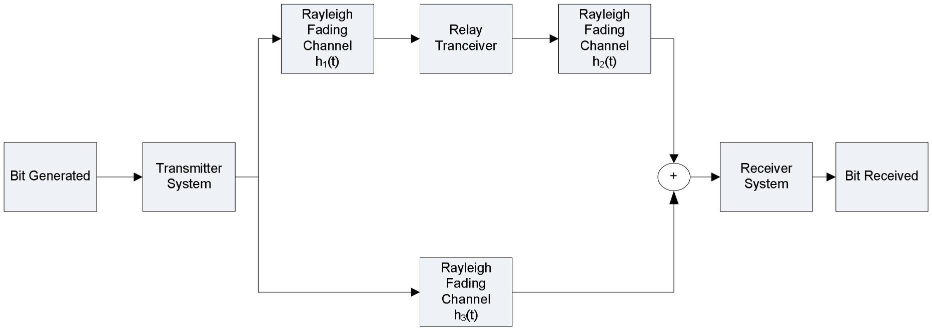
Rayleigh Fading Channel $h_1(t)$
Relay Tranceiver
Rayleigh Fading Channel $h_2(t)$
Bit Generated
Transmitter System
+
Receiver System
Bit Received
Rayleigh Fading Channel $h_3(t)$

Figure 3.1 : Two Hops System Model with Single Antenna [9]

As shown at figure 3.1 the multi hop system introduced 2 hops, such as : 1. the hop between base station (BS) and mobile station (MS) via relay, 2. the hop between BS and mobile station (MS) directly without relay. Fading channel distribution realized in 2 hops are Rayleigh fading channel in i.i.d distributed. Because of Rayleigh channel, received signal performance of 2 hops system should be affected by mobility of either relay or MS velocity. Figure 3.2 explained SISO (Single Input Single Output) system model (1 hop system) in which its performance will be compared to 2 hops system performance [9].

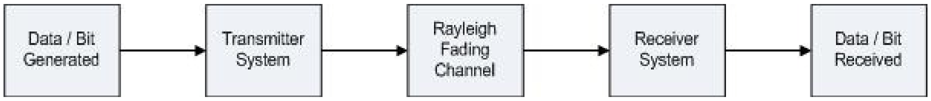

Figure 3.2 : SISO System Model [7]

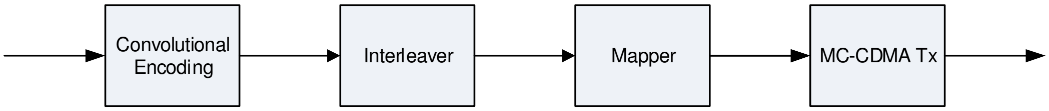

Figure 3.3 : Transmitter System Model

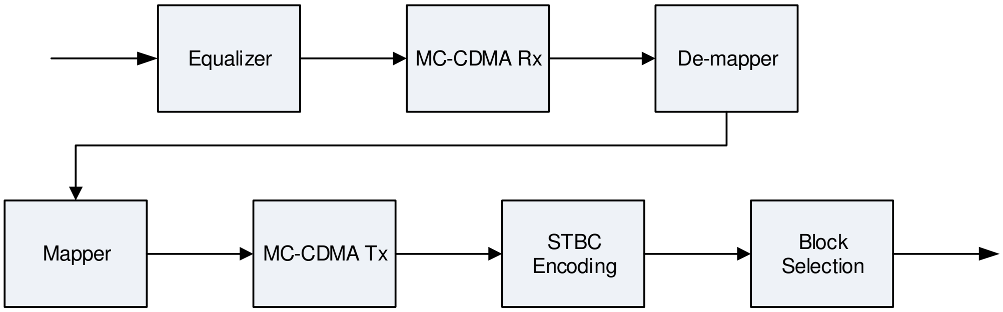

Figure 3.4 : Relay Tranceiver System Model [9]

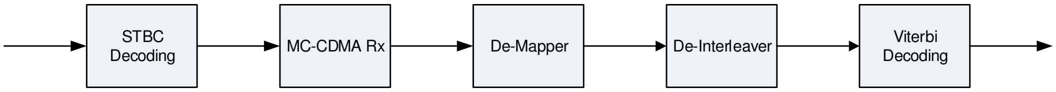

Figure 3.5 : Receiver System Model

The transmitter system of BS or SISO transmitter consists of 3 subsystems processing baseband signal as shown in figure 3.3. While relay transceiver from figure 3.1 consists of 5 subsystems which equalized, normalized, STBC encoded, and selected one block code before transmitting the signal to MS as shown in figure 3.4. As shown in figure 3.5, receiver system consists of several subsystem which decoded combined signal from BS and relay by Alamouti principal, demodulate, deinterleaved, and Viterbi decoded. Next, the data compared to the original data for counting BER performance.

The content of MC CDMA transmitter by frequency domain spreading is shown in figure 3.6. The content of MC CDMA receiver by frequency domain spreading is shown in figure 3.6.

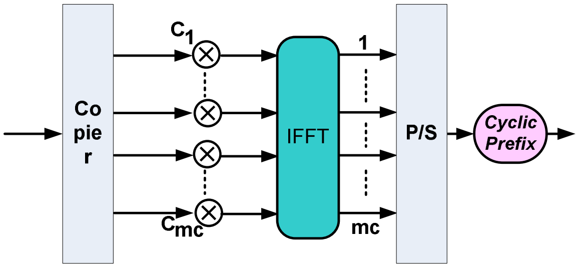

Figure 3.6 : MC CDMA Transmitter Model System [7]

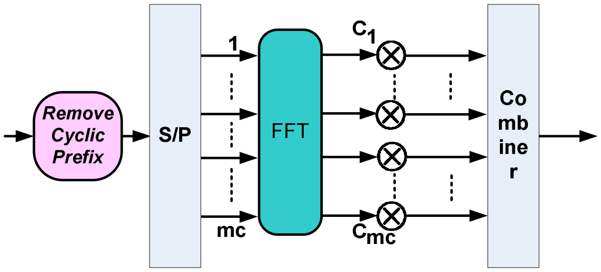

Figure 3.7 : MC CDMA Receiver Model System [7]

The content of MC DS CDMA transmitter by frequency domain spreading is shown in figure 3.8. The content of MC Ds CDMA receiver by time domain spreading is shown in figure 3.9.

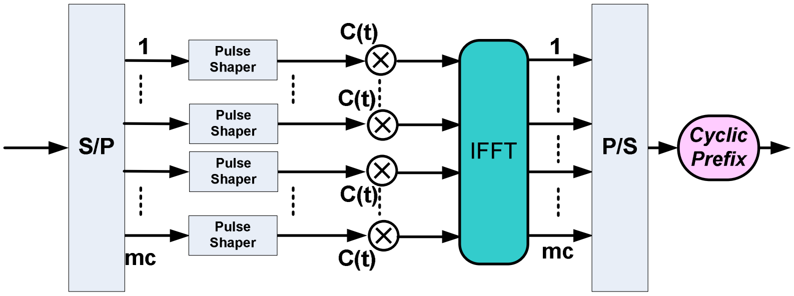

Figure 3.8 : MC DS CDMA Receiver Model System [7]

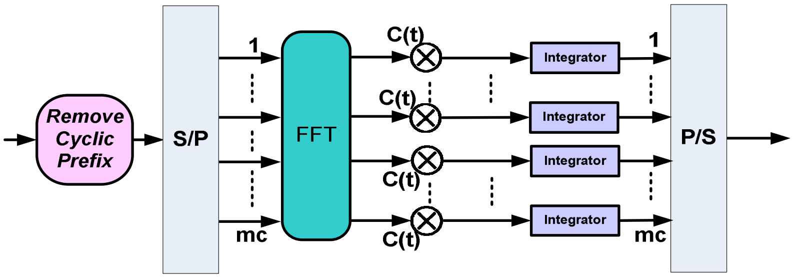

Figure 3.9 : MC DS CDMA Receiver Model System [7]

4. MC CDMA MULTIHOP COOPERATIVE SYSTEM PERFORMANCE

This simulation was running by several scenarios, such as :

1. Comparison between SISO, and MC CDMA with multi hop either frequency domain spreading MC CDMA or time domain spreading MC CDMA at flat fading Rayleigh.
2. Perform how much subcarrier number affected the performance of multi hop MC CDMA.
3. Perform how much subcarrier number affected the performance of multi hop MC DS CDMA.
4. Comparison performance between multihop MC CDMA, MC DS CDMA, and SISO on selective frequency Rayleigh fading.
5. Comparison performance of multi hop MC CDMA and MC DS CDMA in the different fading channel condition.

For the first scenario, the parameter implemented in the simulation has following limitation :

- Flat Fading Rayleigh
- 32 spreading code (Walsh-Hadamard)
- MS Velocity 30 km/h
- QPSK mapper
- Using 32 subcarriers (At Multicarrier system)
- Perfect Channel Estimation

The simulation result is displayed at figure 4.1.

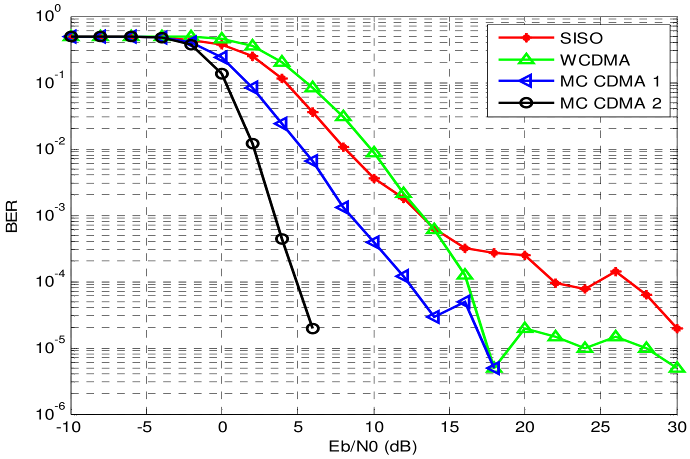

Figure 4.1 : Multi Hop System Performance Comparison

As displayed in figure 4.1, SISO has better performance when Eb/N0 less than 17 dB, but more than 17 dB MC DS CDMA started to have better performance than SISO system. MC CDMA started to have better than SISO at Eb/N0 more than 19 dB. At this simulation it is concluded that both MC CDMA in multi hop communication has a worse performance than SISO when Eb/N0 is still below about 18 dB. But more than 18 dB both MC CDMA has significant performance as the Eb/N0 raises.

For the second scenario, simulation testing was done with following parameter :

- Frequency Selective Fading Rayleigh
- 32 spreading code (Walsh-Hadamard)
- MS Velocity 30 km/h
- BPSK mapper
- Using 32 subcarriers (At Multicarrier system)
- Perfect Channel Estimation

The simulation result is displayed at figure 4.2 and figure 4.3.

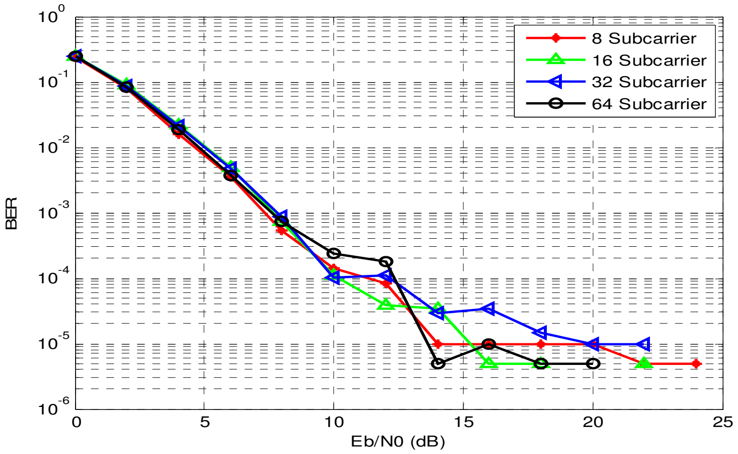

Figure 4.2 : Subcarrier Effect on Multi hop MC CDMA System

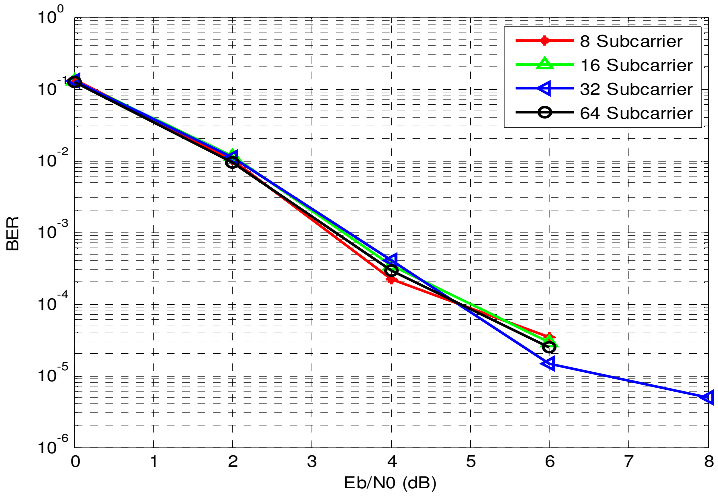

Figure 4.3 : Subcarrier Effect on Multi hop MC DS CDMA System

For the third scenario, simulation testing was done with following parameter :

- Rayleigh Frequency Selective Fading
- 32 spreading code (Walsh-Hadamard)
- MS Velocity 60 km/h
- BPSK mapper
- Using 32 subcarriers (at Multicarrier system)
- Perfect Channel Estimation

The simulation result is displayed at figure 4.4.

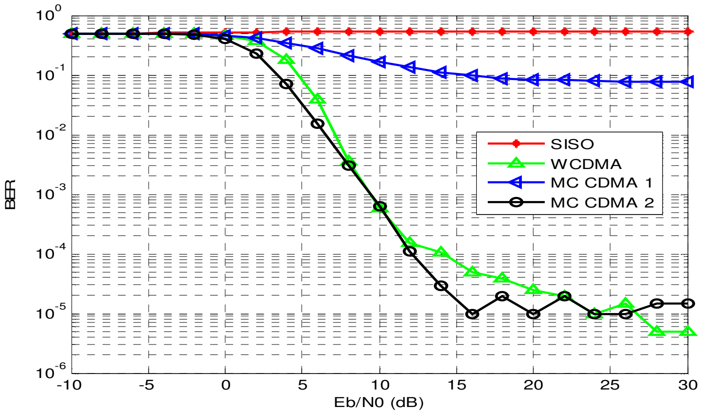

Figure 4.4 : Multihop Performance On Rayleigh Selective Frequency Fading

For the forth scenario, simulation testing was done with following parameter :

- Flat and Frequency Selective on Rayleigh Fading Distribution
- 32 spreading code (Walsh-Hadamard)
- MS Velocity 60 km/h
- QPSK mapper
- Using 32 subcarriers (At Multicarrier system)
- Perfect Channel Estimation

The simulation result is displayed at figure 4.5.

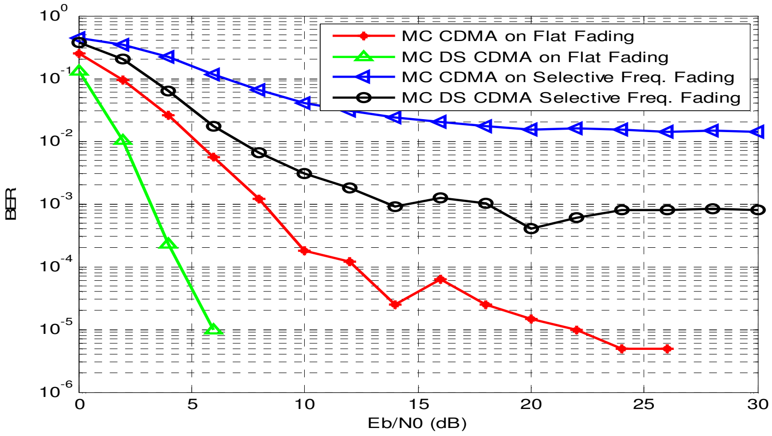

Figure 4.5 : Multihop MC CDMA and MC DS CDMA Performance Comparison On Flat and Frequency Selective Fading

5. CONCLUSION

5.1 Conclusion & Suggestion

1. There will need an improvement formula on MC CDMA Receiver to get better performance. Maximum Likelihood on inner code DSTBC might be improving the performance.
2. Different time symbol received should be simulated and analyzed in the next research as the real condition which needs to be anticipated.
3. Developing system with multi antenna scheme at the transmitter and receiver might perform better performance.

REFERENCES

[1] Alamouti SM, "A Simple Transmit Diversity Technique for Wireless Communication", IEEE Journal on Selected Areas in Communication, vol. 16 No.8, October 1998.

[2] Jaafar W., "On the Performance of Distributed-STBC in Multi-hop Wireless Relay Networks", IEEE European Wireless Conference, 2010.

[3] Adi Nugroho,"Analisis Kinerja Sistem Kooperatif Menggunakan Skema Distributed-Alamouti", Tugas Akhir, ITS, 2010.

[4] Borah D.K, Moreno Crespo, Nammi S., "Distributed Alamouti Transmit Diversity Technique for Co-Operative Communication", Vehicular Technology Conference, 2007. VTC2007-Spring. IEEE 65th, Dublin, 2007.

[5] J. Proakis, "Digital Communications", McGraw Hill, 3rd., 1995.

[6] David Gesbert, Mansoor Shafi, Da-Shan Shiu, Peter J. Smith, Ayman Naguib, "From Theory to Practice : An Overview of MIMO Space-Time Coded Wireless Systems", Tutorial Paper, IEEE Journal On Selected Areas In Communication Vol. 21, No.3 April 2003, Oslo University, Norway.

[7] Gelar Budiman,Suhartono, Rina Pudji Astuti, "Konfigurasi MIMO MC-CDMA Pada Kanal Fading Rayleigh", Jurnal Telekomunikasi IT Telkom Desember 2007 Volume-12 Nomor 2 Hal. 82-88 ISSN : No. 1410-7066, ITTelkom, 2007.

[8] Nur Andini, Ali Muayyadi, Gelar Budiman, "Analisis Performansi WCDMA Diversitas Relay Pada Kanal Fading", Prosiding Konferensi Nasional ICT-M Politeknik Telkom (KNIP) ISSN : 2088-8252, Bandung, 2011.

[9] Ali Muayyadi, Gelar Budiman, Rina Pudji Astuti, "The performance analysis of multiuser WCDMA systems using D-STBC in Rayleigh fading channel", Advanced Communication Technology (ICACT), Pages 1213-1216, South Korea, 2014.

AUTHORS

Gelar Budiman is a lecturer from Electrical Engineering Faculty of Telkom University since 2008. He was graduated from STTTelkom in 2002 as an Electrical Engineering undergraduate student, and same university as Electrical Engineering Master in Telecommunications in 2005. He is an assistant manager of Distance Learning Education Infrastructure in Telkom University, Bandung, Indonesia and has done several researches and lecturer activities such as eLearning grants and community services in relation of his competency. His research competencies are about wireless communication, signal processing, and mobile application.

Ali Muayyadi is a member of IEEE. He finished his BEng degree in electrical engineering from ITB, Bandung, Indonesia in 1990, MSc degree in mobile communicate ons from ENST, Paris in 1997 and PhD degree in digital communications from University of Plymouth, UK in 2003. Now he is the head of Telecommunication Transmission Expert Group of Electrical Engineering Faculty, Telkom University, Bandung, Indonesia.

Rina Pudji Astuti is a lecturer in Electrical Engineering Faculty in Telkom University, Bandung, Indonesia. She finished her undergraduate degree from Electrical Engineering ITS in 1987, Surabaya. She was graduated from Electrical Engineering Master degree from ITB, Bandung, Indonesia in 1999, and Doctoral degree from Electrical and Informatics Engineering in 2009 from ITB. Now she is the Dean of Electrical Engineering Faculty, Telkom university, Bandung, Indonesia. Her interest is in Wireless Communication in speciality of 4G and 5G Telecommunication Technology.

INTENTIONAL BLANK

HIGHLY ACCURATE LOG SKEW NORMAL APPROXIMATION TO THE SUM OF CORRELATED LOGNORMALS

Marwane Ben Hcine[1] and Ridha Bouallegue[2]

[1,2]Innovation of Communicant and Cooperative Mobiles Laboratory,
INNOV'COM
Sup'Com, Higher School of Communication
Univesity of Carthage
Ariana, Tunisia
[1]marwen.benhcine@supcom.tn
[2]ridha.bouallegue@supcom.rnu.tn

ABSTRACT

Several methods have been proposed to approximate the sum of correlated lognormal RVs. However the accuracy of each method relies highly on the region of the resulting distribution being examined, and the individual lognormal parameters, i.e., mean and variance. There is no such method which can provide the needed accuracy for all cases. This paper propose a universal yet very simple approximation method for the sum of correlated lognormals based on log skew normal approximation. The main contribution on this work is to propose an analytical method for log skew normal parameters estimation. The proposed method provides highly accurate approximation to the sum of correlated lognormal distributions over the whole range of dB spreads for any correlation coefficient. Simulation results show that our method outperforms all previously proposed methods and provides an accuracy within 0.01 dB for all cases.

KEYWORDS

Correlated Lognormal Sum, Log Skew Normal, Interference, Outage Probability

1. INTRODUCTION

Multipath with lognormal statistics is important in many areas of communication systems. With the emergence of new technologies (3G, *LTE*, *WiMAX*, Cognitive Radio), accurate interference computation becomes more and more crucial for outage probabilities prediction, interference mitigation techniques evaluation and frequency reuse scheme selection. For a given practical case, Signal-to-Interference-plus-Noise (SINR) Ratio prediction relies on the approximation of the sum of correlated lognormal RVs. Looking in the literature; several methods have been proposed in order to approximate the sum of correlated lognormal RVs. Since numerical methods require a time-consuming numerical integration, which is not adequate for practical cases, we consider only analytical approximation methods. Ref [1] gives an extension of the widely used iterative method known as Schwartz and Yeh (SY) method [2]. Some others resources uses an extended version of Fenton and Wilkinson methods [3-4]. These methods are based on the fact that the sum of dependent lognormal distribution can be approximated by another lognormal

Natarajan Meghanathan et al. (Eds) : NeTCoM, CSIT, GRAPH-HOC, SPTM - 2014
pp. 41–52, 2014. © CS & IT-CSCP 2014 DOI : 10.5121/csit.2014.41304

distribution. The non-validity of this assumption at distribution tails, as we will show later, is the main raison for its fail to provide a consistent approximation to the sum of correlated lognormal distributions over the whole range of dB spreads. Furthermore, the accuracy of each method depends highly on the region of the resulting distribution being examined. For example, Schwartz and Yeh (SY) based methods provide acceptable accuracy in low-precision region of the Cumulative Distribution Function (*CDF*) (i.e., 0.01–0.99) and the Fenton–Wilkinson (FW) method offers high accuracy in the high-value region of the CDF (i.e., 0.9–0.9999). Both methods break down for high values of standard deviations. Ref [5] propose an alternative method based on Log Shifted Gamma (LSG) approximation to the sum of dependent lognormal RVs. LSG parameters estimation is based on moments computation using Schwartz and Yeh method. Although, LSG exhibits an acceptable accuracy, it does not provide good accuracy at the lower region.

In this paper, we propose a very highly accurate yet simple method to approximate the sum of correlated lognormal RVs based on Log Skew Normal distribution (LSN). LSN approximation has been proposed in [6] as a highly accurate approximation method for the sum of independent lognormal distributions, Furthermore a modified LSN approximation method is proposed in [7]. However, LSN parameters estimation relies on a time-consuming Monte Carlo simulation. The main contribution on this work is to provide a simple analytical method for LSN parameters estimation without the need for a time-consuming Monte Carlo simulation or curve fitting approximation. Our analytical fitting method is based on moments and tails slope matching for both distributions. This work can be seen as extension to the correlated case for our work done in [8].

The rest of the paper is organized as follows: In section 2, a brief description of the lognormal distribution and sum of correlated lognormal distributions is given. In section 3, we introduce the Log Skew Normal distribution and its parameters. In section 4, we use moments and tails slope matching method to estimate LSN distribution parameters. In section 5, we provide comparisons with well-known approximation methods (i.e. Schwartz and Yeh, Fenton–Wilkinson, LSG) based on simulation results.

The conclusion remarks are given in Section 6.

2. Sum of Correlated Lognormal RVs

Given *X*, a Gaussian RV with mean μ_X and variance σ_X^2, then $L=e^X$ is a lognormal RV with (PDF):

$$f_L(l,\mu_X,\sigma_X)=\begin{cases}\dfrac{1}{\sqrt{2\pi}l\sigma_X}\exp(-\dfrac{1}{2\sigma_X^2}[\ln(l)-\mu_X]^2) & l>0\\ 0 \quad otherwise & \end{cases} \qquad (1)$$

$$=\phi(\frac{\ln(l)-\mu_X}{\sigma_X})$$

Where $\phi(\mathrm{x})$ is the standard normal cumulative distribution function (*cdf).*

Usually *X* represents power variation measured in dB. Considering X_{dB} with mean μ_{dB} and variance σ_{dB}^2, the corresponding lognormal RV $L=e^{\zeta X_{dB}}=10^{\frac{X_{dB}}{10}}$ has the following pdf:

$$f_L(l,\mu_{dB},\sigma_{dB})=\begin{cases}\dfrac{1}{\sqrt{2\pi}l\sigma_{dB}}\exp(-\dfrac{1}{2\sigma_{dB}^2}[10\log(l)-\mu_{dB}]^2) & l>0\\ 0 \quad otherwise & \end{cases} \qquad (2)$$

Where $\mu_{dB} = \frac{\mu_X}{\xi}$ and $\xi = \frac{\ln(10)}{10}$

$\sigma_{dB} = \frac{\sigma_X}{\xi}$

The first two central moments of L may be written as:

$$m = e^{\mu} e^{\sigma^2/2}$$
$$D^2 = e^{2\mu} e^{\sigma^2} (e^{\sigma^2} - 1) \tag{3}$$

Correlated Lognormals sum distribution corresponds to the sum of dependent lognormal RVs, i.e.

$$\Lambda = \sum_{i=1}^{N} L_n = \sum_{i=1}^{N} e^{X_n} \tag{4}$$

We define $\bar{L} = (L_1, L_2 .. L_N)$ as a strictly positive random vector such that the vector $\bar{X} = (X_1, X_2 ... X_N)$ with $X_j = \log(L_j)$, $1 \leq j < N$ has an n-dimensional normal distribution with mean vector $\mu = (\mu_1, \mu_2 ... \mu_N)$ and covariance matrix M with $M(\mathrm{i,j}) = Cov(X_i, X_j)$, $1 \leq i < N, 1 \leq j < N$. $\bar{L}$ is called an n-dimensional log-normal vector with parameters $\vec{\mu}$ and M. $Cov(L_i, L_j)$ may be expressed as [9, eq. 44.35]:

$$Cov(L_i, L_j) = e^{\mu_i + \mu_j + \frac{1}{2}(\sigma_i^2 + \sigma_j^2)} (\mathrm{e}^{M(i,j)} - 1) \tag{5}$$

The first two central moments of Λ may be written as:

$$\mathrm{m} = \sum_{i=1}^{N} m_i = \sum_{i=1}^{N} e^{\mu_i} e^{\sigma_i^2/2} \tag{6}$$

$$\begin{aligned} D^2 &= \sum_{i=1, j=1}^{N} Cov(L_i, L_j) \\ &= \sum_{i=1, j=1}^{N} e^{\mu_i + \mu_j + \frac{1}{2}(\sigma_i^2 + \sigma_j^2)} (\mathrm{e}^{M(i,j)} - 1) \end{aligned} \tag{7}$$

3. LOG SKEW NORMAL DISTRIBUTION

The standard skew normal distribution was firstly introduced in [10] and was independently proposed and systematically investigated by Azzalini [11]. The random variable X is said to have a scalar $SN(\lambda, \varepsilon, \omega)$ distribution if its density is given by:

$$f_X(\mathrm{x}; \lambda, \varepsilon, \omega) = \frac{2}{\omega} \varphi(\frac{x - \varepsilon}{\omega}) \phi(\lambda \frac{x - \varepsilon}{\omega}) \tag{8}$$

Where $\varphi(\mathrm{x}) = \frac{\mathrm{e}^{-x^2/2}}{\sqrt{2\pi}}$, $\phi(\mathrm{x}) = \int_{-\infty}^{x} \varphi(\zeta) \, \mathrm{d}\zeta$

With λ is the shape parameter which determines the skewness, ε and ω represent the usual location and scale parameters and φ , ϕ denote, respectively, the *pdf* and the *cdf* of a standard Gaussian RV.

The CDF of the skew normal distribution can be easily derived as:

$$F_X(\mathrm{x};\lambda,\varepsilon,\omega)=\phi(\frac{x-\varepsilon}{\omega})-2\,\mathrm{T}(\frac{x-\varepsilon}{\omega},\lambda) \qquad (9)$$

Where function $\mathrm{T}(\mathrm{x},\lambda)$ is Owen's *T* function expressed as:

$$\mathrm{T}(\mathrm{x},\lambda)=\frac{1}{2\pi}\int_0^{\lambda}\frac{\exp\left\{-\frac{1}{2}\mathrm{x}^2(1+\mathrm{t}^2)\right\}}{(1+\mathrm{t}^2)}dt \qquad (10)$$

A fast and accurate calculation of Owen's T function is provided in [12].

Similar to the relation between normal and lognormal distributions, given a skew normal RV X then $L=e^{\xi X_{dB}}=10^{\frac{X_{dB}}{10}}$ is a log skew normal distribution. The cdf and pdf of *L* can be easily derived as:

$$f_L(\mathrm{l};\lambda,\varepsilon_{dB},\omega_{db})=\begin{Bmatrix}\frac{2}{\xi\omega_{db}l}\varphi(\frac{10\log(\mathrm{l})-\varepsilon_{dB}}{\omega_{db}})\phi(\lambda\frac{10\log(\mathrm{l})-\varepsilon_{dB}}{\omega_{db}}) & l>0\\ 0 \quad otherwise & \end{Bmatrix} \qquad (11)$$

$$F_L(\mathrm{l};\lambda,\varepsilon_{dB},\omega_{db})=\begin{Bmatrix}\phi(\frac{10\log(\mathrm{l})-\varepsilon_{dB}}{\omega_{db}})-2\,\mathrm{T}(\frac{10\log(\mathrm{l})-\varepsilon_{dB}}{\omega_{db}},\lambda) & l>0\\ 0 \quad otherwise & \end{Bmatrix} \qquad (12)$$

Where $\varepsilon_{dB}=\frac{\varepsilon}{\xi}$ and $\xi=\frac{\ln(10)}{10}$

$\omega_{dB}=\frac{\omega}{\xi}$

The Moment Generating Function (*MGF)* of the skew normal distribution may be written as [11]:

$$\begin{aligned}\mathrm{M}_X(\mathrm{t})&=\mathrm{E}\left[e^{tX}\right]\\&=2e^{t^2/2}\phi(\beta\,\mathrm{t}),\qquad \beta=\frac{\lambda}{\sqrt{1+\lambda^2}}\end{aligned} \qquad (13)$$

Thus the first two central moments of L are:

$$\zeta = 2e^{\varepsilon}e^{\omega^2/2}\phi(\beta\omega) \qquad (14)$$

$$\varpi^2 = 2e^{2\varepsilon}e^{\omega^2}(e^{\omega^2}\phi(2\beta\omega)-2\phi^2(\beta\omega))$$

4. VALIDITY OF LOGNORMAL ASSUMPTION FOR THE SUM OF LOGNORMAL RVS AT DISTRIBUTION TAILS

Several approximation methods for the sum of correlated lognormal RVs is based on the fact that this sum can be approximated, at least as a first order, by another lognormal distribution. On the one hand, Szyszkowicz and Yanikomeroglu [14] have published a limit theorem that states that the distribution of a sum of identically distributed equally and positively correlated lognormal RVs converges, *in distribution*, to a lognormal distribution as N becomes large. This limit theorem is extended in [15] to the sum of correlated lognormal RVs having a particular correlation structure.

On the other hand, some recent results [16, Theorem 1. and 3.] show that the sum of lognormal RVs exhibits a different behaviour at the upper and lower tails even in the case of identically distributed lognormal RVs. Although the lognormal distribution have a symmetric behaviours in both tails, this is not in contradiction with results proven in [14-15] since convergence is proved *in distribution*, i.e., convergence at every point x not in the *limit behaviour*.

This explain why some lognormal based methods provide a good accuracy only in the lower tail (e.g. Schwartz and Yeh), where some other methods provide an acceptable accuracy in the upper tail (e.g. Fenton–Wilkinson). This asymmetry of the behaviours of the sum of lognormal RVs at the lower and upper tail, motivates us to use the Log Skew Normal distribution as it represents the asymmetric version of lognormal distribution. So, we expect that LSN approximation provide the needed accuracy over the whole region including both tails of the sum of correlated lognormal RVs distribution.

5. LOG SKEW NORMAL PARAMETERS DERIVATION

5.1. Tails properties of sum of Correlated lognormal RVs

Let $\bar{L}$ be an N-dimensional log-normal vector with parameters μ and M. Let $B = M^{-1}$ the inverse of the covariance matrix.

To study tails behavior of sum of correlated lognormal RVs, it is convenient to work on lognormal probability scale [13], i.e., under the transformation G:

$$G : F(\mathrm{x}) \mapsto \tilde{F}(\mathrm{x}) = F(\phi^{-1}(F(\mathrm{e}^{x}))) \qquad (15)$$

We note that under this transformation, the lognormal distribution is mapped onto a linear equation.

We define B_i as row sum of B:

$$B_i = \sum_{k=1}^{N} B(i,k) \ , \quad 1 \le i \le N \qquad (16)$$

We let:

$$\tilde{N} \triangleq Card\{i = 1,..\mathrm{N};\ B_i \neq 0\}$$

$$\tilde{I} \triangleq \{i = 1,..N;\ B_i \neq 0\} \triangleq \{\tilde{k}(1), \tilde{k}(1)...\tilde{k}(\tilde{N})\}$$

We define $\tilde{\mu}$, $\tilde{M}$, $\tilde{B}$ and $\tilde{B}_i$ such that:

$$\tilde{\mu}(i) = \mu(\tilde{k}(i))$$

$$\tilde{M}(i,j) = M(\tilde{k}(i), \tilde{k}(j))$$

$$\tilde{B} = \tilde{M}^{-1}$$

$$\tilde{B}_i = \sum_{k=1}^{\tilde{N}} \tilde{B}(i,k)$$

Since variables L_i are exchangeable, we can assume for the covariance matrix B, with no loss of generality, that $\tilde{I} = \{1, 2, 3 \ldots \tilde{N}\}$ with $\tilde{N} \leq N$.

Let $w \in \Re^{\tilde{N}}$ such that:

$$w = \frac{\tilde{B}^{-1}1}{1^{\perp}\tilde{B}^{-1}1} \tag{17}$$

So that, we may write:

$$w_i = \frac{\tilde{A}_i}{\sum_{j=1}^{\tilde{N}} \tilde{A}_j} \quad j = 1, \ldots \tilde{N} \tag{18}$$

Now, we set $\tilde{w} \in \Re^{N}$ as

$$\tilde{w}_i = \begin{cases} w_i \ \mathit{if} \ i \leq \tilde{N} \\ 0 \ \ \mathit{Otherwise} \end{cases} \tag{19}$$

Assuming that for every $i \in \{1, 2, 3 \ldots N\} \setminus \tilde{I}$

$$(e^i - \tilde{w})^{\perp} B\tilde{w} \neq 0 \tag{20}$$

Where $e^i \in \Re^N$ satisfies $e^i_j = 1 \text{ if } i = j$ and $e^i_j = 0$ otherwise.

In [16, Theorem 3.], Gulisashvili and Tankov proved that the slope of the right tail of the SLN *cdf* on lognormal probability scale is equal to $1/\underset{i}{\mathrm{Max}}\{\tilde{B}(i,i)\}$ when assumption (20) is valid.

$$\lim_{x \to +\infty} \frac{\delta}{\delta x} \tilde{F}_{SCLN}(x) = \frac{1}{\underset{i}{\mathrm{Max}}\{\tilde{B}(i,i)\}} \tag{21}$$

Considering the left tail slope, they proved that the slope of the left tail of the SLN *cdf* on lognormal probability scale is equal to $\sqrt{\sum_{i=1}^{N} \tilde{B}_i}$ [16, Theorem 1.].

$$\lim_{x \to -\infty} \frac{\delta}{\delta x} \tilde{F}_{SCLN}(x) = \sqrt{\sum_{i=1}^{N} \tilde{B}_i} \tag{22}$$

In general, we can assume that $B_i \neq 0$ for $1 \leq i \leq N$, so that $N = \tilde{N}$ and tails slope can be expressed as:

$$\lim_{x \to +\infty} \frac{\delta}{\delta x} \tilde{F}_{SCLN}(x) = \frac{1}{\max\limits_{i}\{B(i,i)\}} \tag{23}$$

$$\lim_{x \to -\infty} \frac{\delta}{\delta x} \tilde{F}_{SCLN}(x) = \sqrt{\sum_{i=1}^{N} B_i} \tag{24}$$

5.2. Tail properties of Skew Log Normal

In [17], it has been showed that the rate of decay of the right tail probability of a skew normal distribution is equal to that of a normal variate, while the left tail probability decays to zero faster. This result has been confirmed in [18]. Based on that, it is easy to show that the rate of decay of the right tail probability of a log skew normal distribution is equal to that of a lognormal variate. Under the transformation G, skew lognormal distribution has a linear asymptote in the upper limit with slope

$$\lim_{x \to +\infty} \frac{\delta}{\delta x} \widetilde{F}_{LSN}(x) = \frac{1}{w} \qquad (25)$$

In the lower limit, it has no linear asymptote, but does have a limiting slope

$$\lim_{x \to -\infty} \frac{\delta}{\delta x} \widetilde{F}_{LSN}(x) = \frac{\sqrt{1+\lambda^2}}{w} \qquad (26)$$

These results are proved in [8, Appendix A]. Therefore, it will be possible to match the tail slopes of the LSN with those of the sum of correlated lognormal RVs distribution in order to find LSN optimal parameters.

5.3. Moments and lower tail slope matching

In order to derive log skew normal optimal parameters, we proceed by matching the two central moments of both distributions. Furthermore, use we lower slope tail match. By simulation, we point out that upper slope tail match is valid only for the sum of high number of lognormals RVs. However we still need it to find an optimal starting guess solution to the generated nonlinear equation. Thus we define λ_{opt} as solution the following nonlinear equation:

$$\frac{\sum_{i=1}^{N} e^{2\mu_i} e^{\sigma_i^2} (e^{\sigma_i^2} - 1)}{(\sum_{i=1}^{N} e^{\mu_i} e^{\sigma_i^2/2})^2} = e^{\frac{1+\lambda^2}{\sqrt{\sum_{i=1}^{N} \tilde{B}_i}}} \frac{\phi(2\frac{\lambda}{\sqrt{\sum_{i=1}^{N} \tilde{B}_i}})}{2\phi^2(\frac{\lambda}{\sqrt{\sum_{i=1}^{N} \tilde{B}_i}})} - 1 \qquad (27)$$

Such nonlinear equation can be solved using different mathematical utility (e.g. fsolve in matlab). Using upper slope tail match we derive a starting solution guess λ_0 to (23) in order to converge rapidly (only few iterations are needed):

$$\lambda_0 = \sqrt{\left[\underset{i}{\mathrm{Max}} \{\tilde{B}(i,i)\}^2 \sum_{i-1}^{N} \tilde{B}_i) \right] - 1} \qquad (28)$$

Optimal location and scale parameters, ε_{opt}, ω_{opt} are obtained according to λ_{opt} as.

$$\begin{cases} \omega_{opt} = \sqrt{\dfrac{1+\lambda_{opt}^2}{\sum_{i=1}^{N} \overline{B}_i}} \\ \varepsilon_{opt} = \ln\left(\sum_{i=1}^{N} e^{\mu_i} e^{\sigma_i^2/2}\right) - \dfrac{\omega_{opt}^2}{2} - \ln\left(\phi\left(\dfrac{\lambda_{opt}}{\sqrt{\sum_{i=1}^{N} \overline{B}_i}}\right)\right) \end{cases} \tag{29}$$

6. Simulation Results

In this section, we propose to validate our approximation method and compare it with other widely used approximation methods. The comparison of the Complementary Cumulative Distribution Function (*CDF*) of the sum of *N* ($N=2,8,20$) correlated lognormal RVs $P[\Lambda > \lambda]$ of Monte Carlo simulations with LSN approximation and lognormal based methods for low value of standard deviation $\sigma = 3\,dB$ with $\mu = 0dB$ and $\rho = 0.7$ are shown in Fig.1. Although these methods are known by its accuracy in the lower range of standard deviation, it obvious that LSN approximation outperforms them. We note that fluctuation at the tail of sum of lognormal RVs distribution is due to Monte Carlo simulation, since we consider 10^7 samples at every turn. We can see that LSN approximation results are identical to Monte Carlo simulation results.

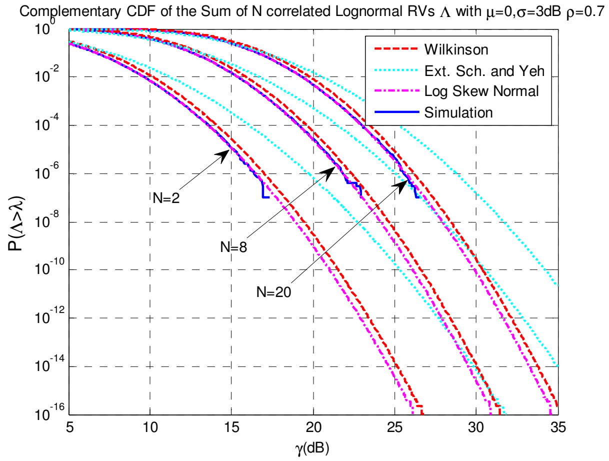

Figure 1. Complementary CDF of the sum of N correlated lognormal RVs with $\mu = 0\,dB$, $\sigma = 3\,dB$ and $\rho = 0.7$

Fig.2 and Fig.3 show the complementary *CDF* of the sum of *N* correlated lognormal RVs for higher values of standard deviation $\sigma = 6,\ 9\,dB$ and two values of correlation coefficients $\rho = 0.9,\ 0.3$.We consider the Log Shifted Gamma approximation for comparison purposes. We consider the Log Shifted Gamma approximation for comparison purposes. We can see that LSN approximation highly outperforms other methods especially at the *CDF* right tail $(1 - CDF < 10^{-2})$. Furthermore, LSN approximation give exact Monte Carlo simulation results even for low range of the complementary CDF of the sum of correlated lognormal RVs $(1 - CDF < 10^{-6})$.

To further verify the accuracy of our method in the left tail as well as the right tail of *CDF* of the sum of correlated lognormal RVs, Fig. 4 and Fig. 5 show respectively the *CDF* $P[\Lambda < \lambda]$ of the sum of 6 correlated lognormal RVs with $\mu = 0dB$ $\rho = 0.7$

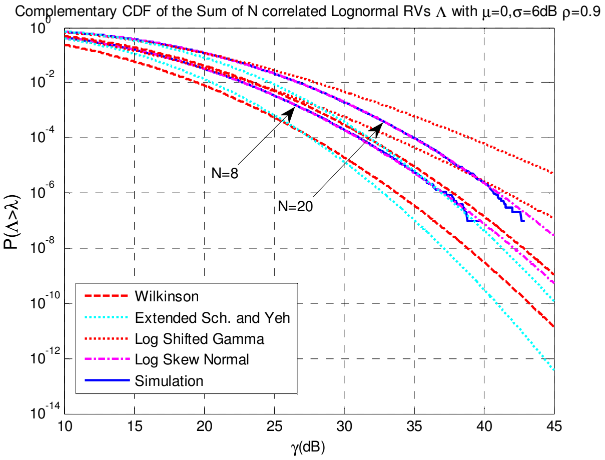

Figure 2. Complementary CDF of the sum of N correlated lognormal RVs with $\mu = 0\,dB$, $\sigma = 6\,dB$ and $\rho = 0.9$

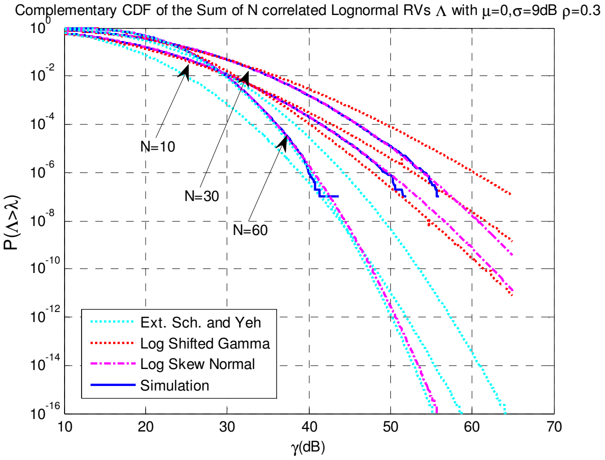

Figure 3. Complementary CDF of the sum of N correlated lognormal RVs with $\mu = 0\,dB$ $\sigma = 9\,dB$ $\rho = 0.3$

and the complementary *CDF* of the sum of 20 correlated lognormal RVs with $\mu = 0dB$ $\rho = 0.3$ for different standard deviation values. It is obvious that LSN approximation provide exact Monte Carlo simulation results at the left tail as well as the right tail. We notice that accuracy does not depend on standard deviation values as LSN performs well for the highest values of standard deviation of the shadowing.

To point out the effect of correlation coefficient value on the accuracy of the proposed approximation, we consider the *CDF* of the sum of 12 correlated lognormal RVs for different combinations of standard deviation and correlation coefficient values with $\mu = 0dB$ (Fig. 6). One can see that LSN approximation efficiency does not depend on correlation coefficient or standard deviation values. So that, LSN approximation provides same results as Monte Carlo simulations for all cases.

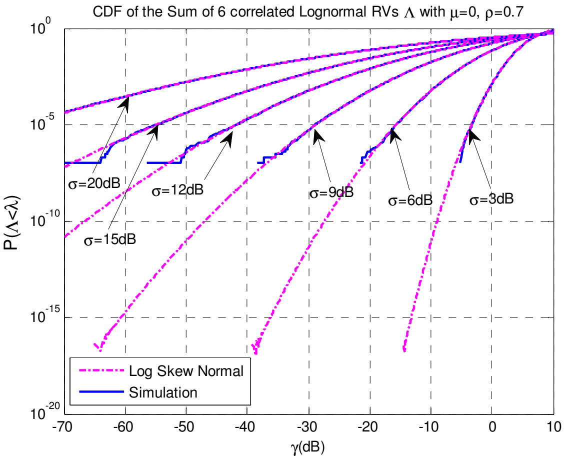

Figure 4. CDF of the sum of 6 correlated lognormal RVs with $\mu = 0\,dB$, $\rho = 0.7$

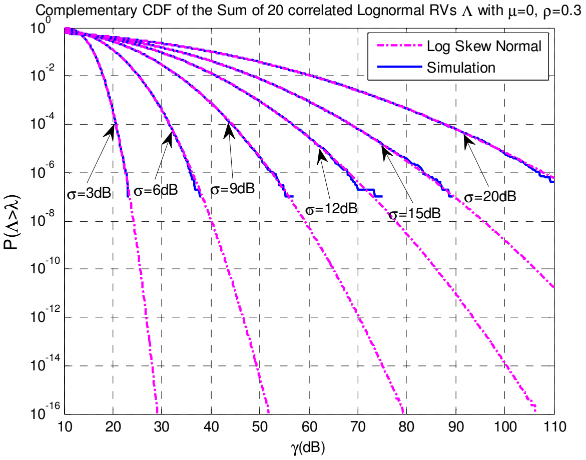

Figure 5. Complementary CDF of the sum of 20 correlated lognormal RVs with $\mu = 0\,dB$, $\rho = 0.3$

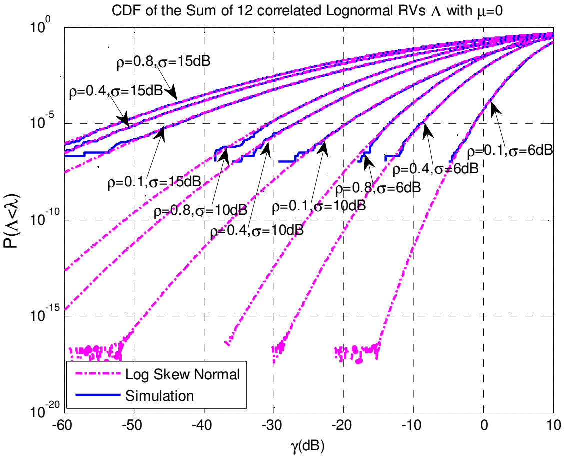

Figure 6. CDF of the sum of 12 correlated lognormal RVs with different correlation coefficients ρ,
$\mu = 0\,dB$

7. CONCLUSIONS

In this paper, we proposed to use the Log Skew Normal distribution in order to approximate the sum of correlated lognormal RV distribution. Our fitting method uses moment and tails slope matching technique to derive LSN distribution parameters. LSN provides identical results to Monte Carlo simulations results and then outperforms other methods for all cases. Such approximation can be effectively used for accurate and fast computation of interference and outage probabilities in cellular networks.

REFERENCES

[1] A. Safak, “Statistical analysis of the power sum of multiple correlated log-normal components”, IEEE Trans. Veh. Tech., vol. 42, pp. 58–61, Feb. 1993.

[2] S.Schwartz and Y.S. Yeh, “On the distribution function and moments of power sums with log-normal components”, Bell System Tech. J., Vol. 61, pp. 1441–1462, Sept. 1982.

[3] M. Pratesi , F. Santucci , F. Graziosi and M. Ruggieri "Outage analysis in mobile radio systems with generically correlated lognormal interferers", IEEE Trans. Commun., vol. 48, no. 3, pp.381 -385 2000.

[4] A. Safak and M. Safak "Moments of the sum of correlated log-normal random variables", Proc. IEEE 44th Vehicular Technology Conf., vol. 1, pp.140 -144 1994.

[5] C. L. Joshua Lam,Tho Le-Ngoc " Outage Probability with Correlated Lognormal Interferers using Log Shifted Gamma Approximation” , Wireless Personal Communications, Volume 41, Issue 2, pp 179-192, April 2007.

[6] Z. Wu, X. Li, R. Husnay, V. Chakravarthy, B. Wang, and Z. Wu. A novel highly accurate log skew normal approximation method to lognormal sum distributions. In Proc. of IEEE WCNC 2009.

[7] X. Li, Z. Wu, V. D. Chakravarthy, and Z. Wu, "A low complexity approximation to lognormal sum distributions via transformed log skew normal distribution," IEEE Transactions on Vehicular Technology, vol. 60, pp. 4040-4045, Oct. 2011.

[8] M. Benhcine, R. Bouallegue, “Fitting the Log Skew Normal to the Sum of Independent Lognormals Distribution”, accepted in the sixth International Conference on Networks and Communications (NetCom-2014) .

[9] Samuel Kotz, N. Balakrishnan, Norman L. Johnson "Continuous Multivariate Distributions", Volume 1, Second Edition, John Wiley & Sons, avril 2004.

[10] O’Hagan A. and Leonard TBayes estimation subject to uncertainty about parameter constraints, Biometrika, 63, 201–202, 1976.

[11] Azzalini A, A class of distributions which includes the normal ones, Scand. J. Statist., 12, 171–178, 1985.

[12] M. Patefield, “Fast and accurate calculation of Owen’s t function,” J. Statist. Softw., vol. 5, no. 5, pp. 1–25, 2000.

[13] N. C. Beaulieu, Q. Xie, “Minimax Approximation to Lognormal Sum Distributions”, IEEE VTC Spring, Vol. 2, pp. 1061-1065, April 2003.

[14] S. S. Szyszkowicz and H. Yanikomeroglu "Limit theorem on the sum of identically distributed equally and positively correlated joint lognormals", IEEE Trans. Commun., vol. 57, no. 12, pp.3538 -3542 2009

[15] N. C. Beaulieu, "An extended limit theorem for correlated lognormal sums," IEEE Trans. Commun., vol. 60, no. 1, pp. 23-26, Jan. 2012

[16] Archil Gulisashvili, Peter Tankov, “Tail behavior of sums and differences of log-normal random variables”, ARXIV 09/2013.

[17] Antonella Capitanio, “On the approximation of the tail probability of the scalar skew-normal distribution”, in METRON (2010).

[18] W. Hürlimann, “Tail Approximation of the Skew-Normal by the Skew-Normal Laplace: Application to Owen’s T Function and the Bivariate Normal Distribution”, Journal of Statistical and Econometric Methods, vol. 2, no.1, 2013, 1-12, Scienpress Ltd, 2013.

AUTHORS

Marwane Ben Hcine was born in Kébili, Tunisia, on January 02, 1985. He graduated in Telecommunications Engineering, from The Tunisian Polytechnic School (TPS), July 2008. In June 2010, he received the master's degree of research in communication systems of the Higher School of Communication of Tunisia (Sup'Com). Currently he is a Ph.D. student at the Higher School of Communication of Tunisia. His research interests are network design and dimensioning for LTE and beyond Technologies.

Pr. Ridha BOUALLEGUE was born in Tunis, Tunisia. He received the M.S degree in Telecommunications in 1990, the Ph.D. degree in telecommunications in 1994, and the HDR degree in Telecommunications in 2003, all from National School of engineering of Tunis (ENIT), Tunisia. Director and founder of National Engineering School of Sousse in 2005. Director of the School of Technology and Computer Science in 2010. Currently, Prof. Ridha Bouallegue is the director of Innovation of COMmunicant and COoperative Mobiles Laboratory, INNOV'COM Sup'COM, Higher School of Communication. His current research interests include mobile and cooperative communications, Access technique, intelligent signal processing, CDMA, MIMO, OFDM and UWB systems.

FITTING THE LOG SKEW NORMAL TO THE SUM OF INDEPENDENT LOGNORMALS DISTRIBUTION

Marwane Ben Hcine[1] and Ridha Bouallegue[2]

[1,2]Innovation of Communicant and Cooperative Mobiles Laboratory,
INNOV'COM
Sup'Com, Higher School of Communication
Univesity of Carthage
Ariana, Tunisia
[1]marwen.benhcine@supcom.tn
[2]ridha.bouallegue@supcom.rnu.tn

ABSTRACT

Sums of lognormal random variables (RVs) occur in many important problems in wireless communications especially in interferences calculation. Several methods have been proposed to approximate the lognormal sum distribution. Most of them requires lengthy Monte Carlo simulations, or advanced slowly converging numerical integrations for curve fitting and parameters estimation. Recently, it has been shown that the log skew normal distribution can offer a tight approximation to the lognormal sum distributed RVs. We propose a simple and accurate method for fitting the log skew normal distribution to lognormal sum distribution. We use moments and tails slope matching technique to find optimal log skew normal distribution parameters. We compare our method with those in literature in terms of complexity and accuracy. We conclude that our method has same accuracy than other methods but more simple. To further validate our approach, we provide an example for outage probability calculation in lognormal shadowing environment based on log skew normal approximation.

KEYWORDS

Lognormal sum, log skew normal, moment matching, asymptotic approximation, outage probability, shadowing environment.

1. INTRODUCTION

The sum of Lognormals (SLN) arises in many wireless communications problems, in particular in the analyses the total power received from several interfering sources. With recent advances in telecommunication systems (Wimax, LTE), it is highly desired to compute the interferences from others sources to estimate signal quality (*Qos*). Such interference can be modelled as sum of lognormal distribution. Several approaches were proposed to obtain the resulting sum of lognormal distributions. Approximation methods can be categorized into three main classes: lognormal approximations [2-6], numerical methods [7-10] and closed form approximations methods [11-15]. Lognormal approximations methods are based on the fact that lognormal sum can be modelled by another lognormal distribution; these methods are simple yet not accurate particularly in upper and lower regions. Numerical methods are accurate but it need extensive

Natarajan Meghanathan et al. (Eds) : NeTCoM, CSIT, GRAPH-HOC, SPTM - 2014
pp. 53–67, 2014. © CS & IT-CSCP 2014 DOI : 10.5121/csit.2014.41305

numerical integrations. Closed form approximations methods are generally not accurate at some regions .i.e. does not catch the whole body of the SLN distribution.

Furthermore, the main drawback of almost all of these methods is the need for an extensive Monte Carlo simulation in order to find optimal parameters of the proposed distribution. Except from [2], [12] and [16], all closed form approximations methods need a prior knowledge of the SLN *cdf* for curve fitting and parameters estimation. In [2], a simple lognormal approximation of the SLN is proposed. Using Moment Matching Method (MOM), distribution parameters could be estimated yet this approximation is not accurate in upper and lower regions of the *cdf.* In [12], a Type IV Pearson Approximation method is proposed. For parameters estimation, they used moment matching in the logarithm domain which is handy to implement. This method has good accuracy in a wide region, but it did not offer good approximations all the cases (i.e. large spread powerσ_i *).* In [16], a Modified–Power–Lognormal (MPLN) approximation method is used. Distribution parameters are estimated using some properties of the upper and lower tails of the SLN distribution [17]. It is easy to implement but it did not offer a tight approximation of the SLN distribution in all the cases (different/lower spread powerσ_i *).*

Recently, it has been shown that Log Skew Normal distribution (LSKN) could approximate the SLN distribution over a wide range. In [18] Wu and Li showed that Log Skew Normal provide a very tight approximation to the SLN distribution. In [19], they proposed a transformed LSN to control the skewness of samples in the transform logarithm domain. However, to estimate distribution parameters, they used in both approximations the moment matching method in the logarithm domain, which require prior knowledge of the SLN distribution.

In this paper, we propose a simple method based on moment matching method (in linear domain) and tails slope match of both SLN and LSKN distributions. Given a set of pairs $\{(\mu_{i,}\sigma_i^2)\}_{i=1}^N$, the goal of our work is to estimate optimal parameters for log skew normal distribution. We derive the expression of the first two central moments of SLN and LSKN distributions. Using moments and tails slope matching, we provide an accurate approximation to optimal parameters values for LSKN distribution. We validate our approach by an example for outage probability calculation in lognormal shadowing environment.

The rest of the paper is organized as follows: In section 2, a brief description of the lognormal and sum of lognormal distribution is given. Moment and tails properties of SLN distribution are investigated. In section 3, we introduce the log skew normal distribution and its parameters. Moment and tails properties of the LSKN distribution are studied, then, we use MoM and tails slope matching to estimate distribution parameters. In section 4, we compare our method with moment matching method in logarithm domain [18-19]. Also, we provides comparisons with some existing approximation method (Lognormal approximation and Modified Power Lognormal) with the simulation results on the cumulative distribution function *(CDF)* of sum of *N* lognormal random variables in different conditions. In section 5, we give an example for outage probability calculation in lognormal shadowing environment based on our method.
The conclusion remarks are given in Section 6.

2. LOGNORMAL SUM DISTRIBUTION

2.1. Lognormal PDF

Let X be a RV with a normal distribution then $L = e^X$ has a lognormal distribution. Likewise, if L is lognormally distributed, then ln(L) is normally distributed. Given X, a Gaussian RV with mean μ_X and varianceσ_X^2 , $L = e^X$ is a lognormal RV with (PDF):

$$f_L(l,\mu_X,\sigma_X)=\begin{cases}\dfrac{1}{\sqrt{2\pi}l\sigma_X}\exp(-\dfrac{1}{2\sigma_X^2}\left[\ln(l)-\mu_X\right]^2) & l>0\\ 0 \quad \mathit{otherwise} & \end{cases} \qquad (1)$$

$$=\phi(\frac{\ln(l)-\mu_X}{\sigma_X})$$

Where $\phi(x)$ is the standard normal cumulative distribution function (*cdf)*. In communications, *X* usually represents power variation measured in dB. Considering X_{dB} with mean μ_{dB} and variance σ_{dB}^2, the corresponding lognormal RV $L=e^{\xi X_{dB}}=10^{\frac{X_{dB}}{10}}$ has the following pdf:

$$f_L(l,\mu_{dB},\sigma_{dB})=\begin{cases}\dfrac{1}{\sqrt{2\pi}l\sigma_{dB}}\exp(-\dfrac{1}{2\sigma_{dB}^2}\left[10\log(l)-\mu_{dB}\right]^2) & l>0\\ 0 \quad \mathit{otherwise} & \end{cases} \qquad (2)$$

Where $\xi=\dfrac{\ln(10)}{10}$

and $\mu_X=\xi\mu_{dB}$

$\sigma_X^2=\xi^2\sigma_{dB}^2$

Lognormal sum distribution corresponds to the sum of independent lognormal RVs, i.e.

$$\Lambda=\sum_{i=1}^{N}L_n=\sum_{i=1}^{N}e^{X_n} \qquad (3)$$

2.2. Lognormal sum moments computation

It is well known that lognormal sum distribution function has no closed form, but it is possible to derive its moment. Let L_i be a lognormal RV with mean m_i and variance D_i^2. Let μ_i, σ_i^2 be the mean and the variance of the corresponding normal distribution.

To compute m_i, D_i^2, the *p*th moment $\alpha_{i,p}$, about the origin is first calculated for a lognormal distribution :

$$\alpha_{i,p}=\int_0^{+\infty}t^p\frac{1}{\sqrt{2\pi}}e^{-(\ln(t)-\mu_i)^2/2\sigma_i^2}dt \qquad (4)$$

With the substitution:

$$z=\frac{\ln(t)-\mu_i}{\sigma_i}, \quad \frac{dz}{dt}=\frac{dt}{t\sigma_i}, \quad t=e^{\sigma_i z+\mu_i}$$

The *p*th moment $\alpha_{i,p}$ of RV L_i is:

$$\alpha_{i,p}=e^{\mu_i p}\int_{-\infty}^{+\infty}e^{\sigma_i pz}\frac{1}{\sqrt{2\pi}}e^{-z^2/2}dz \qquad (5)$$

With $\sigma_i p=iw$, the integral reduces to the characteristic function of the standard normal distribution, which has the value $e^{-w^2/2}$, so that:

$$\alpha_{i,p}=e^{\mu_i p}e^{\sigma_i^2 p^2/2} \qquad (6)$$

Then, we get

$$m_i = e^{\mu_i} e^{\sigma_i^2/2} \qquad (7)$$

$$D_i^2 = \alpha_{i,2} - \alpha_{i,1}^2 = e^{2\mu_i} e^{\sigma_i^2} (e^{\sigma_i^2} - 1) \qquad (8)$$

Based on lognormal moment's computation, we derive the first two central moment of the sum of lognormal distribution:

$$\mathrm{m} = \sum_{i=1}^{N} m_i = \sum_{i=1}^{N} e^{\mu_i} e^{\sigma_i^2/2} \qquad (9)$$

$$D^2 = \sum_{i=1}^{N} D_i^2 = \sum_{i=1}^{N} e^{2\mu_i} e^{\sigma_i^2} (e^{\sigma_i^2} - 1) \qquad (10)$$

2.3. Tails properties of Lognormals sum

SLN distribution has linear asymptotes with simple closed–form expressions in both tails. To study tails behaviour of lognormal sum, it is convenient to work on lognormal probability scale [6], i.e., under the transformation G:

$$G : F(\mathrm{x}) \mapsto \widetilde{F}(\mathrm{x}) = \mathrm{F}(\phi^{-1}(\mathrm{F}(\mathrm{e}^{x}))) \qquad (11)$$

Under this transformation, the lognormal distribution is mapped onto a linear equation. It has been shown in [20] that the slope of the right tail of the SLN *cdf* on lognormal probability scale is equal to $1/\max_i\{\sigma_i\}$.

$$\lim_{x \to +\infty} \frac{\delta}{\delta x} \widetilde{F}_{SLN}(x) = \frac{1}{\max_i\{\sigma_i\}} \qquad (12)$$

In [21] Szyszkowicz and Yanikomeroglu argued that the slope of the left tail of the SLN *cdf* on lognormal probability scale is equal to $\sqrt{\sum_{i=1}^{N} \sigma_i^{-2}}$. A result which has been proved formally by Gulisashvili and Tankov in [22].

$$\lim_{x \to -\infty} \frac{\delta}{\delta x} \widetilde{F}_{SLN}(x) = \sqrt{\sum_{i=1}^{N} \sigma_i^{-2}} \qquad (13)$$

3. Log Skew Normal Distribution

3.1. Log Skew Normal PDF

The standard skew normal distribution appeared firstly in [26] and was independently proposed and systematically investigated by Azzalini [27]. The random variable X is said to have a scalar $SN(\lambda, \varepsilon, \omega)$ distribution if its density is given by:

$$f_X(\mathrm{x}; \lambda, \varepsilon, \omega) = \frac{2}{\omega} \varphi\left(\frac{x-\varepsilon}{\omega}\right) \phi\left(\lambda \frac{x-\varepsilon}{\omega}\right) \qquad (14)$$

Where $\varphi(\mathrm{x}) = \frac{\mathrm{e}^{-x^2/2}}{\sqrt{2\pi}}$, $\phi(\mathrm{x}) = \int_{-\infty}^{x} \varphi(\zeta)\, \mathrm{d}\zeta$

With λ is the shape parameter which determines the skewness, ε and ω represent the usual location and scale parameters and φ , ϕ denote, respectively, the *pdf* and the *cdf* of a standard Gaussian RV.

The cdf of the skew normal distribution can be easily derived as:

$$F_X(\mathrm{x};\lambda,\varepsilon,\omega)=\phi(\frac{x-\varepsilon}{\omega})-2\,\mathrm{T}(\frac{x-\varepsilon}{\omega},\lambda) \tag{15}$$

Where function $\mathrm{T(x,}\lambda)$ is Owen's *T* function expressed as:

$$\mathrm{T(x,}\lambda)=\frac{1}{2\pi}\int_0^{\lambda}\frac{\exp\left\{-\frac{1}{2}\mathrm{x}^2(1+\mathrm{t}^2)\right\}}{(1+\mathrm{t}^2)}dt \tag{16}$$

Similar to the relation between normal and lognormal distributions, given a skew normal RV X then $L=e^{\xi X}=10^{\frac{X}{10}}$ is a log skew normal distribution. The cdf and pdf of *L* can be easily derived as:

$$f_L(\mathrm{l};\lambda,\varepsilon,\omega)=\begin{Bmatrix}\frac{2}{\omega l}\varphi(\frac{\ln(\mathrm{l})-\varepsilon}{\omega})\phi(\lambda\frac{\ln(\mathrm{l})-\varepsilon}{\omega}) & l>0\\ 0 \quad otherwise & \end{Bmatrix} \tag{17}$$

$$F_L(\mathrm{l};\lambda,\varepsilon,\omega)=\begin{Bmatrix}\phi(\frac{\ln(\mathrm{l})-\varepsilon}{\omega})-2\mathrm{T}(\frac{\ln(\mathrm{l})-\varepsilon}{\omega},\lambda) & l>0\\ 0 \quad otherwise & \end{Bmatrix} \tag{18}$$

3.2. Log Skew Normal moments computation

In [18], computation of log skew normal moments is done in logarithm domain, then parameters λ,ε and ω are derived by matching the moment in logarithm domain which require Monte Carlo simulation. In this section we propose to derive the expression of moments of log skew normal distribution (in linear domain), then we can use the moment matching in linear domain to find optimal distribution parameters.

Let L be a log skew normal RV with mean ξ and variance ϖ^2, ε , ω^2 mean and variance of the corresponding skew normal distribution.
To compute ξ,ϖ^2, the *p*th moment α_p, about the origin is first calculated for a log skew normal distribution :

$$\alpha_p=\int_0^{+\infty}t^p\frac{2}{\omega t}\varphi(\frac{\ln(\mathrm{t})-\varepsilon}{\omega})\phi(\lambda\frac{\ln(\mathrm{t})-\varepsilon}{\omega})dt \tag{19}$$

Using same variable substitution as in (4):

$$z=\frac{\ln(\mathrm{t})-\varepsilon}{\omega}\ ,\qquad dz=\frac{dt}{t\omega},\qquad t=e^{\omega z+\varepsilon}$$

The *p*th moment α_p of RV L is:

$$\begin{aligned}\alpha_p &= 2e^{\varepsilon p}\int_{-\infty}^{+\infty} e^{\omega pz}\varphi(\mathrm{z})\phi(\lambda z)\ dz \\ &= e^{\varepsilon p}\,\mathrm{M}_X(p\omega)\end{aligned} \tag{20}$$

In [27], Azzalini showed that the *MGF* of the skew normal distribution is:

$$\begin{aligned}\mathrm{M}_X(\mathrm{t}) &= \mathrm{E}\left[e^{tX}\right] \\ &= 2e^{t^2/2}\phi(\beta\,\mathrm{t}), \qquad \beta = \frac{\lambda}{\sqrt{1+\lambda^2}}\end{aligned} \tag{21}$$

Then the pth moment α_p can be expressed as:

$$\begin{aligned}\alpha_p &= e^{\varepsilon p}\,\mathrm{M}_X(p\omega) \\ &= 2e^{\varepsilon p}e^{\omega^2 p^2/2}\phi(\beta\omega p), \qquad \beta = \frac{\lambda}{\sqrt{1+\lambda^2}}\end{aligned} \tag{22}$$

Then

$$\xi = 2e^{\varepsilon}e^{\omega^2/2}\phi(\beta\omega) \tag{23}$$

$$\varpi^2 = 2e^{2\varepsilon}e^{\omega^2}(e^{\omega^2}\phi(2\beta\omega) - 2\phi^2(\beta\omega)) \tag{24}$$

3.3. Tail properties of Skew Log Normal

In [21] Szyszkowicz and Yanikomeroglu defined the concept of *best lognormal fit* to a tail i.e. that the approximating distribution function have a similar behavior to lognormal sum at a given tail. It is possible to show that LSKN has a best lognormal fit at both tails (see Appendix A). In [23] Capitanio showed that the rate of decay of the right tail probability of a skew normal distribution is equal to that of a normal variate, while the left tail probability decays to zero faster. This result has been confirmed by Hürlimann in [24]. Based on that, it is easy to show that the rate of decay of the right tail probability of a log skew normal distribution is equal to that of a lognormal variate.

Under the transformation G, skew lognormal distribution has a linear asymptote in the upper limit with slope

$$\lim_{x\to+\infty}\frac{\delta}{\delta x}\tilde{F}_{LSKN}(x) = \frac{1}{w} \tag{25}$$

In the lower limit, it has no linear asymptote, but does have a limiting slope

$$\lim_{x\to-\infty}\frac{\delta}{\delta x}\tilde{F}_{LSKN}(x) = \frac{\sqrt{1+\lambda^2}}{w} \tag{26}$$

These results are proved in Appendix A. Therefore, it will be possible to match the tail slopes of the LSKN with those of the SLN distribution in order to find LSKN optimal parameters.

3.4. Moments and lower tail slope matching

It is possible to extend moment matching method in order to include the third and fourth central moment; however by simulation it seems that higher moments introduce errors to computed parameters. Also upper slope tail match is valid only for the sum of high number of lognormal

RVs. In order to derive log skew normal optimal parameters, on consider only the first two central moment and lower slope tail match. We define λ_{opt} as solution the following nonlinear equation:

$$\frac{\sum_{i=1}^{N} e^{2\mu_i} e^{\sigma_i^2} (e^{\sigma_i^2} - 1)}{(\sum_{i=1}^{N} e^{\mu_i} e^{\sigma_i^2/2})^2} = e^{\frac{1+\lambda^2}{\sum_{i=1}^{N} \sigma_i^{-2}}} \frac{\phi(2\frac{\lambda}{\sqrt{\sum_{i=1}^{N} \sigma_i^{-2}}})}{2\phi^2(\frac{\lambda}{\sqrt{\sum_{i=1}^{N} \sigma_i^{-2}}})} - 1 \qquad (27)$$

Moments and lower tail slope matching leads us to a nonlinear equation which can be solved using different mathematical utility such as “fsolve” in Matlab. Such nonlinear equation need a starting solution guess to converge rapidly, we propose to use upper tail slope match for optimal starting guess solution:

$$\lambda_0 = \sqrt{\max_i (\sigma_i)^2 \sum_{i=1}^{N} \sigma_i^{-2} - 1} \qquad (28)$$

Optimal location and scale parameters $\varepsilon_{opt}, \omega_{opt}$ are obtained according to λ_{opt}.

$$\begin{cases} \omega_{opt} = \sqrt{\frac{1+\lambda_{opt}^2}{\sqrt{\sum_{i=1}^{N} \sigma_i^{-2}}}} \\ \varepsilon_{opt} = \ln(\sum_{i=1}^{N} e^{\mu_i} e^{\sigma_i^2/2}) - \frac{\omega_{opt}^2}{2} - \ln(\phi(\frac{\lambda_{opt}}{\sqrt{\sum_{i=1}^{N} \sigma_i^{-2}}})) \end{cases} \qquad (29)$$

4. SIMULATION RESULTS

In this section, we examine the results of the proposed matching method and compare with other priori methods (lognormal approximation, MPLN approximation) in some cases. Monte Carlo simulation results are used as reference.

Table I. compares calculated values of LSKN parameters for different case of sum of lognormal RVs using proposed method and Monte Carlo simulation. It is obvious that our fitting method performs well especially in case of low value of standard deviation.

Fig. 1 and Fig. 2 show the results for the cases of the sum of 20 lognormal RVs with mean 0dB and standard deviation 3dB and 6dB. The CDFs are plotted in lognormal probability scale [6]. Simulation results show that the accuracy of our approximation get better as the number of lognormal distributions increase. We can see that LSKN approximation offers accuracy over the entire body of the distribution for both cases.

Table 1.LSKN parameters for different cases of sum of Lognormals

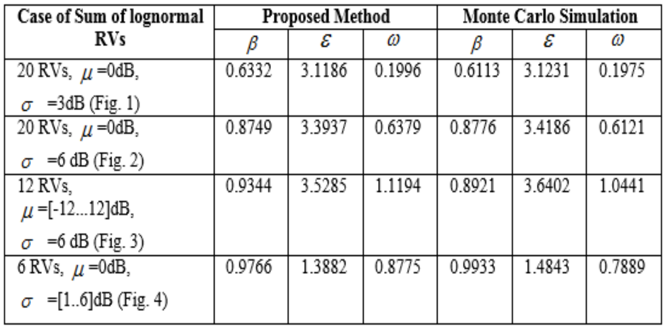

Case of Sum of lognormal RVs	Proposed Method			Monte Carlo Simulation		
	β	ε	ω	β	ε	ω
20 RVs, μ =0dB, σ =3dB (Fig. 1)	0.6332	3.1186	0.1996	0.6113	3.1231	0.1975
20 RVs, μ =0dB, σ =6 dB (Fig. 2)	0.8749	3.3937	0.6379	0.8776	3.4186	0.6121
12 RVs, μ =[-12...12]dB, σ =6 dB (Fig. 3)	0.9344	3.5285	1.1194	0.8921	3.6402	1.0441
6 RVs, μ =0dB, σ =[1..6]dB (Fig. 4)	0.9766	1.3882	0.8775	0.9933	1.4843	0.7889

In Fig. 3, we consider the sum of 12 lognormal RVs having the same standard deviation of 3dB, but with different means. It is clear that LSN approximation catch the entire body of SLN distribution. In this case, both LSKN and MPLN provides a tight approximation to SLN distribution. However LSKN approximation outperform MLPN approximation in lower region. Since interferences modeling belongs to this case (i.e. same standard deviation with different means), it is important to point out that log skew normal distribution outperforms other methods in this case.

Fig. 4 show the case of the sum of 6 lognormal RVs having the same mean 0dB but with different standard deviations. We can see that Fenton-Wilkinson approximation method can only fit a part of the entire sum of distribution, while the MPLN offers accuracy on the left part of the SLN distribution. However, it is obvious that LSKN method provides a tight approximation to the SLN distribution except a small part of the right tail.

It is worthy to note that in all cases, log skew normal distribution provide a very tight approximation to SLN distribution in the region of CDF less than 0.999.

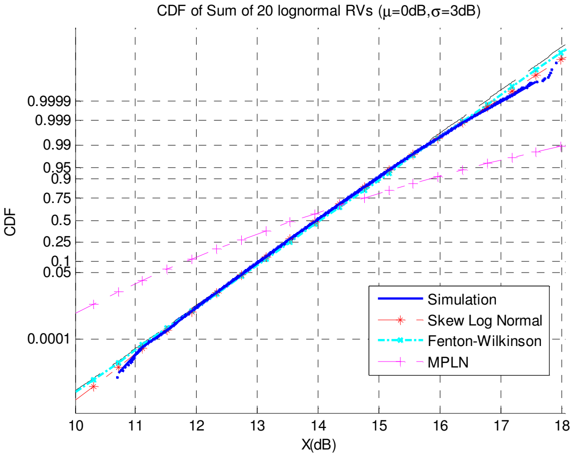

Figure 1. CDF of a sum of 20 i.i.d. lognormal RVs with μ = 0 dB and σ = 3dB.

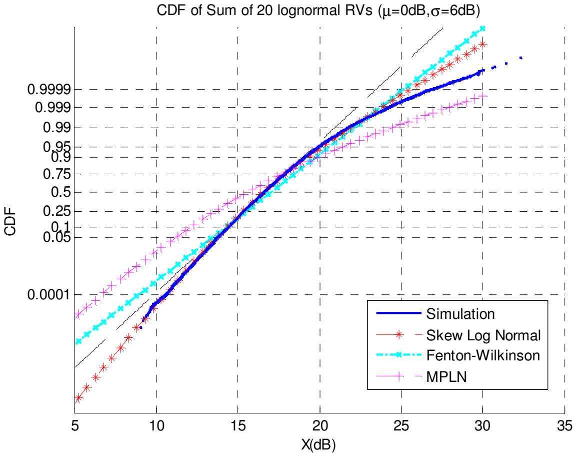

Figure 2. CDF of a sum of 20 i.i.d. lognormal RVs with $\mu = 0$ dB and $\sigma = 6$dB.

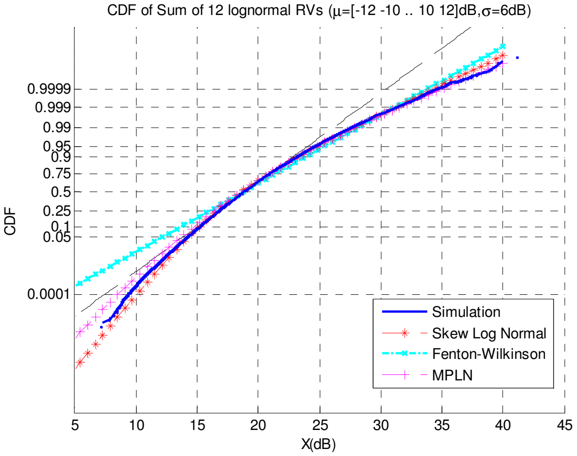

Figure 3. CDF of a sum of 12 lognormal RVs with $\mu = [-12\ -10\ -8\ \ ...\ \ 8\ 10\ 12]$ dB and $\sigma = 6$dB.

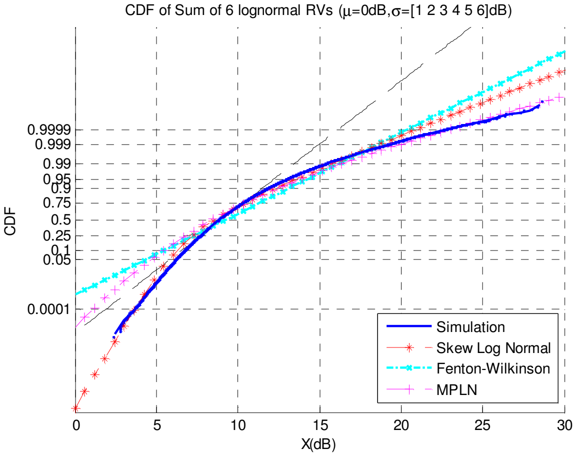

Figure 4. CDF of a sum of 6 lognormal RVs with $\mu = 0$ dB and $\sigma = [1\ 2\ 3\ 4\ 5\ 6]$ dB.

5. Application: Outage Probability in Lognormal Shadowing Environment

In this section, we provide an example for outage probability calculation in lognormal shadowing environment based on log skew normal approximation.

We consider a homogeneous hexagonal network made of 18 rings around a central cell. Fig. 5 shows an example of such a network with the main parameters involved in the study: R, the cell range (1 km), Rc, the half-distance between BS. We focus on a mobile station (MS) u and its serving base station (BS), BS_i, surrounded by M interfering BS

To evaluate the outage probability, the noise is usually ignored due to simplicity and negligible amount. Only inter-cell interferences are considered. Assuming that all BS have identical transmitting powers, the SINR at the u can be written in the following way:

$$SINR=\frac{S}{I+N}=\frac{P_i K r_{i,u}^{-\eta}.\mathrm{Y}_{i,u}}{\sum_{j=0,j\neq i}^{M} P_j K r_{j,u}^{-\eta}.\mathrm{Y}_{j,u}+N}=\frac{r_i^{-\eta}.\mathrm{Y}_{i,u}}{\sum_{j=0,j\neq i}^{M} r_j^{-\eta}.\mathrm{Y}_{j,u}} \qquad (30)$$

The path-loss model is characterized by parameters K and η>2. The term $P_l K r_l^{-\eta}$ is the mean value of the received power at distance r_l from the transmitter BS_l.Shadowing effect is represented by lognormal random variable $Y_{l,u}=10^{\frac{x_{1,u}}{10}}$ where $x_{1,u}$ is a normal RV, with zero mean and standard deviation σ, typically ranging from 3 to 12 dB.

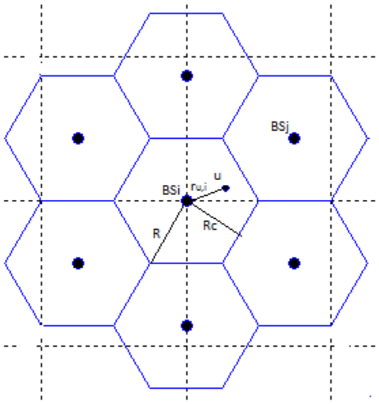

Figure 5. Hexagonal network and main parameters

The outage probability is now defined as the probability for the γ SINR to be lower than a threshold value δ :

$$P(\gamma < \delta) = P(\frac{P_{\text{int}}}{P_{ext}} < \delta) = P(\frac{r_i^{-\eta}.\Upsilon_{i,u}}{\sum_{j=0,\,j\neq i}^{M} r_j^{-\eta}.\Upsilon_{j,u}} < \delta)$$

$$= P(10\log(\frac{r_i^{-\eta}.\Upsilon_{i,u}}{\sum_{j=0,\,j\neq i}^{M} r_j^{-\eta}.\Upsilon_{j,u}}) < \delta_{dB}) \qquad (31)$$

$$= P(P_{\text{int,dB}} - P_{ext,dB} < \xi\delta_{dB})$$

Where:

$P_{\text{int,dB}} = \ln(r_i^{-\eta}.\Upsilon_{i,u})$ a normal RV with mean $m = \ln(r_i^{-\eta})$ and standard deviation $\xi\sigma$.

$P_{\text{ext,dB}} = \ln(\sum_{j=0,\,j\neq i}^{M} r_j^{-\eta}.\Upsilon_{j,u})$ a skew normal RV with distribution $SN(\lambda,\varepsilon,\omega)$.

It is easy to show that the difference $P_{\text{int,dB}} - P_{ext,dB}$ has a skew normal distribution $SN(\lambda_1,\varepsilon_1,\omega_1)$
Where

$$\varepsilon_1 = \text{m} - \text{e}$$

$$\omega_1 = \sqrt{\xi^2\sigma^2 + \omega^2}$$

$$\lambda_1 = \frac{\lambda}{\sqrt{(1+\lambda^2)(\frac{\xi^2\sigma^2}{\omega^2}) + 1}}$$

Fig. 6 and Fig. 7 show the outage probability at cell edge (r=Rc) and inside the cell (r=Rc/2), resp. for =3dB and 6dB assuming η=3. Difference between analysis and simulation results is less than few tenths of dB. This accuracy confirms that the LSKN approximation considered in this work is efficient for interference calculation process.

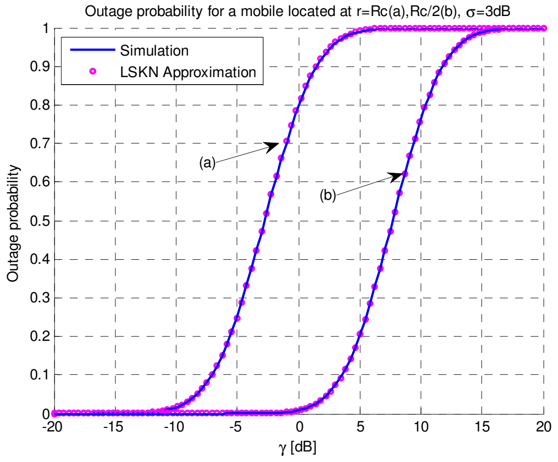

Figure 6. Outage probability for a mobile located at r=Rc (a), r=Rc /2(b), σ =3dB, η=3

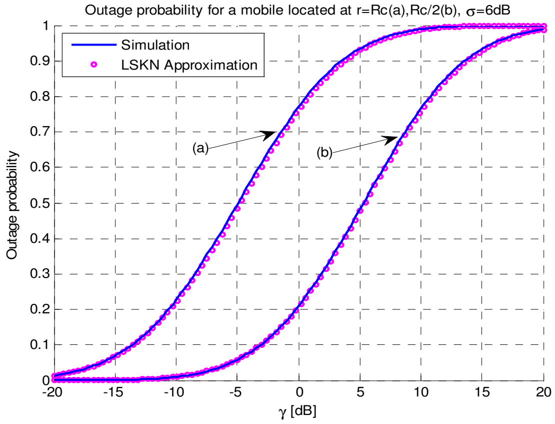

Figure 7. Outage probability for a mobile located at r=Rc (a), r=Rc /2(b), σ =6dB, η=3

6. CONCLUSIONS

In this paper, we proposed a fitting method to log skew normal distribution in order to approximate the sum of lognormal distributions. The proposed fitting method uses moment and tails slope matching technique to generate distribution parameters. By obtaining such parameters through a simple procedure, the LSN random variable approximates the entire lognormal sum distribution with high accuracy, especially at the lower region. Simulations confirm that our fitting method outperforms other priori methods for all cases except for the case when lognormal distributions have different standard deviation. Using an example for outage probability calculation in lognormal shadowing environment, we proved that LSKN approximation, considered in this work, is efficient for interference calculation process.

Appendix A

We begin by showing that the LSKN distribution has a *best lognormal fit* [27] at the right tail. Using [22, Lemma 1], for a given $\lambda > 0$

$$\lim_{x\to+\infty}\frac{1-F_{LSKN,\lambda}(\mathrm{x})}{1-\phi(\frac{\ln(\mathrm{x})-\varepsilon}{w})}$$

$$=\lim_{x\to+\infty}\frac{1-F_{SKN,\lambda}(\mathrm{x})}{1-\phi(\frac{\mathrm{x}-\varepsilon}{w})}$$

$$=\lim_{x\to+\infty}(1-F_{SKN,\lambda}(\mathrm{x}))\frac{\mathrm{x}}{\varphi(\mathrm{x})}=2$$

Because this ratio converges to a finite non–zero value, we may conclude from [21, Lemma 2] that $\phi(\frac{\mathrm{x}-\varepsilon}{w})$ is a *best lognormal fit* to F_{SKLN} at the right tail. The corresponding slope is $1/\omega$ on lognormal paper, which proves (25)

In order to prove the lower tail slope, a few steps are needed. Using [22, Lemma 1], for a given $\lambda > 0$ we have:

$$\begin{aligned}&\lim_{x\to-\infty} F_{SKN,\lambda}(x)\\ &= \lim_{x\to-\infty}(1-F_{SKN,-\lambda}(-x))\\ &= \lim_{x\to+\infty}(1-F_{SKN,-\lambda}(x))\\ &= \lim_{x\to+\infty}\sqrt{\frac{2}{\pi}}\frac{\varphi(x\sqrt{1+\lambda^2})}{\lambda(1+\lambda^2)x^2}\\ &= \lim_{x\to+\infty}\frac{\mathrm{e}^{-\frac{(1+\lambda^2)x^2}{2}}}{\pi\lambda(1+\lambda^2)x^2}\end{aligned}$$

Using approximation from [25]:

$$\phi^{-1}\xrightarrow{x\to 0^+}-\sqrt{-2\ln(2x)-\ln(-\pi\ln(2x))}$$

After some manipulation, we may write:

$$\begin{aligned}&\lim_{x\to-\infty}\frac{\delta}{\delta x}\tilde{F}_{LSKN}(x)=\frac{1}{\omega}\lim_{x\to-\infty}\frac{\delta}{\delta x}\phi^{-1}(\mathrm{F}_{LSKN}(x))\\ &=-\frac{1}{\omega}\lim_{x\to-\infty}\frac{\delta}{\delta x}\sqrt{(1+\lambda^2)x^2+o(\ln(-x))}\\ &=-\frac{1}{\omega}\lim_{x\to-\infty}\frac{2(1+\lambda^2)x}{2\sqrt{(1+\lambda^2)x^2}}\\ &=\frac{\sqrt{(1+\lambda^2)}}{\omega}\end{aligned}$$

Which proves (26).

REFERENCES

[1] J. M. Kelif , M. Coupechoux and P. Godlewski "On the dimensioning of cellular OFDMA networks", Phys. Commun., vol. 5, no. 1, pp.10 -21 2012.

[2] L. F. Fenton,"The sum of log-normal probability distributions in scatter transmission systems", IRE Trans. Commun., Vol. 8, pp.57-67, March 1960.

[3] N. Beaulieu and Q. Xie, "An optimal lognormal approximation to lognormal sum distributions," IEEE Trans. Vehicular Tech., vol. 53, pp. 479–489, Mar. 2004.

[4] J. Wu, N. B. Mehta, J. Zhang, "Flexible lognormal sum approximation method," IEEE GLOBECOM 2005, vol. 6, Nov. 2005, pp. 3413–3417.

[5] Z. Liu, J. Almhana, F. Wang, and R. McGorman, "Mixture lognormal approximations to lognormal sum distributions," IEEE Commun. Lett., vol. 11, pp. 711-713, Sept. 2007.

[6] N. C. Beaulieu, Q. Xie, "Minimax Approximation to Lognormal Sum Distributions", IEEE VTC Spring, Vol. 2, pp. 1061-1065, April 2003.

[7] Tellambura, C., Senaratne, D.,"Accurate computation of the MGF of the lognormal distribution and its application to sum of lognormals", Communications, IEEE Transactions on, Vol. 58, No. 5, pp. 1568-1577, May 2010.

[8] Damith Senaratne, Chintha Tellambura: Numerical Computation of the Lognormal Sum Distribution. GLOBECOM, page 1-6. IEEE, 2009.

[9] N. C. Beaulieu "Fast convenient numerical computation of lognormal characteristic functions", IEEE Trans. Commun., vol. 56, no. 3, pp.331 -332 2008.

[10] Mahmoud, A.S.H. "New Quadrature-Based Approximations for the Characteristic Function and the Distribution Function of Sums of Lognormal Random Variables", Vehicular Technology, IEEE Transactions on, On page(s): 3364 - 3372 Volume: 59, Issue: 7, Sept. 2010.

[11] H. Nie and S. Chen, "Lognormal sum approximation with type IV Pearson distribution," IEEE Commun. Lett., vol. 11, no. 10, pp. 790-792, Oct. 2007.

[12] M. Di Renzo , F. Graziosi and F. Santucci "Further results on the approximation of lognormal power sum via Pearson type IV distribution: a general formula for log moments computation", IEEE Trans. Commun., vol. 57, pp.893 -898 2009.

[13] N. C. Beaulieu, F. Rajwani, “Highly accurate simple closed-form approximations to lognormal sum distributions and densities,” IEEE Communications Letters, vol.8, Dec. 2004, pp. 709–711.

[14] C. L. J. Lam and T. Le-Ngoc "Estimation of typical sum of lognormal random variables using log shifted gamma approximation", IEEE Commun. Lett., vol. 10, no. 4, pp.234 -235 2006.

[15] Z. Liu, J. Almhana, and R. McGorman, “Approximating lognormal sum distributions with power lognormal distributions,” IEEE Trans. Vehic. Tech., vol. 57, pp. 2611–2617, July 2008.

[16] Szyszkowicz, S.S, Yanikomeroglu, H, “Fitting the Modified–Power–Lognormal to the Sum of Independent Lognormals Distribution”, Global Telecommunications Conference, 2009. GLOBECOM 2009.

[17] S. S. Szyszkowicz and H. Yanikomeroglu "On the tails of the distribution of the sum of lognormals", Proc. IEEE International Conf. Commun. (ICC), pp.5324 -5329, 2007.

[18] Z. Wu, X. Li, R. Husnay, V. Chakravarthy, B. Wang, and Z. Wu. A novel highly accurate log skew normal approximation method to lognormal sum distributions. In Proc. of IEEE WCNC 2009.

[19] X. Li, Z. Wu, V. D. Chakravarthy, and Z. Wu, "A low complexity approximation to lognormal sum distributions via transformed log skew normal distribution," IEEE Transactions on Vehicular Technology, vol. 60, pp. 4040-4045, Oct. 2011.

[20] S. Asmussen and L. Rojas-Nandayapa, “Asymptotics of sums of lognormal random variables with Gaussian copula,” Statistics & Probability Letters, vol. 78, pp. 2709–2714, Nov. 2008.

[21] S. Szyszkowicz and H. Yanikomeroglu, “On the tails of the distribution of the sum of lognormals,” IEEE ICC, pp. 5324–5329, June 2007.

[22] Archil Gulisashvili, Peter Tankov, “Tail behavior of sums and differences of log-normal random variables”, ARXIV 09/2013

[23] Antonella Capitanio, “On the approximation of the tail probability of the scalar skew-normal distribution”, in METRON (2010)

[24] W. Hürlimann, “Tail Approximation of the Skew-Normal by the Skew-Normal Laplace: Application to Owen’s T Function and the Bivariate Normal Distribution”, Journal of Statistical and Econometric Methods, vol. 2, no.1, 2013, 1-12, Scienpress Ltd, 2013

[25] H. E. Fettis, “A stable algorithm for computing the inverse error function in the “tail-end” region,” Mathematics of Computation, vol. 28, pp. 585–587, Apr. 1974.

[26] O’Hagan A. and Leonard TBayes estimation subject to uncertainty about parameter constraints, Biometrika, 63, 201–202, 1976.

[27] Azzalini A, A class of distributions which includes the normal ones, Scand. J. Statist., 12, 171–178, 1985.

AUTHORS

Marwane Ben Hcine was born in Kébili, Tunisia, on January 02, 1985. He graduated in Telecommunications Engineering, from The Tunisian Polytechnic School (TPS), July 2008. In June 2010, he received the master’s degree of research in communication systems of the Higher School of Communication of Tunisia (Sup’Com). Currently he is a Ph.D. student at the Higher School of Communication of Tunisia. His research interests are network design and dimensioning for LTE and beyond Technologies.

Pr. Ridha BOUALLEGUE was born in Tunis, Tunisia. He received the M.S degree in Telecommunications in 1990, the Ph.D. degree in telecommunications in 1994, and the HDR degree in Telecommunications in 2003, all from National School of engineering of Tunis (ENIT), Tunisia. Director and founder of National Engineering School of Sousse in 2005. Director of the School of Technology and Computer Science in 2010. Currently, Prof. Ridha Bouallegue is the director of Innovation of COMmunicant and COoperative Mobiles Laboratory, INNOV'COM Sup'COM, Higher School of Communication. His current research interests include mobile and cooperative communications, Access technique, intelligent signal processing, CDMA, MIMO, OFDM and UWB systems.

INTENTIONAL BLANK

SELECTIVE IMAGE ENCRYPTION USING DCT WITH AES CIPHER

Belazi Akram, Benrhouma Oussama, Hermassi Houcemeddine and Belghith Safya

SysComLab, Ecole Nationale d'Ingénieurs de Tunis (ENIT), Tunis, Tunisia
belazi.akram@gmail.com

ABSTRACT

Selective encryption presents a great solution to optimize time efficiency during encryption process. In this paper a novel selective encryption scheme based on DCT transform with AES algorithm is presented. In the DCT method, the basic idea is to decompose the image into 8×8 blocks and these blocks are transformed from the spatial domain to the frequency domain by the DCT. Then, the DCT coefficients correlated to the lower frequencies of the image block are encrypted. The proposed cryptosystem is evaluated using various security and statistical analysis; results show that the proposed algorithm is strong against attacks and suitable for practical application.

KEYWORDS

DCT, Selective Encryption, AES Cipher

1. INTRODUCTION

Nowadays, multimedia content (image, audio and video) presents an enormous importance giving the fact of the rapid growth of high technologies. The rate of exchanges these types of information is growing and the need to protect it is more and more essential. However increasing number of digital documents, multimedia processing tools, and the worldwide availability of Internet access has created an ideal way to uncontrollable distribution of multimedia content [1]. To protect data, various encryption schemes has been proposed for image encryption, [2,3,4] however in these schemes (total encryption schemes) all data has to be encrypted which will generally take some time, complicated calculations and high memory occupation, which makes these schemes hard to use in real time applications.

Total encryption schemes are not necessary when we talking about most multimedia content. Given to the fact that the content is already voluminous and not all the content represents a significant importance we choose to encrypt only significant parts of the data and leave the rest to enhance time encryption and reduce memory occupation and make the encryption scheme suitable in practical application given to the fact that selective crypto-systems presents a simple architecture.

Selective encryption protects the most visually important parts of an image or video representation [5,6,7]. Encrypting only parts of the image data must be sufficient to satisfy the needed security [8,9]. There are two basic ways to encrypt digital images: in the spatial domain or in the transform domain [10]. Since wavelet based compression appeared and was adopted in the

Natarajan Meghanathan et al. (Eds) : NeTCoM, CSIT, GRAPH-HOC, SPTM - 2014
pp. 69–77, 2014. © CS & IT-CSCP 2014 DOI : 10.5121/csit.2014.41306

JPEG2000 standard, suggestions for image encryption techniques based in the wavelet domain have been abundant. However, many of these are not secure as they are based exclusively on random permutations making them vulnerable to known or chosen-plaintext attacks [11, 12, 13, 19]. For example, in DCT codec several selective encryption schemes have been proposed. Droogenbroeck and Benedett [14] selected AC coefficients from compressed images for encryption. In their method the DC coefficients are not ciphered because they carry important visible information and they are highly predictable. The compression and encryption operations are separated in this approach and this requires an additional operating cost. Jiang-Lung Liu [15] proposes to encrypt the low-frequency DCT coefficients only and leave the high-frequency ones unencrypted in the JPEG compression.

In this paper we propose a selective encryption scheme based on DCT transformation and AES algorithm to cipher digital images.

The rest of the paper is organized as follow: section 2 presents a mathematical preliminary for the DCT transform, section 3 we present our encryption, experimental results are presented in section and we conclude in section 5.

2. FREQUENCY BAND ENCRYPTION IN A DCT BLOCK

In a DCT-based codec, media data are partitioned into blocks (typically, 8 × 8 or 4 × 4), and each block is transformed by DCT, quantized and encoded with entropy coding. Generally, the DCT block is scanned in zigzag order, which generates the coefficient sequence ordered from the highest frequency to the lowest frequency. In this coefficient sequence, the first coefficient denotes the DCT block's energy, and the other coefficients denote detailed information on the image block. The DCT block is scanned from the bottom- left to the top- right, as shown in Figure 1. Thus, the first coefficient in the coefficient sequence denotes the block's energy.

In perceptual encryption, the 64 coefficients can be selected from the first one to the last one according to the quality factor Q. Thus, set N = 64 for each DCT block. Figure 2 shows the relation between n and the PSNRs of the encrypted images. As can be seen, with increase in n, the quality of the images decreases.

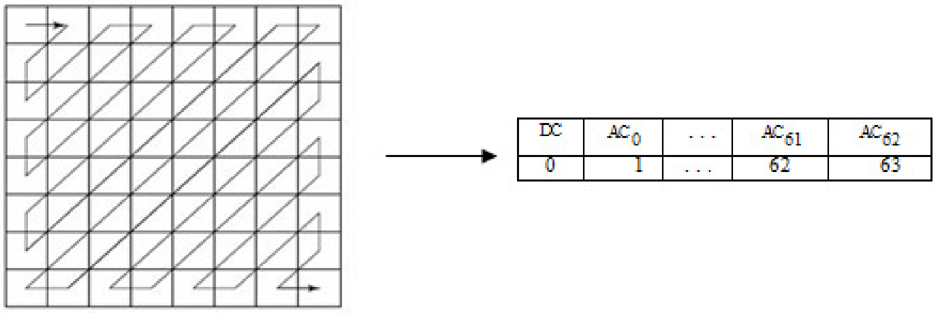

Figure 1. Coefficient sequence generation in a DCT block

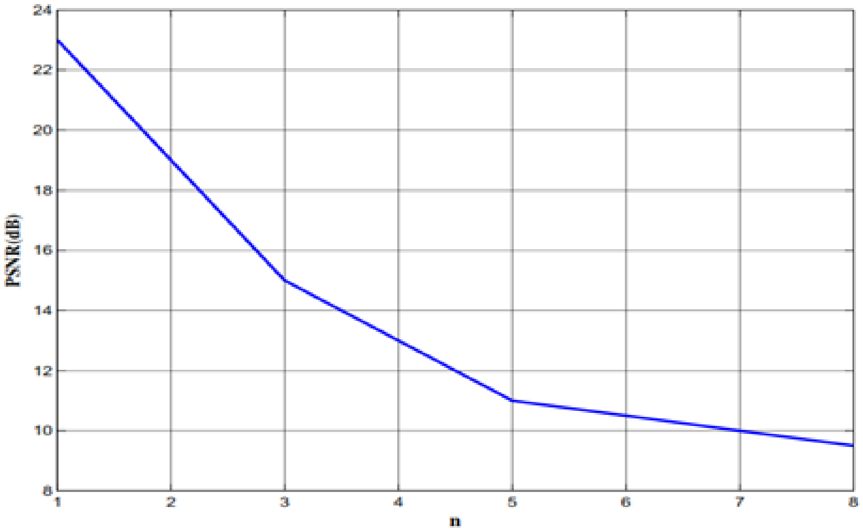

Figure 2. Relation between the quality of the encrypted images and n

For example in JPEG compressed images, there are many techniques that were developed to encrypt parts of JPEG compressed images [15,17]. One technique suggested encrypting some of the Discrete Cosine Transform (DCT) coefficients in each 8x8 blocks [15], as shown in Figure 3. The first value of the DCT coefficients matrix is called the DC coefficient, and the rest are called AC coefficients [16]. The unencrypted high-frequency coefficients provide little information about the original 8 x 8 blocks. However, when the image blocks are considered together, the unencrypted high frequency coefficients often show outlines of objects in the image [15]. An alternative technique is to encrypt the bits that indicate the sign and magnitude of nonzero AC coefficients [17]. Since they are highly predictable, the DC coefficients are left unencrypted.

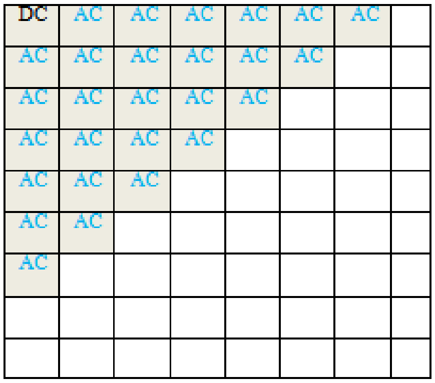

DC	AC	AC	AC	AC	AC	AC	
AC	AC	AC	AC	AC	AC		
AC	AC	AC	AC	AC			
AC	AC	AC	AC				
AC	AC	AC					
AC	AC						
AC							

Figure 3. The DCT coefficients matrix and the encrypted coefficients

3. THE PROPOSED ENCRYPTION SCHEME

The proposed method based on the idea of decomposing the image into 8x8 blocks, these blocks are transformed from the spatial domain to frequency domain by the DCT. Then, the DCT coefficients related to the higher frequencies of the image block are encrypted using the AES cipher. The concept behind encrypting only some selective DCT coefficients based on the fact that the image details are situated in the higher frequencies, In fact the image encryption algorithm obtains higher security when DCT coefficients related to the lower frequencies are encrypted than those related to higher frequencies. Fig. 4 shows the general block diagram of the proposed method of selective image encryption. We propose a secure encryption scheme:

(i) Block 1: All coefficients are encrypted.

(ii) Blocks 2, 3. . . n: The 24 most significant bit-planes are encrypted.

Where n is the number of block.

The general block diagram of the proposed method of selective image encryption is shown in Figure 4, which combines encryption process with DCT codec, and is composed of data encoding, parameter encryption and data decoding. Here, P, K and C are the plaintext, key and ciphertext, respectively. X and Y are the parameters in the data stream, among which, X is encrypted into Z according to Z = E(X, K) while Y is left unchanged. Without losing the generality, the data stream composed of two parameters is investigated. If the data steam is composed of more parameters, the similar results can be obtained.

4. EXPERIMENTAL RESULTS

In this section, the performance of the proposed image encryption scheme is analyzed in detail. It is well known that statistical analysis is of crucial importance. Indeed, an ideal cipher should be robust against any statistical attack. In order to prove the robustness of proposed image encryption scheme, we have performed some statistical tests which are described in the following.

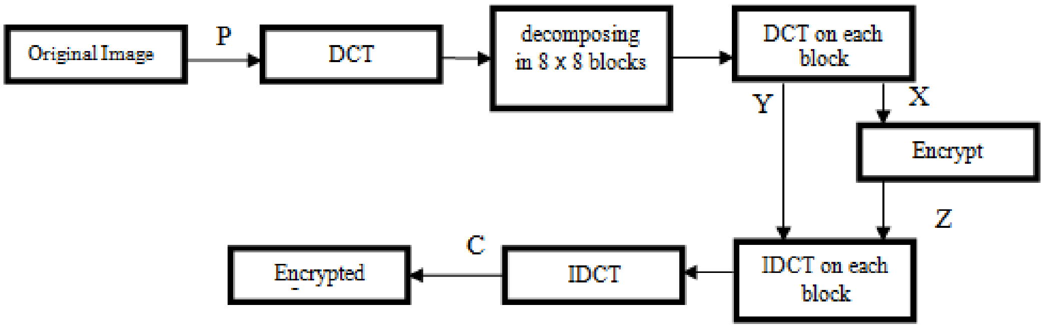

Figure 4. Block diagram of the proposed method

4.1. Histogram

To demonstrate that our proposed algorithm has strong resistance to statistical attacks, test is carried out on the histogram of enciphered image. Several gray-scale images of size 256×256 are selected for this purpose and their histograms are compared with their corresponding ciphered image. One typical example is shown below. The histogram of the original image contains large spikes as shown in Figure 5 but the histogram of the ciphered image as shown in Figure 6, is more uniform. It is clear that the histogram of the encrypted image is, significantly different from the respective histogram of the original image and bears no statistical resemblance to the plain image. Hence statistical attack on the proposed image encryption procedure is difficult.

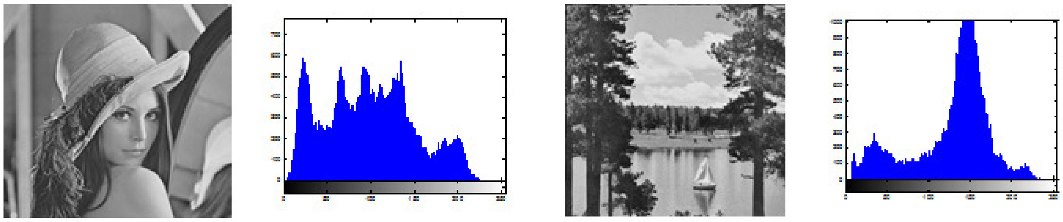

Figure 5. Histogram of Original Image

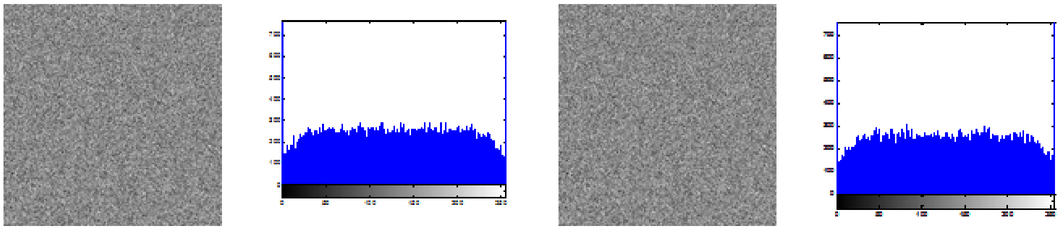

Figure 6. Histogram of Encrypted Image

4.2. Correlation of adjacent pixels

It is well known that adjacent image pixels are highly correlated either in horizontal, vertical or diagonal directions. Such high correlation property can be quantified by means of correlation coefficients which are given by:

$$r = \frac{\operatorname{cov}(p,q)}{\sqrt{D(p)}\sqrt{D(q)}} \qquad (1)$$

Where,

$$D(p) = \frac{1}{S}\sum_{i=1}^{S}(p_i - \overline{p})^2$$

$$\operatorname{cov}(p,q) = \frac{1}{S}\sum_{i=1}^{S}(p_i - \overline{p})(q_i - \overline{q})$$

q_i and p_i denote two adjacent pixels (either horizontal or vertical). S is the total number of duplets (p_i,q_i) obtained from the image; $\bar{p}$ and $\bar{q}$ are the mean values of p_i and q_i , respectively. The correlation coefficients of the plain and ciphered images of Lena and Boat are given in the Table 1. It can be observed that the encrypted images obtained from the proposed scheme have small correlation coefficients in horizontal, vertical and diagonal directions. The result are illustrated in Figure 7 and Figure 8, which presents the distribution of two adjacent pixels in the original and encrypted images of Lena and Boat for horizontal (a-b), vertical (c-d) and diagonal (e-f) directions.

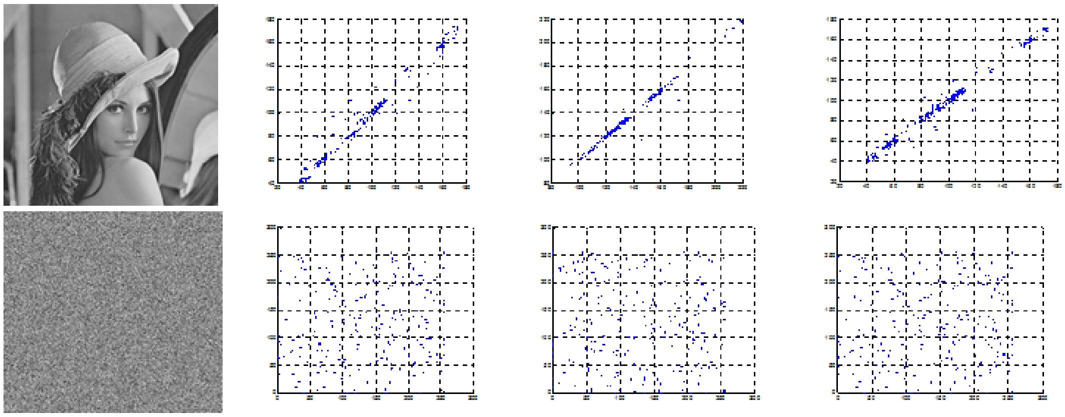

Figure 7. the distribution of two adjacent pixels in the original and encrypted lena.

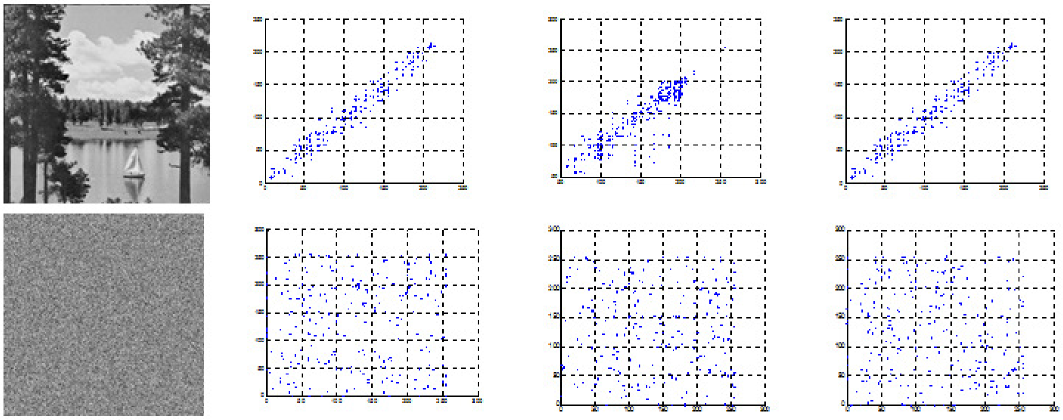

Figure 8. the distribution of two adjacent pixels in the original and encrypted boat.

Table 1. Correlation coefficients of two adjacent pixels in original and encrypted images.

Image	Horizontal		Vertical		Diagonal	
	Original	Encrypted	Original	Encrypted	Original	Encrypted
Lena	0.9888	0.0138	0.9917	-0.0383	0.9923	0.0171
Boat	0.9829	-0.0016	0.9818	-0.0682	0.9769	-0.1169

4.3. Differential attack

As a general requirement for all the image encryption schemes, the encrypted image should be greatly different from its original form. Such difference can be measured by means of two criteria namely, the NPCR (Number of Pixel Change Rate) and the UACI (Unied Average Changing Intensity) [18]. The NPCR is used to measure the number of pixels in difference between two images. Let S(i,j) and S’(i,j) be the (i,j)th pixel of two images S and S’ ,respectively.

The NPCR can be defined as:

$$NPCR = \frac{\sum_{i;j} D(i,j)}{L} \times 100\% \tag{2}$$

Where L is the total number of pixels in the image and D(i,j) is defined as :

$$D(i,j)\begin{cases} 0 \; if \;\; S(i,j) = S'(i,j) \\ 1 \; if \;\; S(i,j) \neq S'(i,j) \end{cases}$$

Where S(i,j) and S'(i,j) are the pixel values of the two images, respectively. For instance, for two random images:

$$NPCR = 99.609375\%$$

The second criterion, UACI, is used to measure the average intensity difference and can be defined as:

$$UACI = \frac{1}{L}(\sum \frac{|S(i,j) - S'(i,j)|}{2^B - 1} \times 100\% \qquad (3)$$

Where B is the number of bits used to represent a grey scale pixel value. In the case of two random images, the expected value of UACI is:

$$UACI = 33.46354\%$$

The NPCR and UACI measured between the plain and ciphered images of Lena and Boat with the proposed cryptosystem are given in Table 2.

Table 2. Sensitivity to differential attacks.

Image	**NPCR%**	**UACI%**
Lena	99.5941	33.7715
Boat	99.5895	33.4626

4.4. Information entropy

Entropy is a statistical measure of randomness. Ideally, the information entropy should be 8 bits for gray scale images. Table 3 shows the entropy of different test images of size 256×256.

Table 3. Entropy results for encrypted images.

Image	**Entropy of Encrypted Image**
Lena	7.8683
Boat	7.8745

It's seen that the value of entropy for encrypted images is very close to the 8 bits, then the loss of information is negligible, and the proposed algorithm is strong against entropy attack.

5. CONCLUSIONS

Selective Image Encryption Using DCT with AES Cipher has been presented in this paper. The algorithm will not encrypt bit by bit the whole image but only selective DCT coefficients will be encrypted. Indeed the proposed encryption method uses the Selective Encryption approach where the DC coefficients and some selective AC coefficients are encrypted, hence the DC coefficients carry important visual information, and it's difficult to predict the selective AC coefficients, this give a high level of security in comparison with methods mentioned above. Several security and statistical analysis tests are carried out in order to check the robustness of the proposed algorithm. Both simulations and analysis results prove the efficiency of the proposed cryptosystem.

REFERENCES

[1] IEEE Transactions on Circuits and Systems for Video Technology (2003) : Special Issue on Authentication, Copyright Protection, and Information Hiding, Vol. 13, No. 8.

[2] Liansheng Sui, Kuaikuai Duan, Junli Liang, Zhiqiang Zhang & Haining Meng , (2014) Asymmetric multiple-image encryption based on coupled logistic maps in fractional Fourier transform domain", Optics and Lasers in Engineering, Volume 62, Pages 139-152

[3] A. Alfalou, C. Brosseau & N. Abdallah, (2015) "Simultaneous compression and encryption of color video images", Optics Communications, Volume 338, Pages 371-379

[4] Tieyu Zhao, Qiwen Ran & Yingying Chi, (2015) "Image encryption based on nonlinear encryption system and public-key cryptography", Optics Communications, Volume 338, Pages 64-72

[5] Li-feng WANG, Wen-dong WANG, Jian MA, Chen XIAO & Kong-qiao WANG, (2008) "Perceptual video encryption scheme for mobile application based on H.264", The Journal of China Universities of Posts and Telecommunications, Volume 15, Supplement, Pages 73-78.

[6] Sukalyan Som & Sayani Sen, (2013) "A Non-adaptive Partial Encryption of Grayscale Images based on Chaos", Procedia Technology, Volume 10, Pages 663-671.

[7] Xinjun Zhang & Xingyuan Wang, (2013) "Chaos-based partial encryption of SPIHT coded color images", Signal Processing, Volume 93, Pages 2422-2431.

[8] Nidhi Taneja, Balasubramanian Raman & Indra Gupta, (2011) "Selective image encryption in fractional wavelet domain", AEU - International Journal of Electronics and Communications, Volume 65, Issue 4, Pages 338-344.

[9] Gaurav Bhatnagar & Q.M. Jonathan Wu, (2012) "Selective image encryption based on pixels of interest and singular value decomposition", Digital Signal Processing, Volume 22, Issue 4, July 2012, Pages 648-663.

[10] S. Li & G. Chen, (2004) "Chaos-Based Encryption for Digital Images and Videos", in Multimedia Security Handbook, B. Furht and D. Kirovski, CRC Press.

[11] Akram Belazi, Houcemeddine Hermassi, Rhouma Rhouma & Safya Belghith, (2014) "Algebraic analysis of a RGB image encryption algorithm based on DNA encoding and chaotic map", Nonlinear Dynamics June, Volume 76, Issue 4, pp 1989-2004.

[12] Houcemeddine Hermassi, Akram Belazi, Rhouma Rhouma & Safya Mdimegh Belghith, (2014) "Security analysis of an image encryption algorithm based on a DNA addition combining with chaotic maps", Multimedia Tools and Applications ,Volume 72, Issue 3, pp 2211-2224.

[13] Rhouma Rhouma, Ercan Solak & Safya Belghith, (2010) "Cryptanalysis of a new substitution–diffusion based image cipher, Communications in Nonlinear Science and Numerical Simulation, Volume 15, Issue 7, Pages 1887-1892.

[14] M. Van Droogenbroeck & R. Benedett, (2002) "Techniques for a Selective Encryption of Uncompressed and Compressed Images", in Proceedings of Advanced Concepts for Intelligent Vision Systems (ACIVS) 2002, Ghent, Belgium.

[15] Jiang-Lung Liu (2006) "Efficient selective encryption for JPEG 2000 images using private initial table". Pattern Recognition, Volume 39, Issue 8, Pages 1509-1517.

[16] K. Sayood, (2000) "Introduction to Data Compression", 2nd edition, USA, Morgan Kauffman Publishers.

[17] Saeed Bahrami & Majid Naderi, (2013) "Encryption of multimedia content in partial encryption scheme of DCT transform coefficients using a lightweight stream algorithm", Optik - International Journal for Light and Electron Optics, Volume 124, Issue 18, Pages 3693-3700.

[18] G. Chen, Y. Mao, & C. K Chui, (2004) "A symmetric image encryption based on 3D chaotic maps," Chaos Soliton Fractals, vol. 21, pp. 749–761.

[19] Oussama Benrhouma •Houcemeddine Hermassi & Safya Belghith, (2013) "Security analysis and improvement of a partial encryption scheme," Multimedia Tools and Applications DOI 10.1007/s11042-013-1790-4.

AUTHORS

Akram BELAZI has received his engineering diplomat in “Telecommunication & Networks” in 2011 at the National Engineering School of Gabes, ENIG Tunisia and his Master degree in “Electronic Systems and Networks Communications” in 2013 at the Polytechnic School of Tunisia, EPT. He is now a Phd student at the Syscom Laboratry, ENIT Tunisia. His researcher domain is focused on the conception of partial encryption scheme for multimedia content and cryptanalysis of chaos-based cryptosystem

Oussama Benrhouma is a PhD student in the Syscom laboratory at the ENIT Ecole Nationale d’Ingénieurs de Tunis (ENIT). His domain of interest includes cryptography, Multimedia watermarking and steganography.

Houcemeddine Hermassi has received his engineering diploma in “Telecommunications & Networks” in 2005 from the National School of Engineering Gabès ENIG, Tunisia, and his MS degree in “Communication Systems” in 2010 from the National School of Engineering Tunis ENIT, Tunisia. He is now a PhD student at the Syscom Laboratory, ENIT Tunisia. His researcher domain is focused on the cryptanalysis and the conception of the new multimedia cryptographic approaches like the chaos-based cryptography and the DNA cryptography.

Prof. Safya Belghith has received his engineering diploma in “Electricity” (1981) and his D.E.A (1982) and the PhD degree (1985) in “Automatic and Signal Processing” from the High School of Electricity, Lab Signals & Systems, University Paris XI Orsay. In 1997, she received her Status Doctorate in “Physical Sciences” from the Faculty of Sciences Tunis FST with collaboration of the Laboratory Signals & Systems, High School of Electricity University Paris XI Orsay. She is now a Professor at the National School of Engineering Tunis ENIT, Tunisia and a senior researcher at SysCom Laboratory in the ENIT, Tunisia. His research domain is focused on the analysis of nonlinear systems and chaotic communication, the generation of the pseudo random sequences from chaotic systems and studying their performance in mobile radio communications particularly in a DS/CDMA and on the Synchronization of chaotic systems and its application to secure the transmission by chaotic carrier – Cryptography.

INTENTIONAL BLANK

DYNAMIC OPTIMIZATION OF OVERLAP-AND-ADD LENGTH OVER MBOFDM SYSTEM BASED ON SNR AND CIR ESTIMATE

Nouri Naziha and Bouallegue Ridha

Innov'Com Laboratory, Higher School of Communications of Tunis, Sup'Com,
University 7th November at Carthage, Tunisia.
nourinaziha@yahoo.fr
ridha.bouallegue@supcom.rnu.tn

ABSTRACT

An important role performed by Zero Padding (ZP) in multi-band OFDM (MB-OFDM) System. This role show for low-complexity in résistance against multipath interference by reducing inter-carrier interference (ICI) and eliminating the inter-symbol interference (ISI) Also, zero-padded suffix can be used to eliminate ripples in the power spectral density in order to conform to FCC requirements.

At the receiver of MB-OFDM system needs to use of a technique called as overlap-and-add (OLA). Which maintain the circular convolution property and take the multipath energy of the channel.

In this paper, we proposed a method of performing overlap-and-add length for zero padded suffixes. Then, we studied the effect of this method, dynamic optimization of overlap-and-add (OLA) equalization, on the performance of MBOFDM system on Bit Error Rate (BER) with AWGN channel and Saleh-Valenzuela (S-V) Multipath channel Model.

In the dynamic optimization OLA, the Length of ZP depends on length of channel impulse response (CIR). These measures, based on SNR, insert the ZP according to the measurement.

Dynamic optimization of length of ZP improves the Performance of MBOFDM system. In fact we developed a technique to select the length of ZP as function of SNR and CIR estimate(repetition). In our simulation this technique improve to 3 dB at BER=10^{-2} with a multipath channels CM4.

KEYWORDS

UWB, ECMA-368, MB-OFDM, OLA, ZPS, SNR, CIR, BER.

Natarajan Meghanathan et al. (Eds) : NeTCoM, CSIT, GRAPH-HOC, SPTM - 2014
pp. 79–96, 2014. © CS & IT-CSCP 2014 DOI : 10.5121/csit.2014.41307

1. INTRODUCTION

Ultra-wideband (UWB) has tremendous potential for high-rate [1] low-power communication due to its high data rates and resistance to interference. Since its lowly beginning in the decade of 1940, UWB technology has traveled a wealthy path, from lab to military, back to lab [2] and this technology has received significant attention from industry, media and academia [3] especially in wireless universal serial bus (WUSB) and wireless personal area network (WPAN) domain [2]. The reason for all this excitement is that this technology promises to deliver high data rates that can scale from 110 Mbit/s at a distance of 10 meters up to 480 Mbit/s at a distance of two meters in realistic multipath environments all while consuming very little power communication and resistance to interference [1]. It is expected that UWB devices will provide low cost solutions [3].The United States Federal communications commission (FCC) officially defined UWB in 2002 as a signal with a 10 dB bandwidth of at least 500 MHz and a maximum equivalent isotropic radiated power spectral density (PSD) of no more than -41.3 dBm/MHz in the 3.1-10.6 GHz band [4]. FCC ruled that UWB system must have instantaneous spectrum of more than 500 MHz or more than 20% of its central frequency [2]. In order that UWB systems appear in the thermal noise floor of the existing narrowband services like GSM, GPS etc., and coexist with them without affecting their performance [5][6].Efficient utilization of such a large bandwidth of 7.5 GHz creates a huge challenge to the system designer community [2]. Furthermore the power constraints limits the range of communication to a short range only around 2 m to 15 m with scalable data rate of 53.3 Mbps to 480 Mbps.

A promising new high-speed wireless communication technology, called Multiband-Orthogonal Frequency Division Multiplexing (MB-OFDM) approach, designers can overcome many of barriers [3] such as complexity, cost, power consumption, and flexibility.

Pulsed multiband technique presented many disadvantages that can overcome if we use symbol which is much longer in time domain and integrating a modulation technique that can efficiently capture multipath energy [2]. MB-OFDM approach is the right candidate for this choice [7]. The main advantage of this approach is that information is processed over a much smaller bandwidth, this approach can reduce the system design complexity, the power consumption, cost, and also improving spectral flexibility which in turn helps UWB systems to follow global compliance [2][3]. Other advantages of this scheme include using lower-rate ADCs and simplifying the digital complexity. Systems built using this type of approach are often referred to as multiband systems [3].

The MB-OFDM is the first UWB technology obtained international standardization Thanks to their multiple benefits [8],[9] developed by the WiMedia alliance. Also this technology has been enabled by the FCC's recent allocation of 7500MHz. The MB-OFDM support data from 53.3 Mb/s to 480 Mb/s and divides the several gigahertz of spectrum allocated by the FCC into 14 bands, each with 528 MHz bandwidth. These bands are then bundled into 5 band groups with only the first defined as mandatory [10]. ECMA-368 is one of such principal standard employing MB-OFDM technique [11].

MB-OFDM based UWB system takes all the positives offered by the multi-banding scheme such as low power, low cost, simple analog design and also is capable of capturing sufficient multipath energy using a single RF chain due to adopted OFDM scheme [2].

Multicarrier schemes are supported to high data rate. OFDM is an attractive air-interface for next-generation wireless network without complex equalizer. OFDM is an emerging multi-carrier modulation scheme. It has been adopted by several wireless standards such as IEEE 802.11a, IEEE 802.16 and HiperLAN2. OFDM is designed such a way that it sends data over hundreds of parallel carrier which increases data rate. OFDM distributes data across a large number of carries that are spaced apart at accurate frequencies is modulated by the data.
The Orthogonal FDM (OFDM) reaps its own advantage to this approach [12], [13] in terms of spectral efficiency, narrow band interference (NBI) mitigation, excellent robustness against multipath channel, and smoothing the use of low complexity equalizer in receiver [2].

OFDM scheme suffered from inter-symbol interference (ISI) problem. ISI is distortion in a signal in which one symbol interferes with subsequent symbols, this will degrade performance of OFDM system. There are several methods for reducing the effects of ISI by affording time for reflection multipath energy mitigation and to allow a transmitter and a receiver for switching between different frequency bands. A receiving device can use an operation called overlap and add to restore the orthogonality.

There are diversities of techniques to represent the noise at the receiver. Characteristically, more noise that affects the modulated signals, this noise can be measure with the distance error between the received signal and the ideal symbol associated with them.

When the distance error is greater more difficult it becomes to map received signal to their associated ideal symbol and may prevent the communication to occur in some cases. Thus, the problem of relatively overly noise being added during overlap-and-add operation is very important issue that must be addressed with solutions that overcome the deficiencies of the prior technique.

In this paper, we proposed a dynamic optimization of length of ZP technique based on SNR and CIR estimate, in addition, we evaluate its effects on performance of MB-OFDM system. Section II present a brief description of the main component of MB-OFDM system, especially by using Zero-Pad OFDM Signal and Overlap and adds operation over AWGN Channel and the SV/ IEEE 802.15.3a Channel Model. A dynamic overlap and add length technique based on SNR and CIR estimate is provided in Section III. In particular, we proposed our process of computing dynamic OLA size based on SNR and CIR estimation. Simulation Results are discussed in Section IV with four different channel models (CM) defined by the IEEE 802.15.3a. Finally, we conclude with a summary of this work given in Section V.

2. SYSTEM MODEL

2.1. MB-OFDM System

MB-OFDM is the primary applicant for high data rate UWB applications. Today, this approach is supported by the WiMedia Alliance and adopted by the ECMA-368 standard. Our system is presented in Figure 1.

The MB-OFDM solution consists in combining OFDM with a multiband technique. That divides the available spectrum into 14 sub-bands of 528 MHz each, as presented in Figure 2. The modulation OFDM with 128 subcarriers is applied separately on each sub-band. As illustrate in the Figure 2, these sub-bands are combined to form several groups. Each group from the four groups contains three subbands and the five group contain only two subbands. This division has the advantage of reducing the complexity and hence the costs of components including converters. A WiMedia compatible device should actually only use the first group (3.1 - 4.6GHz).

Table 1. Characteristics a MB-OFDM symbol

Parameter	Description	value
fs	Sampling frequency	528 MHZ
N_{FFT}	Total number of subcarriers (FFT size)	128
N_D	Number of data subcarriers	100
N_P	Number of pilot subcarriers	12
N_G	Number of guard subcarriers	10
N_T	Total number of subcarriers used	122(=N_D+N_P+N_G)
D_f	Subcarries frequency spacing	4.125 MHZ (=f_s/N_{FFT})
T_{FFT}	IFFT and FFT period	242.42 ns ($\triangle_f^{-1}$)
N_{ZPS}	Number of samples in zero-padded suffix	37
T_{ZPS}	Zero-padded suffix duration in time	70.08 ns(=N_{ZPS}/f_s)
T_{SYM}	Symbol interval	312.5 ns (=T_{FFT} + T_{ZPS})
F_{SYM}	Symbol rate	3.2 MHZ (=$T_{SYM}^{-1)}$
N_{SYM}	Total number of samples per symbol	165(=N_{FFT} + N_P)

The characteristics of the OFDM symbols, used in the MBOFDM system, are listed in Table 2. The OFDM symbols are generated by a 128 point IFFT. Which 100 are dedicated to user data, 12 and 10 pilot to data guards. The inter-carrier interval $\triangle_f$=4.125 MHz can satisfy the orthogonality condition of the OFDM multiplex.

The duration of the suffix zero-padding is Tzps = 70.08 ns, 37 samples. Only the first 32 samples are devoted to the guard interval is a period T_{ZP} = 60.61 ns. The last 9.47 ns themselves being used to effect the change of central frequency of OFDM symbols. Each OFDM symbol transmitted has a duration Ts = 312.5 ns and therefore includes 165 samples. The MB-OFDM system, which presented in Figure 1, uses three sub-bands of the group, to which is applied a frequency hopping called time-frequency code (TFC). The TFC is used to control frequency hopping between different subbands. Moreover this method specifies for each OFDM symbol its central transmission frequency. Thus, as shown in Figure 2, each symbol has a different subband of the preceding symbol.

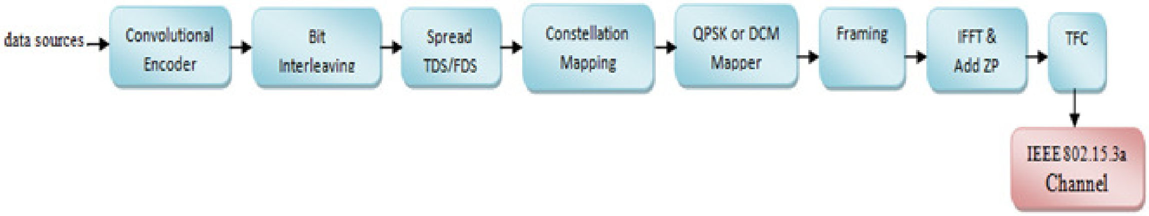

Figure 1. MBOFDM system

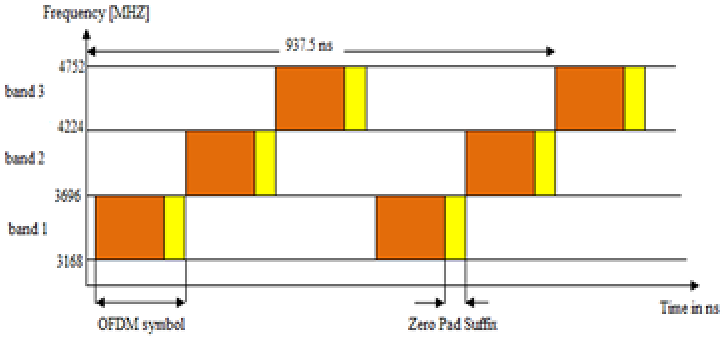

Figure 2. Example of time-frequency coding for MB-OFDM systems in the group1, TFC = {1,2,3,1,2,3,...}

Furthermore the MB-OFDM system transmits information at different data rates varying from 53.3 to 480 Mbps, listed in Table1. These data rates are established by the use of different convolutional coding rates and puncturing technique.

As well this system include bit interleaving, constellation mapping QPSK/DCM, frequency-domain spreading (FDS) and time-domain spreading (TDS) techniques. To retrieve the data, a receiver can put technical implementation as removing ZP overlap and add, channel estimation, equalization, de-spread, de-mapping, de-interleaving, de-puncture, de-coding.

Table 2. WiMedia-based MB-OFDM data rates

Data Rate (MB/s)	**Modulation**	**Code Rate (R)**	**FDS**	**TDS**	**Coded Bits/6 OFDM Symbol (N_{CBP6S})**	**Info Bits/6 OFDM Symbol (N_{IB6S})**
53.3	QPSK	1/3	YES	YES	300	100
80	QPSK	1/2	YES	YES	300	150
106.7	QPSK	1/3	NO	YES	600	200
160	QPSK	1/2	NO	YES	600	300
200	QPSK	5/8	NO	YES	600	375
320	DCM	1/2	NO	NO	1 200	600
400	DCM	5/8	NO	NO	1 200	750
480	DCM	3/4	NO	NO	1 200	900

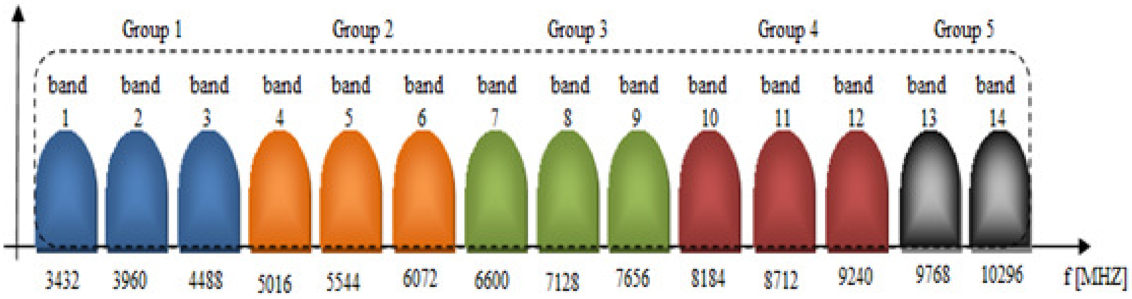

Figure 3. UWB spectrum bands in the MB-OFDM solution

2.2. The SV/ IEEE 802.15.3a Channel Model

Since UWB channels take a some special propagation process and models which possess considerable difference with the conventional narrowband models, many investigation on the propagation and the channel models for UWB signaling have been delivered since the late 1990s [14].

The implementation of system simulation requires the use of model taking into account the effect of the channel on the link [15]. To study MBOFDM system, we will interest in the IEEE 802.15.3a broadband model.

The IEEE 802.15.3a channel model was developed from a dozen all contributions based on different experimental measurements, carried out in residential indoor environment or office [16]. The proposed model is a model derived from Saleh and Valenzuela (SV) model [17] for indoor channels that Appropriate with the properties of UWB channels.

The IEEE 802.15.3a model is a statistical model based on the assumption when the multipath components (MPCs) arrive in clusters, formed by the multiple reflections from the objects in the vicinity of receiver and transmitter [18]. a log-normal distribution is used for the multipath gain magnitude. Furthermore, independent fading is appreciated for each cluster and each ray within the cluster. The impulse response of the multipath channel is given by:

$$h(t) = X \sum_{l=0}^{L} \sum_{k=0}^{K} \beta_{k,l} e^{i\theta_{k,l}} \delta(t - T_l - \tau_{k,l}) \qquad (1)$$

Where l is the index of clusters, k is the index of paths within clusters, T_l is the delay of cluster l, $\tau_{k,l}$ is the delay of the k th path cluster l, relative to the arrival time of the first path of T_l cluster, $\beta_{k,l}$ is the amplitude coefficient of the path k in the cluster, $\theta_{k,l}$ is associated with path k in phase of the cluster ($\theta_{k,l} \in [0,2\pi)$) and X is random variable amplitude that follows a log-normal type.

The clusters, as well as the path arrival times, may be modeled according to Poisson random variables processes with different rates and have interarrival times that are exponentially distributed. The MPCs amplitudes follow a log-normal distribution, whereas the corresponding phase angles are a uniform random variable over $[0,2\pi]$.The power decays exponentially with cluster decay likewise as excess delay within a cluster [18].

The UWB system modeling defined four different channel models (CM1 to CM4) each with decay factors and arrival rates selected to match different employment scenarios and to adapt line-of-sight (LOS) and non-line-of-sight (NLOS) cases. The channel models characteristics are presented in following table.

Table 3. IEEE 802.15.3a channel configurations

	CM1	**CM2**	**CM3**	**CM4**
Distance Tx-Rx (m)	< 4	< 4	From 4 To 10	
Situation	LOS	NLOS	NLOS	NLOS
τ_{RMS} (ns)	5.28	8.03	14.28	25

2.3. CP vs ZP in OFDM based System

The use of the guard interval, which it is kind of cyclic prefix or zero-padding, is a clever solution which allows both to remove the ISI and to ensure the absence of ICI at the entrance of the FFT reception. The main advantage of ZP compared to CP for applications UWB that [15] the insertion of the cyclic prefix inserted in the temporal redundancy symbol which causes undulations in the PSD of the transmitted signal [8]. However, the use of zero padding does not provide temporal redundancy, so, PSD signal emitted is flat. Therefore, the ZP enhances the transmission power while maintaining the PSD mask [15] and hence to a longer distance [3]. ZP technique was therefore chosen for UWB applications instead cyclic-prefix.

2.4. Zero-Pad OFDM Signal

Used in the MB-OFDM approach, this technique involves inserting a guard interval of zero at the end of each OFDM symbol. This is called a type suffix-Zero Padding (ZP) [7].

Draws a series of samples is added to the end of each OFDM symbol at the output of the IFFT. The ith symbol ZP-OFDM $s_{zp}(i)$ the output of the transmitter is given by [15]:

$$\mathbf{S}_{zp}(i)=\mathbf{F}_{zp}\mathbf{x}_{N}(i), \qquad (2)$$

With $F_{ZP}=\mathbf{I}zp\ \mathrm{F}_{\mathbf{N}}^{\mathrm{H}}$ où $\mathbf{I}_{zp}=[\mathbf{I}_{N},\mathbf{0}_{N\times D}]^{T}$, P×N is the matrix for adding ZP, $\mathbf{0}_{N\times D}$ is a matrix of N×D zeros. Vector $\mathbf{s}_{zp}(i)$ is a vector of N samples from the time of operation applied to IFFT $x_{N}(i)$ tracking zero samples D. At the receiver input presented in fig.1, expression of the i-th symbol is given by:

$$\mathbf{r}_{zp}(i)= \widetilde{\mathbf{H}}\ \mathbf{F}zp\ \mathbf{x}_{N}(i)+ \widetilde{\mathbf{H}}_{ISI}\,\mathbf{F}_{zp}\,\mathbf{x}_{N}(i-1)+ \tilde{n}_{p}(i). \qquad (3)$$

The intersymbol interference is eliminated by the matrix of zeros $\mathbf{0}_{D\times N}$ of $\mathbf{F}$zp.

Product $\widetilde{\mathbf{H}}_{ISI}\,\mathbf{F}_{zp}$ in last equation is zero. $\widetilde{\mathbf{H}}=[\widetilde{\mathbf{H}}_{0}, \widetilde{\mathbf{H}}zp]$ where $\widetilde{\mathbf{H}}_{0}$ and $\widetilde{\mathbf{H}}zp$ respectively represent firsts N and D Last column $\widetilde{\mathbf{H}}$, This previous equation simplifies to:

$$\mathbf{r}_{zp}(i)=\widetilde{\mathbf{H}}_{0}\,\mathbf{F}_{\mathbf{N}}^{\mathrm{H}}\,\mathbf{x}_{N}(i)+ \tilde{n}_{p}(i). \qquad (4)$$

2.5. Overlap and Add (OLA)

However, unlike the CP-OFDM, the matrix $\widetilde{\mathbf{H}}_{0}$ is not circulating. An additional operation called Overlap and Add to make $\widetilde{\mathbf{H}}_{0}$ circulating is required. It consists to adding the last D samples received, corresponding to the ZP at the beginning of the symbol before the FFT demodulation. This therefore allows restoring the orthogonality between the subcarriers. The vector rzp(i) is split into two distinct parts. Its upper part is defined by dimension $\mathbf{r}_{u}(i)= \widetilde{\mathbf{H}}_{u}\ s_{N}(i)$ of N×1, its lower part is in turn defined by dimension $\mathbf{r}_{l}(i)= \widetilde{\mathbf{H}}_{l}\ s_{N}(i)$ of D×1 with $\widetilde{\mathbf{H}}_{u}$ (respectively $\widetilde{\mathbf{H}}_{l}$) the corresponding matrix of dimensions N×N (respectively D×N) of $\widetilde{\mathbf{H}}_{0}$. N-D zeros are inserted after $\mathbf{r}_{l}(i)$, the resulting vector is added to $\mathbf{r}_{u}(i)$. This amount corresponds to the OLA is given by the following equation:

$$
\begin{aligned}
\mathbf{r}_{\mathrm{N}}(\mathrm{i}) = \mathbf{r}_{\mathrm{u}}(\mathrm{i}) + \begin{bmatrix} \mathbf{r}\mathrm{l}(\mathrm{i}) \\ 0_{(\mathrm{N}-\mathrm{D})\times\mathrm{N}} \end{bmatrix} \\
= \left(\widetilde{\mathbf{H}}\mathrm{u} + \begin{bmatrix} \widetilde{\mathbf{H}}\mathrm{l} \\ 0_{(\mathrm{N}-\mathrm{D})\times\mathrm{N}} \end{bmatrix}\right) \mathbf{s}_{\mathbf{n}}(\mathbf{i}) + \left(\tilde{\mathrm{n}}_{\mathbf{u}} + \begin{bmatrix} \tilde{\mathrm{n}}_{\mathbf{l}}(\mathbf{i}) \\ \mathbf{0}_{(\mathrm{N}-\mathrm{D})\times 1} \end{bmatrix}\right) \\
= \boldsymbol{C}_{\boldsymbol{N}}(\widetilde{\boldsymbol{h}})\boldsymbol{s}_{\boldsymbol{N}}(\boldsymbol{i}) + \widetilde{\boldsymbol{n}}_{\boldsymbol{N}}^{\boldsymbol{zp}}(\boldsymbol{i}) \qquad (5)
\end{aligned}
$$

This equation obtained after the OLA has exactly the same form to the equation with the CP-OFDM except that the OLA colors noise term $\widetilde{\boldsymbol{n}}_{\boldsymbol{N}}^{\boldsymbol{zp}}(\boldsymbol{i})$ slightly. In the same manner as in the case of CP-OFDM, a circulant matrix is diagonalized by then the demodulation FFT.

At the receiver side, ZP removal demand uses of a method called as overlap and add (OLA) so as to capture the channel multipath energy and maintain the orthogonality in the received [2].

ZPS affords a mechanism to minimize the multipath energy and allows both transmitter and a receiver for switching between different frequency bands.

3. PROPOSED DYNAMIC OVERLAP-ADD TECHNIQUE BASED on SNR and CIR ESTIMATE

3.1. Practical Estimation of Dynamic ZPS

We offer methods to decrease the quantity of noise. Which is introduced into the samples during an operation overlap-and-add is used with ZPS. The dynamic operations overlap and add can perform on the fly for each OFDM packet received, using the overlap-and-add length (OLAL) that provide better performance.

In our work that perform multiband OFDM, operations of overlap and add are made when the data is received to overlap and add less than all of the samples of a zero-padded suffix for corresponding samples of symbol information before ZPS.

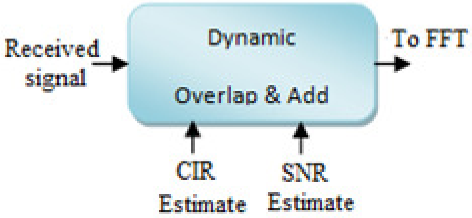

Figure 4. Dynamic OLA based on CIR and SNR estimate

As shown in Figure 1 the receiver comprises dynamic overlap and adding (OLA) receiving an incoming signal. Also dynamic OLA receives a channel impulse response (CIR) estimate and a signal-to-noise-ratio (SNR) estimate.

In this paper, based on the CIR and SNR estimation, OLA dynamically performs activities of overlap-and-add and provides overlap-and-add samples modified and unmodified samples to FFT, OLA also conducts operations of overlap and add when CIR estimate, SNR estimate, or both are absent. Operations of overlap-and-add are portion of a convolution process using additional samples of ZPS to permit the multiplication in the frequency domain for use in forming the desired output. Spectral data extracted from FFT frequency of the incoming signal and outing frequency spectrum data to channel estimator.

The channel estimator defines channel impulse response that is used by the frequency equalizer for removing the frequency shaping produced by the communication channel. The frequency spectrum data equalized to constellation de-mapper by the Frequency equalizer outputs. The frequency equalizer output is received by the constellation de-mapping, that converts the data of the frequency spectrum of the equalized to information symbols whether can be decoded by a decoder.

3.2. OLA Size based SNR and CIR Estimate

Dynamic OLA control (OLAC) which accepts an SNR estimate and CIR estimate. Based on the SNR and CIR estimates or a default value DEFVALM is 24, the OLAC sets the OLA length (OLAL) that is used in the overlap-and-add operation. Then buffer store the current OLAL at a time this new value can be used in the later iteration. Where OLAL value is 32, this number can vary depending upon the system. The following Figure illustrates the process to set the Dynamic OLA size.

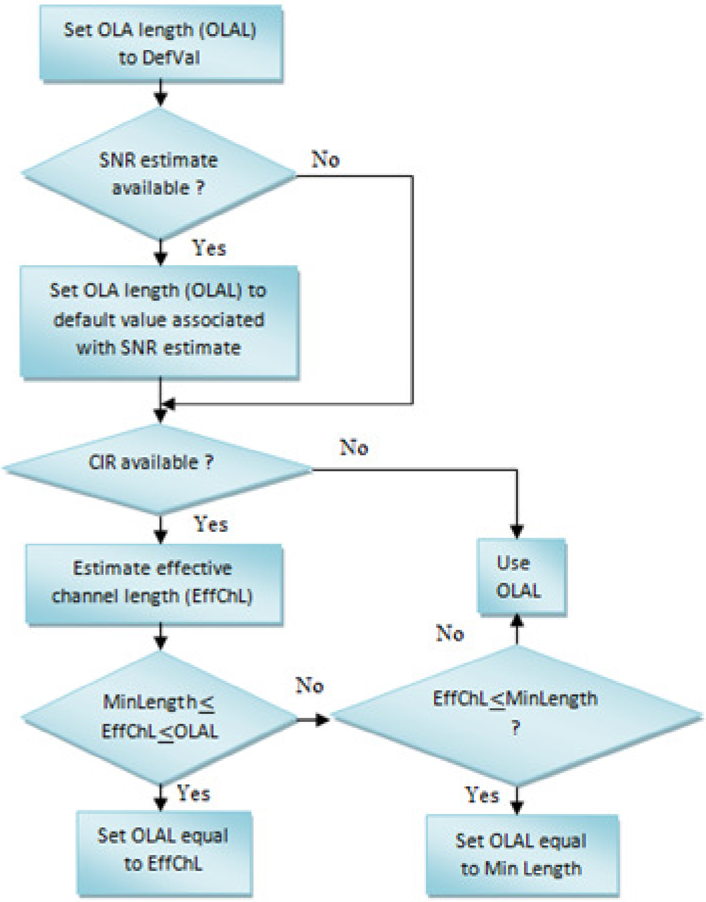
Set OLA length (OLAL) to DefVal
SNR estimate available ?
No
Yes
Set OLA length (OLAL) to default value associated with SNR estimate
CIR available ?
No
Yes
Estimate effective channel length (EffChL)
Use OLAL
No
MinLength≤ EffChL≤OLAL
No
EffChL≤MinLength ?
Yes
Yes
Set OLAL equal to EffChL
Set OLAL equal to Min Length

Figure 5. Process to dynamically evaluate the OLAL length based on the estimated SNR and CIR

OLAC define if an SNR estimate is available for the packet being received, OLAC fix OLAL to a value which correspond to SNR estimate. The SNR assessments are divided into three categories high SNR, medium SNR, and low SNR and each category has a linear correspondence with a value OLAL presented in following table.

Table 4. Evaluate OLAL based on SNR estimate

SNR	OLAL
high	24
Medium	16
Low	8

OLAC then control if the channel impulse response CIR is available. In the first case when an evaluation of CIR is not available OLAC employs OLAL like previously regulated based on the process presented in Figure 5. In the second case When the evaluation of CIR is available, OLAC evaluate the length of channel effective (EffChL). To continue with the process in Figure 5 OLAC determines then if EffChL is equal to or higher than a length minimum of OLA (OALML) and less than or equal to the current value of OLAL.

When EffChl is not higher or equal to a OLA minimal length (OALML) or not lower or equal to the OLAL current value.

OLAC specific if EffChL is less than or equal to OALML. Whenever EffChL is less than or equal to OALML OLAC put OLAL to OALML. When OLAC decide that EffChL is not less than or equal to OALML, OLAC uses the current value of OLAL (i.e.default value, DEFVALM). Exploiting the received CIR and SNR approximates, OLA perform a process like described in Figure 5.

3.3. SNR Estimate based EVM Technique

There are a variety of techniques to produce an assessment of SNR; in our system we chose an EVM technique. Figure 6 illustrate an evaluation of SNR generator based on a vector magnitude metric of error. SNR appreciate generator receive symbol from constellation de-mapper. This SNR set the error distance between the received symbol and their corresponding ideal constellation symbol which is specified by the type of modulation being used. This SNR set the error distance between the received symbol and the symbol of the corresponding ideal constellation that is specified by the type of modulation used. Based on distances from the error, the generator determines an amplitude error vector magnitude (EVM) metric and maps the EVM metric with an estimated SNR and provides SNR approximation.

Generator of estimate SNR produces a more precise estimate SNR by the determination of the metric EVM for the data. Thus, OLAC uses a new more accurate assessment of SNR by performing a process as shown in Figure 5.

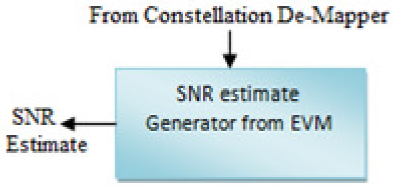

Figure 6. SNR estimation

3.3.1. Error Vector Magnitude

EVM is defined as the value of the root mean square (RMS) of the difference between a collection of symbols measurement and ideal symbols. These differences are averaged over a given symbols. Also these differences are often presented as a percent of the average power per symbols of the constellation. As such EVM can be mathematically given as [19],[20]

$$EVM_{RMS} = \frac{\frac{1}{N}\sum_{n=1}^{N}\left|S_n - S_{0,n}\right|^2}{\frac{1}{N}\sum_{n=1}^{N}\left|S_{0,n}\right|^2} \qquad (6)$$

Where S_n is the nth normalized symbol in the stream of measured symbols, $S_{0,n}$ is the ideal normalized constellation point of the nth symbol and N is the number of unique symbols in the constellation.[19] . The previous equation can be extended by using standardization factors

$$EVM_{RMS} = \left[\frac{\frac{1}{T}\sum_{t=1}^{T}\left|I_t - I_{0,t}\right|^2 + \left|Q_t - Q_{0,t}\right|^2}{\frac{1}{T}\sum_{n=1}^{N}\left[(I_{0,n})^2 + (Q_{0,n})^2\right]}\right]^{\frac{1}{2}} \qquad (7)$$

This is the definition which is now being used as the standard definition of the EVM in IEEE802.11a–1999 T M [21], [22].

3.3.2. Relationship Among EVM and SNR

From last equation, it is evident that EVM is essentially the normalized error magnitude between the measured constellation and the ideal constellation [19].

For Gaussian noise model, also this equation can be simplified in terms of noise in-phase component, $n_{I,t}$ and quadrature component, $n_{Q,t}$ as [19]:

$$EVM_{RMS} = \left[\frac{\frac{1}{T}\sum_{t=1}^{T}\left|n_{I,t}\right|^2 + \left|n_{Q,t}\right|^2}{P0}\right]^{\frac{1}{2}} \qquad (8)$$

Whither P0 is the power of the standardized ideal constellation or the transmitted constellation. The numerator of this equation provides the power of normalized noise. Yet, for T >> N, the noise power normalized ratio to the ideal constellation normalized power can be replaced by non-standard quantities, i.e. likewise this equation rewritten as [19]:

$$EVM_{RMS} \approx \left[\frac{1}{SNR}\right]^{\frac{1}{2}} = \left[\frac{N_0}{E_s}\right]^{\frac{1}{2}} \qquad (9)$$

So as to establish relationship between BER and EVM, SNR in this equation can be expressed in terms of EVM as [19]:

$$SNR \approx \frac{1}{EVM^2} \qquad (10)$$

3.4. CIR Estimation

The receiver contains an estimator for channel which provides a CIR for OLAC.

3.4.1. Cross-correlation

Detector generate CIR estimation a cross-correlation process and the averaging when a packet is received.

With sequence data transmitted represented by x (n), the_sequence data received can be characterized via the following equation:

$$r(n) = \sum_{i=0}^{N-1} x(i-k)h(k) + n(i) \quad (11)$$

With n(i) is additive white Gaussian noise (AWGN) that has variance Γ^2, h(k) is the CIR. whether the sequence data is supposed to have ideal autocorrelation as shown as:

$$\phi\mathrm{xx(m)} = \sum_{i=0}^{N-1} x(i+m)x(i) = \delta(m) \qquad (12)$$

Next, the cross-correlation between the transmitted and received signals will be writen as:

$$\phi\mathrm{rx(m)} = \sum_{i=0}^{N-1} x(i+m)x(i) = \hat{h}(m) \qquad (13)$$

Where $\hat{h}(m)$ is the appreciated CIR. This $\hat{h}(m)$ is approximated on various symbols. These results are averaged and afforded to OLA. In this paper we use this method to estimate CIR.

3.4.2. Least mean square (LMS)

Detector produces a CIR estimate by employing a least means square (LMS) technique in the course of the channel estimation sequence. The LMS approximate may be defined by the following two equations as follows:

$$e_k = r_k - y_k \qquad (14)$$

$$\hat{h}_{k+1} = \hat{h}_{k+}\mu e_k x^*_k \qquad (15)$$

Where e_k is an appreciation error, r_k is the received signal, y_k is the approximation of received signal, x_k is the channel estimation input sequence, and μ is an adaptative step-size.

Monitoring performance and stability of LMS estimation usually depends on the adaptive step size, μ, and would be able to select the step-size that might work for a particular implementation.

3.5. Effective channel length (EffChL)

OLAC estimate the effective channel length by determining the number of coefficients in the CIR estimating magnitude exceeding a threshold value which is X% of the largest magnitude coefficient.

Figure 7 illustrates a channel impulse magnitude response and some of whose coefficients surpass a threshold.

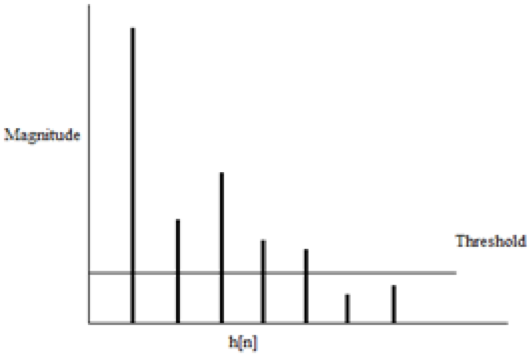

Figure 7. Channel impulse magnitude response

The Figure 8 shows a method for setting a threshold value used to determine the effective channel length.

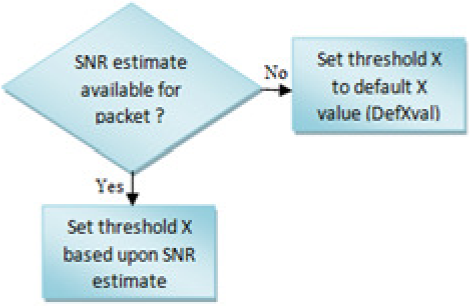
SNR estimate available for packet ?
No
Set threshold X to default X value (DefXval)
Yes
Set threshold X based upon SNR estimate

Figure 8. Setting a threshold value

X is 20% or in our system X is determined based on approximated SNR received by OLAC.
In process OLAC set if an SNR estimate is ready for a packet. In the first case when an estimated SNR is available for a packet, OLAC regulated X to a value based on the approximated SNR. A larger value of X is used for a low SNR value, and vice versa.

Table 4. Evaluate X based on SNR estimate

SNR	X
high	$\leq$ 20
Medium	[20,40]
Low	$\geq$ 40

In the second case when an assessment of SNR is not available for a package, OLAC set X to the default value, in our system, we use the default value of X is 20.

4. SIMULATION RESULTS AND DISCUSSION

The simulation results are obtained using the complete MB-OFDM PHY [9], including forward error correction, TFI, TDS, FDS and DCM. The process to estimate and perform the dynamic OLA length for a given SNR and CIR is illustrated in Figure 5. SNR estimate generates a more accurate SNR by determining the EVM metric for data portion of a packet described in section 3.

When the rate is high, the SNR estimate is high and vice versa. So for high SNR X is less than 20 so the effective channel length (EffChL) is high so the OLAL is high as show in Figure for each channel model for data rate 480 Mbit/s with time frequency code in our case TFC 5 for dynamic OLAL and fixed OLAL is ZP=32 samples.

These simulations use 9000 byte packet transmitted at low rate 53.3 Mbit/s and high rate 480 Mbit/s. It can be seen that the dynamic OLA, based on the simplified process of Figure 5, outperform a fixed OLA of 32 samples in all cases. Since longer channels have more energy in the ZP, the higher order channel models such as CM4 offer high improvement since their optimal OLA size is further than 32 sample maximum. In other words, CM4 channels experience an average improvement of 1.6 dB illustred in Figure 9 wheras CM1cahnnels show no dicernable difference an average gain about 0.4 dB presented in fig ure12 in case of data rate 480 Mbit/s and at BER=10^{-2}.

This confirms an intuitive expectation that dynamic OLA is advantageous in all but extremely long channels.

As discussed previously, the maximum OLA size L can be 32 samples, 37 samples or between the two equal to EffchL. If we compared the result of Figure 9 and Figure 12, we can expect that 25% of CM4 channels would benefit by this technique.

We simulate the performance for MB-OFDM based UWB system with and without dynamic ZP length for overlap and add operation by changing channels, in fact the Figure 9 and Figure 10 and Figure 11 an Figure 12 corresponds respectively to channel model 4,3,2 and 1. For large delay-spread channels presented in Figure 9, the mean excess delay is more compared to small delay-spread channel as shown in Figure 12, the estimation of FFT window will be more away from the true FFT window resulting in more ISI incursions from next OFDM symbol. Hence the proposed technique is more promising for large delay-spread channels, this confirmed by the following simulation result. The curves show a significant amount of performance improvement, for instance in Figure 9, the gain is around 1.6 dB of Eb/No saving at 10^{-2} BER for MB-OFDM system, is achieved for large delay spread channels.

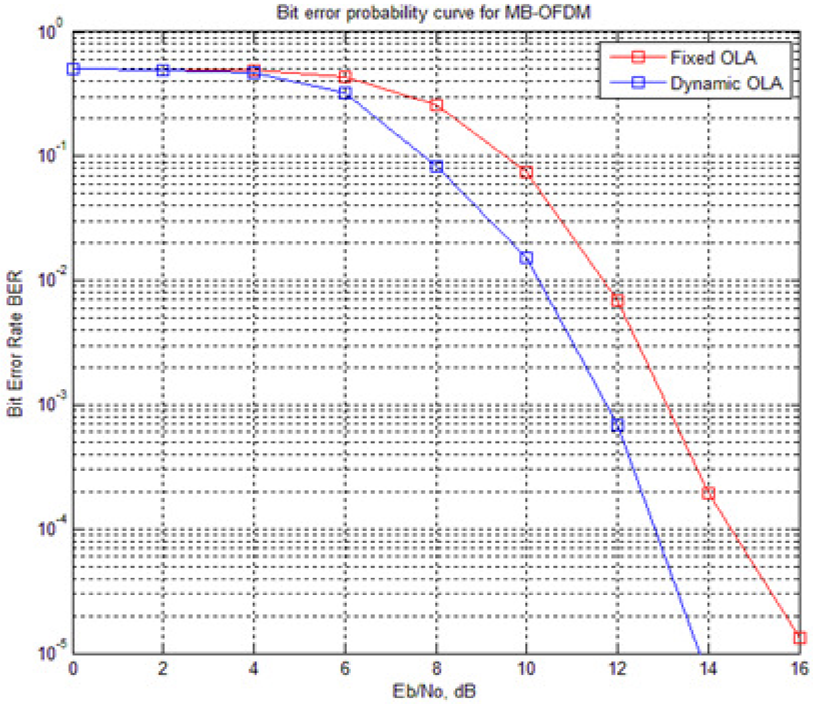

Figure 9. Comparison performance between fixed OLA and Dynamic OLA in the case of CM4 for 480 Mbit/s with TFC

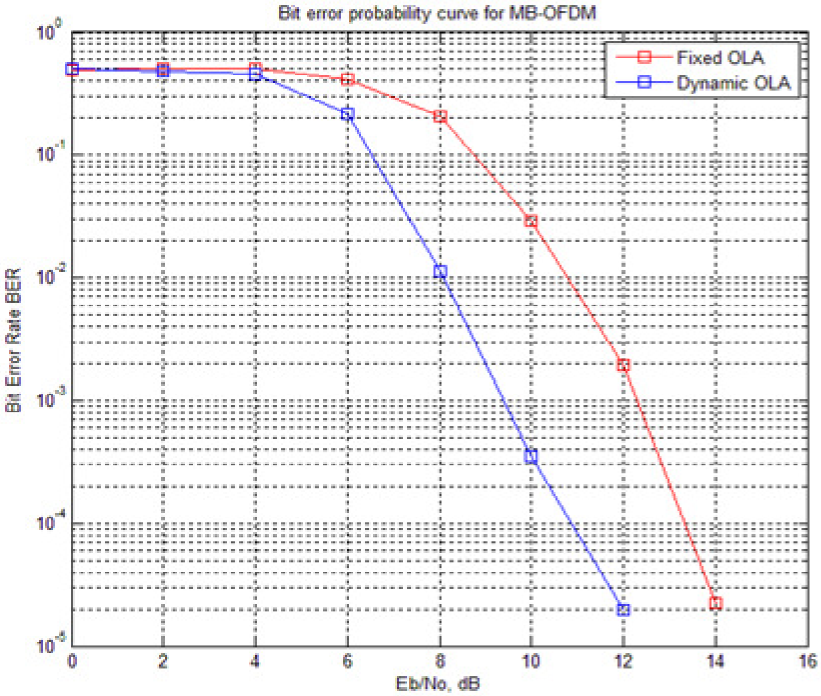

Figure 10. Comparison performance between fixed OLA and Dynamic OLA in the case of CM3 for 480 Mbit/s with TFC

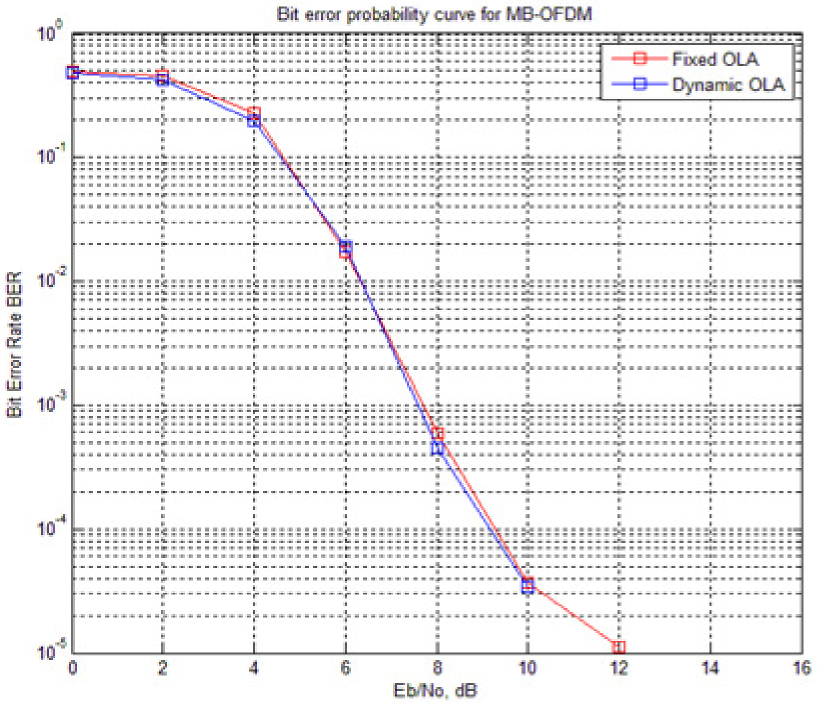

Figure 11. Comparison performance between fixed OLA and Dynamic OLA in the case of CM2 for 480 Mbit/s with TFC

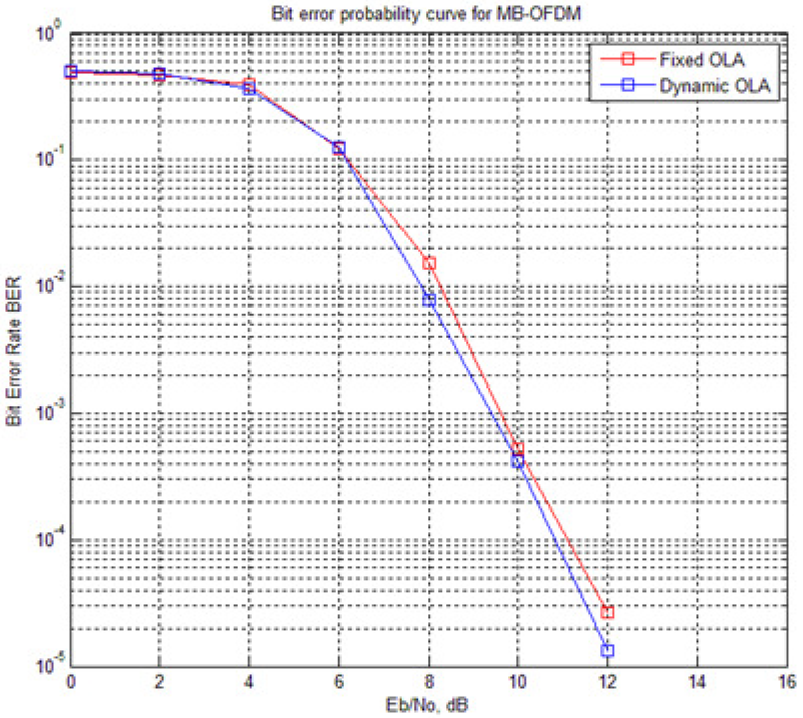

Figure 12. Comparison performance between fixed OLA and Dynamic OLA in the case of CM1 for 480 Mbit/s with TFC

5. CONCLUSION

In this paper, we proposed a method of performing overlap-and-add length dynamically for zero-padded suffixes. This method based on SNR and CIR estimate. Also our technique avoid picking up noise in the OLA process. It is shown that dynamic overlap-and-add technique is important for MBOFDM based receivers in terms of BER performance which tries to minimize ISI. In addition our simulation results indicate that Eb/No can be reduced by around 1.6 dB for the channel CM4 at 10^{-2} BER in multipath channels may be obtained by using dynamic OLA technique. Therefore the method is more promising and fruitful to channels having large delay spread channels(e.g. CM4) and provides a significant Eb/N0 improvement in the detection process.

REFERENCES

[1] K.Siwiakand and D. McKeown, Ultra-wideband Radio Technology. Chichester, England: Wiley and Sons, 2004.

[2] P.Haseena bhanu, C. Venkata sudhakar. Performance Analysis of Aola technique for Wireless communication. International Journal of engineering Trends and Technology (IJETT), May 2013 , Vol.4, n°5, pp. 1893-1898. ISSN: 2231-5381.

[3] P. Srilakshmi, N Gopi Chand. Analaysis and Implementation of UWB Receiver in Multi-Band OFDM systems. International Journal of Modern engineering Research (IJMER), July-Aug. 2012, vol.2, n°4, pp. 2641-2645.

[4] First Report and Order, Revision of Part 15of the Commission's Rules Regarding Ultra-Wideband Transmission Systems, Federal Communications Commission ET Docket 98-153, Feb. 2002.

[5] Saswat Chakrabarti, member, IEEE Adaptive overlap and add technique in MB-OFDM based UWB receiver design.

[6] Dr.R.S.kawitkat performance analysis of UWB system.

[7] B. Muquet, Z. Wang, G. B. Giannakis, M. De Courvilleet P.Duhamel, “Cyclic Prefixing or Zero Padding for Wireless Multicarrier Transmissions? “. IEEE Transaction on Communications, vol. 50, no12, pages 2136–2148, Décembre 2002.

[8] A. Batra, J. Balakrishnan, G. R. Aiello, J. R. Foersteret A.Dabak,” Design of a Multiband OFDM System for Realistic UWB Channel Environ-ments”. IEEE Transaction on Microwave Theory and Techniques, vol. 52, no9, pages 2132–2138, Septembre 2004.

[9] High Rate Ultra Wideband PHY and MAC Standard, ECMA International ECMA-368, Dec. 2005.

[10] Darryn Lowe and Xiaojing Huang,”Adaptative Overlap-Add equalization for MB-OFDM Ultra-wideband”, International Symposium on Communications and Information Technologies (ISCIT’06), Page 644 – 648, October 2006.

[11] Lowe, D & Huang, X, “Adaptive Overlap-Add Equalization for MBOFDM Ultra-Wideband”, International Symposium on Communications and Information Technologies (ISCIT), Bangkok, Thailand, 18-20 October 2006.

[12] A. Batra, et. al, “Multi-band OFDM physical layer proposal,”IEEE P802.15-03/268r0-TG3a, July 2003.

[13] June Chul Ron, Batra. A, and Waters. D, “Adaptive overlap-and-add techniques for MB-OFDM systems,” IEEE Asilomar Conference on Signals, Systems and Computers (ACSSC), Nov. 2007.

[14] Ayman Khalil, Matthieu Crussière and Jean-François Hélard, “Cross-Layer Resource Allocation for MB-OFDM UWB Systems”.

[15] GUÉGUEN Emeric.Etude et optimisation des techniques UWB haut débit multibandes OFDM . thèse de doctorat d’université. Rennes : Institut National des Sciences Appliquées de Rennes, Oct. 2009, 201 p.

[16] Jeff Foerster, “ Channel Modeling Sub-committee Report Final”. IEEE P802.15-02/490r1-SG3a, Février 2003.

[17] A. Salehet R.Valenzuela, “A statistical Model for Indoor Multipath Pro-pagation”. IEEE Journal on Selected Areas in Communications (JSAC), vol. 5,no7, pages 128–137, Février 1987.

[18] A. A. M Saleh and R. A. Valenzuela, “A statistical model for indoor multipath propagation,” IEEE Journal on Selected Areas in Communications, vol. 5, pp. 128-137, Feb. 1987.

[19] Rishad Ahmed Shafik, Md. Shahriar Rahman, AHM Razibul Islam, “On the Extended Relationships Among EVM, BER and SNR as Performance Metrics”. 4th International Conference on Electrical and Computer Engineering, 19-21 December 2006.

[20] S. Forestier, P. Bouysse, R. Quere, A. Mallet, J. Nebus, and L. Lapierre. “Joint optimization of the power-aided efficiency and error vector mea-surement of 20-GHz pHEMT amplifier through a new dynamic bias-control method”. IEEE Transactions on Microwave Theory and Techniques, vol.52(no.4):pp.1132–1140, Apr. 2004.

[21] IEEE, IEEE Standard 802.11b-1999. IEEE Standard for Wireless LAN Medium Access Control (MAC) and Physical Layer (PHY) Specifications: High Speed Physical Layer Extension in the 2.4GHz Band.

[22] IEEE, IEEE Standard 802.11a-1999. IEEE Standard for Wireless LAN Medium Access Control (MAC) and Physical Layer (PHY) Specifications: High Speed Physical Layer in the 5GHz Band.

AUTHORS

Nouri Naziha

Was born in Sousse, Tunisia. She received the M.S degree in Telecommunications engineering in 2007 and the M.Sc. degree in Telecommunications in 2009 from the National Engineering School of Tunis (ENIT), Tunisia.She is currently working toward the Ph.D. Degree in Telecommunication systems at the High School of Telecommunication of Tunis (SUP’com) in the Laboratory research of Innovation of Communication and Cooperative Mobiles (Innov’COM), Tunisia. His current research interests include Wireless Communication, CDMA, MBOFDM and Ultra Wideband Systems.

Bouallegue Ridha

received the Ph.D degrees in electronic engineering from the National Engineering School of Tunis. In Mars 2003, he received the Hd.R degrees in multiuser detection in wireless communications. From September 1990 he was a graduate Professor in the higher school of communications of Tunis (SUP’COM), he has taught courses in communications and electronics. From 2005 to 2008, he was the Director of the National engineering school of Sousse. In 2006, he was a member of the national committee of science technology. Since 2005, he was the Innov’COM laboratory research in telecommunication Director’s at SUP’COM. From 2005, he served as a member of the scientific committee of validation of thesis and Hd.R in the higher engineering school of Tunis. His current research interests include wireless and mobile communications, OFDM, space-time processing for wireless systems, multiuser detection, wireless multimedia communications, and CDMA systems.

EDD CLUSTERING ALGORITHM FOR WIRELESS SENSOR NETWORKS

Awatef Ben Fradj Guiloufi, Salim El Khediri, Nejah Nasri
and Abdennaceur Kachouri

National Engineering School of Sfax, Sfax, Tunisia
benfradj_awatef@yahoo.fr

ABSTRACT

Power consumption is an important metric tool in the context of the wireless sensor networks (WSNs). In this paper, we described a new Energy-Degree (EDD) Clustering Algorithm for the WSNs. A node with higher residual energy and higher degree is more likely elected as a clusterhead (CH). The intercluster and intracluster communications are realized on one hop. The principal goal of our algorithm is to optimize the energy power and energy load among all nodes. By comparing EDD clustering algorithm with LEACH algorithm, simulation results have showen its effectiveness in saving energy.

KEYWORDS

wireless sensor networks (WSNs), clustering, clusterhead, energy, LEACH.

1. INTRODUCTION

A WSNs is a set of nodes called sensors which are able to detect a particular information and to send it to the Base Station (BS). The sensors are inter-connected using a wireless radio communication ([1] ,[2]).

The WSNs are characterized by an absence of infrastructure a resources constraints, an heterogeneity and a dynamics structure. For that, it is important to design an auto-organized virtual topology ([3] ,[4]).

For these virtual topology, several methods were defined in the literature such as clustering algorithm and the dorsal structure [5].

The clustering procedure is to cut the structure in small zones (called cluster) which are managed by a leader called Cluster Head (CH) ([6], [7]).

For clustering method, the WSNs architecture can be presented into three layers: a sensors nodes which are the receivers of the data, the CHs, and the BS [3].

For WSNs, the important metric tool is generally energy consumption (network lifetime) [8]. In fact, the lifetime is a fundamental parameter in the context of availability in the WSNs ([9] ,[10]).

Natarajan Meghanathan et al. (Eds) : NeTCoM, CSIT, GRAPH-HOC, SPTM - 2014
pp. 97–104, 2014. © CS & IT-CSCP 2014 DOI : 10.5121/csit.2014.41308

In this paper, we proposed an energy efficient clustering algorithm called EDD. The objective of this algorithm is to minimize the energy consumption among all nodes. We propose also to compare between the performances of dynamic clustering and static clustering.

The rest of this paper is organized as follows. Section 2 describes the model of the network. Section 3 presents the proposed algorithm. The simulation results are described in the last section.

2. EDD CLUSTERING ALGORITHM

In this section, we define a new clustering algorithm called EDD (Energy-Degree) Clustering Algorithm for WSNs of which the goal is the minimization of the energy consumption and the maximization of network lifetime.

2.1. Energy Consumption Model

The energy consumption is generally the most important parameter for WSNs evaluation phase. It depends in fact on the nodes' characteristics (nature of data processing, transmitted power, standby mode, …), and nodes role during the communication [11].

The consumed energy is defined by this equation [12]:

$$E_{\chi} = E_{c/capture}+E_{c/treatment}+E_{c/communication} \qquad (1)$$

Where:

- $E_{c/capture}$: is the consumed energy by a sensor during the capture unit activation.
- $E_{c/treatment}$: is the consumed energy by the sensor during the activation of its treatment unit.
- $E_{c/communication}$ is the consumed energy by the sensor during the activation of its communication unit.

The consumed power by the communication unit is generally very high than the consumed energy by the treatment unit and the capture unit. In fact, the transfer of one bit can consume as much as the execution of a thousands instructions [13]. For this, we can neglect the consumed energy of the capture unit, and the treatment unit compared to the energy consumed by the communication unit. In this case, the equation (1) will be thus:

$$E_{\chi} = E_{c/communication} \qquad (2)$$

The communication energy is equal to the sum of the emission energy and the reception energy:

$$E_{c/communication} = E_{TX}+E_{RX} \qquad (3)$$

Referring to [14], the transmission the energy and the reception energy can be defined as follows:

$$E_{TX}(K,d) = E_{elec} * K + \varepsilon_{amp} * K * d^{\lambda}. \qquad (4)$$

$$E_{RX}(K) = E_{elec} * K. \qquad (5)$$

Where:

- K: message length (bits).
- D: distance between transmitting node and receiving node (m).

- λ: of way loss exhibitor, λ>=2.
- Eelec: emission /reception energy, Eelec = 50 nJ/bit.
- εamp: transmission amplification coefficient, εamp = 100 pJ/bit/m2

2.2. ClusterHeads election procedure

Step 1: Each sensor transmits a "hello" message to its neighbors, for the discovery of 1-hop neighborhood.

Step 2: Sensors calculate their weights, the weight is defined as follows:

$$\text{Weight}(u) = E_{c/com}(u) + 1/D(u) \qquad (6)$$

Step 3: The sensors distribute their weights to their neighbors.

Step 4: The sensor which has the weakest weight is declared as a CH, it puts its state = "CH" and transmits a message "clusterhead_elected" (containing its ID) to its neighbors.

Step 5: These laters, after receiving this message, declare themselves like "Nm", transmit to the CH a message "clusterhead_accepted", and note the identity of their CHs in their databases.

The EDD clustering algotithm can be described by this organigram:

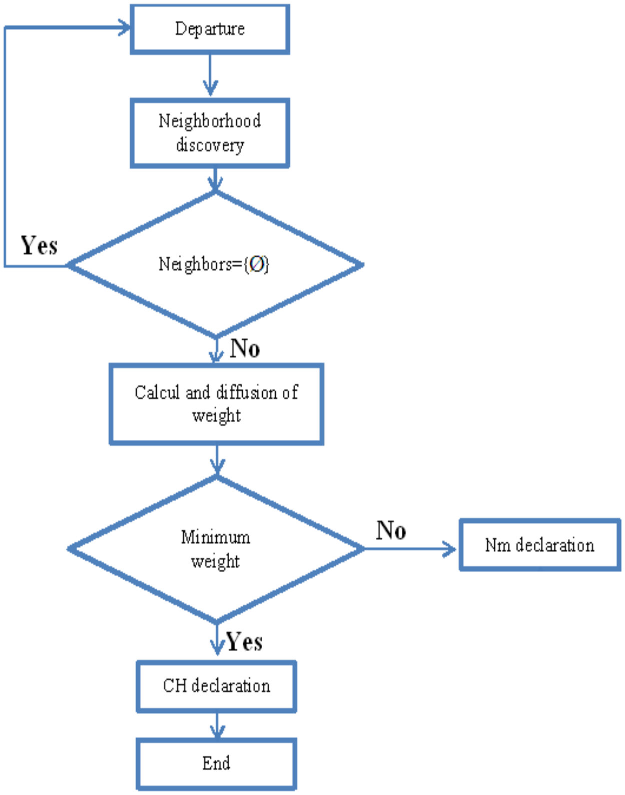

Figure 1. Organigram

2.3. Dynamic clustering VS static clustering

There exist two method of clustering: dynamic clustering and static clustering. For the dynamic clustering, the update of the cluster and CHs is done each round, in the other hands, the change relates to the totality of the structure.

For the static cluster, the cluster are static and for each cluster, the change only relates to CH, in this case, the number of clusters is always the same and CH of each cluster changes according to its properties.

3. SIMULATION RESULTS

The simulation results are implemented using *Matlab 7.0.1* tool. The WSNs is composed of a number of nodes which varies between 10 and 200 nodes.

The simulation of the proposed algorithm was carried out during 10 deactivation intervals T (standby mode) in a space of 150 m × 150 m and the range of the nodes (Tx-Arranges) is 40 m. The size of a measured data package for sensors and send towards their clusterheads is 4000 bits. Fig. 2 shows the communication structure of network with 30 nodes.

In Figure. 2, red o represent the CH, yellow triangle represent the ordinary sensor node, blue lines represent the communication between CH and its members, and black * represent the BS.

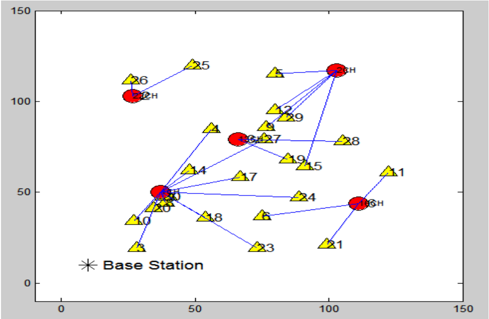

Figure 2. Communication structure of network

Then, we suppose to make a comparison between the dynamic clustering method (DC) and the static clustering method (SC) by applying the proposed clustering algorithm EDD.

Figure.3 represents the control traffic for both method: EDD- DC indicates that the update is done in a dynamic way and EDD- SC indicates that the method of clustering is static.

We notice that the control traffic is higher for the dynamic method, more control packages are transmitted during the cluster construction phase.

For the static method, control packages are transmitted only if there is a CH change procedure. A higher control traffic can represent a cause of energy over consumption, but, the energy consumption for the control traffic is generally negligible than that consumed during the transmission of information.

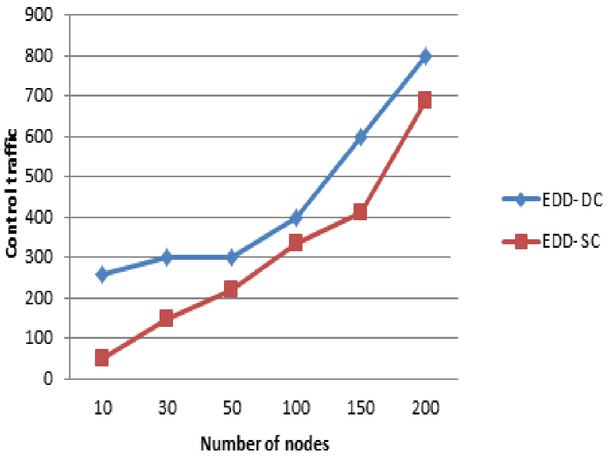

Figure 3. Control traffic

Figure.4 represents the average energy consumption for both methods. We notice that the average energy consumption of the dynamic method is higher, this method consumes more energy during the cluster head election phase and the clusters update phase.

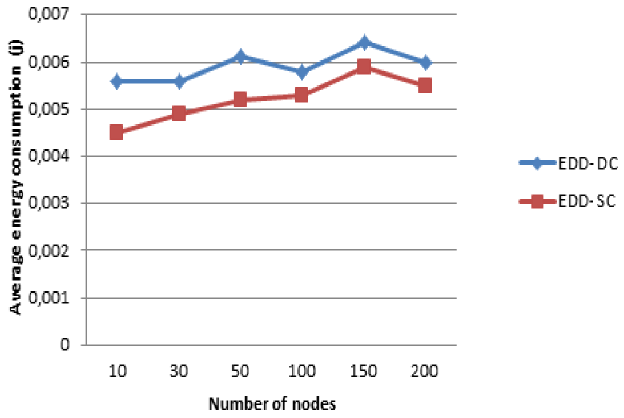

Figure 4. Energy consumption

Figure. 5 represents the first node die for two methods. The best results are given by EDD- DC, this method tends to balance the load of energy consumption between nodes, in this case the network lifetime increases. EDD- SC set up of the static clusters and the update concerne only the CHs. This method can involves the choice of CHs having a weak energy reserve, which results the crushing of its battery.

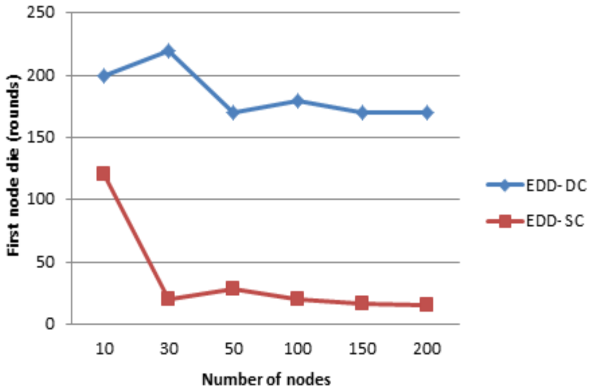

Figure 5. First node die

Among the most known clustering algorithms in literature, we distinguish, LEACH algorithm [8]. LEACH is a famous algorithm which the goal is the minimization of the energy consumption in the WSNs.

We wish in this part to compare our algorithm with the LEACH clustering algorithm. Figure. 6 represents the energy consumption VS the network size. We can note that the values obtained by our algorithm are rather low compared to those obtained by LEACH. These results indicate that our algorithm is more effective and can prolong the network lifetime and ensure its good performance.

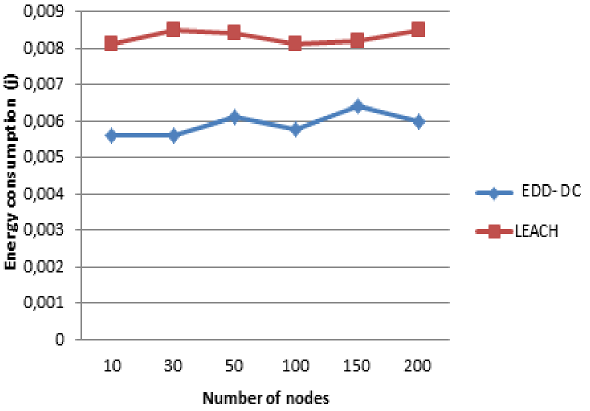

Figure 6. EDD-DC VS LEACH

3. CONCLUSIONS

We presented in this paper a new clustering algorithm for the WSNs called EDD. The principal goal of our algorithm is the prolongation of the network life time, two parameters were taken into account for the choice of CHs: the nodes energy consumption and their degree.

The simulation results show that our algorithm is more effective in energy and increase the network lifetime.

REFERENCES

[1] C. Tidjane Kone, (2011) ‘’Conception de l’architecture d’un réseau de capteurs sans fil de grande dimension,’’PHD, University of Henri Poincaré Nancy I.

[2] G. Chalhoub, (2010) ‘’Les réseaux de capteurs sans fil’’, Ph.D, University of Clermont, Auvergne.

[3] L. Samper, (2008) ‘‘Modélisations et analyses de Réseaux de capteurs’’, PHD, VERIMAG laboratory.

[4] R. Kacimi, (2009)’’Techniques de conservation d’énergie pour les réseaux de capteurs sans fil,’’ PHD, TOULOUSE UNIVERSITY.

[5] M. Khan & J. Misic. (2009) ‘’On the lifetime of wireless sensor networks,’’ ACM Transactions on Sensor Networks (TOSN), Vol, 5, No. 5.

[6] R. Kuntz, (2010) ‘‘Medium access control facing the dynamics of wireless sensor networks, ‘‘PHD, University of Strasbourg.

[7] D. Kumar, D. Trilok, C. Aseri & R. B. Patel, (2009) ‘’EEHC : energy efficient heterogeneous clustered scheme for wireless sensor networks,’’ *Computer Communication.*, Vol. 32, No. 4, pp 662–667.

[8] W. B. Heinzelman, (2000) ‘’Application-specific protocol architectures for wireless networks,’’ PHD, B.S.Cornell University.

[9] Y. Ossama & S. Fahmy, (2004) ‘’HEED : A hybrid energy-efficient distributed clustering approach for ad hoc sensor networks,’’ IEEE Transactions on Mobile Computing, Vol. 3, No. 4, pp 366 – 379.

[10] Duan, Changmin & Hong Fan, (2007) ‘' A distributed energy balance clustering protocol for heterogeneous wireless sensor neworks". In : Proc. Int. Conf. Wireless Communications, Networking and Mobile Computing WiCom. pp. 2469–2473.

[11] V. Raghunathan, C. Schurgers, S. Park & M.B. Srivastava, (2002) ‘’Energy- aware wireless micro-sensor networks,’’ IEEE Signal Processing Magazine, Vol. 19, No. 2, pp 40 –50.

[12] Mitton, Nathalie, Busson, Anthony & Fleury, Eric. (2004) ‘’Self-organization in large scale adhoc networks‘’. In : Mediterranean ad hoc Networking Workshop (Med-Hoc-Net’04). Bodrum, Turquie.

[13] Wendi Rabiner Heinzelman, Anantha Chandrakasan, & Hari Balakrishnan, (2000) “Energy-efficient communication protocol for wireless microsensor networks,” In : Proc IEEE 33rd Hawaii International Conference on System Sciences.

[14] G. J. Pottie & W. J. Kaiser, (2000) ‘’Wireless integrated network sensors,’’ Commun. ACM, Vol. 43, No. 5, pp. 51-58.

AUTHORS

Awatef BENFRADJ was born in Gabes, Tunisia in 1983. She received the engineering degree in Telecommunications and Networks from the University of Gabes, in 2007. In 2009, she obtained the master degree in Networks from Higher School of Communication of Tunisia. Since 2011, she has been a researcher within the laboratory of electronics and information technology, Sfax University.

Salim El Khediri, a Ph.D student at the National School of Engineers of Sfax, Tunisia (Laboratory of Electrical and Information Technology) and in partnership collaboration education with CEDRIC laboratory of CNAM (National Conservatory of Arts and Crafts , Paris). Since 2009 working in the capacity of assistant teacher of computer sciences at the Faculty of Sciences Gafsa – Tunisia.

Nejah NASRI was born in Menzel Bouzaienne Village, in 1981. He received the B.S. and M.S. degrees in electronic engineering from the University of Sfax, in 2006 and the Ph.D. degree in electronic and telecommunication engineering from Toulouse University, France, in 2010. From 2006 to 2009, he was a Research Assistant with Higher Institute of Computer and Communication Techniques (ISITCom), Hammam Sousse, Tunisia. Since 2010, he has been an Assistant Professor with the Informatics Engineering Department, Gafsa University. He is the author of more than 50 articles. His research interests include engineering of wireless sensors networks and wireless underwater communication.

Abdennaceur KACHOURI was born in Sfax, Tunisia, in 1954. He received the engineering diploma from National school of Engineering of Sfax in 1981, a Master degree in Measurement and Instrumentation from National school of Bordeaux (ENSERB) of France in 1981, a Doctorate in Measurement and Instrumentation from ENSERB, in 1983. He “works” on several cooperation with communication research groups in Tunisia and France. Currently, he is Permanent Professor at ENIS School of Engineering and member in the “LETI” Laboratory ENIS Sfax

VIDEOCONFERENCING WEB APPLICATION FOR CARDIOLOGY DOMAIN USING FLEX/J2EE TECHNOLOGIES

Imen Debbabi and Ridha Bouallegue

Innov'COM Research laboratory, University of Carthage, Tunis, Tunisia.
debbabi.imen@gmail.com
ridha.bouallegue@gnet.tn

ABSTRACT

The recent advances in computer technology and data networking have made videoconferencing system a popular medium for users to interact with one another from remote locations. This system offers communication between more than two users, who are able to interact through their webcams, microphone and other components. The use of this system has been increased recently due to many reasons, for one thing, progress in Internet access in different networks like companies, universities and houses, with the increase of available bandwidth whereas the decrease of delay in sending and receiving packets . On the other hand, the coming of Rich Internet Applications (RIA) means that a large part of web application started to be implemented on the web browsers. This paper discusses the conception of multiparty videoconferencing systems using technologies of Web 2.0. For our conceptual Videoconferencing Platform, we have developed many feature : live audio video, text chat, video recording, user and room management and quality control. Videoconferencing modules have been carried out using open source technologies Flex and J2EE.

KEYWORDS

Videoconferencing System, RIA, web2.0, Flex, Red5, J2EE .

1. INTRODUCTION

Telemedicine is defined as the use of telecommunication and information technologies in order to provide clinical health care at distance. It helps eliminate distance barriers and can improve access to medical services that would often not be consistently available in distant rural communities using two-way videos, emails, smart phones, wireless tools and other forms of telecommunication technology [1].

It may be as simple as two health professionals discussing medical problems of a patient and seeking advice from over a simple telephone to more complex transmission of electronic medical records of clinical information, diagnostic tests such as E.C.G, radiological images etc . and carrying out real time interactive medical video conference with the help of Information Technologies.

This paper describes a videoconferencing system using open source technologies for a group of cardiologists connected through internet. There may be a situation where a cardiologist in a remote hospital may need to contact an expert to take his advice about a better treatment of a patient. Videoconferencing enables a group of cardiologists to organize meetings, conferences,

Natarajan Meghanathan et al. (Eds) : NeTCoM, CSIT, GRAPH-HOC, SPTM - 2014
pp. 105–117, 2014. © CS & IT-CSCP 2014 DOI : 10.5121/csit.2014.41309

training or other distant meetings while giving the impression of being all present in the same room.

In the recent years, the videoconferencing systems have become more complex due to increasing demands of this type of systems in the internet and the heterogeneity of terminals, such as laptops, mobile phones, tablets, etc with a variety of network access connections including ADSL, cable Modem, Wi-Fi, UMTS, etc. On the other hand, the maturity of multimedia codecs, formats and protocols has become a reality in the last decade. Therefore, a lot of videoconferencing applications and solutions arise every year.

I.debbabi and al**. [2]** give a survey of the videoconferencing standards and videoconferencing solutions and compare them. These systems are provided in two different ways. The first type is the **centralized system.** Generally, drawbacks of the centralized system are not scalable and the operations of the MCUs (Multipoint Conference Unit) are very complex and expensive. The outgoing bandwidth of the server is shared by all the concurrent participants. Specifically, the more clients there are, the lesser the bandwidth each participant can have. The more expensive multipoint control units are capable of handling more connections, the faster data transfer rate is and the more participants can be displayed on the video screen at one time. In addition, MCU requires a higher bandwidth to disseminate a single video signal among participants. The second kind of videoconferencing system is the ***multicast videoconferencing system***. It is often free of charge and easy to install and use, although quality cannot be guaranteed.

In the traditional systems, videos, audios and document information encoding, decoding and transfer are implemented by the developers, which makes the systems more difficult to be developed, and the deployment and maintenance more expensive. These Desktop applications have a difficult installation, maintenance and access flexibility for many reasons like the increasing number of clients with different hardware and operating systems. Web developers have always tried to build one type of client which is richer, more powerful and sensitive and have more interesting visual characteristics than the traditional HTML. The appearance of RIA technology makes it possible to deploy rich client program as easily as to use the web on the Internet.

In this paper, we present a technical overview of technologies for Rich Internet applications, Red5 Media Server, J2EE framework and Flex technologies .We also present architecture of videoconferencing system using these technologies. The remainder of this paper is organized as follows: Section 2 presents some technologies of RIA .Section 3 presents the design of our system. In Section 4, we present the realization of the system. Section 5 describes the conclusion and future work.

2. TECHNICAL OVERVIEW

2.1 Technologies for Rich Internet application

The term ”Rich Internet Applications” was introduced in a Macromedia whitepaper [3] to designate a unification of desktop and traditional Web applications whose goal is to take the advantages of both architectures and overcome their disadvantages. “Macromedia “define RIAs as combining the best user interface functionality of desktop software applications with the broad reach and low-cost deployment of the web applications and the best of interactive multimedia communication.

Typically, a RIA is a web application running in a web browser as part of a web site and is loaded by the client along with some initial data, then it manages the data rendering and event processing, communicating with the server only when the user requires further information or must submit the data. However, this type of application shares several characteristics like a rich user experience and complex user interfaces with traditional desktop applications, and can be accessed using only the web browser with the use of JavaScript; via a browser plug-ings or sandboxes. It forces the users to install a plug-in before launching the application. Once installed, the application runs inside a sandbox delivered within the plug-in.

Before viewing a list of Rich Internet Application frameworks, we should know that a framework is a collection of software libraries providing an application programming interface (API), which provides generic functionality that separates them from other normal libraries.

In the case of RIAs, there is an extensive list of software frameworks that can be useful in different contexts, with different programming languages and operating systems. The vast majority of frameworks are intended to run over almost all the operating systems.

These Frameworks are Adobe Flash, Microsoft Silverlight, Oracle Java FX, AJAX or HTML5. They have to be installed on clients that are going to run these applications.

Many studies regarding the installation made depict the market penetration and global usage comparing different technologies. They show that Adobe Flash, Microsoft Silverlight and Java are installed in more than 60% of machines.

2.1.1 Adobe Flash Player

Adobe Flash (formerly Macromedia Flash) is a multimedia platform used to add animation, videos, and interactivity to web pages. Flash is frequently used for advertisements and games. More recently; it has been positioned as a tool for the Rich Internet Application .It is mainly based on an object-oriented language named ***ActionScript***.

In order to run the Flash content, the users need to install the Flash Player plug-in previously. Nowadays, Flash content may be displayed on various computer systems and devices using Adobe Flash Player, which is free for common web browsers, some mobile phones and a few other electronic devices (using Flash Lite).When Flash Player starts running the application, it manipulates vector graphics to provide animation to various components, like text, drawings, images, and UI objects. It also provides advanced APIs, such as the possibility of manipulating images directly, audios and videos. It supports multimedia streaming applications, such as videos and audios streaming as well as bidirectional multimedia communication and can capture the user’s input via a mouse, a keyboard, a microphone, and a camera.

2.1.2 Real Time Messaging Protocol (RTMP)

The protocol called **Real Time Messaging Protocol** (RTMP) was initially implemented by Macromedia in 2002 and now it is owned by Adobe. It was first used to stream the content across the internet from the servers to the clients which were applications running in a web browser plug-in (Macromedia Flash Player). It was then used to implement web conferences, by accessing the user’s camera and microphone through the same clients, and then sending them using RTMP to send and receive media flows. In 2009, having acquired Macromedia, Adobe decided to publish an open specification of this protocol in [4].

According to those specifications, the RTMP protocol has multiple variations, i.e. the “plain” RTMP protocol; RTMPS which is RTMP over a TLS/SSL connection, RTMPE which is RTMP encrypted using Adobe's own security mechanism, and **RTMPT** which is encapsulated within ***HTTP requests*** to go through firewalls [4].

RTMP works on top of TCP which maintains persistent connections and allows ***low-latency*** communication. It originally follows client-server architecture by defining requests and responses. This protocol splits media streams into fragments and their size is negotiated dynamically between the client and the server. Thus, it transmits as much information as possible with a little overhead.

RTMP defines several virtual channels to provide multiplexing of audios, videos and data sent in the same TCP connection. It defines headers like a timestamp, size of packet, id of the channel, as shown in Fig 1.

AT higher level, RTMP encapsulates MP3, AAC and Speex audio, FLVI and H.264 video, and can make remote procedure calls (RPCS) using a specific format for the representation of the data, named Action Message Format (AMF)[4].

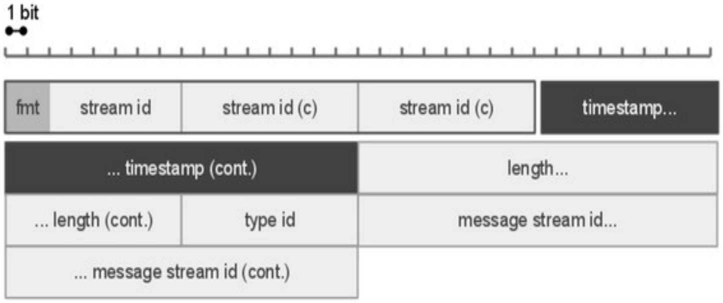

Figure 1 : RTMP packet structure

2.2 Red5 Media Server

The development of Flash-based applications requires the implementation of a centralized Server architecture based on a multimedia server, which redirects all the traffic sent between clients, for example ***Adobe Flash Media Server***. This server is a new platform used for communication between users. It integrates Flash multimedia interactive features, and adds real-time audio, real-time video and real-time data streams and other new features like broadcasting. This server is proprietary media server from Adobe Systems but not free. In this work, we need an open system server. There is an open source technology, called **Red5 Media Server,** which delivers a powerful video streaming and multi-user solution to the Adobe Flash Player and other exciting client technologies [4].

Red5 is an open source software package written in the Java language. Its purpose is to consolidate communication between Adobe flash applications. It offers the same functionality as ***Adobe Flash Server***. It supports live stream publishing, audios and videos streaming, object sharing as well as the recording of streams [6, 7].

By using this platform, you can save recorded audios, videos from a network, share data objects, and transfer the audios, videos and shared data objects with multiple clients. Therefore, it stands as a solid solution for businesses of all sizes, such as enterprises and it is widely used for developing videoconferencing systems, multi-user gaming and enterprise application software.
Red5 includes a support for the latest multi-user APIs such as **NetConnection**, **NetStream** and **SharedObject** while providing a powerful RTMP / Servlet implementation. In addition to

supporting the RTMP protocol, the application server has an embedded Tomcat Servlet container for JEE Web Applications.

In Red5, we developed a browser based videoconferencing application. Here, the client uses Adobe Flash Player to capture videos and audios from players continuous media clips from a web server. This platform integrates communication and application functions, via a flash player on the client, captures and shares audios, videos and data streams. By using Red5 and Flex, we can easily create a real-time communication system, which allows two or more end-users to communicate instantly. For example, we can use the Red5 to easily create video conferencing systems, video telephone system and video chatting systems [6, 7].The system presented here is designed based on Flex. It uses extended UI component library and defines rich user interface on MXML.

Macromedia Flex is a representing server and application program framework, which meets the needs of enterprise-class programmers who hope to develop RIA and run on J2EE. It can run in the application server and provide standard-based, declarative programming methods and processes, run-time services, application integration and management capabilities.

Flex can integrate Java object access or xml using the existing code and information. Furthermore, Flex can also be integrated with some of the existing presentational technology and framework, such as JSP, Struts, etc [8].

In addition, it deals with procedure logic by using script towards objects, and runs **swf** client program translated by Flex server into Flash Player. Combining with audio, video and some real-time communication technologies, the RIA has highly interactive user experience.

2.3 J2EE Framework

J2EE is a set of specifications, which define the standard for developing multi-tier enterprise applications with Java. This platform provides a complete framework for design, development, assembly, and deployment of Java applications built on multi-tiered distributed application model. This specification defines numerous API services and multiple application programming models for developing applications and integrating them with the enterprise systems as shown in Figure 2.

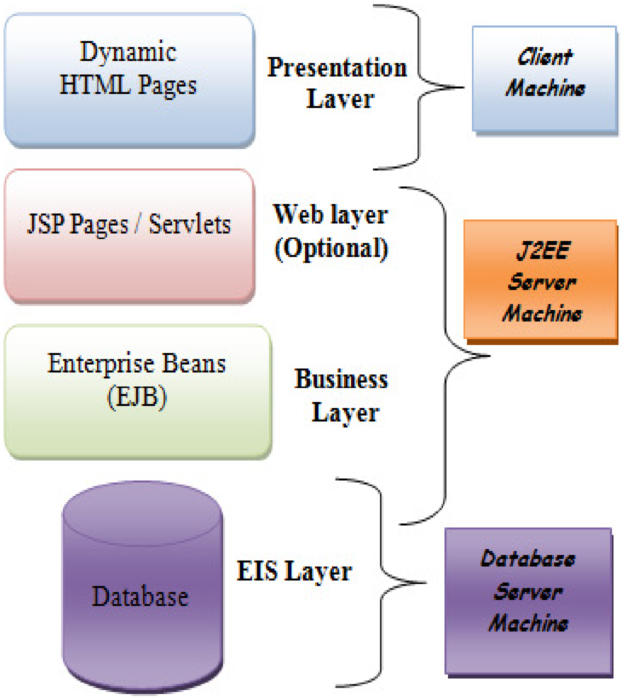

Figure 2: Architecture of J2EE framework

A J2EE application is divided into multiple layers, as seen in Figure 2. Applications can have three or four layers, although most of them only have three [8, 9].

The top layer exists on the client's machine called The ***Presentation Layer***. It consists mainly of interactive webpage interfaces, but occasionally contains some functionality. This layer is responsible for the management of the user's request and for making the corresponding response. Example of the frameworks **is Struts** [9].

The next level is the Web tier. This level may contain Java Server Pages (**JSPs**) and s**ervlets**, which dynamically handle requests to the server. The Web tier is usually excluded, in which case the Client tier interacts directly with the ***Business layer***. This latter layer holds the enterprise beans, which retrieve and process the data from the database.

This layer is responsible for dealing with application procedure business logic and business checking, and responsible for the management services .An example of this framework is **Spring[9]**.

Finally, the Enterprise Information System (EIS) layer is the database in which the information is stored. This layer is responsible for building a relationship between the java domain objects and the database tables. An example of this framework **is Hibernate** [9].

The Business layer is responsible for dealing with application procedure's business logic and business checking, and responsible for the management services. An example of this framework is **Spring**.

2.4 Integration of Flex and J2EE

Prior to the release of Flex, J2EE developers could tightly integrate their middleware with a Flash-based client by using the Flash Remoting technology. This was introduced by one of the authors in **the Macromedia Press title Reality J2EE—Architecting for Flash MX.**

As shown in Fig.3, Flex is integrated in the Presentation Layer. Flex communicates with the **Business Layer** through the AMF gateway. The advantage of this model is that it can quickly and conveniently integrate the Flex into the existing J2EE framework without affecting the original structure [8].

Introducing Flex into data services will affect the performance of Flex. Flex offers several ways to send data: calling the Java classes loaded in Flex classpath; sending a request to the web proxies service or HTTP server [8]. Flex data services can be divided into Web Service Agent, remote object proxy and HTTP services, etc. Two better choices are the XML of HTTP Service and AMF's Remote Object [8].

In this framework, a statement which appeared in the Flex page announces that a Remote object (FlexFacade type) run on the server-side. Flex is responsible for the data transfer between Flex pages and Java objects. We need to define a corresponding method in an object when the Java method is necessary in all the Flex pages which will call the corresponding method in Flex Facade object, and then the method will call the Java method which realizes the business logic in the background [8].

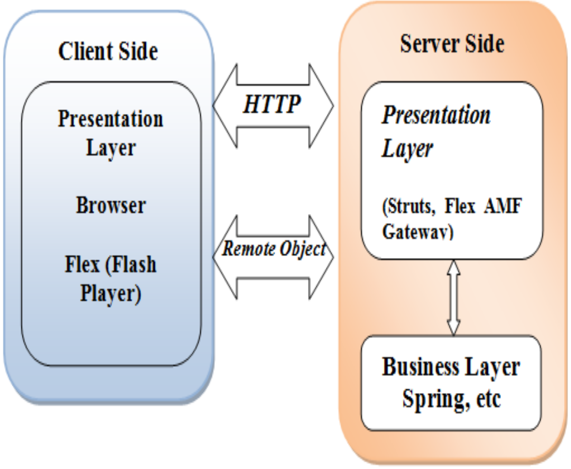

Figure 3: Integrable framework of Flex/Struts

3. SYSTEM DESIGN

3.1 Design of Videoconferencing system

In recent years, more and more multimedia conference systems have been deployed on the Internet. A typical Videoconferencing System has the following functionalities : Live Audio / Video, Text Chat and Video Recording .Firstly, the live audio / video tool supports multiple video displays, showing the video streams from the cameras focusing on the different remote cardiologists. Next, the Text Chat facilitates chatting amongst cardiologists sitting in remote place. Finally, the video Recording helps automatically record and save all the videos in a central archive, where cardiologists can access them conveniently when they need to review them.

Our videoconferencing prototype has four main modules as demonstrated in Fig. 4.

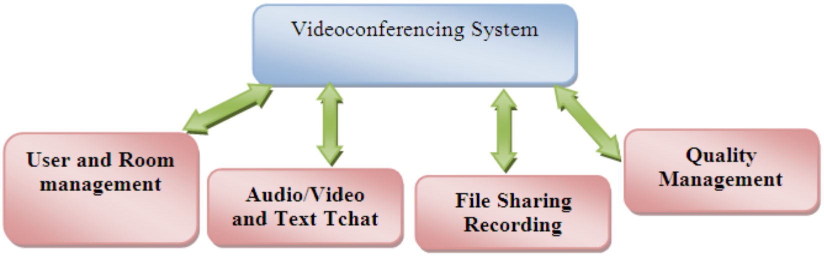

Figure 4: Prototype Videoconferencing System

- **Audio/Video and Text Tchat Module:** This module captures the videos, relays it to the receiver's end to enable cardiologist sitting in remote place chat with one another.

- **File Sharing and Recording Module**: This module helps the users share files and record their video/audio conferencing and text chatting through the internet.

- **User and Room Management Module**: The purpose of this module is the authentication and identification of the registered users. It also facilitates the connection between the user groups for audio/video conferencing.

- **Quality Control Module**: The role of this module is to control the quality of images and audios and capture the videos and relays them to the receiver's end with a desired quality of service.

3.2 Implementation of Videoconferencing system

The architecture of our application is client-server, where a computer interacts with others on the Internet.

As we mentioned earlier, our application consists of three parts: User and Room management developed in Jsp / Servlet / JavaBeans, some for streaming videos developed in Flex (MXML, Action Script) and a portion for controlling a PC remotely with suitable tools like VNC viewer open sources and VNC server.

To do so, we need:

- **On the application server:** ***Apache Tomcat*** is used as an application server for the management of the rooms and users.

- **On the streaming server (Red5)**: It is responsible for disseminating all the information Multimedia (video, micro, slides) to all the participants.

- **On the MySQL database server:** handles the data storage.

- **A thin client**: a web browser (Google Chrome, Firefox ...)

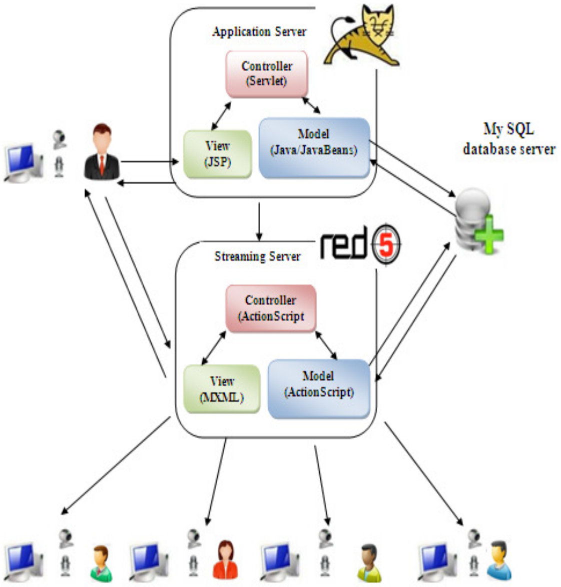

Figure 5: Architecture of application

In the realization of our project, we opted for MVC architecture to provide insurance maintainability, scalability of the application and the speed of development. The Figure 5 shows the architecture of our application.

4. Realization

The implementation of the proposed architecture in this paper has resulted in the provision of a system that consists of a set of classes and methods that we will detail in this section.

4.1 Several important classes and methods

4.1.1 Class Application

Application class contains information about a ***Red5 Server*** application. It maintains this information until the application program is unloaded.

There are several important events in the application class:

- **AppStart:** it is called when the applications are loaded.
- **AppStop:** it is called when the applications are uninstalled.
- **Connect:** it is called when a client connects with the application.
- **Disconnect**: it is called when a client disconnects with the application.

There are several important methods in the class Application:

- **acceptConnection:** it accepts the connection from a client to an application procedure.
- **broadcastMsg**: it announces the news to all the connected clients.
- **disconnect**: it disconnects the connection between the server and the clients.
- **rejectConnection**: it refuses an application to another.

4.1.2 Class NetConnection

NetConnection is used for the management of a two-way connection between Flash Player and red5 Server. It can let you connect to the remote Flash object and red5 Server, while red5 Server allows you to use macromedia Real-Time Messaging Protocol to share audio, video and data information.

4.1.3 Class NetStream

NetStream realizes a data stream connection between Flash Player and Red5 Server. A NetStream object is just like a channel of a NetConnection objects. This channel can, by using the publication method of NetStream object, publish audio and video data, or by using Play() method of NetStream objects, subscribe a pubished flow or data. When necessary, we can also, using NetStream object, publish or broadcast live video and audio information, or play previously recorded video and audio information. There are two important methods in NetStream object: NetStream.attachAudio() and NetStreamattachVideo(). These two methods are essential for the network video call. We can make use of these two methods to bind the audio from the microphone, and the video from the camera with a network stream.

4.1.4 Server-side programming

Service-side scripting can be used to control log-in processes, and control the events in connection Micromedia Flash program which determine the data that the users get from the Flash program. Server-side script file is generally main.asc**.** When the system is running, the file is placed in the Applications directory of the Flash Media Server. Service-side scripting main code is as following:

```
userList=[];
application.onConnect = function(currentClient)
{
application.acceptConnection(currentClient);
currentClient.communicateServer= function(value)
{
currentClient.username=value;
userList.push(value);
trace("The current user list"+userList);
application.broadcastMsg("playOtherVideo",userList);
}
}
```

4.1.5 Client Programming

The release and acceptance of video and audio signals is realized by NetStream object of red5 Server. It mainly constructs a TCP-based connection by using the RTMP agreement, between the client and FMS. A connection can contain several RTMP data circulation channels. When the clients log in video conferencing systems successfully, FMS uses a data flow channel to publish the user's video and audio streams. At the same time, FMS, by using several data flow channels, receives other client user's video and audio stream.

The following is the registered user’ video, audio stream core code, published by FMS.
First of all, the client to establish connection:

```
var RTMP = " rtmp ://localhost:5080/Videoconference" ;
_global.out_nc = new NetConnection () ;
out_nc. connect (RTMP ,PhoneID) ;
var mic = Microphone.get() ;
mic.setRate (11) ;
mic.setUseEchoSuppression (t rue) ;
mic.setSilenceLevel (0 , 0) ;
Publish the audio stream of our side to the user:
outAudio_ns = new NetStream(out_nc) ;
outAudio_ns.attachAudio(mic) ;
```

```
outAudio_ns.publish("Audio" + PhoneID) ;
Publish the video stream of our side to the user:
outVideo_ns =new NetStream(out_nc) ;// New data streams
outVideo_ns.attachVideo (Camera.get()) ;
outVideo_ns.publish("Video" + OutID) ;
Accepting the video stream of other side:
inVideo_ns = new NetStream(out_ nc); // new data streams.
Video_AV.attachVideo(inVideo_ns);//
inVideo_ns.play("Video " + PhotoNum_ mc.CallOutNum) ;
```

4.2 Comparative study and discussions

Traditional video conference systems have problems of development, expensive deployment and maintenance. Flex and Red5 Server provide a new and better solution to develop videos, webcast, MP3 streaming audios, videos conferencing and audio and video chat. This application combines the best user 's interface functionality of desktop software applications with the broad reach and low-cost deployment of Web applications and the best of interactive, multimedia communication.

Among the different applications of videoconferencing proposed in literature we have described only a few examples in this section.

Ponec et al. [11] considered P2P multi-rate multi-party conferencing systems. In a multi-rate setting, different receivers in the same group can receive video at different rates using layered videos. In particular, their study focuses on issues related to multi-rate setting in comparison to the case of single rate videos. It studies the optimal usage of peer uplink capacities of P2P utility maximization in a multi-rate multicast which provides a novel multi-tree formulation.

Nefsis [10] provides dedicated cloud computing resources for video conferencing. The users automatically connect to geographically close servers distributed on the Internet to have a low-latency experience.

We now consider well known, free or commercial conferencing systems such as Skype, Gmail chat and Apple's iChat, and discuss how they address the challenge of Multipoint conferencing. Skype provides multipoint audio conferencing, but video conferencing in Skype is only point-to-point. Recently, the developers have added a group feature which is limited to 5 persons; however, it is not known what the bandwidth requirements are.

GMail chat has a video conferencing module (Google gmail chat), but it works only for two persons. Moreover, it uses a special hardware provided by Vidyo.

Apple's iChat provides multipoint video conferencing; however, one of the peers has to have enough download and upload bandwidth to initiate the conference where it presumably acts as a software MCU (Multipoint Multipoint Control Unit : Apple iChat).

Many other popular online chatting applications (like Skype, Msn, Yahoo, messenger, Google talk, etc.) support multi-party videoconference but they have not a good quality of service therefore, they are not utilizable for professional use like in telemedicine and therefore not considered here.

We have considered Tree applications, of which we list the maximum bandwidth, the delay, the technique of video coding, the maximum number of simultaneous conference participants, and the architecture (S/C or P2P) they belong to Table 1.

From Table 1, we observe that all the applications support only a very limited number of participants and the applications that support more than 10 simultaneous participants,who all use a centralized or P2P network structure.

Table 1 : A comparison of videoconferencing solutions

	Delay in ms	Bandwidth kbps	Number of Video participants	Video coding	Architecture
Ponec and al.,[11]	<100	2000	15	H.264/AVC	Distributed P2P
Nefsis [10]	20	14Mbps	8	-	centralized
Our application	<100	2500	8	-	centralized

We observe that the maximum bandwidth is 14 Mbps which corresponds to cloud computing solutions whereas the second bandwidth is ***2.5 Mbps*** which corresponds to our web application. The solutions based on P2P architecture features of the best bandwidth and the best delay is inferior to ***100 ms***.

3. CONCLUSIONS

Videoconferencing systems have problems of development and expensive deployment. In this paper, we provide a new method using open source technologies based on the Flex and J2EE video conferencing network system to develop a low cost one. It is intended to support consultations for a group of cardiologists connected through the internet.

For future work, Videoconferencing System with 3G and 4G mobile telephony and virtual reality technologies can be developed.

REFERENCES

[1] http://www.americantelemed.org/about-telemedicine/what-is-telemedicine.

[2] I.Debbabi,"A Survey of multimedia videoconferencing system and a proposal for a novel hybrid cloud and P2P architecture". ISSN 22773061. 1641 | Page. Aug 20, 2013.

[3] J. Duhl. White paper: Rich Internet Applications.Technical report, IDC, November 2003.

[4] Adobe Systems Incorporated, Adobe's Real Time Messaging Protocol specification , 21 December, 2012.

[5] http://www.red5.org/

[6] Liu Lu and Dong XiaoGuo, 2010. Red5 flash server analysis and video call service implement-tation. In Proceedings of IEEE symposium on web society, pages 397-400.

[7] X. C. Peng, "The Integration of Flex RIA with J2EE Application," Application Technology and Research, June, 2008, pp. 37-39 (in Chinese).

[9] http:/java.sun.com/j2ee.

[10] http://www.nefsis.co Nefsis. Online: http://www.nefsis.com/How-Multipoint-Conferencing-Works/index-multipoint-video-conferencing.htmlS.

[11] Ponec, M., S. Sengupta, M. Chen, L. Jin and P.A. Chou, 2009. "Multi-rate peer-to-peer video conferencing: A distributed approach using scalable coding. Proceedings of the IEEE International Conference on Multimedia and Expo, Ju. 28-Jul. 3, IEEE Xplore Press, New York, pp: 1406-1413. DOI: 10.1109/ICME.2009.5202767

AUTHORS

Imen debbabi was born in Monastir ,Tunisia, in 1984. She received the B.S. degree in Computer engineering from National Engineering School of Sousse, Tunisia, in 2008, and a master degree of "Intelligent and Communicating Systems "from National Engineering School of Sousse, Tunisisa, in 2010. She is currently pursuing Ph.D degree in Higher School of communication, Tunis, Tunisia. Her research interests include, Multiparty Video Conference and multimedia System .

INTENTIONAL BLANK

ALAMOUTI OFDM/OQAM SYSTEMS WITH TIME REVERSAL TECHNIQUE

Ilhem Blel and Ridha Bouallegue

Innov'Com Laboratory Higher School of Communications,
University of Carthage, Tunis, Tunisia
ilhem.bilel@supcom.tn
ridha.bouallegue@gmail.com

ABSTRACT

Orthogonal Frequency Division Multiplexing with Offset Quadrature Amplitude Modulation (OFDM / OQAM) is a multicarrier modulation scheme that can be considered as an alternative to the conventional Orthogonal Frequency Division Multiplexing (OFDM) with Cyclic Prefix (CP) for transmission over multipath fading channels. In this paper, we investigate the combination of the OFDM/OQAM with Alamouti system with Time Reversal (TR) technique.

TR can be viewed as a precoding scheme which can be combined with OFDM/OQAM and easily carried out in a Multiple Input Single Output (MISO) context such as Alamouti system.

We present the simulation results of the performance of OFDM/OQAM system in SISO case compared with the conventional CP-OFDM system and the performance of the combination Alamouti OFDM / OQAM with TR compared to Alamouti CP-OFDM. The performance is derived by computing the Bit Error Rate (BER) as a function of the transmit signal-to-noise ratio (SNR).

KEYWORDS

OFDM/OQAM, Alamouti, OSTBC, Time Reversal

1. INTRODUCTION

The use of radio communication systems with multiple transmit and receive antennas also referred to as MIMO system can be used to increase capacity. Because of the time-dispersion that occurs in radio mobile communications, the MIMO channel is frequency selective.

OFDM presents the property to convert such a frequency selective MIMO channel into a set of parallel frequency flat MIMO channels. This makes CP-OFDM a suitable scheme to be associated with MIMO.

Standards such as IEEE802.11a have already implemented the CP-OFDM. Other standards like IEEE802.11n combine CP-OFDM and MIMO in order to increase the bit rate and to provide a better use of the channel spatial diversity.

Natarajan Meghanathan et al. (Eds) : NeTCoM, CSIT, GRAPH-HOC, SPTM - 2014
pp. 119–130, 2014. © CS & IT-CSCP 2014 DOI : 10.5121/csit.2014.41310

Nevertheless, CP-OFDM technique causes a loss of spectral efficiency due to the CP as it contains redundant information. Moreover, the rectangular prototype filter used in CP-OFDM has poor frequency localization which makes it difficult for CP-OFDM systems to respect stringent specifications of spectrum masks.

To overcome these drawbacks, OFDM/OQAM was proposed as an alternative approach to CPOFDM. Indeed, OFDM/OQAM does not need any CP, and it furthermore offers the possibility to use different time-frequency well localized prototype filters such as Isotropic Orthogonal Transform Algorithm (IOTA). One of the characteristics of OFDM/OQAM is that the demodulated transmitted symbols are accompanied by interference terms caused by the neighboring transmitted data in time-frequency domain. The presence of this interference is an issue for some MIMO schemes and until today their combination with OFDM/OQAM remains an open problem.

Some interesting researches [1] [2] [3] propose a modification in the conventional OFDM/OQAM modulation by transmitting complex QAM symbols instead of OQAM ones. This proposal allows to reduce considerably the inherent interference but at the expense of the orthogonality condition. Indeed, the data symbol and the inherent interference term are both complex.

Regarding Alamouti coding, some works have been carried out such as [4] where the authors showed that Alamouti coding can be performed when it is combined with code division multiple access (CDMA). A pseudo-Alamouti scheme was introduced in [5] but at the expense of the spectral efficiency since it requires the appending of a CP to the OFDM/OQAM signal. Another solution was proposed in [6] where the Alamouti coding is performed in a block-wise manner inserting gaps (zero-symbols and pilots) in order to isolate the blocks. The main objective of this paper is to analyze and study the combination of OFDM/OQAM technique with Alamouti system using Time Reversal approach.

Firstly experimented in acoustics and ultrasound domains [7] [8] [9], Time Reversal (TR) has also received attention recently for wireless communications [10] [11] [12]. Owing to its inherent time and spatial focusing properties, TR is now studied as a solution for future green wireless communications [12]. Its time focusing property allows having low intersymbol interferences (ISI) at the receiver side.

In fact, TR was highlighted to be suitable for MISO systems as it is simple prefiltering techniques for any number of transmit antennas and leads to low complexity receivers [13]. Moreover, it reduces the delay spread of the channel [14]. However, to achieve good performance in terms of delay spread reduction and spatial focusing TR must be realized either over a large frequency bandwidth or with multiple antennas [15].

Multicarrier systems such as OFDM are commonly used to deal with time-dispersive channels and can be combined with TR to accommodate any residual intersymbol interference.

The combination of TR and OFDM has recently been studied in [11] [12] and has been proven to allow designing of simple and efficient MISO-OFDM systems [16] [17]. In this paper we investigate the combination of Alamouti OFDM/OQAM with TR.

The remaining of this paper is organized as follow: In section II we describe the OFDM/OQAM modulation in SISO case, and we show that the introduction of appropriate pulse shaping can efficiently combat time and frequency distortions caused by the channel. In section III we present the combination of OFDM/OQAM with multiple transmit antennas and especially with classical Alamouti scheme using TR technique. In section IV we provide simulation results, and finally we give the general conclusions in section V.

2. SINGLE-INPUT SINGLE-OUTPUT OFDM-OQAM

The OFDM/OQAM signal in baseband and discrete time for M subcarriers can be expressed, at time kTe, as follows:

$$s_{OFDM/OQAM}[k] = \sum_{m=0}^{M-1} \sum_{n=-\infty}^{+\infty} a_{m,n} \underbrace{f[k - n\frac{M}{2}] e^{j\frac{2\pi}{M}m(k-\frac{LF-1}{2})} e^{j\Phi_{m,n}}}_{f_{m,n}[k]} \tag{1}$$

Where Te denotes the sampling period, $a_{m,n}$ are the real coefficients, f[] is a prototype filter of length LF and $\Phi_{m,n}$ denotes a phase term selected for example equal to $\frac{\pi}{2}(m+n)$. Thus, the OFDM/OQAM modulation overcomes the presence of a guard interval or cyclic prefix thanks to a judicious choice of the prototype filter modulating each subcarrier signal which enables well localization in time and frequency, and which verifies the constraint of real orthogonality between subcarriers resulting in:

$\Re\{\langle f_{m,n}, f_{m',n'}\rangle\} = \Re\{\sum_{k=-\infty}^{+\infty} f_{m,n}[k] f^*{}_{m',n'}[k]\} = \delta_{m,n}\delta_{m',n'}$. Where $\langle g, h\rangle$ denotes the scalar product between g and h. The scalar product $\langle f_{m,n}, f_{m',n'}\rangle$ is a pure imaginary number for $(m,n) \neq (m',n')$. In the following description we use for simplicity the following notation: $\langle f\rangle_{p,q}^{m,n} = -j\langle f_{m,n} f_{p,q}\rangle$.

The prototype filter has to satisfy the orthogonality conditions or at least must be nearly orthogonal. It can be derived directly in continuous-time, as it is the case for instance in [18] with the IOTA filter.

Naturally, the resulting prototype filter has to be truncated and discretized to be implemented. The IOTA prototype filter used in this paper is of length L = 4M and it is denoted by IOTA4. Prototype filters can also be directly derived in discrete time with a fixed length [19]. This is the case of the time frequency localization (TFL) [19] prototype filter. In this paper, it is taken of length L = M and denoted by TFL1.

The block diagram in Figure 1 illustrates our OFDM/OQAM transmission scheme in SISO case. The pre-modulation steps corresponds to a single multiplication by an exponential which argument depends on the phase term Φm,n and on the prototype length. The polyphase block contains the coefficients of the prototype filter. At the receiver side the dual operation are carried out that, at the end taking the real part of the post-demodulator output, allows us to exactly recover the transmitted symbols in the case of a distortion-free channel.

However, in the general case, the propagation channel breaks the real orthogonality condition thus equalization must be performed at the receiver side to restore this orthogonality. Let us consider a channel $\mathrm{h}(\mathrm{t},\tau)$ that can also be represented by a complex-valued number $\mathrm{H}_{\mathrm{m,n}}^{(\mathrm{c})}$ for subcarrier m at symbol time n. At the receiver side, the received signal is the summation of the $\mathrm{S}_{\mathrm{OFDM/OQAM}}$ signal convolved with the channel impulse response and of a noise component. For a locally invariant channel, we can define a neighborhood, denoted $\Omega_{\Delta\mathrm{m},\Delta\mathrm{n}}$ around the (m, n) position, with $\Omega_{\Delta\mathrm{m},\Delta\mathrm{n}} = \left\{(\mathrm{p},\mathrm{q}), |\mathrm{p}| \leq \Delta\mathrm{m}, |\mathrm{q}| \leq \Delta\mathrm{n} \left|\mathrm{H}_{\mathrm{m+p,n+q}}^{(\mathrm{c})}\right| \approx \mathrm{H}_{\mathrm{m,n}}^{(\mathrm{c})}\right\}$

And we also define $\Omega^{*}{}_{\Delta\mathrm{m},\Delta\mathrm{n}} = \Omega_{\Delta\mathrm{m},\Delta\mathrm{n}} - \{(0,0)\}$

Indeed, despite the use of a prototype filter well localized in time and frequency, OFDM/OQAM modulation produced by building an imaginary term of intrinsic interference. For a SISO system, after transmission over a frequency selective channel and additive noise terms noted η, the demodulated signal can be written as:

$$\mathrm{y}_{\mathrm{m,n}} = \mathrm{H}_{\mathrm{m,n}}^{(\mathrm{c})}\left(\mathrm{a}_{\mathrm{m,n}} + \mathrm{j}\mathrm{a}_{\mathrm{m,n}}^{(\mathrm{i})}\right) + \mathrm{J}_{\mathrm{m,n}} + \eta_{\mathrm{m,n}} \tag{2}$$

$\mathrm{H}_{\mathrm{m,n}}^{(\mathrm{c})}$ denotes the value of the complex channel on subcarrier m at time n, $\eta_{\mathrm{m,n}}$ denotes the noise component at time n and subcarrier m, $\mathrm{j}\mathrm{a}_{\mathrm{m,n}}^{(\mathrm{i})}$is a purely imaginary term of intrinsic interference affecting the symbol $\mathrm{a}_{\mathrm{m,n}}$ and dependent on its neighbors symbols at time n given by:

$$\mathrm{a}_{\mathrm{m,n}}^{(\mathrm{i})} = \sum\nolimits_{(\mathrm{p,q}) \in \Omega_{\Delta\mathrm{m},\Delta\mathrm{n}-(0,0)}} \mathrm{a}_{\mathrm{m+p,n+q}} \langle \mathrm{f} \rangle_{\mathrm{p,q}}^{\mathrm{m,n}} \tag{3}$$

And with $\langle f \rangle_{p,q}^{m,n} = -j\langle f_{m,n} f_{p,q} \rangle$.

$J_{m,n}$, the interference term created by the data symbols outside $\Omega_{\Delta m,\Delta n}$, given by [20]:

$$J_{m,n} = j \sum\nolimits_{(p,q) \in \Omega_{\Delta m,\Delta n}} a_{m+p,n+q} H_{m+p,n+q}^{(c)} \langle f \rangle_{p,q}^{m,n} \tag{4}$$

It can be shown that, even for small size neighborhoods, if the prototype functions is well localized in time and frequency, $\mathrm{J}_{\mathrm{m,n}}$ becomes negligible when compared to the noise term $\eta_{\mathrm{m,n}}$.Thus the received signal can be approximated by:

$$\mathrm{y}_{\mathrm{m,n}} \approx \mathrm{H}_{\mathrm{m,n}}^{(\mathrm{c})}\left(\mathrm{a}_{\mathrm{m,n}} + \mathrm{j}\mathrm{a}_{\mathrm{m,n}}^{(\mathrm{i})}\right) + \eta_{\mathrm{m,n}} \tag{5}$$

Based on this approximation, various techniques can then be considered at the receiver side to remove the intrinsic interference term $\mathrm{j}\mathrm{a}_{\mathrm{m,n}}^{(\mathrm{i})}$ in case of a SISO system.

If the channel is known at the receiver side, the estimate of the real transmit symbol can be easily obtained by a simple ZF or MMSE [21] equalization as:

$$\hat{\mathrm{a}}_{\mathrm{m,n}} \approx \Re\left\{\frac{\mathrm{y}_{\mathrm{m,n}}}{\mathrm{H}_{\mathrm{m,n}}^{(\mathrm{c})}}\right\} \approx \mathrm{a}_{\mathrm{m,n}} + \Re\left\{\frac{\eta_{\mathrm{m,n}}}{\mathrm{H}_{\mathrm{m,n}}^{(\mathrm{c})}}\right\} \tag{6}$$

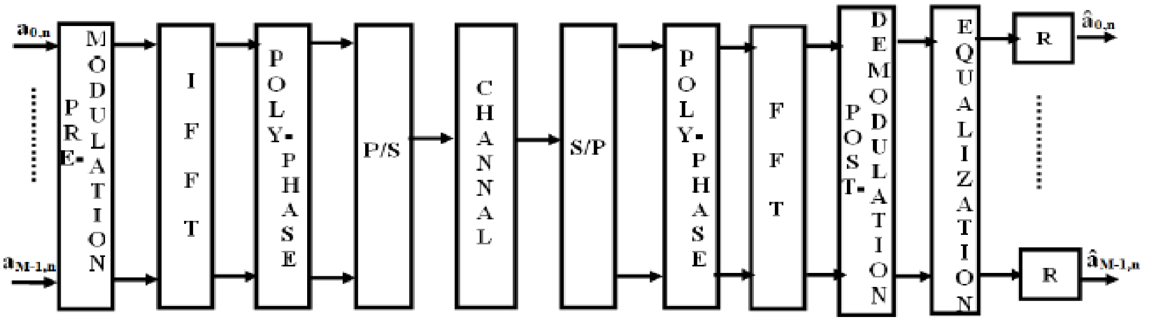

Figure 1. OFDM/OQAM transmission scheme in SISO case

3. ALAMOUTI-OFDM/OQAM WITH TIME REVERSAL

Some works [1][2][3] show that when combining OFDM/OQAM with MIMO techniques such as STBC, the presence of the interference term causes problems and makes the detection process very hard if not impossible.

In this section, we shall propose a new Alamouti-OFDM/OQAM scheme in order to get rid of the inherent interference term. Indeed, we will apply the time reversal technique on the outside of the OFDM/OQAM modulator on each transmission antenna.

TR principles are presented in detail for acoustic and electromagnetic waves in [12] and [13] respectively. Applied to wireless communications, TR consists in prefiltering the signal with the time reversed and conjugated version of the channel impulse response (CIR) between transmit and receive antennas. Without loss of generality, such an operation can be represented in discrete time domain as depicted in Figure 2. In this figure, c[l] is the transmit shape filter, h[l] the discrete complex-baseband CIR, h*[−l] the time reversal filter, and c[l] the so-called equivalent channel obtained by convolving h[l] and h*[−l].

Consequently, in the time domain, c[l] is made of a central peak of high amplitude and some side lobes. For rich propagation environments, a time focusing effect is obtained as the channel autocorrelation peak is getting sharper and narrower and as side lobes are reduced. In other words, TR leads to time dispersion compression, here by reducing the ISI occurring between symbols [14].

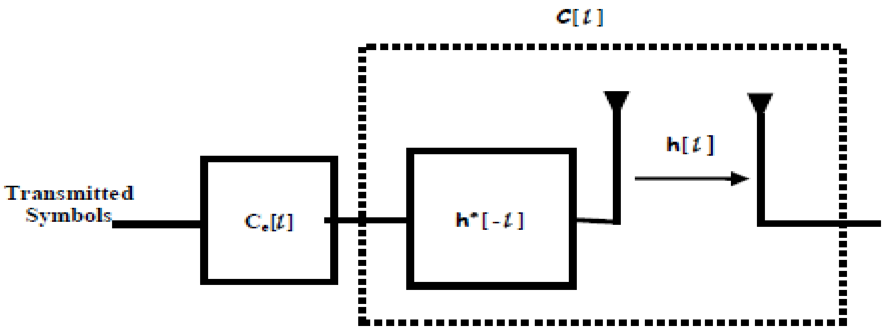

Figure 2. Transmission with Time Reversal technique

If time focusing is sufficiently strong for a given symbol duration, the receiver could merely be reduced to a threshold detector. Nevertheless, for systems exploiting a restricted bandwidth or a limited number of transmit antennas, residual ISI can be efficiently treated through multicarrier approach. The TR and multicarrier approaches can be viewed as complementary and compatible processes applied on the signal before transmission, the former trying to compress the channel time dispersions and the latter accommodating with the residual ISI.

In some preliminary work [16] [17], it has been demonstrated that TR can be applied in an OFDM system either in the time or in the frequency domain. For both implementations, the achieved performance is equivalent.

On that basis, applying TR to an OFDM/OQAM signal amounts to precoding the symbols on each subcarrier by the conjugated channel coefficients. These channel coefficients are obtained from the frequency version of the CIR through a Fourier transform.

More precisely, we proposes to transmit OFDM/OQAM symbols associated with a transmit antenna on an equivalent channel resulting from the convolution of the TR prefilter and the CIR.

Let us suppose that the transmission channel is a frequency selective channel consisting of L paths. We denote h = (h_0,h_1,….,h_{L-1}) the vector of the complex channel coefficients. In the following description, are used indifferently channel coefficients, the temporal impulse response or its transformation in Z to describe and qualify the transmission channel. These various representations are equivalent. It will be the same for the TR prefilter.

These coefficients are distributed according to a centered Gaussian distribution. The transform in Z of the impulse response h(t) of the transmission channel is H(z).

The time reversed from the transmission channel has as a transform $\widehat{H}^*(z^{-1})$ and its impulse response is h *(-t)

The equivalent channel seen by OFDM/OQAM modulation in frequency domain is thus:

$$C(\exp(jw)) = \underbrace{\sum_{l=0}^{L-1} \|h_l\|^2}_{c_0} + 2\sum_{k\neq l} \Re(h_k h_l^*)\cos\big((k-l)w\big) - \Im(h_k^* h_l)\sin((k-l)w)) \tag{7}$$

The equivalent channel is thus a symmetric conjugate channel which central path c0 is a real coefficient. It also appears, in light of the above equations, that because of the symmetry of the coefficients of the equivalent channel, its transform C(z) is a real function. It will be noted that this reasoning is valid for a discrete or continuous representation of the considered channel. This means that the constraint of real orthogonality between the subcarriers verified by the prototype filter is advantageously verified after passing through this equivalent channel since its equivalent frequency response filter is real, even if the transmission channel associated with each antenna is complex. This avoids the generation of an intrinsic interference term purely imaginary difficult to remove such as that generated for a modulation OFDM/OQAM state of the art.

The diagram in Figure 3 illustrates the principal steps of an OSTBC-MISO-OFDM/OQAM transmission scheme with TR technique. In this paper, we consider the Alamouti system with two transmit antennas and one receiver antenna.

Indeed a sequence of bits is transformed into a sequence of real symbols of QAM constellation. Real symbols are then distributed over M subcarriers and two antennas in a step of serial-parallel conversion, so as to form OFDM/OQAM symbols in the frequency domain for each transmit antenna. There is a real symbol a_{nm} associated with the subcarrier m at time n. The real symbols a_{nm} are then coded at OSTBC coding step according its spatial and temporal dimension to generate two sequences of coded symbols for two transmit antennas. Such codes are described in particular in [20] and in [21] for any number of transmit antennas. In this paper, we consider a space-time coding of real symbols a_{mn} distributed over M subcarriers, defined by the following real orthogonal coding matrix GR2:

$$\mathrm{GR2} = \begin{bmatrix} a_{m,n} & -a_{m,n+1} \\ a_{m,n+1} & a_{m,n} \end{bmatrix}$$

Thus, during the OSTBC coding step, the matrix GR2 is applied to each subcarrier m. Thus obtaining two sequences of coded symbols which are then respectively modulated for the two transmit antennas in accordance with the OFDM/OQAM modulation scheme, and then converted according to an operation of parallel-serial conversion carried out independently for each antenna.

Then, for each Txj antenna, j=1,2, the OFDM/OQAM symbols forming coded OFDM/OQAM multicarrier signal S(j) are filtered by a TRj prefilter defined from an estimate transmission channel.

The vector of the coefficients of the TRj prefilter for the transmit antenna Txj are given by: $h^{TR(j)} = (\hat{h}_{L-1}^{(j)\,*}, \hat{h}_{L-2}^{(j)\,*}, \ldots, \hat{h}_{0}^{(j)*})$ where $\hat{h}^{(j)} = (\hat{h}_{0}^{(j)}, \hat{h}_{1}^{(j)}, \ldots, \hat{h}_{L-1}^{(j)})$ is the estimated coefficients of the propagation channel between the transmit antenna Txj and the reception antenna Rx. The resulting multicarrier signal for each antenna is noted:

$$x^{(j)} = s^{(j)} \otimes h^{TR(j)} \qquad (8)$$

Multicarrier filtered signals x(j) are then transmitted over the propagation channel via their respective transmit antennas.

Figure 4 illustrates the principal steps of an OSTBC-Alamouti-OFDM/OQAM reception scheme where the received signal equal to the sum of the received signals from each transmit antenna is:

$$y^{'} = \sum_{j=1}^{N} x^{(j)} \otimes h^{(j)} + \eta \qquad (9)$$

Where η denotes an additive white Gaussian noise.

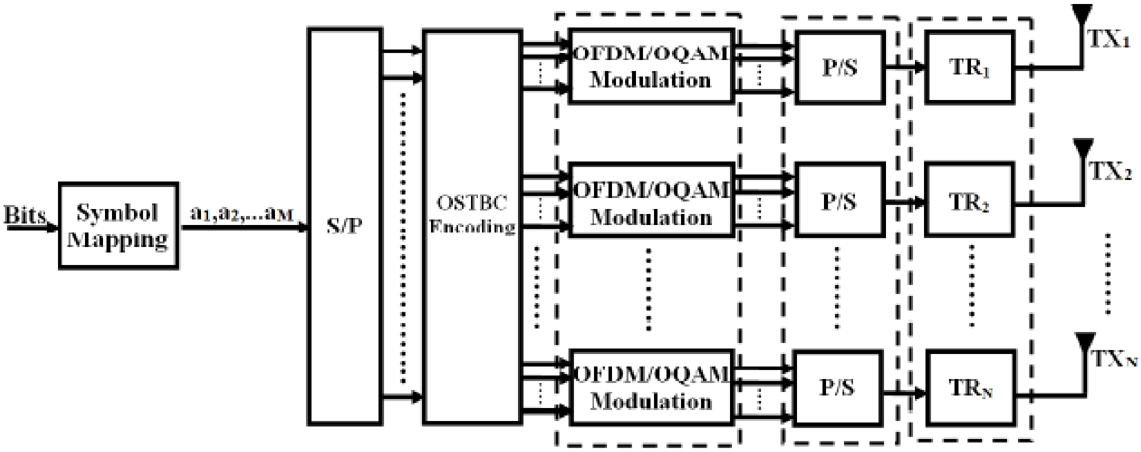

Figure 3. OSTBC-MISO-OFDM/OQAM transmission

The multicarrier signal y', as depicted in Figure 4, are distributed in a serial-parallel conversion of M subcarriers, and then an FFT operation is applied to demodulate OFDM/OQAM symbols.

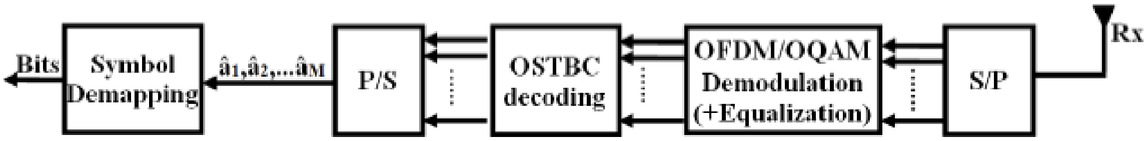

Figure 4. OSTBC-Alamouti-OFDM/OQAM reception scheme

We note HR the equivalent channel obtained by convolution of h^{TR} and h.

With space-time coding GR2 matrix considered previously, the symbols obtained after FFT transformation for each subcarrier m at nT and (n+1)T times are given by the following equations:

$$\begin{aligned} y'_{m,n} &= H^{R(0)}_{m,n} a_{m,n} + H^{R(1)}_{m,n} a_{m,n+1} + \eta_{m,n} \\ y'_{m,n+1} &= -H^{R(0)}_{m,n} a_{m,n+1} + H^{R(1)}_{m,n} a_{m,n} + \eta_{m,n+1} \end{aligned} \tag{10}$$

Where $\eta_{m,n}$ and $\eta_{m,n+1}$ denote the components of the additive white Gaussian noise for the carrier m at time nT. This expression can also be written in matrix form according to the following expression:

$$\begin{bmatrix} y'_{m,n} \\ y'_{m,n+1} \end{bmatrix} = \underbrace{\begin{bmatrix} H^{R(0)}_{m,n} & H^{R(1)}_{m,n} \\ H^{R(1)}_{m,n} & -H^{R(0)}_{m,n} \end{bmatrix}}_{HC} \begin{bmatrix} a_{m,n} \\ a_{m,n+1} \end{bmatrix} + \begin{bmatrix} \eta_{m,n} \\ \eta_{m,n+1} \end{bmatrix} \tag{11}$$

Where HC is an orthogonal matrix. An estimate real symbols $\tilde{a}_{mn}$ is thus obtained from the symbols $y'_{m,n}$ resulting from the FFT using the OSTBC decoding for each subcarrier m. After parallel-serial conversion of the real symbols estimated for each subcarrier, the symbols are converted into bits, in accordance with the selected transmission constellation.

Thus, the principle of TR can advantageously eliminate the intrinsic interferences terms generated by the use of the OFDM/OQAM modulation, including MISO system.

4. SIMULATIONS RESULTS

In this section, we provide the simulation results of the proposed SISO-OFDM/OQAM system and Alamouti-OSTBC-OFDM/OQAM with TR previously presented with two transmit antenna and one receive antenna.

Our simulations have been carried out with sampling frequency fs=10 MHz; FFT size M = 1024; QPSK modulation is used; Prototype filter IOTA4 and TFL1 is used; 3paths with Power profile (in dB):-0,-3,-2.2 and Delay profile (µ s): 0, 0.2527, 0.32 and finally the ZF equalization technique is used.

The simulations are carried out with a discrete-time signal model and prototype filter of finite length, denoted by L. The first prototype filter is a truncated version of IOTA leading a prototype filter containing L = 4M = 4096 taps, designated by IOTA4. We also use another prototype filter that results from a direct optimization, with L = M = 1024 coefficients, of the time-frequency localization (TFL) criterion [17], designated by TFL1.

As usual, the performance is evaluated by a comparison of the Bit Error Rate (BER) as a function of the SNR ratio.

Figure 5 presents the BER performance comparison between OFDM/OQAM and conventional CP-OFDM systems over multipath channels. Results show that OFDM/OQAM outperforms CP-OFDM. This gain corresponds to the no use of CP.

Figure 6 shows the BER performance comparison between OSTBC-Alamouti-OFDM/OQAM with TR and OSTBC-CP-OFDM system over multipath channels. Simulation results confirm that OSTBC-Alamouti-OFDM/OQAM based TR with IOTA4 prototype filter outperforms Alamouti CP-OFDM. But Alamouti CP-OFDM is better than OSTBC-Alamouti-OFDM/OQAM based TR with TFL1 prototype filter.

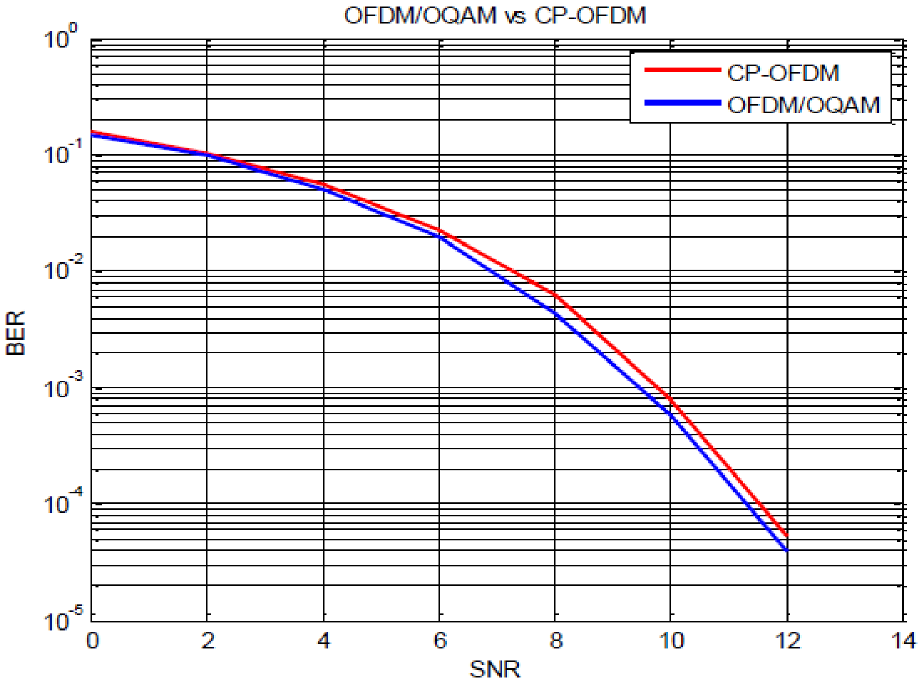

Figure 5. BER performance comparison between OFDM/OQAM and CP-OFDM sytems over multipath fading channel in SISO system

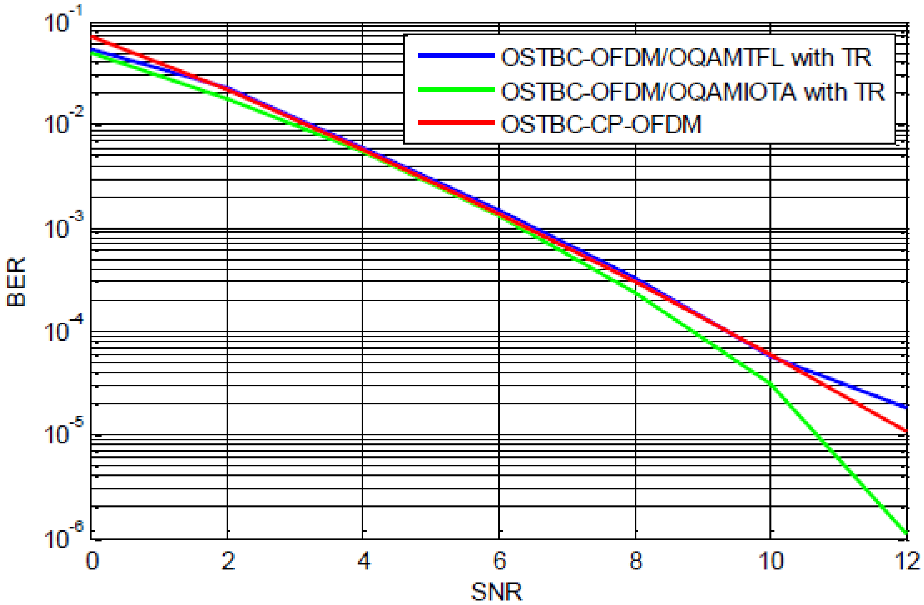

Figure 6. BER performance comparison between OSTBC-OFDM/OQAM with TR and OSTBC-CP-OFDM system with 2×1 Alamouti system

5. CONCLUSIONS

This paper addresses the issue of the association of OFDM/OQAM modulation to OSTBC-Alamouti system using TR technique. OFDM/OQAM in a SISO system is presented. OSTBC-Alamouti-OFDM/OQAM-TR is shown to be very simple as the channel becomes purely real in the frequency domain. The receiver only requires a threshold detector in the case of QPSK symbols. This only comes with a TR prefiltering at the transmitter side.

Simulations results prove that OFDM/OQAM performs better than conventional CP-OFDM thanks to the use of special prototype filter such as IOTA and TFL filter and the no use of cyclic prefix. Moreover, OSTBC-Alamouti-OFDM/OQAM based TR with IOTA prototype filter outperforms the OSTBC Alamouti CP-OFDM.

ACKNOWLEDGMENT

T is work was supported by Innov'Com Laboratory located at Hig er Sc ool of Communications Technological Park of Communications, 2083, Tunis, Tunisia.

REFERENCES

[1] C. Lélé, P. Sio an, R. Legouable, and M. Bellanger "CDMA Transmission with Complex OFDM/OQAM" EURASIP Journal on Wireless Communications and Networking, Article ID 748063, 12 pages, 2008.

[2] R. G arsalla and R. Bouallegue "Comparison between MC-CDMA and CDMA OFDM/OQAM systems in presence of MIMO c annel" IJCSI International Journal of Computer Science Issues, Vol. 9, Issue 4, No 3,2012.

[3] R. Gharsallah and R. Bouallegue "MULTI USER DETECTION FOR CDMAOFDM/OQAM SYSTEM COMBINED WITH SPACE TIME CODING » International Journal of Wireless & Mobile Networks (IJWMN) Vol. 4, No. 4, 2012.

[4] C. Lélé, P. Siohan and R. Legouable "T e Alamouti Sc eme wit CDMA OFDM/OQAM", EURASIP J. Adv. Sig. Proc., vol. 2010.

[5] H. Lin, C. Lélé, and P. Sio an "A pseudo alamouti transceiver design for OFDM/OQAM modulation with cyclic prefix", in Signal Processing Advances in Wireless Communications, 2009. SPAWC '09. IEEE 10t Works op, pp. 300 –304.

[6] M. Renfors, T. I alainen, and T.H. Stitz "A block-Alamouti scheme for filter bank based multicarrier transmission" in Wireless Conference, pp. 1031 –1037, 2010.

[7] M. Fink "Time Reversal of Ultrasonic Fields - Part I Basic Principles." IEEEtran on Ultrasonics, Ferro-electrics, And Frequency Control, 39, 1992.

[8] G.F. Edelmann, T. Akal,W.S. Hodgkiss, Kim.Seongil, W.A. Kuperman, Hee C un Song "An initial demonstration of underwater acoustic communication using time reversal" IEEE Journal of Oceanic Engineering, , vol.27, no.3, pp. 602- 609, 2002.

[9] F. Edelmann, H.C. Song, S. Kim,W.S. Hodgkiss, W.A. Kuperman, T. Akal "Underwater acoustic communications using time reversal," IEEE Journal of Oceanic Engineering, vol.30, no.4, pp.852-864, 2005.

[10] D.Abbasi-Mog adam, V.Vakili "A SIMO one-bit time reversal for UWB communication systems," EURASIP Journal on Wireless Communications and Networking 2012, vol.2012, no.1, pp.1-9.

[11] Y. Wang, J. Coon "Full Rate Ort ogonal Space-Time Block Coding in OFDM transmission Using Time Reversal," WCNC 2009.pp.1-6.

[12] B. Wang, Y. Wu, F. Han, Y.H. Yang, , K.J.R Liu "Green Wireless Communications: A Time-Reversal Paradigm," Selected Areas in Communications, IEEE Journal on , vol.29, no.8, pp.1698-1710, 2011.

[13] R.C. Qiu, Z. C enming, G. Nan, J.Q. Z ang “Time Reversal With MISO for Ultrawideband Communications: Experimental Results,” IEEE Antennas and Wireless Propagation Letters, vol.5, no.1, pp.269-273, 2006.

[14] P. Kyritsi, G. Papanicolaou, P. Eggers, A. Oprea “MISO time reversal and delay-spread compression for FWA c annels at 5 GHz,”IEEE Antennas and Wireless Propagation Letters, vol.3, no.1, pp.96-99, 2004.

[15] T.Dubois, M.Crussière, M. Hélard “On t e use of Time Reversal for digital communications with non-impulsive waveforms,” Signal Processing and Communication Systems (ICSPCS), 2010 4th International Conference, pp.1-6.

[16] T. Dubois, M. Hélard, M. Crussière “ Time Reversal in a MISO OFDM system: Guard Interval design, dimensioning and synchronisation aspects »WWRF29, Berlin, Germany 2012.

[17] T.Dubois, M.Hélard, M.Crussière, C.Germond ” Performance of time reversal precoding technique for MISO-OFDM systems” EURASIP Journal on Wireless Communications and Networking 2013.

[18] B. Le Floch, M. Alard and C. Berrou "Coded Orthogonal Frequency Division Multiplex", Proceedings of the IEEE, Vol. 83, pp. 982-996., 1995.

[19] P. Siohan, C. Siclet and N. Lacaille "Analysis and design of OFDM/OQAM systems based on filterbank theory", IEEE Transactions on Signal Processing 2002, Vol. 50(5), pp. 1170-1183.

[20] C.Lélé “ C annel estimation met ods for preamble-base OFDM/OQAM modulation”European Wireless 2007.

[21] J. Bibby, H. Toutenburg “Prediction and Improved Estimation in Linear Models”, Wiley, New York 1997.

[22] S. Alamouti “ A simple Transmis Diversity Tec nique for Wireless Communications”, IEEE, Journal of Selected Areas Communication, 1998, n°16, pages 1451-1458.

[23] V .Tarokh “Space-time block codes from ort ogonal designs”, IEEE Transactions on Information Theory 1999, vol. 45.

AUTHORS

Ilhem BLEL received the Engineering Degrees from the High School of Communications of Tunis (SUP'COM) in 2007. In Juin 2009, she received the master degree on electronic and telecommunications systems from National Engineer School of Monastir (ENIM). Since January 2009, she has worked as a university assistant in the high Institute of Mathematic and Informatic of Monastir (ISIMM). She is currently working toward the Ph.D. degree in Telecommunications systems at the High School of Communications of Tunis in Innov’Com laboraotory.

Ridha BOUALLEGUE received the Ph.D degrees in electronic engineering from the National Engineering School of Tunis. In Mars 2003, he received the Hd.R degrees in multiuser detection in wireless communications. From September 1990 he was a graduate Professor in the higher school of communications of Tunis (SUP’COM), e as taug t courses in communications and electronics. From 2005 to 2008, he was the Director of the National engineering school of Sousse. In 2006, he was a member of the national committee of science technology. Since 2005, he has been the Innov’COM laboratory researc in telecommunication Director’s at SUP’COM. From 2005, he served as a member of the scientific committee of validation of thesis and Hd.R in the higher engineering school of Tunis. His current research interests include wireless and mobile communications, OFDM, space-time processing for wireless systems, multiuser detection, wireless multimedia communications, and CDMA systems.

ISSUES, CHALLENGES, AND SOLUTIONS: BIG DATA MINING

Jaseena K.U.[1] and Julie M. David[2]

[1,2] Department of Computer Applications,
M.E.S College, Marampally, Aluva, Cochin, India
[1]jaseena.mes@gmail.com,[2]julieeldhosem@yahoo.com

ABSTRACT

Data has become an indispensable part of every economy, industry, organization, business function and individual. Big Data is a term used to identify the datasets that whose size is beyond the ability of typical database software tools to store, manage and analyze. The Big Data introduce unique computational and statistical challenges, including scalability and storage bottleneck, noise accumulation, spurious correlation and measurement errors. These challenges are distinguished and require new computational and statistical paradigm. This paper presents the literature review about the Big data Mining and the issues and challenges with emphasis on the distinguished features of Big Data. It also discusses some methods to deal with big data.

KEYWORDS

Big data mining, Security, Hadoop, MapReduce

1. INTRODUCTION

Data is the collection of values and variables related in some sense and differing in some other sense. In recent years the sizes of databases have increased rapidly. This has lead to a growing interest in the development of tools capable in the automatic extraction of knowledge from data [1]. Data are collected and analyzed to create information suitable for making decisions. Hence data provide a rich resource for knowledge discovery and decision support. A database is an organized collection of data so that it can easily be accessed, managed, and updated. Data mining is the process discovering interesting knowledge such as associations, patterns, changes, anomalies and significant structures from large amounts of data stored in databases, data warehouses or other information repositories. A widely accepted formal definition of data mining is given subsequently. According to this definition, data mining is the non-trivial extraction of implicit previously unknown and potentially useful information about data [2]. Data mining uncovers interesting patterns and relationships hidden in a large volume of raw data. Big Data is a new term used to identify the datasets that are of large size and have grater complexity [3]. So we cannot store, manage and analyze them with our current methodologies or data mining software tools. Big data is a heterogeneous collection of both structured and unstructured data. Businesses are mainly concerned with managing unstructured data. Big Data mining is the capability of

Natarajan Meghanathan et al. (Eds) : NeTCoM, CSIT, GRAPH-HOC, SPTM - 2014
pp. 131–140, 2014. © CS & IT-CSCP 2014 DOI : 10.5121/csit.2014.41311

extracting useful information from these large datasets or streams of data which were not possible before due to its volume, variety, and velocity.

The extracted knowledge is very useful and the mined knowledge is the representation of different types of patterns and each pattern corresponds to knowledge. Data Mining is analysing the data from different perspectives and summarizing it into useful information that can be used for business solutions and predicting the future trends. Mining the information helps organizations to make knowledge driven decisions. Data mining (DM), also called Knowledge Discovery in Databases (KDD) or Knowledge Discovery and Data Mining, is the process of searching large volumes of data automatically for patterns such as association rules [4]. It applies many computational techniques from statistics, information retrieval, machine learning and pattern recognition. Data mining extract only required patterns from the database in a short time span. Based on the type of patterns to be mined, data mining tasks can be classified into summarization, classification, clustering, association and trends analysis [4].

Enormous amount of data are generated every minute. A recent study estimated that every minute, Google receives over 4 million queries, e-mail users send over 200 million messages, YouTube users upload 72 hours of video, Facebook users share over 2 million pieces of content, and Twitter users generate 277,000 tweets [5]. With the amount of data growing exponentially, improved analysis is required to extract information that best matches user interests. Big data refers to rapidly growing datasets with sizes beyond the capability of traditional data base tools to store, manage and analyse them. Big data is a heterogeneous collection of both structured and unstructured data. Increase of storage capacities, Increase of processing power and availability of data are the main reason for the appearance and growth of big data. Big data refers to the use of large data sets to handle the collection or reporting of data that serves businesses or other recipients in decision making. The data may be enterprise specific or general and private or public. Big data are characterized by 3 V's: Volume, Velocity, and Variety [6].

Volume -the size of data now is larger than terabytes and peta bytes. The large scale and rise of size makes it difficult to store and analyse using traditional tools.

Velocity – big data should be used to mine large amount of data within a pre defined period of time. The traditional methods of mining may take huge time to mine such a volume of data.

Variety – Big data comes from a variety of sources which includes both structured and unstructured data. Traditional database systems were designed to address smaller volumes of structured and consistent data whereas Big Data is geospatial data, 3D data, audio and video, and unstructured text, including log files and social media. This heterogeneity of unstructured data creates problems for storage, mining and analyzing the data.

Big Data mining refers to the activity of going through big data sets to look for relevant information. Big data samples are available in astronomy, atmospheric science, social networking sites, life sciences, medical science, government data, natural disaster and resource management, web logs, mobile phones, sensor networks, scientific research, telecommunications [7]. Two main goals of high dimensional data analysis are to develop effective methods that can accurately predict the future observations and at the same time to gain insight into the relationship between the features and response for scientific purposes. Big data have applications in many fields such as Business, Technology, Health, Smart cities etc. These applications will allow people to have better services, better customer experiences, and also to prevent and detect illness much easier than before [8].

The rapid development of Internet and mobile technologies has an important role in the growth of data creation and storage. Since the amount of data is growing exponentially, improved analysis of large data sets is required to extract information that best matches user interests. New technologies are required to store unstructured large data sets and processing methods such as Hadoop and Map Reduce have greater importance in big data analysis. To process large volumes of data from different sources quickly, Hadoop is used. Hadoop is a free, Java-based programming framework that supports the processing of large data sets in a distributed computing environment. It allows running applications on systems with thousands of nodes with thousands of terabytes of data. Its distributed file system supports fast data transfer rates among nodes and allows the system to continue operating uninterrupted at times of node failure. It runs Map Reduce for distributed data processing and is works with structured and unstructured data [6]. This paper is organized as follows. Section 1 gives introduction and Section 2 presents literature review. Section 3 presents the issues and challenges of big data mining. Section 4 provides an overview of security and privacy challenges of big data and Section 5 describes some technologies to deal with big data analysis. Section 6 concludes this paper with summaries.

2. LITERATURE REVIEW

Puneet Singh Duggal, Sanchita Paul, "Big Data Analysis : Challenges and Solutions", international Conference on Cloud, Big Data and Trust 2013, Nov 13-15, RGPV

This paper presents various methods for handling the problems of big data analysis through Map Reduce framework over Hadoop Distributed File System (HDFS). Map Reduce techniques have been studied in this paper which is implemented for Big Data analysis using HDFS.

Chanchal Yadav, Shullang Wang, Manoj Kumar, "Algorithm and Approaches to handle large Data- A Survey", IJCSN, Vol 2, Issuue 3, 2013 ISSN:2277-5420

This paper presents a review of various algorithms from 1994-2013 necessary for handling big data set. It gives an overview of architecture and algorithms used in large data sets. These algorithms define various structures and methods implemented to handle Big Data and this paper lists various tools that were developed for analyzing them. It also describes about the various security issues, application and trends followed by a large data set [9].

Wei Fan, Albert Bifet, "Mining Big Data: Current Status, and Forecast to the Future", SIGKDD Explorations, Volume 14, Issue 2

The paper presents a broad overview of the topic big data mining, its current status, controversy, and forecast to the future. This paper also covers various interesting and state-of-the-art topics on Big Data mining.

Priya P. Sharma, Chandrakant P. Navdeti, "Securing Big Data Hadoop: A Review of Security Issues, Threats and Solution", IJCSIT, Vol 5(2), 2014, 2126-2131
This paper discusses about the big data security at the environment level along with the probing of built in protections. It also presents some security issues that we are dealing with today and

propose security solutions and commercially accessible techniques to address the same. The paper also covers all the security solutions to secure the Hadoop ecosystem.

Richa Gupta, Sunny Gupta, Anuradha Singhal, “Big Data : Overview”, IJCTT, Vol 9, Number 5, March 2014

This paper provides an overview on big data, its importance in our live and some technologies to handle big data. This paper also states how Big Data can be applied to self-organizing websites which can be extended to the field of advertising in companies.

3. ISSUES AND CHALLENGES

Big data analysis is the process of applying advanced analytics and visualization techniques to large data sets to uncover hidden patterns and unknown correlations for effective decision making. The analysis of Big Data involves multiple distinct phases which include data acquisition and recording, information extraction and cleaning, data integration, aggregation and representation, query processing, data modeling and analysis and Interpretation. Each of these phases introduces challenges. Heterogeneity, scale, timeliness, complexity and privacy are certain challenges of big data mining.

3.1. Heterogeneity and Incompleteness

The difficulties of big data analysis derive from its large scale as well as the presence of mixed data based on different patterns or rules (heterogeneous mixture data) in the collected and stored data. In the case of complicated heterogeneous mixture data, the data has several patterns and rules and the properties of the patterns vary greatly. Data can be both structured and unstructured. 80% of the data generated by organizations are unstructured. They are highly dynamic and does not have particular format. It may exists in the form of email attachments, images, pdf documents, medical records, X rays, voice mails, graphics, video, audio etc. and they cannot be stored in row/ column format as structured data. Transforming this data to structured format for later analysis is a major challenge in big data mining. So new technologies have to be adopted for dealing with such data.

Incomplete data creates uncertainties during data analysis and it must be managed during data analysis. Doing this correctly is also a challenge. Incomplete data refers to the missing of data field values for some samples. The missing values can be caused by different realities, such as the malfunction of a sensor node, or some systematic policies to intentionally skip some values. While most modern data mining algorithms have inbuilt solutions to handle missing values (such as ignoring data fields with missing values), data imputation is an established research field which seeks to impute missing values in order to produce improved models (compared to the ones built from the original data). Many imputation methods exist for this purpose, and the major approaches are to fill most frequently observed values or to build learning models to predict possible values for each data field, based on the observed values of a given instance.

3.2. Scale and complexity

Managing large and rapidly increasing volumes of data is a challenging issue. Traditional software tools are not enough for managing the increasing volumes of data. Data analysis, organization, retrieval and modeling are also challenges due to scalability and complexity of data that needs to be analysed.

3.3. Timeliness

As the size of the data sets to be processed increases, it will take more time to analyse. In some situations results of the analysis is required immediately. For example, if a fraudulent credit card transaction is suspected, it should ideally be flagged before the transaction is completed by preventing the transaction from taking place at all. Obviously a full analysis of a user's purchase history is not likely to be feasible in real time. So we need to develop partial results in advance so that a small amount of incremental computation with new data can be used to arrive at a quick determination.

Given a large data set, it is often necessary to find elements in it that meet a specified criterion. In the course of data analysis, this sort of search is likely to occur repeatedly. Scanning the entire data set to find suitable elements is obviously impractical. In such cases Index structures are created in advance to permit finding qualifying elements quickly. The problem is that each index structure is designed to support only some classes of criteria.

4. SECURITY AND PRIVACY CHALLENGES FOR BIG DATA

Big data refers to collections of data sets with sizes outside the ability of commonly used software tools such as database management tools or traditional data processing applications to capture, manage, and analyze within an acceptable elapsed time. Big data sizes are constantly increasing, ranging from a few dozen terabytes in 2012 to today many petabytes of data in a single data set.

Big data creates tremendous opportunity for the world economy both in the field of national security and also in areas ranging from marketing and credit risk analysis to medical research and urban planning. The extraordinary benefits of big data are lessened by concerns over privacy and data protection.

As big data expands the sources of data it can use, the trust worthiness of each data source needs to be verified and techniques should be explored in order to identify maliciously inserted data. Information security is becoming a big data analytics problem where massive amount of data will be correlated, analyzed and mined for meaningful patterns. Any security control used for big data must meet the following requirements:

- It must not compromise the basic functionality of the cluster.
- It should scale in the same manner as the cluster.
- It should not compromise essential big data characteristics.
- It should address a security threat to big data environments or data stored within the cluster.

Unauthorized release of information, unauthorized modification of information and denial of resources are the three categories of security violation. The following are some of the security threats:

- An unauthorized user may access files and could execute arbitrary code or carry out further attacks.
- An unauthorized user may eavesdrop/sniff to data packets being sent to client.
- An unauthorized client may read/write a data block of a file.
- An unauthorized client may gain access privileges and may submit a job to a queue or delete or change priority of the job.

Security of big data can be enhanced by using the techniques of authentication, authorization, encryption and audit trails. There is always a possibility of occurrence of security violations by unintended, unauthorized access or inappropriate access by privileged users. The following are some of the methods used for protecting big data:

Using authentication methods: Authentication is the process verifying user or system identity before accessing the system. Authentication methods such as Kerberos can be employed for this.

Use file encryption: Encryption ensures confidentiality and privacy of user information, and it secures the sensitive data. Encryption protects data if malicious users or administrators gain access to data and directly inspect files, and renders stolen files or copied disk images unreadable. File layer encryption provides consistent protection across different platforms regardless of OS/platform type. Encryption meets our requirements for big data security. Open source products are available for most Linux systems, commercial products additionally offer external key management, and full support. This is a cost effective way to deal with several data security threats.

Implementing access controls: Authorization is a process of specifying access control privileges for user or system to enhance security.

Use key management: File layer encryption is not effective if an attacker can access encryption keys. Many big data cluster administrators store keys on local disk drives because it’s quick and easy, but it’s also insecure as keys can be collected by the platform administrator or an attacker. Use key management service to distribute keys and certificates and manage different keys for each group, application, and user.

Logging: To detect attacks, diagnose failures, or investigate unusual behavior, we need a record of activity. Unlike less scalable data management platforms, big data is a natural fit for collecting and managing event data. Many web companies start with big data particularly to manage log files. It gives us a place to look when something fails, or if someone thinks you might have been hacked. So to meet the security requirements, we need to audit the entire system on a periodic basis.

Use secure communication: Implement secure communication between nodes and between nodes and applications. This requires an SSL/TLS implementation that actually protects all network communications rather than just a subset.

Thus the privacy of data is a huge concern in the context of Big Data. There is great public fear regarding the inappropriate use of personal data, particularly through linking of data from multiple sources. So, unauthorized use of private data needs to be protected.

To protect privacy, two common approaches used are the following. One is to restrict access to the data by adding certification or access control to the data entries so sensitive information is accessible to a limited group of users only. The other approach is to anonymize data fields such that sensitive information cannot be pinpointed to an individual record. For the first approach, common challenges are to design secured certification or access control mechanisms, such that no sensitive information can be misconduct by unauthorized individuals. For data anonymization, the main objective is to inject randomness into the data to ensure a number of privacy goals [10].

5. TECHNIQUES FOR BIG DATA MINING

Big data has great potential to produce useful information for companies which can benefit the way they manage their problems. Big data analysis is becoming indispensable for automatic discovering of intelligence that is involved in the frequently occurring patterns and hidden rules. These massive data sets are too large and complex for humans to effectively extract useful information without the aid of computational tools. Emerging technologies such as the Hadoop framework and MapReduce offer new and exciting ways to process and transform big data, defined as complex, unstructured, or large amounts of data, into meaningful knowledge.

5.1. Hadoop

Hadoop is a scalable, open source, fault tolerant Virtual Grid operating system architecture for data storage and processing. It runs on commodity hardware, it uses HDFS which is fault-tolerant high bandwidth clustered storage architecture. It runs MapReduce for distributed data processing and is works with structured and unstructured data [11]. For handling the velocity and heterogeneity of data, tools like Hive, Pig and Mahout are used which are parts of Hadoop and HDFS framework. Hadoop and HDFS (Hadoop Distributed File System) by Apache is widely used for storing and managing big data.

Hadoop consists of distributed file system, data storage and analytics platforms and a layer that handles parallel computation, rate of flow (workflow) and configuration administration [6]. HDFS runs across the nodes in a Hadoop cluster and together connects the file systems on many input and output data nodes to make them into one big file system. The present Hadoop ecosystem, as shown in Figure 1, consists of the Hadoop kernel, MapReduce, the Hadoop distributed file system (HDFS) and a number of related components such as Apache Hive, HBase, Oozie, Pig and Zookeeper and these components are explained as below [6]:

- HDFS: A highly faults tolerant distributed file system that is responsible for storing data on the clusters.
- MapReduce: A powerful parallel programming technique for distributed processing of vast amount of dataon clusters.
- HBase: A column oriented distributed NoSQL database for random read/write access.
- Pig: A high level data programming language for analyzing data of Hadoop computation.
- Hive: A data warehousing application that provides a SQL like access and relational model.
- Sqoop: A project for transferring/importing data between relational databases and Hadoop.
- Oozie: An orchestration and workflow management for dependent Hadoop jobs.

Figure 2 gives an overview of the Big Data analysis tools which are used for efficient and precise data analysis and management jobs. The Big Data Analysis and management setup can be understood through the layered structured defined in the figure. The data storage part is dominated by the HDFS distributed file system architecture and other architectures available are Amazon Web Service, Hbase and CloudStore etc. The data processing tasks for all the tools is Map Reduce and it is the Data processing tool which effectively used in the Big Data Analysis [11].

For handling the velocity and heterogeneity of data, tools like Hive, Pig and Mahout are used which are parts of Hadoop and HDFS framework. It is interesting to note that for all the tools used, Hadoop over HDFS is the underlying architecture. Oozie and EMR with Flume and Zookeeper are used for handling the volume and veracity of data, which are standard Big Data management tools [11].

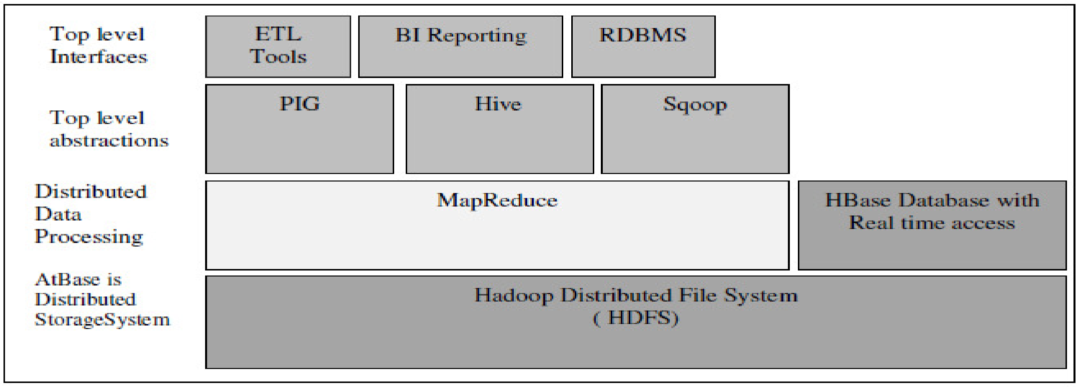
Top level Interfaces
ETL Tools
BI Reporting
RDBMS
Top level abstractions
PIG
Hive
Sqoop
Distributed Data Processing
MapReduce
HBase Database with Real time access
AtBase is Distributed StorageSystem
Hadoop Distributed File System (HDFS)

Figure 1 : Hadoop Architecture Tools

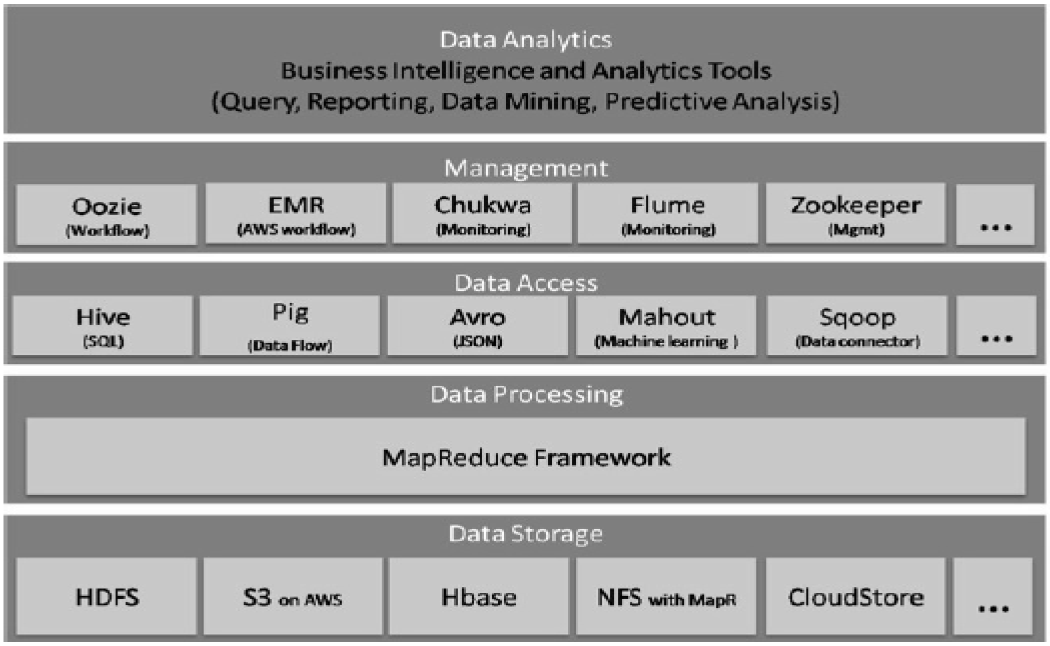

Figure 2: Big data analysis tools

5.2. MapReduce

MapReduce is a programming model for processing large data sets with a parallel, distributed algorithm on a cluster. Hadoop MapReduce is a programming model and software framework for writing applications that rapidly process vast amounts of data in parallel on large clusters of compute nodes [11].

The MapReduce consists of two functions, map() and reduce(). Mapper performs the tasks of filtering and sorting and reducer performs the tasks of summarizing the result. There may be multiple reducers to parallelize the aggregations [7]. Users can implement their own processing logic by specifying a customized map() and reduce() function. The map() function takes an input key/value pair and produces a list of intermediate key/value pairs. The MapReduce runtime system groups together all intermediate pairs based on the intermediate keys and passes them to reduce() function for producing the final results. Map Reduce is widely used for the Analysis of big data.

Large scale data processing is a difficult task. Managing hundreds or thousands of processors and managing parallelization and distributed environments makes it more difficult. Map Reduce provides solution to the mentioned issues since it supports distributed and parallel I/O scheduling. It is fault tolerant and supports scalability and it has inbuilt processes for status and monitoring of heterogeneous and large datasets as in Big Data [11].

6. CONCLUSION

The amounts of data is growing exponentially worldwide due to the explosion of social networking sites, search and retrieval engines, media sharing sites, stock trading sites, news sources and so on. Big Data is becoming the new area for scientific data research and for business applications. Big data analysis is becoming indispensable for automatic discovering of intelligence that is involved in the frequently occurring patterns and hidden rules. Big data analysis helps companies to take better decisions, to predict and identify changes and to identify new opportunities. In this paper we discussed about the issues and challenges related to big data mining and also Big Data analysis tools like Map Reduce over Hadoop and HDFS which helps organizations to better understand their customers and the marketplace and to take better decisions and also helps researchers and scientists to extract useful knowledge out of Big data. In addition to that we introduce some big data mining tools and how to extract a significant knowledge from the Big Data. That will help the research scholars to choose the best mining tool for their work.

REFERENCES

[1] Julie M. David, Kannan Balakrishnan, (2011), Prediction of Key Symptoms of Learning Disabilities in School-Age Children using Rough Sets, Int. J. of Computer and Electrical Engineering, Hong Kong, 3(1), pp163-169

[2] Julie M. David, Kannan Balakrishnan, (2011), Prediction of Learning Disabilities in School-Age Children using SVM and Decision Tree, Int. J. of Computer Science and Information Technology, ISSN 0975-9646, 2(2), pp829-835.

[3] Albert Bifet, (2013), “Mining Big data in Real time”, Informatica 37, pp15-20

[4] Richa Gupta, (2014), “Journey from data mining to Web Mining to Big Data”, IJCTT, 10(1),pp18-20

[5] http://www.domo.com/blog/2014/04/data-never-sleeps-2-0/

[6] Priya P. Sharma, Chandrakant P. Navdeti, (2014), " Securing Big Data Hadoop: A Review of Security Issues, Threats and Solution", IJCSIT, 5(2), pp2126-2131

[7] Richa Gupta, Sunny Gupta, Anuradha Singhal, (2014), "Big Data:Overview", IJCTT, 9 (5)

[8] Wei Fan, Albert Bifet, "Mining Big Data: Current Status and Forecast to the Future", SIGKDD Explorations, 14 (2), pp1-5

[9] Chanchal Yadav, Shullang Wang, Manoj Kumar, (2013) "Algorithm and Approaches to handle large Data- A Survey", IJCSN, 2(3), ISSN:2277-5420(online), pp2277-5420

[10] Xindong Wu, Xingquan Zhu, Gong-Qing Wu, Wei Ding, "Data Mining with Big Data"

[11] Puneet Singh Duggal, Sanchita Paul, (2013), "Big Data Analysis:Challenges and Solutions", Int. Conf. on Cloud, Big Data and Trust, RGPV

AUTHORS

Jaseen K.U. received her Master's Degree in Computer Science and Engineering in the year 2011 from Indira Gandhi National Open University, New Delhi, India. She is working as an Assistant Professor in the Department of Computer Applications with MES College, Aluva, Cochin, India. She has published two papers in International Journals and one paper in National Conference Proceedings. Her research interests include Data Mining and Information Security. She has coordinated various National Conferences.

Dr. Julie M. David received her Master's Degree in Computer Applications and Masters of Philosophy in Computer Science in the years 2000 and 2009 from Bharathiyar University, Coimbatore, India and from Vinayaka Missions University, Salem, India respectively. She has also received her Doctorate in the research area of Artificial Intelligence from Cochin University of Science and Technology, Cochin, India in 2013. During 2000-2007, she was with Mahatma Gandhi University, Kottayam, India, as Lecturer in the Department of Computer Applications. Currently she is working as an Assistant Professor in the Department of Computer Applications with MES College, Aluva, Cochin, India. Also, she is serving as the Programme Officer of the National Service Scheme Unit at the college. She has published several papers in International Journals and International and National Conference Proceedings. She has received Best Paper Awards in International Conferences. Her research interests include Artificial Intelligence, Data Mining, and Machine Learning. She is a life member of various professional organizations like International Association of Engineers & Computer Scientists, IAENG Societies of Artificial Intelligence & Data Mining, Computer Society of India, etc. She is a Reviewer of Elsevier International Journal of Knowledge Based Systems. She is a reviewer as well as an Editorial Board Member of various other International Journals also. She has coordinated various International and National Conferences.

DT-BAR: A DYNAMIC ANT RECOMMENDER TO BALANCE THE OVERALL PREDICTION ACCURACY FOR ALL USERS

Abdelghani Bellaachia[1] and Deema Alathel[2]

[1,2]School of Engineering and Applied Science,
The George Washington University, Washington, DC, USA
[1]bell@gwu.edu, [2]atheld@gwmail.gwu.edu

ABSTRACT

Ant colony algorithms have become recently popular in solving many optimization problems because of their collaborative decentralized behavior that mimics the behavior of real ants when foraging for food. Recommender systems present an optimization problem in which they aim to accurately predict a user's rating for an unseen item by trying to find similar users in the network. Trust-based recommender systems make use of trust between users. T-BAR was the first successful application of an ant colony algorithm to trust-based recommender systems but it lacked the ability to deal with cold start users. In this paper we propose a dynamic trust-based ant recommender (DT-BAR) that solves the problem of cold start users by locally initializing the pheromone level on edges using the dynamically changing information within each neighborhood as ants pass by. DT-BAR increases the communication between ants and emphasizes the importance of trust in the pheromone initialization process.

KEYWORDS

Ant Colony Optimization, Artificial Agents, Bio-inspired Algorithms, Recommender Systems, Trust.

1. INTRODUCTION

Collaborative filtering (CF) is the most common technique applied to recommender systems (RS) to suggest to users items that may be of interest to them [1]. CF techniques generate recommendations based on the items that are highly rated by users similar to the active user [2]. Such techniques suffer from their inability to deal with cold start users who have rated only a few items, which makes it hard for the system to find similar users. There have been several attempts to overcome this problem, such as allowing the users to express their trust level in other users in the network in hopes of utilizing the trust to enhance the system's performance. Such systems are known as trust-based recommender systems (TBRS) and one of the major trust-based algorithms applied to such systems is Massa et al.'s MoleTrust [3], which at the time it was presented showed to outperform traditional CF techniques and Golbeck's TidalTrust [4]. The MoleTrust approach is based on propagating the trust over the network to predict the active user's trust in other distant users and then use the propagated trust to reach the target users with the rating for the target item. However, we recently proposed our ant colony inspired algorithm, Trust-Based

Natarajan Meghanathan et al. (Eds) : NeTCoM, CSIT, GRAPH-HOC, SPTM - 2014
pp. 141–151, 2014. © CS & IT-CSCP 2014 DOI : 10.5121/csit.2014.41312

Ant Recommender (T-BAR), which surpassed the performance of other algorithms for TBRS, including MoleTrust [5]. T-BAR's major advantage over other popular algorithms is that unlike other algorithms that only consider a single user at the end of each search path, it considers all users with a rating for the target item that are encountered in the search process. The paths are constructed by combining both trust and semi-similarity between the users, which guarantees the quality of the constructed solutions.

2. RELATED BACKGROUND

2.1. Trust-Based Recommender Systems

RS provide an adaptive web environment for users by filtering the vast amount of information available online and delivering the right information to the right user. At their core RS suggest to users items that may be of interest to them. One of the major techniques applied to accomplish this goal is CF, which recommends items that were liked by likeminded users in the network. However, in recent years many researchers shifted their focus to TBRS based on the popular belief that users tend to trust people they know rather than depending on a RS to find similar *unknown* people in the network. The incorporation of trust in such networks results in neighborhoods of trust where a web of trust for a user *x* WOT_x refers to the group of users that are trusted by user *x*. In this manner, users trusted though chains of trust (i.e. friends of friends) are considered part of an extended WOT. Trust metrics in TBRS usually utilize trust by propagating it to reach a wider range of users who would not be otherwise reached if traditional CF techniques were used [4, 3].

2.2. Ant Colony Optimization Algorithms

Ant colony optimization (ACO) is a family of algorithms that falls under swarm intelligence. An ACO algorithm applies a probabilistic technique to solve optimization problems by mimicking the behavior of ants when they forage for food [6, 8]. In the context of RS, the active user can be considered the ants' nest while the target users that have a rating for the target item are considered the *good* food sources [5]. Within such a framework, artificial ants are dispatched from the active user into a network of users connected through multiple WOT and they construct paths that lead to possible target users in the solution space. Just like real ants, artificial ants deposit pheromone on paths leading to *good* users, and just like in real ant colonies, pheromone on edges evaporates as time passes by to allow exploration of other possible solutions. The combined effect of pheromone deposit and evaporation increases the probability of other ants traversing *good* paths while decreasing the probability of crossing others. The ants are usually dispatched from the active user over several iterations so the system moves from an unstable stage, where no solution is necessarily better than another, to a stable one where certain paths emerge as being the best solutions leading to the *best* food sources.

2.3. Trust-Based Ant Recommender

T-BAR [5] is a bio-inspired algorithm that is based on the ant colony system (ACS) algorithm proposed by Dorigo et al. [9]. T-BAR is the first successful application of an algorithm derived from ACS to TBRS. When compared to other popular algorithms for TBRS [4, 3], T-BAR greatly enhanced the accuracy of rating predictions and ratings coverage especially for heavy raters. However just like other techniques, it suffers from its inability to deal with cold start users.

At each step within an iteration in T-BAR, an ant *k* located at user *x* calculates the probability p^k_{xy} of crossing the edge connecting to a user *y* that belongs to WOT_x. The edge that yields the highest probability is the one that is crossed. The probability p^k_{xy} is calculated as:

$$p^k_{xy} = \frac{(\tau_{xy})^{\alpha}(\eta_{xy})^{\beta}}{\sum\limits_{z \in WOT_x}(\tau_{xz})^{\alpha}(\eta_{xz})^{\beta}} \tag{1}$$

where τ_{xy} is the pheromone level on the edge *xy*, η_{xy} is the trust T_{xy} expressed by user *x* towards user *y*, and α and β are influence parameters. Each ant stops constructing its solution once a certain search depth *d* is reached.

Pheromone update is accomplished on two levels in T-BAR, a local one and a global one. The *local pheromone update* occurs whenever an ant k crosses an edge *xy*, which results in adjusting τ_{xy} using:

$$\tau_{xy} = (1-\rho).\, \tau_{xy} + \rho.\, \tau^0_{xy} \tag{2}$$

where ρ is the pheromone evaporation coefficient and τ^0_{xy} is the initial pheromone level on *xy* calculated within each WOT_x as [10]:

$$\tau^0_{xy} = \frac{1}{\sum\limits_{z \in WOT_x} T_{xz}} \tag{3}$$

The *global pheromone update* takes place at the end of each iteration where first each constructed path's quality is evaluated by calculating its *path trust* PT_k [5, 3] and the paths that satisfy $PT_k \geq PT_{threshold}$ are considered the best paths so far. The pheromone level on the edges belonging to the best paths is further incremented by a quantity that is proportional to the path's PT_k. At the end of the last iteration, the system should have converged to the *best* solutions and the *good* users found on those paths are used to predict the rating for the target item *i*.

3. Proposed Dynamic Trust-Based ANT Recommender

Our proposed Dynamic Trust-Based Ant Recommender (DT-BAR) is a different variation of T-BAR that focuses on solving the problem of cold start users. DT-BAR applies a dynamic approach based on ACO algorithms' probabilistic methodology and emphasizes on utilizing trust and information sharing among ants to predict item ratings for users in a TBRS.

3.1. Rationale behind Proposed Approach

T-BAR's success is greatly credited to incorporating trust to strengthen the paths constructed by ants based on user popularities and user similarities and thus to ultimately find *good* users with *good* quality solutions [5]. In other words, the quality of *good* users reached through T-BAR was high due to its ability to find users that have many items in common with the active user *and* that have a high trust level. T-BAR's approach guarantees great results for heavy raters because such users have rated many items and therefore it is easier for the algorithm to find *good* quality solutions. However, the same argument cannot be applied to cold start users due to their lack of item ratings, which would explain T-BAR's inability to perform well for them.

A solution to the cold start problem would require expanding the ants' exploration scope of the solution space to increase the probability of finding better users that can contribute to providing more accurate predictions. In T-BAR, the ants' edge selection mechanism is dictated by the trust between two users and the evaluation of the best paths is determined by the number of co-rated items between users. For cold start users, the ants would be guided only by trust, so the role of trust needs to be further emphasized for such users to compensate for the lack of item ratings and co-rated items.

To overcome this problem we propose to:

1) Allow the artificial ants to share more information among them about the paths that have been explored and thus to support the exploration of the other undiscovered paths.

2)

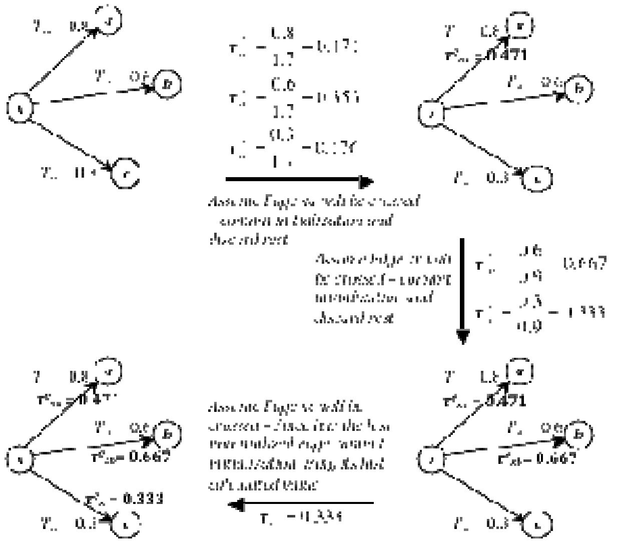

Figure 1. Example of DT-BAR's pheromone initialization process

3) Increase the role of trust in the pheromone initialization process so that the initial pheromone levels on edges within WOT_x would reflect the different trust levels on those edges.

4)We propose to accomplish both goals during the pheromone initialization process. To attain the first goal, we suggest allowing each ant to commit the initial pheromone level only on the edge that will be crossed while discarding the other initializations. This is closely related to the second goal though, because if we opt to calculate the initial pheromone level in a manner similar to the way it is done in T-BAR (Eq. 3), then the probability of crossing undiscovered edges would still be relatively unaffected especially if the previously crossed edges keep accumulating pheromone on them. Therefore, the initial pheromone level should be calculated in a way that reflects the trust assigned to each edge within WOT_x.

3.2. DT-BAR Algorithm

DT-BAR follows the same methodology proposed in [5] to predict ratings for unseen items for the active user in TBRS. DT-BAR's major difference from T-BAR is evident in the pheromone initialization step. Instead of calculating a single initial pheromone level τ^0_{xy} for all nodes within

WOT$_x$, our proposed algorithm would calculate a different value for each edge within WOT$_x$ that reflects its associated trust level as follows:

$$\tau_{xy}^{0} = \frac{T_{xy}}{\sum_{z \in WOT_{x*}} T_{xz}} \tag{4}$$

where WOT$_{x*}$ refers to users in WOT$_x$ with *uninitialized* edges. After calculating the probabilities of crossing those edges, DT-BAR allows an ant k to commit the pheromone initialization only on the edge that yielded the highest probability. So we can see how committing the initialization only on the crossed edges serves as a message to subsequent ants about which edges have been explored and thus those edges are not included later in the pheromone initialization of edges in the dynamically updated WOT$_{x*}$. Also, DT-BAR emphasizes the role of trust on the different edges with WOT$_x$ by calculating an initial pheromone level that is proportional to T_{xy}. Figure 1 is an example that demonstrates DT-BAR's pheromone initialization process.

The effect of the introduced change in the pheromone initialization will impact:

1) The probability $p^{k}{}_{xy}$ (Eq. 1) because the initial pheromone level on an edge xy determines the initial probability of crossing that edge and since the calculated $\tau^{0}{}_{xy}$ will dynamically change as ants continue to cross edges, we would expect the probability of selecting uncrossed edges to increase as ants keep passing by the neighborhood.

2) The local pheromone update of τ_{xy} (Eq. 2) because it involves the initial pheromone level to determine the amount of pheromone to be deposited. So, once an edge is initialized to a value that is large enough to increase its probability of being crossed, then that *successful* initial pheromone level would be committed and will determine the rate at which pheromone is deposited on that edge.

4. EXPERIMENTAL EVALUATION

4.1. Dataset and Evaluation Metrics

The Epinions dataset was used to test our proposed algorithm DT-BAR. Epinions is one of the few publically available datasets that provides access to both user ratings and explicit trust values between users. It is composed of 49,290 users who rated 139,738 unique items at least once and 487,181 distinct trust statements. The two major user categories of utmost importance in Epionions are *cold start users*, who comprise more than half of the users in the dataset, and *heavy raters*. *Cold start users* are users who rated less than 5 items each in the dataset, while *heavy raters* are the ones who rated more than 10 items each [11]. Some other user and item categories that are worth considering in Epinions include *opinionated users* who rated 5 or more items and whose standard deviation is greater than 1.5; *black sheep users* who rated 5 or more items and the average distance of their rating for item i with respect to the mean rating of item i is greater than 1; *niche items* that received less than 5 ratings each; and *controversial items* received ratings whose standard deviation is greater than 1.5.

We applied the *leave-one-out* technique to measure DT-BAR's prediction ability. We compared our obtained results to the results reported from running a basic CF algorithm that uses the Pearson Similarity and to Massa's MoleTrust algorithm [3]. Massa's work is one of the early major techniques applied to TBRS and it has been compared to many contributions in the literature [12, 13, 14, 15]. The results of our empirical evaluation were analyzed in terms of the

Mean Absolute Error (MAE) along with the *ratings coverage* (RC) [16], which measures an algorithm's ability to predict a rating for a certain item (regardless of the accuracy of the prediction). One of the major drawbacks in the MAE is that it has the same weight for all user categories in the dataset without taking into account, for example, the percentage of cold start users and heavy raters in the system, so in the case of Epinions the error for heavy raters shadows the one for cold start users [3]. In order to gain a better understanding of an algorithm's performance the *Mean Absolute User Error* (MAUE) is usually used because it averages the MAE by the number of users in each category. In the same perspective, the *users coverage* (UC) represents the percentage of users in the dataset for which the algorithm was able to provide with at least one prediction.

4.2. Experimental Results

We compare DT-BAR's performance results to the ones reported by running several other algorithms on the Epinions dataset, namely: *CF* which is Massa's implementation of a basic CF algorithm that uses the Pearson Similarity [11], *MT* which is the MoleTrust algorithm [3], and T-BAR which is our basic trust-based ant recommender [5].

At first glance, a quick look at Table 1 and Table 2 would show that T-BAR has the best overall performance since it achieves the lowest MAE of ~ 0.3 and the highest ratings coverage of 93%.

Table 1. The MAE of the algorithms across different views.

Views	**Algorithm**			
	CF	**MT**	**T-BAR**	**DT-BAR**
All	0.843	0.832	0.298	0.723
Cold start users	1.094	0.674	1.459	0.714
Heavy raters	0.850	0.873	0.212	0.778
Controversial items	1.515	1.425	1.995	1.629
Niche items	0.822	0.734	0.572	0.222
Opinionated users	1.200	1.020	1.308	0.411
Black sheep	1.235	1.152	1.973	0.812

Table 2. The RC of the algorithms across different views.

Views	**Algorithm**			
	CF	**MT**	**T-BAR**	**DT-BAR**
All	51%	28%	93%	84%
Cold start users	3%	11%	91%	55%
Heavy raters	58%	31%	93%	87%
Controversial items	45%	25%	59%	39%
Niche items	12%	8%	48%	84%
Opinionated users	50%	23%	94%	34%
Black sheep	56%	24%	77%	37%

Table 3. The MAUE of the algorithms across different views.

Views	Algorithm			
	CF	MT	T-BAR	DT-BAR
All	0.938	0.790	1.203	0.790
Cold start users	1.173	0.674	1.581	0.784
Heavy raters	0.903	0.834	0.282	0.806
Controversial items	1.503	1.326	1.967	1.750
Niche items	0.854	0.671	0.896	0.323
Opinionated users	1.316	0.938	1.262	0.498
Black sheep	1.407	1.075	1.973	0.895

Table 4. The UC of the algorithms across different views.

Views	Algorithm			
	CF	MT	T-BAR	DT-BAR
All	41%	47%	96%	68%
Cold start users	3%	17%	97%	50%
Heavy raters	86%	80%	93%	90%
Controversial items	16%	12%	92%	73%
Niche items	11%	10%	74%	85%
Opinionated users	61%	61%	94%	39%
Black sheep	68%	61%	81%	43%

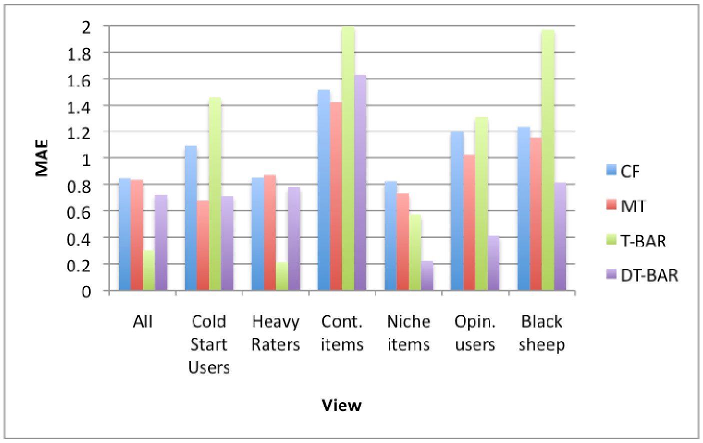

Figure 2. The MAE of the algorithms across different views

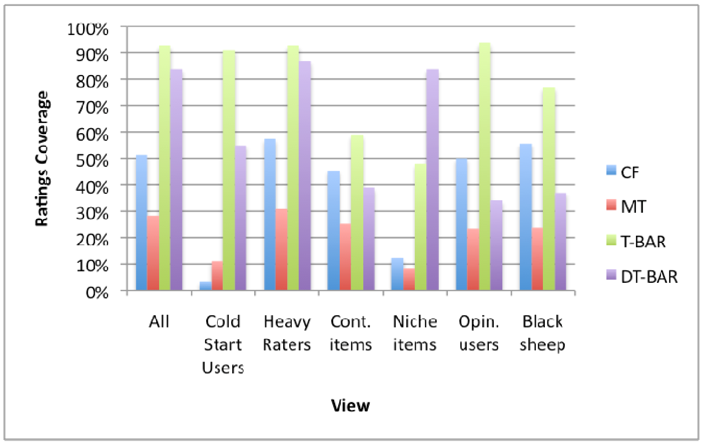

Figure 3. The RC of the algorithms across different views

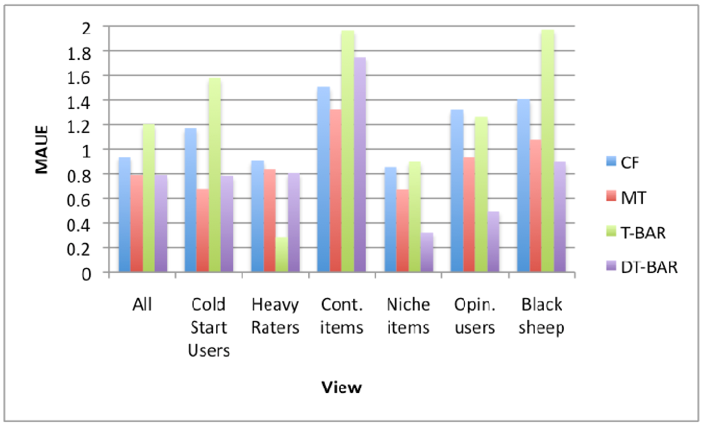

Figure 4. The MAUE of the algorithms across different views

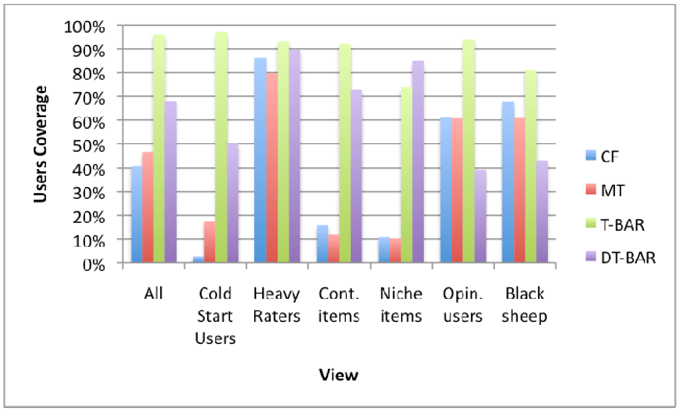

Figure 5. The UC of the algorithms across different views

However, a closer look at Table 1 and remembering how the MAE is calculated we can see how the overall accuracy does not reflect the results for the majority of users in the dataset, i.e. cold start users, but is rather affected by the ones for heavy raters due to the big difference in the accuracy between the two user categories. The same observation can be noticed with respect to

CF and MT. However, DT-BAR does not suffer from the same problem because it achieves almost similar MAEs for both cold start users and heavy raters (~ 0.7 and ~0.78 respectively) which results in the overall MAE of 0.723 not being misleading as it is in the case of the other three algorithms. DT-BAR's overall RC of 84% is a bit lower than T-BAR's 93% but given DT-BAR's acceptable consistent overall performance, the drop in coverage can be considered reasonable. On the other hand, Table 3 and Table 4 show how the MAUE and UC are better indicators of all four algorithms' performances since the overall accuracies are direct reflections of the results obtained for cold start users. Even when averaging the results by the number of users/items in each category, DT-BAR outperforms the other algorithms because its overall MAUE of ~0.8 reflects the results achieved for both cold start users and heavy raters (both ~ 0.8). One might argue that DT-BAR's MAUE levels for the two major user categories are close to the ones obtained by MT, however Table 4 shows that DT-BAR provides better levels of UC (50% vs. 17% for cold start users and 90% vs. 80% for heavy raters). When it comes to heavy raters alone, T-BAR is still considered to beat all other algorithms in terms of both accuracy and coverage by reaching a MAUE as low as ~ 0.28 and a UC of 93%.

Another major advantage of DT-BAR is its superior performance for niche items, which can be a challenge to deal with in RSs just like cold start users due to the scarcity of ratings available for those items. DT-BAR achieved a low MAE of 0.2 and a RC of 84%, which are better than any of the results achieved by the other three algorithms. Our proposed algorithm also achieved lower MAE and MAUE for black sheep and opinionated users however that came with the price of lower coverage percentage for both user categories. DT-BAR's performance for controversial items was almost similar to the average performance achieved by the other algorithms.

Overall, it is evident that T-BAR is always the better choice if the dataset is composed mostly of heavy raters since it provides an amazing performance that outperforms the ones achieved by all other algorithms (MAE ~ 0.2 and 93% RC). On the other hand, if the distribution of user categories in the dataset is unknown then DT-BAR would be a more suitable option since it delivers an acceptable consistent performance across the different discussed views. Another case where DT-BAR should be considered is when a RS consists of a substantial number of niche items whose accuracy of predictions could affect a user's confidence in the system's performance.

5. CONCLUSION

In this paper we proposed our Dynamic Trust-Based Ant Recommender (DT-BAR) to achieve a consistent performance for the two major user categories in RS: cold start users and heavy raters. Proposed algorithms in the literature can only deliver good results for one user category at the expense of the other, but DT-BAR managed to balance the performance by attaining a consistent acceptable accuracy levels across the two categories. DT-BAR achieves that by allowing the artificial ants to share information about the explored edges and by initializing the pheromone level on edges to values proportional to their corresponding trust level. DT-BAR allows each ant to locally calculate the initial pheromone level for each edge within the neighborhood but only commit the initialization on the edge to be crossed which would serve as a message to the other ants to indicate which edges have been crossed and at the same time increase the possibility of crossing other edges by dynamically calculating the new initial pheromone level using the newly available information about the uninitialized edges.

The initial pheromone level is a determining factor in any ACO algorithm's convergence speed and accuracy, and DT-BAR's proposed dynamic pheromone initialization approach proved to be successful in terms of allowing the ants to expand the scope of their edge exploration, which benefited both cold start users and niche items. Our proposed algorithm loosely preserved the ants' ability to exploit the good discovered paths for heavy raters, which resulted in finding *acceptable* good users with a rating for the target item in general. However, DT-BAR's performance for heavy raters is not as good as the ones achieved by T-BAR but at least it matched the average results obtained by a basic CF algorithm or Massa's MoleTrust (in other words, it was not worse than their results for heavy raters).

DT-BAR's expanded exploration mechanism proved to be feasible for cold start users and niche items. In general, DT-BAR achieved an acceptable, good, consistent performance for both cold start users and heavy raters as opposed to the other algorithms in the literature.

REFERENCES

[1] Resnick, Paul & Varian, Hal R., (1997) "Recommender systems", Commun. ACM, Vol. 40, pp 56-58.

[2] Schafer, J. Ben, Frankowski, Dan, Herlocker, Jon & Sen, Shilad, (2007) "Collaborative filtering recommender systems", The Adaptive Web, Springer-Verlag.

[3] Massa, Paolo & Avesani, Paolo, (2007) "Trust-aware recommender systems", Proceedings of the 2007 ACM Conference on Recommender Systems, pp 17-24.

[4] Golbeck, Jennifer, (2005) "Computing and applying trust in web-based social networks," Doctoral Dissertation, University of Maryland at College Park.

[5] Bellaachia, Abdelghani & Alathel, Deema, (2012) "Trust-Based Ant Recommender (T-BAR)", IEEE Conference of Intelligent Systems, Sofia, Bulgaria, pp 130-135.

[6] Dorigo, Marco, (1992) "Learning and natural algorithms", Doctoral Dissertation, Politecnico di Milano.

[8] Dorigo, Marco, Bonabeau, Eric & Theraulaz, Guy, (2000) "Ant algorithms and stigmergy", Future Generation Computer Systems, Vol. 16, pp 851-871.

[9] Dorigo, Marco & Stützle, Thomas, (2004) "Ant colony optimization", MIT Press.

[10] Bellaachia, Abdelghani & Alathel, Deema, (2014) "A Local Pheromone Initialization Approach for Ant Colony Optimization Algorithms", IEEE International Conference on Progress in Informatics and Computing, Shanghai, China.

[11] Massa, Paolo & Avesani, Paolo, (2004) "Trust-aware collaborative filtering for recommender systems", Proceedings of the Federated International Conference on the Move to Meaningful Internet, Larnaca, Cyprus, Springer-Verlag, pp 492-508.

[12] Avesani, Paolo & Massa, Paolo, (2005) "Moleskiing.it: A Trust-aware recommender system for ski mountaineering", International Journal for Infonomics, pp 1-10.

[13] Golbeck, Jennifer, (2006) "Generating predictive movie recommendations from trust in social networks", Lecture Notes in Computer Science, Vol. 3986, pp 93-104.

[14] O'Donovan, John & Smyth, Barry, (2005) "Trust in recommender systems", Proceedings of the 10th International Conference on Intelligent User Interfaces, San Diego, California, USA, pp 167-174.

[15] Victor, Patricia, Cornelis, Chris, Cock, Martine De & Teredesai, AM, (2008) "Key figure impact in trust-enhanced recommender systems", AI Commun., Vol. 21, pp 127-143.

[16] Herlocker, Jonathan L., Konstan, Joseph A., Terveen, Loren G. & Riedl, John T., (2004) "Evaluating collaborative filtering recommender systems", ACM Transactions on Information Systems, Vol. 22, pp 5-53.

AUTHORS

Abdelghani Bellaachia received his B.S. and M.S. degrees in electrical engineering from Mohammadia School of Engineering, Rabat, Morocco in 1983. He later received his second M.S. degree in computer science from the George Washington University, Washington, DC, in 1991. He earned his Ph.D. from the same university in software systems a year later. Since then he has been a faculty member at the George Washington University and is currently an associate professor there. His research interests include data mining, multi-lingual information retrieval systems, bio-informatics, design and analysis of algorithms, and parallel processing.

Deema Alathel is a doctoral student at the George Washington University, Washington, DC. She received her B.S. and M.S. degrees in computer science from King Saud University, Riyadh, Saudi Arabia. She has worked at the Institute of Public Administration in Riyadh for 2 years as a faculty staff member. Her research interests include data mining, information retrieval systems, and bio-informatics.

INTENTIONAL BLANK

MEDICAL DIAGNOSIS CLASSIFICATION USING MIGRATION BASED DIFFERENTIAL EVOLUTION ALGORITHM

Htet Thazin Tike Thein[1] and Khin Mo Mo Tun[2]

[1]Ph.D Student, University of Computer Studies, Yangon, Myanmar
[2]Department of Computational Mathematics,
University of Computer Studies, Yangon, Myanmar
[1]htetthazintikethein@ucsy.edu.mm,[2]khinmo2tun@gmail.com

ABSTRACT

Constructing a classification model is important in machine learning for a particular task. A classification process involves assigning objects into predefined groups or classes based on a number of observed attributes related to those objects. Artificial neural network is one of the classification algorithms which, can be used in many application areas. This paper investigates the potential of applying the feed forward neural network architecture for the classification of medical datasets. Migration based differential evolution algorithm (MBDE) is chosen and applied to feed forward neural network to enhance the learning process and the network learning is validated in terms of convergence rate and classification accuracy. In this paper, MBDE algorithm with various migration policies is proposed for classification problems using medical diagnosis.

KEYWORDS

Artificial Neural Network, Differential Evolution, Island Model, Classification, Medical Diagnosis

1. INTRODUCTION

An objective function describing the artificial neural network (ANN) training problem is going to be multimodal. Therefore, algorithm based on gradient methods can easily get stuck in local minima. To avoid this problem, it is possible to use a global optimization technique, such as, for example, the differential evolution (DE) algorithm [1], [2], which is a variant of the evolutionary algorithm [3], [4], or other techniques, such as: a particle swarm optimization algorithm [5], a continuous ant colony optimization algorithm [6], a bee colony optimization algorithm [7], or an evolutionary strategy [8]. The DE algorithm is a heuristic algorithm for global optimization. It was introduced several years ago (in 1997) and has been developed intensively in recent years [9]. Its advantages are as follows: the possibility of finding the global minimum of a multimodal function regardless of the initial values of its parameters, quick convergence, and the small number of parameters that needs to be set up at the start of the algorithm's operation [10]. Since 1997, the DE algorithm has been modified to increase its effectiveness

.

To speed up an evolutionary computation it is a common practice to use multiple machines. Island models behave qualitatively different from standard EAs and even using them on a single

Natarajan Meghanathan et al. (Eds) : NeTCoM, CSIT, GRAPH-HOC, SPTM - 2014
pp. 153–163, 2014. © CS & IT-CSCP 2014 DOI : 10.5121/csit.2014.41313

machine may produce different, possibly better solutions for many problems, especially complex ones (for example in engineering). Separating individuals spatially from each other results in slowing down the information flow between individuals, which may have both desired and undesired results. A slower information flow may stop temporarily best solution from dominating the population and allow different building blocks or solutions to be discovered and later confronted, which is important in the context of engineering design and creativity. On the other hand one can prevent successful mixing, which could otherwise lead to constructing a novel solution.

In this paper, a latest optimization algorithm called DE with island model is applied in feed forward neural network to improve neural network learning mechanism. Island based model works by running multiple algorithms and shares the results at regular interval promoting the overall performance of the algorithm. This paper proposes the migration based differential evolution algorithm for classification medical diagnosis.

2. DIFFERENTIAL EVOLUTION ALGORITHM

Having developed an ANN-based process model, a DE algorithm is used to optimize the N-dimensional input space of the ANN model. Conventionally, various deterministic gradient-based methods are used for performing optimization of the phenomenological models. Most of these methods require that the objective function should simultaneously satisfy the smoothness, continuity, and differentiability criteria. Although the nonlinear relationships approximated by an ANN model can be expressed in the form of generic closed-form expressions, the objective function(s) derived thereby cannot be guaranteed to satisfy the smoothness criteria. Thus, the gradient-based methods cannot be efficiently used for optimizing the input space of an ANN model and, therefore, it becomes necessary to explore alternative optimization formalisms, which are lenient towards the form of the objective function.

In the recent years, Differential Evolution (DE) that are members of the stochastic optimization formalisms have been used with a great success in solving problems involving very large search spaces. The DEs were originally developed as the genetic engineering models mimicking the population evolution in natural systems. Specifically, DE like genetic algorithm (GA) enforces the "survival-of-the-fittest" and "genetic propagation of characteristics" principles of biological evolution for searching the solution space of an optimization problem. The principal features possessed by the DEs are: (i) they require only scalar values and not the second- and/or first-order derivatives of the objective function, (ii) the capability to handle nonlinear and noisy objective functions, (iii) they perform global search and thus are more likely to arrive at or near the global optimum and (iv) DEs do not impose pre-conditions, such as smoothness, differentiability and continuity, on the form of the objective function.

Differential Evolution (DE), an improved version of GA, is an exceptionally simple evolution strategy that is significantly faster and robust at numerical optimization and is more likely to find a function's true global optimum. Unlike simple GA that uses a binary coding for representing problem parameters, DE uses real coding of floating point numbers. The mutation operator here is the addition instead of bit-wise flipping used in GA. And DE uses non-uniform crossover and tournament selection operators to create new solution strings. Among the DEs advantages are its simple structure, ease of use, speed and robustness. It can be used for optimizing functions with real variables and many local optima.

This paper demonstrates a successful application of DE with island model. As already stated, DE in principle is similar to GA. So, as in GA, we use a population of points in our search for the optimum. The population size is denoted by NP. The dimension of each vector is denoted by D.

The main operation is the NP number of competitions that are to be carried out to decide the next generation. To start with, we have a population of NP vectors within the range of the objective function. We select one of these NP vectors as our target vector. We then randomly select two vectors from the population and find the difference between them (vector subtraction). This difference is multiplied by a factor F (specified at the start) and added to the third randomly selected vector. The result is called the noisy random vector. Subsequently, the crossover is performed between the target vector and noisy random vector to produce the trial vector. Then, a competition between the trial vector and target vector is performed and the winner is replaced into the population. The same procedure is carried out NP times to decide the next generation of vectors. This sequence is continued till some convergence criterion is met. This summarizes the basic procedure carried out in differential evolution. The details of this procedure are described below.

Steps performed in DE

Assume that the objective function is of D dimensions and that it has to be optimized. The weighting constants F and the crossover constant CR are specified.

Step 1. Generate NP random vectors as the initial population: generate (NP×D) random numbers and linearize the range between 0 and 1 to cover the entire range of the function. From these (NP×D) numbers, generate NP random vectors, each of dimension D, by mapping the random numbers over the range of the function.

Step 2. Choose a target vector from the population of size NP: first generate a random number between 0 and 1. From the value of the random number decide which population member is to be selected as the target vector (Xi) (a linear mapping rule can be used).

Step 3. Choose two vectors from the population at random and find the weighted difference: Generate two random numbers. Decide which two population members are to be selected (Xa,Xb).Find the vector difference between the two vectors (Xa - Xb).Multiply this difference by F to obtain the weighted difference. Weighted difference = F (Xa - Xb)

Step 4. Find the noisy random vector: generate a random number. Choose the third random vector from the population (Xc). Add this vector to the weighted difference to obtain the noisy random vector (X'c).

Step 5. Perform the crossover between Xi and X'c to find Xt, the trial vector: generate D random numbers. For each of the D dimensions, if the random number is greater than CR, copy from Xi into the trial vector; if the random number is less than CR, copy the value from X'c into the trial vector.

Step 6. Calculate the cost of the trial vector and the target vector: for a minimization problem, calculate the function value directly and this is the cost. For a maximization problem, transform the objective function f(x) using the rule F(x) = 1 / [1 + f(x)] and calculate the value of the cost. Alternatively, directly calculate the value of f(x) and this yields the profit. In case the cost is calculated, the vector that yields the lower cost replaces the population member in the initial population. In case the profit is calculated, the vector with the greater profit replaces the population member in the initial population.

Steps 1–6 are continued till some stopping criterion is met. This may be of two kinds. One may be some convergence criterion that states that the error in the minimum or maximum between two previous generations should be less than some specified value. The other may be an upper bound on the number of generations. The stopping criterion may be a combination of the two. Either way, once the stopping criterion is met, the computations are terminated. Choosing DE key parameters NP, F, and CR is seldom difficult and some general guidelines are available. Normally, NP ought to be about 5 to 10 times the number of parameters in a vector. As for F, it lies in the range 0.4 to 1.0. Initially, F= 0.5 can be tried and then F and/or NP is increased if the population converges prematurely. A good first choice for CR is 0.1, but in general CR should be as large as possible (Price and Storn, 1997). DE has already been successfully applied for solving several complex problems and is now being identified as a potential source for the accurate and faster optimization.

3. ISLAND MODEL

The main difference between the island model and the single population model is the separation of individuals into islands. As against the master-slave model the communication to computation ratio of the island model approach is low, owing to the low communication frequency between the islands. Also, separating individuals separately from each other results in a qualitative change in the behaviour of the algorithm.

In the island model approach, each island executes a standard sequential evolutionary algorithm. The communication between sub-population is assured by a migration process. Some randomly selected individuals (migration size) migrate from one island to another after every certain number of generations (migration interval) depending upon a communication topology (migration topology). The two basic and most sensitive parameters of island model strategy are: migration size, which indicates the number of individuals migrating and controls the quantitative aspect of migration; and migration interval denoting the frequency of migration. Although different aspects of migration size and interval were studied in the past, we are unaware of any work studying directly the influence of these parameters on the behaviour of island model based differential evolution, though [15] presents a similar study on a set of 8 standard functions.

3.1. Migration Topology

The migration topology describes which islands send individuals to which islands. There are many topologies. This system investigates the fully connected topology. In this paper, simulations were run with setups of five islands.

3.2. Migration Policy

A migration policy consists of two parts. The first part is the selection of individuals, which shall be migrated to another island. The second part is to choose which individuals are replaced by the newly obtained individuals. Four migration policies are proposed in this system:

- Select the best individuals replace the worst individuals.
- Select random individuals, replace the worst individuals.
- Select the best individuals replace random individuals.
- Select random individuals, replace random individuals.

This system experiments all of the above migration policies and compare their results.

3.3. Migration Interval

In order to distribute information about good individuals among the islands, migration has to take place. This can either be done in synchronous way every nth generation or in an asynchronous way, meaning migration takes place at non-periodical times. It is commonly accepted that a more frequent migration leads to a higher selection pressure and therefore a faster convergence. But as always with a higher selection pressure come the susceptibility to get stuck in local optima. In this system, various migration intervals are experimented to find the best solution for the neural network training.

3.4. Migration Size

A further important factor is the number of individuals which are exchanged. According to these studies the migration size has to be adapted to the size of a subpopulation of an island. When one migrates only a very small percentage, the influence of the exchange is negligible but if too much individuals are migrated, these new individuals take over the existing population, leading to a decrease of the global diversity. In this system, the migration sizes were chosen to be approximately 10% of the size of a subpopulation as suggested in [19].

4. THE PROPOSED MODEL

As shown in figure 1, the training patterns of medical dataset are used as input data. Attributes are scaled to fall within a small specific range by using min-mix normalization. At the start of the algorithm, dataset were loaded from the database. In the next step, each chromosome or vector is randomly initialized with random neural network weight. Fitness of each chromosome is evaluated using following step. Fitness defined how well a chromosome solves the problem in hand. The first step converts chromosome's genes into neural network and fitness is calculated for each individuals. Mutation operator produce the trial vector from parent vector and randomly selected three vectors. Crossover recombines the parent vector and trial vector to produce offspring. By using mutation and crossover, some genes are modified that mean weights are updated. Fitness of offspring is calculated and compare with fitness of parent vector, the chromosome with high fitness survive and next generation begin. Choose individuals according to migration policy. Migrate and replace individuals according to migration topology. Figure 1 presents the flow of the proposed system.

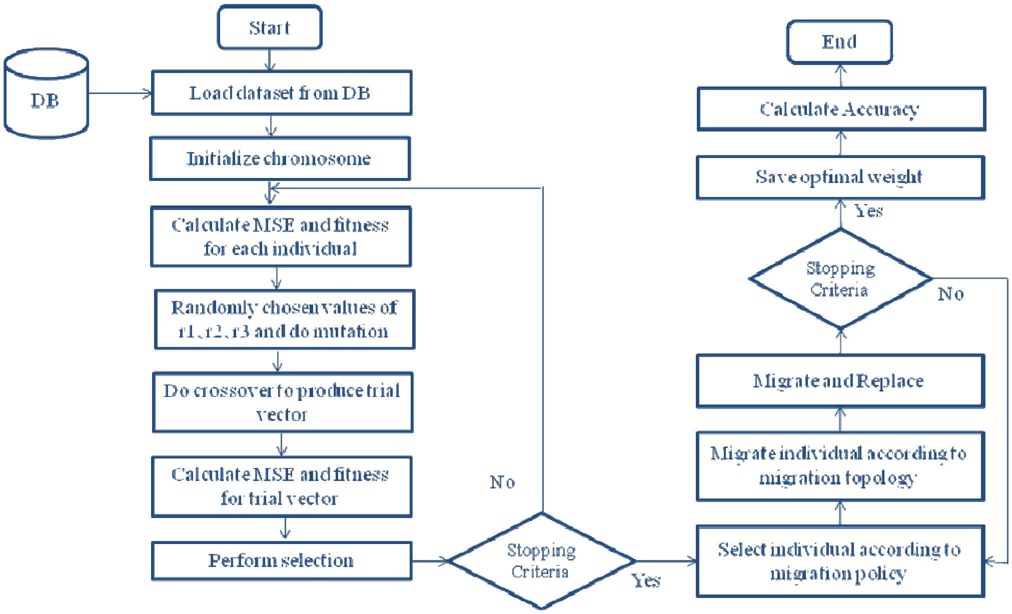
Start
DB
Load dataset from DB
Initialize chromosome
Calculate MSE and fitness for each individual
Randomly chosen values of r1, r2, r3 and do mutation
Do crossover to produce trial vector
Calculate MSE and fitness for trial vector
Perform selection
No
Stopping Criteria
Yes
Select individual according to migration policy
Migrate individual according to migration topology
Migrate and Replace
Stopping Criteria
No
Yes
Save optimal weight
Calculate Accuracy
End

Figure 1. ANNs-MBDE algorithm training process

5. DESCRIPTION OF DATASETS

This paper presents four medical datasets such as Breast Cancer, Heart, Liver and Pima Indian Diabetes from UCI machine learning repository [18]. The size and number of attributes are different for each dataset. The size means number of medical dataset records for training.

5.1. Breast Cancer

The cancer dataset requires the decision maker to correctly diagnose breast lumps as either benign or malignant based on data from automated microscopic examination of cells collected by needle aspiration. The dataset includes 9 inputs and 2 outputs. A total of 345 instances are available in breast cancer data set. 231 instances are used for training and 114 instances are used for testing.

5.2. Heart

The network architecture used for Heart dataset consists of 13 continuous and 2 classes. The attribute are age, sex, chest pain type, resting blood pressure, serum cholestoral, fasting blood pressure, serum cholestoral, fasting blood sugar > 120 mg/dl, resting electrocardiographic results, maximum heart rate achieved, exercise induced angina, oldpeak, the slope of the peak exercise ST segment, number of major vessels and thal. The classes are absent (1) and present (2).. A total of 303 instances are available in heart disease data set. 201 instances are used for training and 100 instances are used for testing.

5.3. Liver

In this paper, we used liver dataset from UCI machine learning repository. There are 345 instances, 6 continuous attributes and 2 classes. The attributes are mean corpuscular volume, alkaline phosphatase, alamine aminotransferase, aspartate, aminotransferase, gamma-glutamyl transpeptidase and number of half-pint equivalents of alcoholic beverages drunk per day. The classes are absents (1) and present (2). The first 5 attributes are all blood tests which are thought to be sensitive to liver disorders that might arise from excessive alcohol consumption. Each record is a single male individual.

5.4. Pima Indian Diabetes Database (PIDD)

There are 768 instances, 8 continuous attributes and 2 classes. PIDD includes the following attributes (1-8 attributes as input and last attributes as target variable) number of times pregnant, plasma glucose concentration a 2 hours in an oral glucose tolerance test, diastolic blood pressure (mm Hg), triceps skin fold thickness (mm), 2 hours serum insulin (mu U/ml), body mass index (weight in kg/ (height in m) ^ 2), diabetes pedigree function and age (years). Class to be predicted is patient is suffering from tested-positive or test-negative.

6. EXPERIMENTAL RESULT

Java programming language, which is the platform independent and a general-purpose development language, is used to implement the proposed system. First of all, the medical datasets are accessed. And then, normalization is made for pre-processing steps according to the different medical data sets. Experiments are performed with four migration policies. Currently the system experiment the island model with fully connected topology and four migration policies. In this system, five islands are used. The island model used the iteration as the migration interval and one-third of the old population is used to migrate and replace. Four medical datasets are used from the UCI, namely Breast Cancer, Heart, Liver and Pima Indian Diabetes. The results for each dataset are compared and analysed based on the convergence rate and classification performance.

6.1. Parameters of Datasets

The table 1 below shows the parameter of four datasets.

Table 1. Datasets Information

Parameter	**Medical Datasets**			
	Breast cancer	***Heart***	***Liver***	***Pima Diabetes***
Train Data	456	201	231	509
Test Data	227	100	114	259
Output Neuron	2	2	2	2

6.2. Data Normalization

The data normalization is considered as the most important pre-processing step using neural networks. To improve the performance of multilayer neural networks, it is better to normalize the data entry such that will be found in the interval of [0 1]. To transform the data into digital form, and use it as inputs of the neural network, scaling or normalization should be realized for each attribute. The nine numerical attributes, in the analog form, are scaled with a range of 0 and 1. There are many types of normalization that are found in the literature. The new values obtained after normalization, follow this equation:

$$New\ value\ (after\ normalization) = \frac{current - min}{\max - min} \qquad (1)$$

6.3. Classifier Accuracy

Estimating classifier accuracy is important since it determines to evaluate how accurately a given classifier will label future data, data on which the classifier has not been trained. Accuracy estimates also help in the comparison of different classifiers. The following classification features are used to train and test the classifier.

Given: A collection of labeled records (training set). Each record contains a set of features (attributes), and the true class (label).

Find: A model for the class as a function of the values of the features.

Gold: Previously unseen records should be assigned a class as accurately as possible. A test set is used to determine the accuracy of the model. Usually, the given data set is divided into training and test sets, with training set used to build the model and test set used to validate it. The Sensitivity and Specificity measures can be used to determine the accuracy measures.

Precision may also be used to access the percentage of samples labeled as for example, “cancer” that actually are “cancer” samples. These measures are defined as

$$Specificity = \frac{t\_neg}{neg} \qquad (2)$$

$$Precision = \frac{t\_pos}{t_{pos} + f\_pos} \qquad (3)$$

$$Sensitivity = \frac{t\_pos}{pos} \qquad (4)$$

Where,

t_pos = the number of true positives (“medical dataset class” samples that were correctly classified as such class),

pos = the number of positive (“medical dataset class”) samples

t_neg = the number of true negative (“not medical dataset class” samples that were correctly classified as such class)

neg = the number of negative samples

f_pos = number of false positive (“not medical dataset class” samples that were incorrectly labeled as such class)

$$accuracy = sensitivity\frac{pos}{pos + neg} + specificity\frac{negs}{pos + neg} \qquad (5)$$

6.4. Accuracy Comparisons for UCI Medical Datasets

Four medical datasets are tested with MBDE neural network classifier for this system. Below the tables show the accuracy of training and testing of MBDE neural network on medical datasets.

Table 2. Results of classification accuracy on breast cancer dataset

Migration Policies	**Error Convergence**	**Convergence Time (sec)**	**Classification Accuracy**	
			Training Accuracy (%)	***Testing Accuracy (%)***
Best-Worst	0.0011	9	97.82	100
Best-Random	0.0021	10	99.31	99.43
Random-Worst	0.0037	13	97.35	98.46
Random-Random	0.0043	13	98.76	97.32

Table 3. Results of classification accuracy on heart dataset

Migration Policies	**Error Convergence**	**Convergence Time (sec)**	**Classification Accuracy**	
			Training Accuracy (%)	***Testing Accuracy (%)***
Best-Worst	0.0021	11	97.32	99.89
Best-Random	0.0107	12	98.09	99.32
Random-Worst	0.0130	13	99.14	98.72
Random-Random	0.0160	14	99.04	98.04

Table 4. Results of classification accuracy on liver dataset

Migration Policies	**Error Convergenc e**	**Convergence Time (sec)**	**Classification Accuracy**	
			Training Accuracy (%)	***Testing Accuracy (%)***
Best-Worst	0.0011	13	99.72	100
Best-Random	0.0167	11	98.62	98.45
Random-Worst	0.0203	11	98.14	97.68
Random-Random	0.0264	12	97.68	97.36

Table 5. Results of classification accuracy on PIDD dataset

Migration Policies	**Error Convergence**	**Convergence Time (sec)**	**Classification Accuracy**	
			Training Accuracy (%)	***Testing Accuracy (%)***
Best-Worst	0.0035	12	98.23	99.01
Best-Random	0.0159	13	98.97	98.34
Random-Worst	0.0159	13	98.35	97.78
Random-Random	0.0178	14	97.65	97.78

The MBDE is successfully applied in neural network and has been tested using Breast Cancer, Heart, Liver and Pima Indian Diabetes datasets.

7. ACCURACY COMPARISON ON MIGRATION POLICIES

This analysis is carried out to compare the results of migration policy. To do this, the learning patterns for the proposed system is compared using all four medical datasets. The comparative correct classification percentage for all datasets is shown in figure 2.

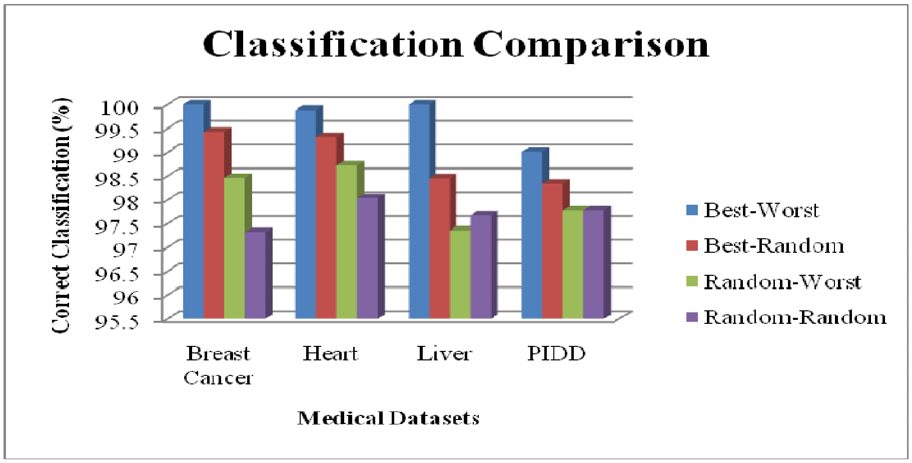

Figure 2. Comparative of correct classification percentage of migration policies

In this paper, we have introduced the various migration policies with fully connected topology and compared their results. Figure 2 shows the accuracy comparison with four migration policies by using medical datasets. Medical datasets are used to implement this proposed system which shows better experiments with higher accuracy. The proposed system also reduces the computing time. For all medical datasets, the experiments show that best-worst migration policy has better results on convergence time and correct classification percentage. The proposed algorithm converges in a short time with high correct classification percentage.

8. CONCLUSIONS

The proposed system (MBDE) algorithm is successfully applied in neural network and has been tested using breast cancer, heart, liver and pima indian diabetes database datasets. The analysis is done by comparing the results for each dataset. The results produced by ANNs are not optimal before using migration based differential evolution algorithm. Therefore, this paper improves the performance of ANNs by using the proposed algorithm, MBDE. The main difficulty of neural network is to adjust weight in order to reduce the error rate. This system presents the neural network training algorithm using migration based differential evolution algorithm. By exploiting the global search power of differential evolution algorithm in conjunction with island model will boost the training performance of the algorithm. The system will converge quickly to the lower mean square error. Island model encourage the diversity among the individual among islands which increase search capability and by migration island model can share the best experiences of each other. By using island model rather than single DE, it can get advantages from parallel problem solving and information sharing which lead to faster global search. This system improves the performance of medical datasets in feed forward neural network and reduces the computing time.

REFERENCES

[1] R. Storn and K. Price, “Differential evolution—A simple and efficient heuristic for global optimization over continuous spaces,” J. Glob. Optim., vol. 11, no. 4, pp. 341–359, Dec. (1997).

[2] K. Price, “An introduction to differential evolution,” in New Ideas in Optimization, D. Corne, M. Dorigo, and F. Glover, Eds. London, U.K.: McGraw-Hill, pp. 79–108 (1999).

[3] D. Goldberg, Genetic Algorithms in Search, Optimization, and Machine Learning. Reading, MA: Addison-Wesley, (1989).

[4] Z. Michalewicz, Genetic Algorithms+Data Structures=Evolution Programs. Berlin, Germany: Springer-Verlag, (1998).

[5] J. Kennedy, R. C. Eberhart, and Y. Shi, Swarm Intelligence. San Francisco, CA: Morgan Kaufmann, (2001).

[6] K. Socha and M. Doringo, “Ant colony optimization for continous domains,”Eur. J. Oper. Res., vol. 185, no. 3, pp. 1155–1173, Mar. (2008).

[7] D. T. Pham, A. Ghanbarzadeh, E. Koç, S. Otri, S. Rahim, and M. Zaidi, “The bees algorithm—A novel tool for complex optimization problems,” in IPROMS 2006. Oxford, U.K.: Elsevier, (2006).

[8] H. G. Beyer and H. P. Schwefel, “Evolution strategies: A comprehensive introduction,” Nat. Comput., vol. 1, no. 1, pp. 3–52, May (2002).

[9] K. V. Price, R. M. Storn, and J. A. Lampinen, Differential Evolution: A Practical Approach to Global Optimization. Berlin, Germany: Springer Verlag, (2005).

[10] R. L. Becerra and C. A. Coello Coello, “Cultured differential evolution for constrained optimization,” Comput. Methods Appl. Mech. Eng., vol. 195, no. 33–36, pp. 4303–4322, Jul. 1, (2006).

[11] A. Slowik and M. Bialko, “Adaptive selection of control parameters in differential evolution algorithms,” in Computational Intelligence: Methods and Applications, L. Zadeh, L. Rutkowski, R. Tadeusiewicz, and J. Zurada, Eds. Warsaw, Poland: EXIT, pp. 244–253, (2008).

[12] J. Liu and J. Lampinen, “A fuzzy adaptive differential evolution algorithm,” Soft Comput.—A Fusion of Foundations, Methodologies and Applications, vol. 9, no. 6, pp. 448–462, Jun. (2005).

[13] M. M. Ali and A. Torn, “Population set-based global optimization algorithms: Some modifications and numerical studies,” Comput. Oper. Res., vol. 31, no. 10, pp. 1703–1725, Sep. (2004).

[14] E. Mezura-Montes, C. A. Coello Coello, J. Velázquez-Reyes, and L. Munoz-Dávila, “Multiple trial vectors in differential evolution for engineering design,” Eng. Optim., vol. 39, no. 5, pp. 567–589, Jul. (2007).

[15] Z. Skolicki and K. De Jong, “The influence of migration sizes and intervals on island models,” in Proceedings of the Genetic and Evolutionary Computation Conference (GECCO-2005), ACM Press, (2001).

[16] R. Storn, “On the usage of differential evolution for function optimization,” in Proc. of the 1996 Biennial Conference of the North American Fuzzy Information processing society- NAFIPS, Edited by: M. H. Smith, M. A. Lee, J. Keller and J. Yen, June 19-22, Berkeley, CA, USA, IEEE Press, New York, pp 519-523, (1996).

[17] F. Amato, A. Lopez, E. Maria, P. Vanhara, A. Hampl, “ Artificial neural networks in medical diagnosis “, J Appl Biomed.11, 2013, DOI 10.2478/v10136-012-0031-x ISSN 1214-0287, pp.47-58, (2013).

[18] https://archive.ics.uci.edu/ml/datasets.html

[19] Z. Skolicki and K. De Jong. The influence of migration sizes and intervals on island models. In GECCO’05: Proceedings of the 2005 conference on Genetic and evolutionary computation, pages 1295-1302, New York, NY, USA, ACM, (2005).

INTENTIONAL BLANK

A NEW SURVEY ON BICLUSTERING OF MICROARRAY DATA

Haifa Ben Saber[1,2] and Mourad Elloumi[1,3]

[1]Laboratory of Technologies of Information and Communication and Electrical Engineering (LaTICE) at National Superior School of Engineers of Tunis (ENSIT) - Tunis university, Tunis, Tunisia
[2]Time université
[3]University of Tunis-El Manar, Tunisia
[2]bensaberhaifa1@gmail.com,[3]Mourad.Elloumi@gmail.com

ABSTRACT

There are subsets of genes that have similar behavior under subsets of conditions, so we say that they coexpress, but behave independently under other subsets of conditions. Discovering such coexpressions can be helpful to uncover genomic knowledge such as gene networks or gene interactions. That is why, it is of utmost importance to make a simultaneous clustering of genes and conditions to identify clusters of genes that are coexpressed under clusters of conditions. This type of clustering is called biclustering.

Biclustering is an NP-hard problem. Consequently, heuristic algorithms are typically used to approximate this problem by finding suboptimal solutions. In this paper, we make a new survey on biclustering of gene expression data, also called microarray data.

KEYWORDS

Biclustering, heuristic algorithms, microarray data,genomic knowledge.

1. INTRODUCTION

A DNA Microarray is a glass slide covered with a chemical product and DNA samples containing thousands of genes. By placing this glass slide under a scanner, we obtain an image in which colored dots represent the expression level of genes under experimental conditions [1]. This process can be summerized by Figure 1. As shown in Figure 2, the obtained colored image can be coded by a matrix *M*, called gene expression data, or microarray data, where the i^{th} row represents the i^{th} gene, the j^{th} column represents the j^{th} condition and the cell m_{ij} represents the expression level of the i^{th} gene under the j^{th} condition. Simultaneous clustering of rows (genes) and columns (conditions) of this matrix enables to identify subsets of genes that have similar behavior under subsets of conditions, so we say that they coexpress, but behave independently under other subsets of conditions. This type of clustering is called biclustering. Biclustering of microarray data can be helpful to discover coexpression of genes and, hence, uncover genomic knowledge such as gene networks or gene interactions. Biclustering is an NP-hard problem [3]. Consequently, heuristic algorithms are typically used to approximate this problem by finding suboptimal solutions. In this paper, we make a new survey on biclustering of microarray data.

Natarajan Meghanathan et al. (Eds) : NeTCoM, CSIT, GRAPH-HOC, SPTM - 2014
pp. 165–183, 2014. © CS & IT-CSCP 2014 DOI : 10.5121/csit.2014.41314

In this paper, we make a survey on biclustering of gene expression data. The rest of the paper is organized as follows: First, we introduce some definitions related to biclustering of microarray data. Then, we present in section 3 some evaluation functions and biclustering algorithms. Next, we show how to validate biclusters via biclustering tools on microarrays datasets. Finally, we present our conclusion.

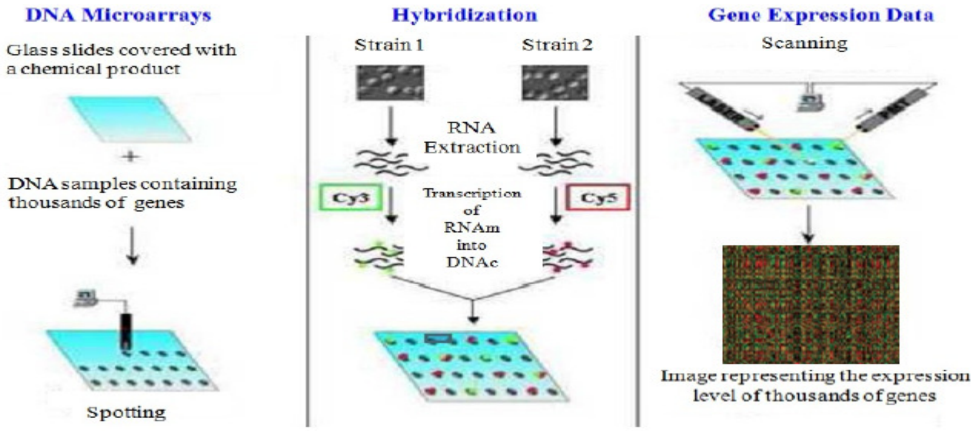
DNA Microarrays
Glass slides covered with a chemical product
+
DNA samples containing thousands of genes
Spotting
Hybridization
Strain 1
Strain 2
RNA Extraction
Cy3
Cy5
Transcription of RNAm into DNAc
Gene Expression Data
Scanning
Image representing the expression level of thousands of genes

Figure 1. Generation from a DNA microarray of an image where colored dots represent the expression level of genes under experimental conditions [2]

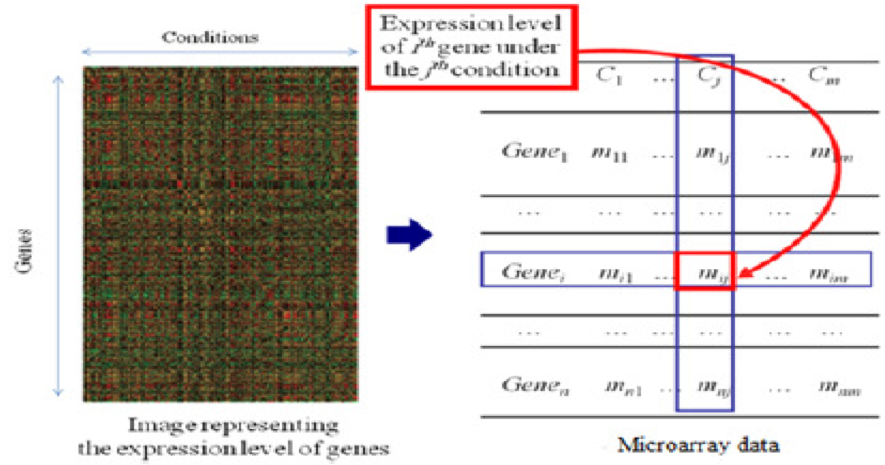
Conditions
Genes
Image representing the expression level of genes
Expression level of i^{th} gene under the j^{th} condition
Microarray data

	C_1	...	C_j	...	C_m
$Gene_1$	m_{11}	...	m_{1j}	...	m_{1m}
...	...	...	...	...	...
$Gene_i$	m_{i1}	...	m_{ij}	...	m_{im}
...	...	...	...	...	...
$Gene_n$	m_{n1}	...	m_{nj}	...	m_{nm}

Figure 2. Coding of the generated colored image to a microarray data

2. BICLUSTERING OF MICROARRAY DATA

Let introduce some definitions related to a biclustering of microarray data [3].

Biclusters : Let $I = \{1,2,...,n\}$ be a set of indices of n genes, $I = \{1,2,...,m\}$ be a set of indices of m conditions and $M(I,J)$ be a data matrix associated with I and J. A bicluster associated with the data matrix $M(I,J)$ is a couple $M(I',J')$ such that $I' \subseteq I$ and $J' \subseteq J$.

Types of biclusters : A bicluster can be one of the following cases:

• Bicluster with constant values on rows:

$$m_{ij} = c + a_i \tag{2.1}$$

$$m_{ij} = c * a_i \tag{2.2}$$

where c is a constant and a_i is the adjustment for the row i.

• Bicluster with constant values on columns:

$$m_{ij} = c + b_j \tag{2.3}$$

$$m_{ij} = c * b_j \tag{2.4}$$

where b_j is the adjustment for the column $_{j}$.

• Bicluster with coherent values: There are two types of biclusters with coherent values. Those with additive model and those with multiplicative model defined respectively by:

Those with additive model:

$$m_{ij} = c + a_i + b_j \tag{2.5}$$

And those with multiplicative model:

$$m_{ij} = c * a_i * b_j \tag{2.6}$$

• Bicluster with coherent evolution: It is a bicluster where all the rows (resp. columns) induce a linear order across a subset of columns (resp. rows).

Groups of biclusters : A group of biclusters can be one of the following types [4]:

1. Single bicluster (Figure 3. (a)),

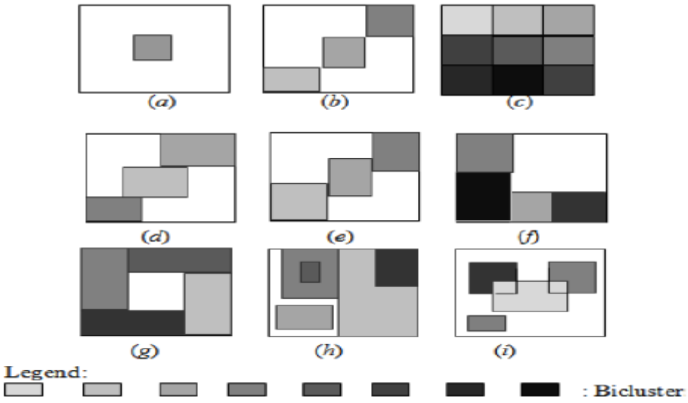

Figure 3.Types of groups of biclusters

2. Exclusive rows and columns group of biclusters (Figure 3. (b)),
3. Non-overlapping group of biclusters with checkerboard structure (Figure 3. (c)),
4. Exclusive rows group of biclusters (Figure 3. (d)),
5. Exclusive columns group of biclusters (Figure 3. (e)),
6. Non-overlapping group of biclusters with tree structure (Figure 3. (f)),
7. Non-overlapping non-exclusive group of biclusters (Figure 3. (g)),
8. Overlapping group of biclusters with hierarchical structure (Figure 3. (h)),
9. Or, arbitrarily positioned overlapping group of biclusters (Figure 3. (i)).

We note also that a natural way to visualize a group of biclusters consists in assigning a different color to each bicluster and in reordering the rows and the columns of the data matrix so that we obtain a data matrix with colored blocks, where each block represents a bicluster.The biclustering problem can be formulated as follows: Given a data matrix *M*, construct a group of biclusters B_{opt} associated with *M* such that:

$$f(B_{opt}) = \max_{B \in BC(M)} f(B) \tag{2.7}$$

where *f* is an objective function measuring the quality, i.e., degree of coherence, of a group of biclusters and *BC*(*M*) is the set of all the possible groups of biclusters associated with *M*. This problem is NP-hard [4,5].

3. EVALUATION FUNCTIONS

An evaluation function is an indicator of the performance of a biclustering algorithm. There are two main classes of evaluation functions: Intra-biclusters evaluation functions and inter-biclusters evaluation functions.

3.1. Intra-biclusters evaluation functions

An intra-biclusters evaluation function is a function that measures the quality of a bicluster, i.e., it quantifies the coherence degree of a bicluster. There are several intra-biclusters evaluation functions.

- The $E_{AVSS}(I',J')$ is defined as follows[6]:

$$E_{AVSS}(I',J') = \frac{\sum_{i \in I'} \sum_{j \in J'} s_{ij}}{|I'||J'|} \tag{3.1}$$

where (I',J') is a bicluster, s_{ij} is a similarity measure among elements of the row *i* and the column *j* with others elements belonging to *I'* and *J'*. It follows that a number of these functions are particular cases of the *AVerage Similarity Score* (AVSS).

- The *Average Row Variance* (ARV) is defined as follows [7]:

$$E_{ARV}(I',J') = \frac{\sum_{i \in I'} \sum_{j \in J'} (m_{ij} - m_{iJ'})^2}{|I'||J'|} \tag{3.2}$$

where $m_{iJ'}$ is the average over the row *i*. It follows that the biclusters that contain rows with large changes in their values for different columns are characterized by a large row variance. The ARV guarantees that a bicluster captures rows exhibiting coherent trends under some subset columns.

- The *Mean Squared Residue* (MSR) is defined as follows [8]:

$$E_{MSR}(I',J') = \frac{\sum_{i\in I'}\sum_{j\in J'}(m_{ij} - m_{iJ'} - m_{I'j} + m_{I'J'})^2}{|I'||J'|} \tag{3.3}$$

where $m_{I'J'}$ is the average over the whole bicluster, $m_{I'j}$ is the average over the column j, $m_{iJ'}$ is the average over the row i. The E_{MSR} represents the variation associated with the interaction between the rows and the columns in the bicluster. It follows that a low (resp. high) E_{MSR} value, i.e., close to 0 (resp. higher than a fixed threshold d), indicates that the bicluster is strongly (resp. weakly) coherent. The E_{MSR} function is inadequate to assess certain types of biclusters. For example, the E_{MSR} function is good for biclusters of coherent values with additive model but not for coherent values with multiplicative model.

- The *Volume* (V) is defined as follows [7]:

$$E_V(I',J') = |I'||J'| \tag{3.4}$$

This function enables to have the maximum-sized bicluster that does not exceed a certain coherence value expressed as a MSR score. $E_V(I',J')$ finds the maximum-sized bicluster that does not exceed a certain coherence value [9] expressed as a MSR score. Hence, discovered biclusters have a high $E_V(I',J')$ maximized and lower E_{MSR} than a given threshold $\delta \geq 0$.

- The *Mean Square Error* (MSE) is defined as follows [10]:

$$E_{MSE}(I,J) = \frac{\sum_{i\in I}\sum_{j\in J}(m_{ij} - m_{iJ'} - m_{Ij} + m_{IJ})^2}{|I||J|} \tag{3.5}$$

where m_{IJ} is the average over the whole matrix, m_{Ij} is the average over the column j of the whole matrix and $m_{iJ'}$ is the average over the row i. This function identifies constant biclusters.

- The *Average Correlation Value* (ACV) is defined as follows [5, 11]:

$$E_{ACV}(I',J') = \max\left\{ \frac{\sum\limits_{i\in I'}\sum\limits_{j\in I'} |r_{ij}| - |I'|}{|I'|(|I'|-1)}, \frac{\sum\limits_{k\in J'}\sum\limits_{l\in J'} |r_{kl}| - |J'|}{|J'|(|J'|-1)} \right\} \tag{3.6}$$

where $r_{ij}(i \neq j)$ (resp. $r_{kl}(k \neq l)$) is the Pearson's correlation coefficient associated with the row indices i and j (resp. k and l) in the bicluster (J',J') [8]. The values of E_{ACV} belong to [0;1], hence, a high (resp. low) E_{ACV} value, i.e., close to 1 (resp. close to 0), indicates that the bicluster is strongly (resp. weakly) coherent. However, the performance of the E_{ACV} function decreases when noise exists in the data matrix [5, 11].

- The *Average Spearman's Rho* (ASR) is defined as follows [2]:

$$E_{ASR}(I',J') = 2\max\left\{ \frac{\sum\limits_{i\in I'}\sum\limits_{j\in I', j\geq i+1} \rho_{ij}}{|I'|(|I'|-1)}, \frac{\sum\limits_{k\in J'}\sum\limits_{l\in J', l\geq k+1} \rho_{kl}}{|J'|(|J'|-1)} \right\} \tag{3.7}$$

where $\rho_{ij}(i \neq j)$ (resp. $\rho_{KL}(k \neq l)$) is the Spearman's rank correlation associated with the row indices i and j in the bicluster (I',J') [12], The values of the E_{ASR} function belong also to *[-1,1]*, hence, a high (resp. low) E_{ASR} value, i.e., close to 1 (resp. close to -1), indicates that the bicluster is strongly (resp. weakly) coherent. On the other hand, like Spearman's rank correlation, the E_{ASR} is less sensitive to the presence of noise in data [2]. There are other intra-biclusters evaluation function like the *Average Correspondance Similarity Index* (ACSI) [2].

3.2. Inter-biclusters evaluation functions

An inter-biclusters evaluation function is a function that measures the quality of a group of biclusters, i.e., it assesses the accuracy of an algorithm to recover true implanted biclusters in a data matrix. There are several inter-biclusters evaluation functions. In what follows, we present some of them:

Let M_1 and M_2 be two groups of biclusters defined as follows:

$M_1 = \{B_1^{(1)}, B_2^{(1)}, \ldots, B_{K_1}^{(1)}\}$, where $B_l^{(1)} = (G_l^{(1)}, C_l^{(1)})$, G_l and C_l are respectively the l^{th} gene and condition, $1 \leq l \leq K_1$: Set of true implanted biclusters in a data matrix M.

$M_2 = \{B_1^{(2)}, B_2^{(2)}, \ldots, B_{K_2}^{(2)}\}$, where $B_m^{(j)} = (G_m^{(2)}, C_m^{(2)})$, G_m and C_m are respectively the m^{th} gene and condition, $1 \leq m \leq K_2$: Set of the biclusters extracted by a biclustering algorithm.

- The *Prelic* index is defined as follows:

$$I_{Prelic}(M_1, M_2) = \frac{1}{K_1} \sum_{i=1}^{n_1} \max_j S_{Prelic}(B_i^{(1)}, B_j^{(2)}) \tag{3.8}$$

where S_{Prelic} is based on the *Jaccard index* for two sets and defined as follows:

$$S_{Prelic}(B_i, B_j) = \frac{|G_i \cap G_j|}{|G_i \cup G_j|} \tag{3.9}$$

This index compares two solutions based on categorization of genes. However, it compares only genes sets.

- The *Liu and Wang index* is defined as follows:

$$I_{Liu\&Wang}(M_1, M_2) = \frac{1}{K_1} \sum_{i=1}^{K_1} \max_j S_{Liu\&Wang}(B_i^{(1)}, B_j^{(2)}) \tag{3.10}$$

where

$$S_{Liu\&Wang}(B_i, B_j) = \frac{|G_i \cap G_j| + |C_i \cap C_j|}{|G_i \cup G_j| + |C_i \cup C_j|} \tag{3.11}$$

It compares two solutions by considering both genes and conditions.

- The *wtjaccard index* is defined as follows:

$$I_{wt\,jaccard}(M_1, M_2) = \frac{\sum_{i=1}^{K_1} |B_i^{(1)}| * \max_j S_{Jaccard}(B_i^{(1)}, B_j^{(2)})}{\sum^{K_1} |B_i^{(1)}|} \tag{3.12}$$

Where

$$S_{Jaccard}(B_i,B_j) = \frac{|C_i \cap B_j| + |G_i \cap G_j|}{|C_i| + |B_j| - |C_i \cap C_j|} \tag{3.13}$$

- The *Dice index* is defined as follows:

$$I_{Dice}(M_1,M_2) = \frac{1}{K_1}\sum_{i=1}^{K_1} \max_j S_{Dice}(B_i^{(1)},B_j^{(2)}) \tag{3.14}$$

where:

$$S_{Dice}(B_i,B_j) = \frac{2 * |C_i \cap C_j|}{|C_i| + |C_j|} \tag{3.15}$$

which is proposed in [13] and called F-measure in biclustering cases to computes the overall relevance of two bicluster solutions.

- The *Santamaría index* is defined as follows:

$$I_{wtDice}(M_1,M_2) = \frac{\sum_{i=1}^{K_1} |B_i^{(1)}| * \max_j S_{Dice}(B_i^{(1)},B_j^{(2)})}{\sum_{i=1}^{K_1} |B_i^{(1)}|} \tag{3.16}$$

The Santamaría index is the most conservative index among above others indices and used for biclustering case [14, 13]. In fact, while the Prelic index compares only object sets and the LW index compares object sets and feature sets independently, the Santamaría index compares two solutions using pairs of genes and conditions.

For gene expression case, the *Gene Match Score* (GMS) function doesn't take into account column match. It is given by:

$$E_{GMS}(B_1,B_2) = \frac{1}{|B_1|}\sum_{(I_1,J_1)\in B_1} \max_{(I_2,J_2)\in B_2} \frac{|I_1 \cap I_2|}{|I_1 \cup I_2|}, \tag{3.17}$$

where B_1 and B_2 are two groups of biclusters and the pair (I,J) represents the submatrix whose rows and columns are given by the set I and J, respectively.

The *Row and Column Match Scores* (RCMS) assess the method's accuracy to recover known biclusters and reveal true ones. Thereafter, more similar measures of match scores have been introduced [5, 15, 6]. For instance, the evaluation functions, herein called Row and Column Match Scores, E_{RCMS1} and E_{RCMS2}, are proposed in [6] and [15], respectively and given by:

$$E_{RCMS_1}(B_1,B_2) = \frac{1}{|B_1|}\sum_{(I_1,J_1)\in B_1} \max_{(I_2,J_2)\in B_2} \frac{|I_1 \cap I_2| + |J_1 \cap J_2|}{|I_1 \cup I_2| + |J_1 \cup J_2|}, \tag{3.18}$$

$$E_{RCMS_2}(B_1,B_2) = \frac{1}{|B_1|}\sum_{(I_1,J_1)\in B_1} \max_{(I_2,J_2)\in B_2} \frac{|I_1 \cap I_2| + |J_1 \cap J_2|}{|I_1| + |J_1|} \tag{3.19}$$

All these measures of match score are used to assess the accuracy of an algorithm to recover known biclusters and reveal true ones. Both E_{RCMS1} and E_{RCMS2} have the advantage of reflecting, simultaneously, the match of the row and column dimensions between biclusters as opposed to E_{GMS} that doesn't take into account column match. They vary between 0 and 1 (the higher the better the accuracy). Let B_{opt} denote the set of true implanted biclusters in the data matrix M and B the set of the output biclusters of a biclustering algorithm. Thus, $E_{GMS}(B_{opt},B)$ and E_{RCMS1} (B_{opt},B) express how well each of the true biclusters are detected by the algorithm under consideration. E_{RCMS2} (B_X,B_Y), where B_X (resp. B_Y) denotes the set of biclusters detected by the algorithm X (resp. Algorithm Y), has the particularity to allow the quantification of how well each bicluster identified by the algorithm X is contained into some bicluster detected by the algorithm Y.

4. BICLUSTERING ALGORITHMS

As we mentioned earlier, the biclustering problem is NP-hard [3, 10]. Consequently, heuristic algorithms are typically used to approximate the problem by finding suboptimal solutions. We distinguish different approaches adopted by biclustering approaches[3].

4.1. Iterative Row and Column Clustering Combination Approach

By adopting the Iterative Row and Column Clustering Combination Approach (IRCCC) approach, we apply clustering algorithms on both rows and columns separately and then combine the results to obtain biclusters [56]. Table 5 is a synoptic table of biclustering algorithms adopting IRCCC approach. The conceptually simpler way to perform biclustering using existing algorithms without searching novels algorithms. But, this approach consider approximatively same advantages and drawbacks that clustering algorithms used. Among the algorithms adopting this approach we mention Croki2 [58], Crobin [58], DCC [59], ITWC [61], CTWC [54] and Bi-SOM [60].

Table 1. Biclustering algorithms adopting IRCCC approach.

Algorithms Bicluster discovery	**Types of biclusters**	**Types of groups of biclusters**	**Data type**	**Time complexity**
Croeuc [57]	Coherent values	–	One at time Continuous	–
Croki2 [58]	Coherent values	–	One at time Continuous	–
CroBin[57]	Coherent values	–	One at time Continuous	–
CemCroki [57]	Coherent values	–	One at time Continuous	–
DCC [59]	Coherent values	Exclusive dimension	One at time Continuous	–
Bi-SOM [60]	Coherent values	–	-	–
ITWC [61]	Coherent values	–	One at time Continuous	–
CTWC[54]	Constant columns	Arbitrarily positioned overlapping	One at time Continuous	–

4.2. Greedy Iterative Search Approach

By adopting the Greedy Iterative Search (GIS), first, we construct submatrices of the data matrix by adding/removing a row/column to/from the current submatrix that optimizes a certain function. Then, we reiterate this process until no other row/column can be added / removed to/from any submatrix. This approach presents the same advantage and drawback as DC. They may make wrong decisions and loose good biclusters, but they have the potential to be very fast. Among the algorithms adopting this approach we mention Spectral [16], Quest [17], Random Walk Biclustering [18], BicFinder [19], MSB [6], ISA [17, 20], OPSM [21] and SAMBA [17, 22]. Table 1 is a synoptic table of biclustering algorithms adopting GIS approach.

Table 2. Biclustering algorithms adopting GIS approach.

Algorithms	**Types of biclusters**	**Types of groups of biclusters**	**Bicluster discovery strategy**	**Data type**	**Time complexity**
d-biclusters[10]	Coherent values	Arbitrarily positioned overlapping	One at a time	Continuous	$O(nm)$
FLOC [23]	Coherent values	Arbitrarily positioned overlapping	All at time	Continuous	$O((n+m)^2kp$
xMotif [17]	Coherent evolution	Single bicluster arbitrarily positioned overlapping	All at time	Discret	–
RMSBE [8]	Constant values	–	All at time	Binary	$O(kC_u(1-p_r)((n+m)+p_r))$
MSB[6]	Constant values	–	All at time	Binary	$O((n+m)^2)$ $O(k(n^2+m^2))$
OPSMs [24]	Coherent evolution	Single bicluster arbitrarily positioned overlapping	One at a time	Continuous	$O(nm^3I)$
Spectral [16]	Coherent values	Checkerboard structure	All at time	Continuous	–
d-Pattern[17, 10]	Constant rows values	Arbitrarily positioned overlapping	All at time	Continuous	$O(nm(n+m)k)$
BISOFT[25]	Coherent values		One at a time	Categorical	–
sv4d [26]	Constant values	A checkerboard structure	All at time	Binary	–
ISA[17]	Coherent values	Overlapping	One at time	Continuous	–
BicBin [27]	Constant values	Overlapping	A set of biclusters	Binary	–

where :

n and *m* are respectively the numbers of genes and conditions in the data matrix,
l is the number of the best partial models of order,

K is the maximum number of iterations,
C_u isthe cost of computing the new residue and the new row variance of the bicluster after performing a move,
p_r is a user-provided probability that the algorithm is allowed to execute a random move.

4.3. Exhaustive Bicluster Enumeration Approach

By adopting the Exhaustive Bicluster Enumeration (EBE), We identify all the possible groups of biclusters in order to keep the best one, i.e., the one that optimizes a certain evaluation function. The advantage of this approach is that it is able to obtain the best solutions. Its drawback is that it is costly in computing time and memory space Among the algorithms adopting this approach we mention BSGP[28, 29], OPC [30, 6], CPB [30], IT[31], e-Bmotif [29], BIMODULE [32], RAP [26], BBK [33] and MSB [6]. Table 2 is a synoptic table of biclustering algorithms adopting EBE approach.

Table 3. Biclustering algorithms adopting EBE approach.

Algorithms	**Types of biclusters**	**Types of groups of biclusters**	**Bicluster discovery strategy**	**Data type**	**Time complexity**
e-BiMotif [34][29]	Coherent values	–	All at time	Contingence	$O(2^n mlog(m))$
CPB [30]	Coherent values	–	All at time	Contingence Categorical	–
OPC [30]	Coherent evolution	Arbitrarily positioned overlapping	All at time		–
PClusters [10]	Coherent values	Non-overlapping non-exclusive	All at time	Binary	$O(n^2m^4(nlog(n)+mlog(m)))$
BSGP [28, 29]	Coherent values	–	All at time	Contingence Categorical	–
Expander [35]	Coherent evolution	–	One a time	Categorical	–
IT [31]	Coherent values	–	All at time	Contingence	–
BIMODULE [32]	Coherent values	–	One a time	Contingence Categorical	–
RAP [26]	Constant row values coherent values	Overlapping	One a time	Continuous	–
SAMBA [17, 22]	Coherent evolution	Arbitrarily positioned Overlapping	All at time	Continuous	$O((n2^{d+1})^{log(r+1)/r(rd)})$
MDS[36]		–			$O(2^m+m^2nlog(n)+n^2mlog(m))$
cHawk [37]	Constant values//coherent Evolution	Overlapping	All at time	Categorial	–
BBK[33]	Constant values	–	One at time	Binary	–

Where

d is the bounded degree of gene vertices in a bipartite graph *G* whose two sides correspond to he set of genes and the set of conditions.
r is the maximum weight edge in the bipartite graph *G*.

4.4. Distribution Parameter Identification Approach

By adopting the Distribution Parameter Identification (DPI) approach use a statistical model to identify the distribution parameters and generate the data by minimizing a certain criterion iteratively. These algorithms certainly find the best biclusters, if they exist, but have a very serious drawback. Due to their high complexity, they can only be executed by assuming restrictions on the size of the biclusters. Among the algorithms adopting this approach we mention QUBIC [38], PRMs [39], FABIA [40], BEM [41] and BCEM [42]. Table 3 is a synoptic table of biclustering algorithms adopting DPI approach.

Table 4. Biclustering algorithms adopting DPI approach.

Algorithms Bicluster discovery	**Types of biclusters**	**Types of groups of biclusters**	**Bicluster discovery strategy**	**Data type**	**Time complexity**
PRMs [43]	Coherent constant values on Columns	Arbitrarily positioned overlapping	All at time	Binary	–
iBBiG[44]	Coherent values	Overlapping	One set at time Binary	Binary	–
Plaid[45, 46]	Coherent values	Arbitrarily positioned overlapping	One at time	Continuous	$O(n^2)$
QUBIC[38]	Constant columns or rows	Exclusive dimension	One at time	Discrete	–
FABIA[40]	Constant values	Overlapping	All at time	Catgeorial binary	–
BEM [41]	Coherent values	–	All at time	Continuous binary	$O(nm)$
BCEM[42]	Coherent values	–	All at time	Continuous binary	–
ISA [20]	Coherent or constant values	–	One at a time	Continuous	–
Gibbs[47]	Constant columns or rows	Exclusive dimension	One at a time	Catgeorial binary	–

4.5. Divide and Conquer Approach

By adopting the Divide-and-Conquer (DC) approach, first, we start by a bicluster representing the whole data matrix then we partition this matrix in two submatrices to obtain two biclusters. Next, we reiterate recursively this process until we obtain a certain number of biclusters verifying a specific set of properties. The advantage of DC is that it is fast, its drawback is that it may ignore good biclusters by partitioning them before identifying them. DC algorithms have the significant advantage of being potentially very fast. However, they have the very significant drawback of being likely to miss good biclusters that may be split before they can be identified. Among the algorithms adopting this approach we mention OWS [48], TWS [49], BiBit [28] and BARTMAP [50] and GS [51].

Table 5. Biclustering algorithms adopting DC approach.

Algorithms Bicluster discovery	**Types of biclusters**	**Types of groups of biclusters**	**Data type**	**Time complexity**
Block Clustering [52]	Constant values	Non-overlapping tree structure	Binary categorial	–
OWS[53]	Constant values	All at time	Continuous	$O(n)$
TWS [54]	Constant values	All at time	Continuous	–
BiBit [28]	Constant values	All at time	Binary	$O(nm\beta \min\{n,m\})$
BiBit [28]	Constant values	All at time	Binary	–
Cmnk [44]	Constant values	One at time	Binary	–
GS [51]	Constant values	One at time	Binary	–

where β is the number of biclusters that are not entirely contained in any other bicluster.

5. BICLUSTERING VALIDATION

There are two types of biclusters validation;

(i) Statistical validation: It is used to validate synthetical data

(ii) Biological validation: It is used to validate biological data

5.1. Statistical validation

Statistical validation can be made by adopting one or many of the following indices:

Separation: It reflects how well the biclusters are separated from each other. Separation between two biclusters

A and B is defined as follows [62]:

$$Sep(A,B) = 1 - \frac{A \cap B}{A \cup B} \tag{5.1}$$

Coverage: We distinguish three types of coverage, matrix coverage, genes coverage and conditions coverage:

$$Matrix\ coverage = \frac{Number\ of\ the\ cells\ covered\ by\ the\ extracted\ biclusters}{Total\ number\ of\ cells\ in\ the\ matrix} \tag{5.2}$$

$$Genes\ coverage = \frac{Number\ of\ the\ genes\ covered\ by\ the\ extracted\ biclusters}{Total\ number\ of\ genes\ in\ the\ matrix} \tag{5.3}$$

$$Conditions\ coverage = \frac{Number\ of\ the\ conditions\ covered\ by\ the\ extracted\ biclusters}{Total\ number\ of\ conditions\ in\ the\ matrix} \tag{5.4}$$

Compactness: It assesses cluster homogeneity, with intra-cluster variance[63].

Connectedness: It assesses how well a given partitioning groups data items together with their nearest neighbours in the data space [63].

Coherence: It expresses how well a bicluster is fitted to a specified model. The coherence is computed thanks to compactness and connectedness.

Significance: It is computed thanks to *p*-value$_B$. Let B be a bicluster, p□value is defined as follows [15]:

$$p\text{-value}_B = 1 - \phi\left(\frac{|1_B|/|B| - p}{\sqrt{\frac{p(1-p)}{|B|}}}\right) \qquad (5.5)$$

where f is the standard normal distribution function, $|1_B|$ is the number of 1's in the bicluster *B* and $p= k/(|I|*|J|)$ of 1's in $M(I,J)$, k is the number of 1's in the binary matrix M_b. A bicluster *B* is considered as potentially significant at a level of significance α if *p*-value$_B$< α .

5.2. Biological validation

Biological validation can qualitatively evaluate the capacity of an algorithm to extract meaningful biclusters from a biological point of view. To assess biologically biclusters, we can use Gene Ontology (GO) annotation [64]. In GO, genes are assigned to three structured, controlled vocabularies, called ontologies: biological process, cellular components and molecular functions. The GO Consortium (GOC)[64] [65] is involved in the development and application of the GO. In what follows, we briefly report some R tools relared to GOC [66, 67]:

- AnnotationDbi: It provides user interface and database connection code for annotation data packages using SQLite data storage.
- FunCluster: It is a functional profiling and analysis of microarray expression data based on GO & KEGG.
- GExMap: It is an intuitive visual tool to perform a GO and to test to unveil genomic clusters, graphical interpretations and statistical results in pdf files.
- GO.db annotation: It provides detailed information about the latest version of the GOs and it is updated biannually.
- GOsummaries: It shows GO enrichment results in the context of experimental data.
- GOstats: It determines which GOs found in gene lists are statistically over/under-represented.
- goTools: It compares the GOs represented by the genes in the three gene lists (biological process, molecular function and cellular component).
- topGO: It provides tools for testing GO terms while accounting for the topology of the GO graph. Different test statistics and different methods for eliminating local similarities and dependencies between GO terms can be implemented and applied.

6. TOOLS

There are also many R microarray biclustering tools. Table 6. presents a few examples on tools and here are some examples [68]:

- arules: It is a mining association rules and frequent itemsets. It provides the infrastructure for representing, manipulating and analyzing transaction data and patterns. It also provides interfaces of the association mining algorithms Apriori and Eclat [69].
- lattice: It is a high-level data visualization system with an emphasis on multivariate data. It supports the creation of trellis graphs to display multivariate relationship between variables, conditioned on one or more other variables via R graphics [69].
- rootSolve: It finds the root of nonlinear functions, solves the steady-state conditions for uni/multi-component and equilibrium analysis of ordinary differential equations via a dynamically running; like gradient and Jacobian matrices, non-linear equations by the Newton-Raphson algorithm.

Table 6. Tools used to evaluate and compare biclustering algorithms

Tool	**Biclustering algorithms**	**Reference**
Lattice	*Galois lattice*	[17]
arules	*rules*	[71]
rootSolve, pracma	*Newton Raphson*	[71]
blockcluster	*Coclustering*	[17]
biclustGUI	CC, *Plaid*, BiMAX,, xMOTIFs, xQuest, Spectral, FABIA, ISA	[20]
biclust	Plaid, BiMAX, xMOTIFs, *xQuest*, *Spectral*	[17]
BcDiag	*biclust, eisa, isa2*	[17]
FABIA, FABIAs, FABIAp,	FABIA	[40]
NMF	NMF	[70]
s4vd	*s4vd*	[26]
qubic	*Rqubic*	[38]
eisa, isa2	ISA	[17]
BicARE	FLOC	[72]
ThreeWayPlaid	*Plaid for three-dimensional data*	[46]
IBBigs	iBBiG	[44]
Superbiclust	*Ensemble Biclustering*	[73, 41]
HSSVD	HSSVD	[46]
FacPad	*Factor analysis for pathways*	[45]
FastICA	*Fast independent component analysis*	[74]
CMonkey	*cMonkey*	[75]

- pracma: It root finds through Newton-Raphson or Secant algorithms [70] via using functions from numerical analysis and linear algebra, numerical optimization, differential equations and some special functions. It also uses Matlab function names where appropriate to simplify porting.
- BicARE: It is based on the FLOC algorithm [23] for biclustering analysis and results exploration.
- BcDiag: It provides methods for data pre-processing, visualization, and statistical validation to diagnostic and visualize in two-dimensional data based on two way anova [40] and median polish residual plots for biclust package output obtained from biclust, eisa-isa2 and fabia packages [17][40]. In addition, the biclust package can be used via biclustGUI, i.e. R commander plug in.

- blockcluster: It performs coclustering of binary, contingency and categorical datasets with utility functions to visualize the coclustered data. It contains a function cocluster which
- performs coclustering and returns object of appropriate class. It also contains coclust strategy function which returns an object of class strategy.
- rqubic: It represents an implementation of the QUBIC algorithm [38] for the qualitative biclustering with gene expression data.
- HSSVD: It discovers and compares subgroups of patients and genes which simultaneously display unusual levels of variability. It detects both mean and variance biclusters by testing the biclustering with heterogeneous variance.
- iBBig: It optimizes applying binary data analysis to meta-gene set analysis of gene expression datasets. It extracts iteratively groups of phenotypes from multiple studies that are associated with similar gene sets without requiring prior knowledge of the number or scale of clusters and allows discovery of clusters with diverse sizes.
- NMF: It provides a framework to perform Non-negative Matrix Factorization (NMF). It implements a set of already published algorithms and seeding methods, and provides a framework to test, develop and plug new/custom algorithms. It performs parallel computations on multicore machines.
- s4vd: It performs a biclustering via sparse singular value decomposition (svd) with a nested stability selection. The result is an biclust object and thus all methods of the biclust package can be applied.
- superbiclust: It generates as a result a number of (or super) biclusters with none or low overlap from a bicluster set, i.e. ensemble biclustering [42], with respect to the initialization parameters for a given bicluster solution. The set of robust biclusters is based on the similarity of its elements, i.e. overlap, and on the hierarchical tree obtained via cut-off points.

7. DATASETS

There are many microarray datasets, related to R package, used to evaluate biclustering algorithms [68]. Table 7. presents a few examples on these datasets.

Table 7. Microarray datasets used to evaluate biclustering algorithms

Package	**List of datasets**
aroma. Copy-number (cn) and aroma. for affyrmetrix anpuce	Spleen
Abd	Analysis of Biological Data (abd)
ICluster	*Breast cancer*, DNA *cn, breast.chr17*
ORCME	*Gene expression*
Adegenet	*Genetic and genomic*
SNPMClust	*Dose-response microarray*
DCGL	*Differential co-expression and regulation analysis*
Opmdata	*OmniLog(R) Phenotype Microarray data (opmdata)*
Knorm	*Across multiple biologically interrelated experiments*
Biclust	*BicatYeast*
DDHFm	*Data-Driven Haar-Fisz for Microarrays (DDHFm)*
integrativeMEdata	*Categorical clinical factors, cancer microarray*
Madsim	*Flexible microarray data simulation model (madsim)*
EMA	*Easy Microarray data Analysis (EMA)*
FBN	*SNP microarray*
BioConductor	*Acute Lymphocytic Leukemia* (ALL), *arrayMissPattern.*

Bioconductor annotation Data	GO.db, GO_dbconn, GOBPANCESTOR, GOBPCHILDREN, GOBPOFFSPRING, GOBPPARENTS, GOCCANCESTOR, GOCCCHILDREN, GOCCOFFSPRING, GOCCPARENTS, GOMAPCOUNTS,
Lemma	*Laplace approximated EM Microarray Analysis (lemma)*
Maanova	*N-dye Micro 18-array affymetrix experiment*
GeneARMA	*Time-course microarray with periodic gene expression*
iGenomicViewer	IGGVex
CLAG	*Breast tumor cells*

8. CONCLUSION

The biclustering of microarray data has been the subject of a large research. No one of the existing biclustering algorithms is perfect. The construction of biologically significant groups of biclusters for large microarray data is still a problem that requires a continuous work. Biological validation of biclusters of microarray data is one of the most important open issues. So far, there are no general guidelines in the literature on how to validate biologically extracted biclusters.

REFERENCES

[1] Ouafae Kaissi. Analyse de Données Transcriptomiques pour La Recherche de Biomarqueurs Liés à Certaines Pathologies Cancéreuses. PhD thesis, University Abdelmalek Essaadi, Tangier, Morocco,, sep 2014.

[2] Sara C. Madeira and Arlindo L. Oliveira. A polynomial time biclustering algorithm for finding approximate expression patterns in gene expression time series. Algorithms for Molecular Biology, 4(8), June 2009.

[3] W. Ayadi and M. Elloumi. Algorithms in Computational Molecular Biology : Techniques,Approaches and Applications. chapter Biclustering of Microarray Data, 2011.

[4] Sara C. Madeira and Arlindo L. Oliveira. Biclustering algorithms for biological data analysis: A survey. IEEE/ACM Trans. Comput. Biol. Bioinformatics, 1:24–45, 2004. ISSN 1545-5963.

[5] Law Ngai-Fong Siu Wan-Chi Cheng, Kin-On and Alan Wee-Chung. Identification of coherent patterns in gene expression data using an efficient biclustering algorithm and parallel coordinate visualization. BMC Bioinformatics, 2008.

[6] Xiaowen Liu and Lusheng Wang. Computing the maximum similarity bi-clusters of gene expression data. Bioinformatics, 23(1):50–56, 2007.

[7] Aguilar-Ruiz and Jesús S. Shifting and scaling patterns from gene expression data. Bioinformatics, 21(20): 3840–3845, 2005.

[8] Hyuk Cho and Inderjit S. Dhillon. Coclustering of human cancer microarrays using minimum sum-squared residue coclustering. IEEE/ACM Trans. Comput. Biol. Bioinformatics, 5(3):385–400, 2008.

[9] Ranajit Das and al. Evolutionary biclustering with correlation for gene interaction networks. In Pattern Recognition and Machine Intelligence, Second International Conference, PReMI 2007, Kolkata, India, December 18-22, 2007, Proceedings, pages 416–424, 2007.

[10] Yizong Cheng and George M. Church. Biclustering of expression data. pages 93–103, 2000.

[11] Li Teng and Laiwan Chan. Discovering biclusters by iteratively sorting with weighted correlation coefficient in gene expression data. Signal Processing Systems, 50:267–280.

[12] Carazo J.-Kochi K. Lehmann-D. Pascual-Montano, A. and R. D. Pascual-Marqui. Nonsmooth nonnegative matrix factorization (nsnmf). IEEE, 2006.

[13] Rodrigo Santamara, Roberto Theran, and Luis Quintales. Bicoverlapper: A tool for bicluster visualization. Bioinformatics, 24:1212–1213, 2008.

[14] Roberto Therón Rodrigo Santamaría and Luis Quintales. A visual analytics approach for understanding biclustering results from microarray data. BMC Bioinformatics, 9(247), 2008.

[15] Pinheiro M. Arrais-J. Gomes A. C. Carreto L. Freitas A. Oliveira J. L. Moura, G. and M. A. Santos. Large scale comparative codon-pair context analysis unveils general rules that fine-tune evolution of mrna primary structure. PLoS ONE., 2007.

[16] Yuval Kluger, Ronen Basri, Joseph T. Chang, and Mark Gerstein. Spectral biclustering of microarray cancer data: Co-clustering genes and conditions. Genome Research, 13:703–716, 2003.

[17] Santamaria R. Khamiakova-T. Sill M. Theron R. Quintales L. Kaiser, S. and F. Leisch. biclust: Bicluster algorithms. R package., 2011.

[18] Eugenio Cesario Fabrizio Angiulli and Clara Pizzuti. Random walk biclustering for microarray data. Information Sciences, 178(6):1479–1497, 2008.

[19] Elloumi M. Ayadi, W. and J.-K. Hao. Bicfinder: a biclustering algorithm for microarray data analysis. Knowledge and Information Systems., 2012.

[20] Jan Ihmels, Sven Bergmann, and Naama Barkai. Defining transcription modules using large-scale gene expression data. Bioinformatics, 20(13):1993–2003, 2004.

[21] Chor B.-Karp R. Ben-Dor, A. and Z. Yakhini. Clustering gene expression patterns. 6, 2002.

[22] Amos Tanay, Roded Sharan, and Ron Shamir. Discovering statistically significant biclusters in gene expression data. In In Proceedings of ISMB 2002, pages 136–144, 2002.

[23] Jiong Yang and al. Enhanced biclustering on expression data.

[24] Chor Benny Karp Richard Ben-Dor, Amir. and Zohar. Yakhini. Discovering local structure in gene expression data: The order-preserving submatrix problem. In Proceedings of the Sixth Annual International Conference on Computational Biology, RECOMB '02, pages 49–57, New York, NY, USA, 2002. ACM.

[25] Hossam S. Sharara and Mohamed A. Ismail. Bisoft: A semi-fuzzy approach for biclustering gene expression data. In BIOCOMP, 2008.

[26] Martin Sill, Sebastian Kaiser, Axel Benner, and Annette Kopp-Schneider. Robust biclustering by sparse singular value decomposition incorporating stability selection. Bioinformatics, 27:2089–2097, 2011.

[27] Miranda van Uitert, Wouter Meuleman, and Lodewyk F. A. Wessels. Biclustering sparse binary genomic data. Journal of Computational Biology, 15(10):1329–1345, 2008.

[28] Perez-Pulido A. J. Rodriguez-Baena, D. S. and J.S. Aguilara-Ruiz. A biclustering algorithm for extracting bit-patterns from binary datasets. Bioinformatics., 2011.

[29] Elloumi M. Ayadi, W. and J.-K. Hao. A biclustering algorithm based on a bicluster enumeration tree: application to dna microarray data. BioData Mining., 2009.

[30] Tze-Haw Huang ; XingXing Song ; Mao Lin Huang. Optimized data acquisition by time series clustering in opc. IEEE., 2011.

[31] Inderjit S. Dhillon, Subramanyam Mallela, and Dharmendra S. Modha. Information-theoretic co-clustering. In Proceedings of the ninth ACM SIGKDD international conference on Knowledge discovery and data mining, pages 89–98. ACM Press, 2003.

[32] Jiun-Rung Chen and Ye-In Chang. A condition-enumeration tree method for mining biclusters from dna microarray data sets. Elsevier, 97:44–59, 2007.

[33] Stefan Bleuler Oliver Voggenreiter and Wilhelm Gruissem. Exact biclustering algorithm for the analysis of large gene expression data sets. Eighth International Society for Computational Biology (ISCB) Student Council Symposium Long Beach, CA, USA.July, pages 13–14, 2012.

[34] Joana P. Gonalves and Sara C. Madeira. e-bimotif: Combining sequence alignment and biclustering to unravel structured motifs. In IWPACBB, volume 74, pages 181–191, 2010.

[35] Shamir and al. Expander - an integrative program suite for microarray data analysis. BMC Bioinformatics, 6: 232, 2005.

[36] Dong Wang and al. Mapping query to semantic concepts: Leveraging semantic indices for automatic and interactive video retrieval. In ICSC '07: Proceedings of the International Conference on Semantic Computing, pages 313–320, 2007.

[37] W. Ahmad. chawk: An efficient biclustering algorithm based on bipartite graph crossing minimization. 2007.

[38] Haibao Tang Andrew H. Paterson Guojun Li, Qin Ma and Ying Xu. Qubic: a qualitative biclustering algorithm for analyses of gene expression data. 2009.

[39] Nir Friedman, Lise Getoor, Daphne Koller, and Avi Pfeffer. Learning probabilistic relational models. In IJCAI, pages 1300–1309, 1999.

[40] Sepp Hochreiter, Ulrich Bodenhofer, Martin Heusel, Andreas Mayr, Andreas Mitterecker, Adetayo Kasim, Tatsiana Khamiakova, Suzy Van Sanden, Dan Lin 0004, Willem Talloen, Luc Bijnens, Hinrich W. H. Göhlmann, Ziv Shkedy, and Djork-Arné Clevert. Fabia: factor analysis for bicluster acquisition. Bioinformatics, 26(12):1520–1527, 2010.

[41] Mohamed Nadif and Gérard Govaert. Block clustering via the block gem and two-way em algorithms. In AICCSA'05, pages –1–1, 2005.

[42] Mohamed Nadif and Gerard Govaert. A comparison between block cem and two-way cem algorithms to cluster a contingency table. In PKDD'05, pages 609–616, 2005.

[43] Baocheng W. Guifen, C. and Y. Helong. The implementation of parallel genetic algorithm based on matlab. Advanced Parallel Processing Technologies., 2007.

[44] Daniel Gusenleitner, Eleanor Howe, Stefan Bentink, John Quackenbush, and Aedin C. Culhane. ibbig: iterative binary bi-clustering of gene sets. Bioinformatics, 28(19):2484–2492, 2012.

[45] Lazzeroni and Owen. Plaid models for gene expression data. Statistica Sinica., 2002.

[46] Shawn Mankad and George Michailidis. Biclustering three-dimensional data arrays with plaid models. Journal of Computational and Graphical Statistics, 2013.

[47] Ole Andreatta, Massimo Lund and Morten Nielsen. Simultaneous alignment and clustering of peptide data using a gibbs sampling approach. Bioinformatics, 29(1):8–14, 2013.

[48] Hartigan. Clustering Algorithms, chapter Direct splitting. 1975.

[49] Gerard GOVAERT. La classification croisee. Modulad, 1983.

[50] Wunsch II Xu, Rui and Donald C. Bartmap: A viable structure for biclustering. Neural Netw., 24:709–716, September, 2011.

[51] Douglas Creighton Saeid Nahavandi. Thanh Nguyen, Abbas Khosravi. Spike sorting using locality preserving projection with gap statistics and landmark-based spectral clustering. Neuroscience Methods., 2014.

[52] I. Llatas, A.J. Quiroz, and J.M. Renom. A fast permutation-based algorithm for block clustering. Test, 6(2): 397–418, 1997.

[53] G. Govaert and M. Nadif. Co-Clustering. FOCUS Series. Wiley, 2013.

[54] G. Getz, E. Levine, and E. Domany. Coupled two-way clustering analysis of gene microarray data. Proc. Natl. Acad. Sci. USA, 97:12079–12084, 2000.

[55] Amela Preli´c, Stefan Bleuler, Philip Zimmermann, Anja Wille, Peter Bühlmann, Wilhelm Gruissem, Lars Hennig, Lothar Thiele, and Eckart Zitzler. A systematic comparison and evaluation of biclustering methods for gene expression data. Bioinformatics, 22:1122–1129, 2006.

[56] J. Caldas and S. Kaski. Hierarchical generative biclustering for microrna expression analysis. Computational Biology., 2011.

[57] M. Charrad. Une approche gnrique pour l-analyse croisant contenu et usage des sites web par des methodes de bipartitionnement. PhD thesis, Paris and ENSI, University of Manouba, 2010.

[58] Yves Lechevallier Malika Charrad, Gilbert Saporta, and Mohamed Ben Ahmed. Determination du nombre des classes dans l'algorithme croki de classification croisee. In EGC'09, pages 447–448, 2009.

[59] Stanislav Busygin and al. Double conjugated clustering applied to leukemia microarray data. 2002.

[60] Khalid Benabdeslem and Kais Allab. Bi-clustering continuous data with self-organizing map. Neural Computing and Applications, 22(7):1551–1562, 2013.

[61] Chun Tang, Li Zhang 0008, Aidong Zhang, and Murali Ramanathan. Interrelated two-way clustering: An unsupervised approach for gene expression data analysis. pages 41–48, 2001.

[62] Eleni Mina. Applying biclustering to understand the molecular basis of phenotypic diversity. Phd. Utrecht University Faculty of Science Department of Information and Computing Sciences, 2011.

[63] Akdes Serin. Biclustering analysis for large scale data. Phd., 2011.

[64] Michael Ashburner. Gene ontology: tool for the unification of biology. Nature Genetics 25, pages 25 –29, 2000.

[65] Gene ontology consortium. Internet:, . URL http://www.geneontology.org/,note= September2014.

[66] Pietro Hiram Guzzi, Marianna Milano, and Mario Cannataro. Mining association rules from gene ontology and protein networks: Promises and challenges. Procedia Computer Science, 29(0):1970 – 1980, 2014. International Conference on Computational Science.

[67] Xuebo Song, Lin Li, Pradip K. Srimani, Philip S. Yu, and James Z.Wang. Measure the semantic similarity of go terms using aggregate information content. IEEE/ACM Trans. Comput. Biol. Bioinformatics, 11:468–476, 2014.

[68] Cran package. Internet:, . URL http://cran.r-project.org/web/packages. July 2014.

[69] Kuznetsov S. O. Macko J. Jr. W. M. Kaytoue, M. and A. Napoli. Mining biclusters of similar values with triadic concept analysis. The Eighth International Conference on Concept Lattices and Their Applications., 2011.

[70] Chris H. Q. Ding, Tao Li, and Wei Peng. Nonnegative matrix factorization and probabilistic latent semantic indexing: Equivalence chi-square statistic, and a hybrid method. In AAAI'06, 2006.

[71] Haifa BenSaber. Classification non supervisiee des donnees des puces a ADN", ESSTT. 2010.

[72] Jiong Yang, HaixunWang,WeiWang 0010, and Philip S. Yu. An improved biclustering method for analyzing gene expression profiles. International Journal on Artificial Intelligence Tools, 14(5):771–790, 2005.

[73] Mehmet Koyuturk. Using protein interaction networks to understand complex diseases. Computer, 45(3): 31–38, 2012.

[74] C Heaton J L Marchini and B D Ripley. fastica: Fastica algorithms to perform ica and projection pursuit. R package, 2013.

[75] Baliga N. S. Reiss, D. J. and Bonneau. cmonkey integrated biclustering algorithm. R package, 2012.

AUTHORS

Professor ELLOUMI Mourad : Full Professor in Computer Science Head of the BioInformatics Group (BIG) of The Laboratory of Technologies of Information and Communication, and Electrical Engineering (LaTICE), National High School of Engineers of T unis (ENSIT), University of Tunis, Tunisia, and Professor at the Faculty of Economic Sciences and Management of Tunis (FSEGT), University of Tunis El Manar, Tunisia.

Mrs BEN SABER Haifa : Phd student on the BioInformatics Group (BIG) of The Laboratory of Technologies of Information and Communication, and Electrical Engineering (LaTICE), National High School of Engineers of Tunis (ENSIT), University of Tunis, Tunisia, and Assistant at the Time Université, Tunisia.

INTENTIONAL BLANK

TTACCA: TWO-HOP BASED TRAFFIC AWARE CONGESTION CONTROL ALGORITHM FOR WIRELESS SENSOR NETWORKS

Prabha R[1], Prashanth Kumar Gouda[1], Manjula S H[1], K R Venugopal[1]
and L M Patnaik[2]

[1]Department of Computer Science and Engineering,
University Visvesvaraya College of Engineering
Bangalore University, Bangalore, India
[2]Honorary Professor, Indian Institute of Science, Bangalore 560 001, India
heshakil@yahoo.com, prashanth333.ece@gmail.com,
shmanjula@gmail.com,
venugopalkr@gmail.com,patnaiklm@cedt.iisc.ernet.in

ABSTRACT

Congestion in Wireless Sensor Networks has negative impact on the Quality of Service. Congestion effects the performance metrics, namely throughput and per-packet energy consumption, network lifetime and packet delivery ratio. Reducing congestion allows better utilization of the network resources and thus enhances the Quality of Service metrics of the network. Traffic Aware Dynamic Routing to Alleviate Congestion in Wireless Sensor Networks reduces congestion by considering one hop neighbor routing in the network. This paper proposed an algorithm for Quality of Service Based Traffic-Aware Data forwarding for congestion control in wireless sensor networks based on two hop neighbor information. On detection of congestion, the algorithm forwards data packets around the congestion areas by spreading the excessive packets through multiple paths. The path with light load or under loaded nodes is efficiently utilized whenever congestion occurs. The main aspect of the algorithm is to build path to the destination using two independent potential fields depth and queue length. Queue length field solves the traffic-aware problem. Depth field creates a backbone to forward packets to the sink. Both fields are combined to yield a hybrid potential field to make dynamic decision for data forwarding. Network Simulator used for simulating the algorithm is NS2. The proposed algorithm performs better.

KEYWORDS

Congestion Control, Depth Potential Field, Queue Length Potential Field, Traffic-Aware, Wireless Sensor Networks.

1. INTRODUCTION

Wireless Sensor Networks (WSN) are emerged as an innovative technology which are applied in a wide range of areas like environment monitoring, military, medical systems etc.. The main task of any WSN is to collect and process information in a coordinated way in the region of

Natarajan Meghanathan et al. (Eds) : NeTCoM, CSIT, GRAPH-HOC, SPTM - 2014
pp. 185–194, 2014. © CS & IT-CSCP 2014 DOI : 10.5121/csit.2014.41315

deployment and deliver the data to the sink node via the communication path. Quality of Service (QoS) requirements in WSN differs from wired networks. The existing researches related to the QoS in WSN are classified into three categories: (i) traditional end-to-end QoS, (ii) reliability assurance, and (iii) application-specific QoS. In case of wired networks QoS routing is performed usually through resource reservation. WSN networks characteristics such as loose network state information, dynamically varying network topology, unrestricted mobility of hosts, and limited availability of bandwidth and battery power make QoS very demanding. While performing a certain task in WSN, when the data traffic becomes heavier in sensor node, packets are stored in the buffer. When the buffer reaches to threshold level, there will be traffic at the node for the data packets. These results in increased contention, increased retransmissions, decreased packet delivery ratios and increased energy consumption. Data loss due to congestion ultimately threatens the Quality of Service parameters namely throughput, packet delivery ratio, latency and energy efficiency. Congestion in the network threatens the network performance [1].

2. MOTIVATION

Traffic-Aware Dynamic Routing to Alleviate Congestion in Wireless Sensor Networks (TADR) [2] work focused on alleviating the congestion in keeping view of fidelity level of the applications as the data generated during crisis state is more important. Whenever there is congestion in the network, congestion is handled by scattering the excessive packets to alternative paths with less load. The main drawbacks of TADR are more energy consumption and throughput is less due the one hop neighbour information used for congestion control.

3. CONTRIBUTION

The QoS parameters emphasized in this paper are throughput, delay and energy. The objective of our Two-hop based Traffic Aware Congestion Control Algorithm (TTACCA) for Wireless Sensor Network is to alleviate congestion and improve throughput by distributing packets in both time and space. Two independent potential fields Depth field and Queue length fields plays an major role in the network to control the congestion due the occurrence of an event. The proposed algorithm works based on two-hop routing technique.

4. RELATED WORK

This section provides a brief overview of existing congestion control techniques. Congestion control in WSN has gained high importance in the field of research. Muhammad *et al.,* [3] proposed a Prioritized Heterogeneous Traffic-oriented Congestion Control Protocol which performs hop-by-hop rate adjustment controlling the congestion and ensures efficient rate for the prioritized diverse traffic. This protocol uses intra-queue and inter-queue priorities along with weighted fair queuing for ensuring feasible transmission rates of Farooq *et al.,* [4] came up with an algorithm that takes a novel and different approach towards congestion control in wireless multimedia sensor networks.Upon detection of congestion, the congested node makes an estimate of the data rate that should be used by the node itself and its one hop away upstream neighbours. While estimating the data rate, the congested node considers the characteristics of the different traffic classes along with their total bandwidth usage. Sohail *et al.,* [5] designed Congestion Control Protocol for mobile sensor networks. It uses the existing TDMA technique with combination of statistical Time Division Multiplexing and enhanced newly proposed Time Sharing Time Division Multiple Access scheme to avoid congestion in WSN. Charalambos *et al.,* [6], proposed two methods to tackle congestion in WSNs. The two methods are either by reducing the load or by increasing resources. Hierarchical Tree Alternative Path algorithm is implemented for resource control. The algorithm attempts through simple steps and minor computations to mitigate congestion in wireless sensor networks by creating dynamic alternative paths to the sink.

In [7] an algorithm which is called Rapid Congestion Control Algorithm (RCCA) for data flow rate control and Cluster Head (CH) selection is proposed. Most of the wireless sensor networks research topics consider how to save the energy of the sensor nodes. In some applications of WSN, like the monitoring of an earthquake or forest wildfire, transmitting emergency data packets to the sink node as soon as possible is much more important than saving power. Liu *et al.,* [8] focused on Priority-based Hybrid Protocol WSN model to provide a feasible WSN architecture, which can save the energy of the sensor nodes in normal situation, and transmits emergency data packets in an efficient manner to the sink node. Gajendra *et al.,* [9] has presented the multiple sink mechanism in which sensor nodes are able to deliver data to multiple sink in the network. Congestion control mechanism used in this work improves the packet delivery ratio, reliability, throughput of the network. It reduces the packet loss ratio, which reduces the number of retransmission, saves the energy of sensor node. This improves the network lifetime. It is able to handle the Black Hole Problem in the wireless sensor network. Kiran *et al.,* [10] focused on many problems starting with the basic problem of eliminating the phenomenon of congestion collapse, and include the problems of effectively using the available network resources in different types of environments. Many other techniques have the ability to measure the loss rate, delay and bottleneck buffer size, and level of congestion in wireless sensor networks.

5. NETWORK MODEL

In this section Network Model used and the Assumptions made are discussed along with preliminaries required for the design of our proposed TTACCA Algorithm.

5.1 Network Model and Assumptions Made

The network is modelled as bowl structure as illustrated in Figure 1. The sink resides at the bottom, and all data packets flow down along the surface just like water. When the traffic load in the network is light, the surface of the bowl is smoother and hence our algorithm acts just like the shortest path routing. In heavily loaded cases (e.g., burst of data packets caused by detection of a monitoring event), the congestion will form bulges on the bowl surface which blocks the packets to flow directly down to the bottom along the shortest path. The excessive packets are driven by the potential field to the appropriate alternative path without obstacles, i.e., idle or less loaded nodes. When the congestion disappears, the bowl surface becomes smoother, and the packets continue to move along the shortest path. Essentially, through spreading the packet transmissions spatially and temporarily, our TTACCA scheme alleviates congestion, while improving the throughput at the same time [2].

Table 1: Symbols used in the Algorithm

Symbols	**Meaning**
N_ID	Neighbour node ID
U_msg	Updated Message
local depth	Depth value of the parent node
Local queue length	Queue length value of parent node
Q(N_ID)	Normalized queue length of the neighbour node
C	Cost of radio link between parent node and neighbour node
D	Depth of neighbour node

Q	Queue length of node
$F_d\ (N\_ID)$	Depth force between parent node and neighbour node
$F_q\ (N\_ID)$	Queue length force between parent node and neighbour node
$F_m(N\_ID)$	Combined force between parent node and neighbour node
A	Combined Co-efficient
P	Data packet

5.2. Preliminaries

This section describes the construction of routing potential fields required for our proposed TTACCA algorithm namely the depth field and the queue length field.

(i) Depth Potential Field: Provides the basic routing function (which the smooth bowl does), namely, to make each packet flow towards the sink. TTACCA defines the depth potential field V_d as $V_d = Depth(v)$ where $Depth(v)$ is the depth of node v. The depth field from node v to its neighbour $w \in nbr(v)$ is given by

$$F_d(v,w) = (V_d(v)-V_d(w))\ /\ c_{v,w} \tag{1}$$

$F_d(v,w)$ denotes the force between the parent node v and the neighbour node w. This force is calculated by taking difference of depth field from parent node v and its neighbour w divided by cost of radio link between the node v and neighbour w.

(ii) Queue Length Field: The priority routing function which determines the number of packets at each and every node in the network. In the bowl structure network model, packets move from a node to a neighbour with lower potential. To avoid a hotspot which is identified by a large queue, the potential at this node should be raised. Now, we define the queue length potential field.

$$Vq(v) \quad = \quad Q(v) \tag{2}$$

$Q(v)$ denotes the normalized queue at node v and it is defined as $Q(v)$ = Number of packets in the queue/Buffer size at node v.

6. PROBLEM DEFINITION

The objective of our TTACCA algorithm is to alleviate congestion and improve throughput by distributing packets in both time and space. The main focus of this work is on detection and reduction of congestion in a particular node in WSN. The algorithm works based on Two-hop routing technique. Two-hop based Traffic-Aware Congestion Control Algorithm forwards data packets around the congestion areas by spreading the excessive along multiple paths. The idle or under loaded nodes are efficiently utilized in response to congestion.

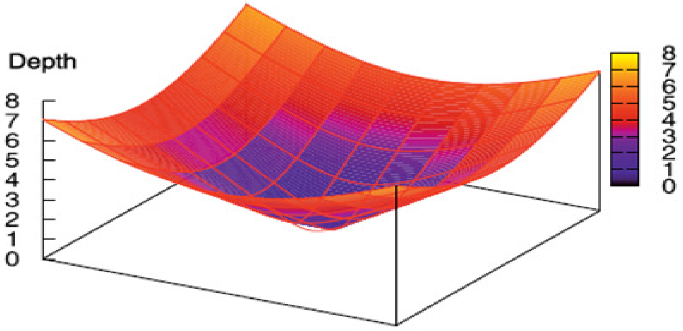

Figure 1: Bowl structure of the network

7. ALGORITHM

This section explains the TTACCA algorithm given in Table 2. TTACCA needs the status information from neighbour nodes, such as queue length and depth, to construct the potential fields.

The WSN is modelled as a bowl structure. In the bowl model each node will send data packets to the neighbours before, it reaches sink node. The data packets generated from source sensor nodes acts as input to the TTACCA algorithm. The neighbour nodes receiving the data packets, finds the shortest paths to the sink by choosing the depth field and congestion free path using queue length potential field. The neighbours receiving the *N_ID*, *U_msg* from the neighbours, updates the parent node information into the routing table. The routing table contains the information like *SINK_ID*, *N_ID*, *C*, *d*, *q*, *Q(N_ID)*, $F_d(N\_ID)$. Routing table contains information of all one hop neighbours and two hop neighbours routing information. Which includes *N_ID*, *C, d, q, Q(N_ID)*, $F_d(N\_ID)$, *Fq(N_ID)*, $F_m(N\_ID)$ (Combined force field between parent and its neighbour).

Table 2: Two-Hop based Traffic Aware Congestion Control Algorithm (TTACCA)

```
Routing Table at node 'v'
Input : A WSN modelled as a bowl structure
Output : Queue length field and depth field
    InsertToRouting Table( N_ID, U_msg )
    local depth = depth( v );
    local queue length = queue length( v )
    Q( v ) = ( local queue length ) / buffer size;
    for each entry in routing table
    if (local depth – d ≤ 2)
        {
            $C$ = cost of radio link to $N\_ID$
            $d$ = depth of $N\_ID$
            $q$ = queue length of $N\_ID$
            $Q(N\_ID) = (q)$ / buffer size
            $Fd(N\_ID) = ($ local depth $- d) / C$
            $Fq(N\_ID) = ($local queue length $- q) / C$
            $n$ = number of neighbour $ID$
            $F_m(N\_ID) = (1 - \alpha) F_d(N\_ID) + \alpha F_q(N\_ID)$
}
end for
```

8. PERFORMANCE EVALUATION

This section details the simulation parameters used for the simulation of the TTACCA algorithm and Performance analysis of the algorithm through the graphs.

8.1 Simulation Setup

Table 3: Simulation Parameters

Parameters	Value
Area Size	500 m * 500m
Number of nodes	18-99
Deployment Type	Random
Transmission Range	212 mtrs
Sink Coordination	250 m * 250 m
Initial Energy	1J
Link layer transmission	8kbps
Interface Queue Type	Queue/DropTail/PriQueue
Antenna	Antenna/OmniAnteena
0.1 seconds	Least Utilization Time
10 seconds	Maximum Utilization Time
Application Type	Event Driven

The simulation parameters used in TTACCA algorithm is shown in Table 3. The sensor nodes are first deployed randomly in square area with dimensions 500m * 500m. The sink node is placed in the centre of the area. The WSN is modelled as bowl structure. The transmission range for all nodes is fixed for 212m. The propagation model used is TwoRayGround. The TTACCA algorithm is simulated under two scenarios: with high load in the network and with low load in the network

8.2 Performance Analysis

In this section, we evaluate the performance of TTACCA algorithm using simulation experiments conducted on the NS2 [11] platform. NS2 uses OTcl and C++ codes to implement the given scenario. For a comprehensive performance evaluation, several QoS quantitative metrics considered are defined below

(i) Energy Consumption: The average consumed energy per packet received by the sink reflects the energy efficiency of the protocols. It is ratio of the total energy consumption to the number of packets received by the sink successfully. The lower the energy consumed per packet, the higher the energy efficiency.

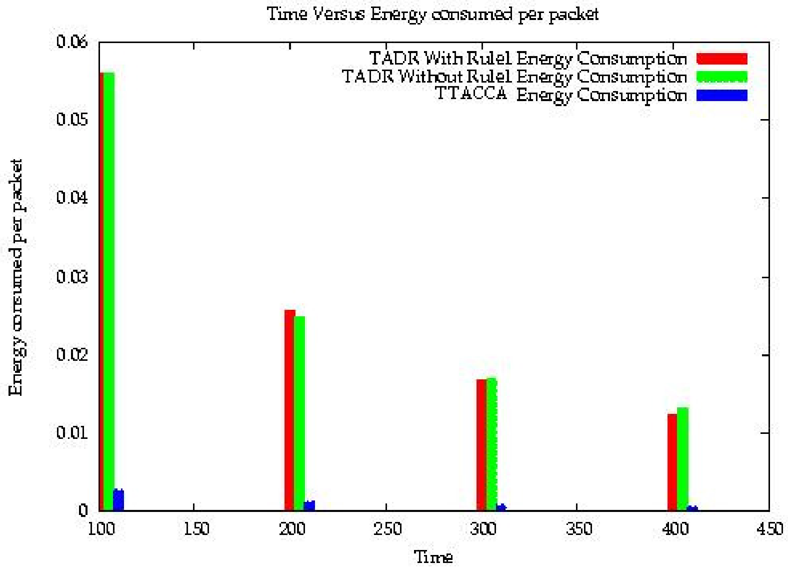

Figure 2: Time versus Throughput

Figure 2 depicts the energy consumption of the TTACCA algorithm. The energy consumed per packet is effectively reduced by 30 % compared to the TADR algorithm. TTACCA algorithm selects the forwarding node by considering distance to sink and forwarder node set information in the one hop neighbourhood or two hop neighbours. Considering distance to sink and forwarder node set information in the one hop neighbourhood or two hop neighbours. The queue length field in the one hop or two hop neighbour set solves the traffic aware problem. The depth filed gives the shortest path from parent node to the destination node. The number of hops travelled by the packet or message to reach the destination is comparatively less. Hence the energy consumed for each packet to reach the destination or sink node is less.

(ii) Throughput: It is the ratio of number of packets received by the sink to the number of packets sent by the source node.

Figure 3 shows the comparison of time versus throughput. TADR routes the packets around the under loaded or idle nodes around the hotspot. Whenever a hotspot occurs in the network this results in packet dropping at the hotspot or near the sink node. Due to this in TADR the overall throughput is comparatively low. TTACCA scatters the packets to under loaded or idle nodes around the hotspot through two hop routing technique or one hop routing technique. Excessive packets in and around the hotspots when congestion occurs in the network are spread evenly through alternate paths with less load. Hence throughput of TTACCA algorithm is improved by 20% compared with the TADR algorithm. Hence the overall throughput is high compared to TADR

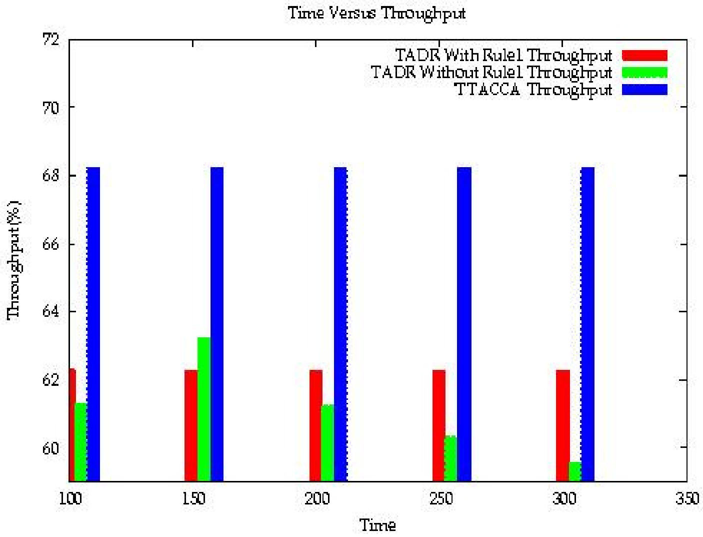

Figure 3: Time versus Throughput

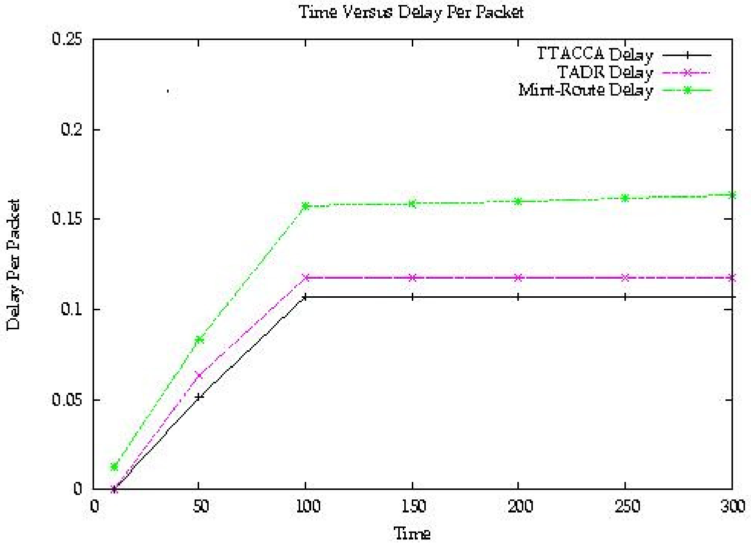

Figure 4 : Time versus Delay per Packet

(iii) Delay: The time taken between the source node sending the packet and the destination node receiving the packet is End-to-End Delay.

Figure 4 shows the comparison of delay per packets versus time.Initially no packet transmission takes place due to this the delay is less. As simulation time increases from 0 to 50 seconds, number of packet transmission and transmission overhead increases due to this there is a gradual increase in delay and finally reaches to saturation. In TADR packet transmission is hop by hop. At each hop packet selects its next hop from the one hop neighbour set. Hence dropping of packets is more. Whereas in TTACCA algorithm follows multihop transmission hence packet dropping is low, implies that in TTACCA delay is comparatively low due to the depth potential field, which selects the routing path based on shortest distance from source to the sink node.

9. CONCLUSIONS

The congestion control in WSN is different from that in tradition networks, such as Wireless LAN and adhoc networks. The pure traffic control is able to alleviate congestion, but hard to satisfy the fidelity required by applications. In this paper, TTACCA algorithms follows the philosophy of dynamic capacity planning to deal with the congestion problem in WSN. Through TTACCA algorithm QoS performance metrics delay is reduced by 10%, improves energy efficiency by 30% and throughput of TTACCA is high compared with TADR. The TACCA algorithm thus mitigates congestion in the network efficiently compared to TADR congestion control algorithm.

REFERENCES

[1] Mansoor-uz-Zafar Dawood, Biztek, Pakistan,Noor Zaman, Abdul Raouf Khan, Mohammad Salih,"Designing of Energy Aware Quality of Service (QoS) Based Routing Protocol for Efficiency Improvement in Wireless Sensor Network", Journal of Information and Communication Technology, Vol. 4, No. 1, 2010.

[2] Fengyuan Ren and Tao He, "Traffic-Aware Dynamic Routing to Alleviate Congestion in Wireless Sensor Networks", IEEE Transactions On Parallel and Distributed Systems, Vol. 22, No. 9, September 2011.

[3] Muhammad Monowar, Obaidur Rahman, Al-Sakib Khan Pathan, and Choong Seon Hong, "Prioritized Heterogeneous Traffic-Oriented Congestion Control Protocol for WSNs" , The International Arab Journal of Information Technology, Vol. 9, No. 1, January 2012.

[4] Muhammad Omer Farooq, Thomas Kunz, and Marc St-Hilaire, "Differentiated Services based Congestion Control Algorithm for Wireless Multimedia Sensor Networks", IEEE, 2011.

[5] Sohail Jabbar, Awais Ahmad, Ataul Aziz Ikram, Murad Khan, "TSEEC - TS/TDMA based Energy Efficient Congestion Control in Mobile Wireless Sensor Network", Proceedings of the World Congress on Engineering and Computer Science, October 19-21, 2011, San Francisco, USA 2011.

[6] Charalambos Sergiou, Vasos Vassiliou and Aristodemos Paphitis, "Hierarchical Tree Alternative Path (HTAP) Algorithm for Congestion Control in Wireless Sensor Networks", University of Cyprus, February 3, 2012.

[7] G Srinivasan and S Murugappan, "Rapid Congestion Control Technique for Wireless Sensor Network for Energy Efficiency and Reliability", International Conference on Computing and Control Engineering, 12 and 13 April, 2012.

[8] Hsu-Jung Liu, Mei-Wen Huang, Wen-Shyong Hsieh, Chenhuan Jack Jan,"Priority-based Hybrid Protocol in Wireless Sensor Networks", 11th IEEE International Conference on High performance Computing and Communications, 2009.

[9] Gajendra Sanjay Vyas, Vivek S Deshpande, "Effect of Multiple Sinks on the Performance of Wireless Sensor Networks", International Journal of Emerging Science and Engineering, Vol. 1, No. 5, March 2013.

[10] Kiran Babu T S, Manoj Challa, Sundeep Kumar K, M Jitendranath, " Congestion Control using Adaptive Buffer Flow Managements in WSN", International Journal of Scientific Engineering Research, Vol. 3, No.8, August 2012.

[11] http://www.isi.edu/nsmam/ns

AUTHORS

Prabha R is currently working as an Associate Professor in the Department of Information Science and Engineering, Dr. Ambedkar Institute of Technology, Bangalore, India. She obtained her Bachelor of Engineering degree in Computer Science and Engineering branch. M.E in Computer Science and Engineering from Computer Science Department, UVCE, Bangalore University in the year 2003. She has 22 years of teaching experience. Currently she is pursuing Ph. D in the Department of Computer Science and Engineering, University Visvesvaraya College of Engineering, Bangalore University, Bangalore. Her research interest is in the area of Wireless Sensor Networks.

Prashanth Kumar Gouda received his B.E in Electronics and Communication Engineering from Dr. Ambedkar Institute of Technology Bangalore from Visvesvaraya Technological University in the year of 2010. M.E in Computer Networks from Computer Science Department, UVCE, Bangalore University in the year2013. His research focus includes QoS and Routing in WSN and Cloud Networking and Communication. He worked as Business Intelligence Developer at GrayMatter Software Service Private limited Bangalore.

Dr. S H Manjula is currently working as an Associate Professor in the Department of Computer Science and Engineering, University Visvesvaraya College of Engineering Bangalore University, Bangalore, India. She obtained her Bachelor of Engineering degree in Computer Science and Engineering branch, Masters of Engineering and Ph D. in Computer Science and Engineering. She has published a book on Wireless Sensor Networks. She has published more than 30 papers in refereed international journals and conferences. Her research interests are in the field of Wireless Sensor Networks, Semantic web and Data Mining.

Dr. Venugopal K R is currently Special Officer, DVG Bangalore University and Principal, University Visveswaraya College of Engineering, Bangalore University Bangalore. He obtained his Bachelor of Engineering from University Visvesvaraya College of Engineering. He received his Master's degree in Computer Science and Automation from Indian Institute of Science Bangalore. He was awarded Ph. D in Economics from Bangalore University and Ph.D in Computer Science from Indian Institute of Technology, Madras. He has a distinguished academic career and has degrees in Electronics, Economics, Law, Business Finance, Public Relations, Communications, Industrial Relations, Computer Science and Journalism. He has authored and edited 39 books on Computer Science and Economics, which include Petrodollar and the World Economy, C Aptitude, Mastering C, Microprocessor Programming, Mastering C++ and Digital Circuits and Systems. During his three decades of service at UVCE he has over 400 research papers to his credit. He was a Post-Doctoral Research Scholar at University of Southern California, USA. His research interests include Computer Networks, Wireless Sensor Networks, Parallel and Distributed Systems, Digital Signal Processing and Data Mining.

Dr L M Patnaik is honorary professor in Department of Computer Science and Auto- mation, Indian institute of Science, Bangalore. During the past 35 years of his service at the Institute he has over 700 research publications in refereed International Conference Proceedings. He is a Fellow of all the four leading Science and Engineering Academies in India. Fellow of the IEEE and the Academy of Science for the developing world. He has received twenty national and international awards. Notable among them is the IEEE Technical Achievement Award for his significant contributions to High performance Computing and Soft Computing. He is an Ex-Vice Chancellor Defence institute of Advanced Technology, Pune India. His area of research interest has been Parallel and Distributed Computing, Mobile Computing, CAD for VLSI circuits, Soft computing and Computational Neuroscience.

PREDICTIVE CYBER SECURITY ANALYTICS FRAMEWORK: A NON-HOMOGENOUS MARKOV MODEL FOR SECURITY QUANTIFICATION

Subil Abraham[1] and Suku Nair[2]

[1]IBM Global Solution Center, Coppell, Texas, USA
smabraha@us.ibm.com
[2]Southern Methodist University, Dallas, Texas, USA
nair@lyle.smu.edu

ABSTRACT

Numerous security metrics have been proposed in the past for protecting computer networks. However we still lack effective techniques to accurately measure the predictive security risk of an enterprise taking into account the dynamic attributes associated with vulnerabilities that can change over time. In this paper we present a stochastic security framework for obtaining quantitative measures of security using attack graphs. Our model is novel as existing research in attack graph analysis do not consider the temporal aspects associated with the vulnerabilities, such as the availability of exploits and patches which can affect the overall network security based on how the vulnerabilities are interconnected and leveraged to compromise the system. Gaining a better understanding of the relationship between vulnerabilities and their lifecycle events can provide security practitioners a better understanding of their state of security. In order to have a more realistic representation of how the security state of the network would vary over time, a nonhomogeneous model is developed which incorporates a time dependent covariate, namely the vulnerability age. The daily transition-probability matrices are estimated using Frei's Vulnerability Lifecycle model. We also leverage the trusted CVSS metric domain to analyze how the total exploitability and impact measures evolve over a time period for a given network.

KEYWORDS

Attack Graph, Non-homogeneous Markov Model, Markov Reward Models, CVSS, Security Evaluation, Cyber Situational Awareness

1. INTRODUCTION

Defending a large scale enterprise from outside threats is a fairly complicated task. At the same time, Cybercriminals are increasingly using sophisticated social engineering techniques leading to disruptions in business operations, damaging the reputation as well as financial stability of these corporations. The recent cyber-attack incident at Target Corp illustrates how these security breaches can seriously affect profits and shareholder value. According to a report by Secunia[1], the number of reported security vulnerabilities in 2013 increased by 32% compared to 2012. However in spite of these increasing rate of attacks on corporate and government systems,

Natarajan Meghanathan et al. (Eds) : NeTCoM, CSIT, GRAPH-HOC, SPTM - 2014
pp. 195–209, 2014. © CS & IT-CSCP 2014 DOI : 10.5121/csit.2014.41316

corporations have fallen behind on ramping up their defenses due to limited budgets as well as weak security practices.

One of the main challenges currently faced in the field of security measurement is to develop a mechanism to aggregate the security of all the systems in a network in order assess the overall security of the network. For example INFOSEC [2] has identified security metrics as being one of the top 8 security research priorities. Similarly Cyber Security IT Advisory Committee [3] has also identified this area to be among the top 10 security research priorities.

In addition, traditional security efforts in corporations have focused on protecting key assets against known threats which have been disclosed publicly. But today, advanced attackers are developing exploits for vulnerabilities that have not yet been disclosed called “zero-day” exploits. So it is necessary for security teams to focus on activities that are beyond expected or pre-defined. By building appropriate stochastic models and understanding the relationship between vulnerabilities and their lifecycle events, it is possible to predict the future when it comes to cybercrime such as identifying vulnerability trends, anticipating security gaps in the network, optimizing resource allocation decisions and ensuring the protection of key corporate assets in the most efficient manner.

In this paper, we propose a stochastic model for security evaluation based on Attack Graphs, taking into account the temporal factors associated with vulnerabilities that can change over time. By providing a single platform and using a trusted open vulnerability scoring framework such as CVSS[4-6], it is possible to visualize the current as well as future security state of the network leading to actionable knowledge. Several well established approaches for Attack graph analysis [7-15] have been proposed using probabilistic analysis as well as graph theory to measure the security of a network. Our model is novel as existing research in attack graph analysis do not consider the temporal factors associated with the vulnerabilities, such as the availability of exploits and patches. In this paper, a nonhomogeneous model is developed which incorporates a time dependent covariate, namely the vulnerability age. The proposed model can help identify critical systems that need to be hardened based on the likelihood of being intruded by an attacker as well as risk to the corporation of being compromised.

The remainder of the paper is organized as follows. In Section 2, we discuss about previous research proposed for security metrics and quantification. In Section 3, we explore the Cyber-Security Analytics Framework and then realize a non-homogenous Markov Model for security evaluation that is capable of analyzing the evolving exploitability and impact measures of a given network. In Section 4, we present the results of our analysis with an example. Finally, we conclude the paper in Section 5.

2. BACKGROUND AND RELATED WORK

Here we briefly discuss about Attack Graphs and then provide an overview of some of the most prominent works that have been proposed for quantifying security in a network.

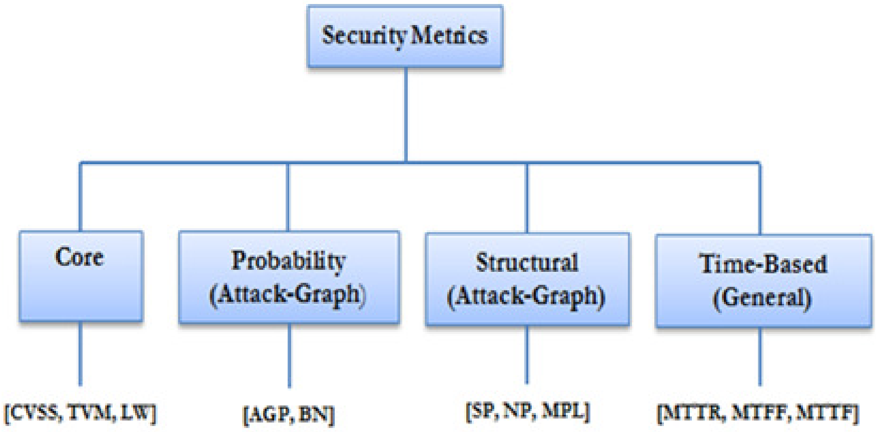

Figure 1. Security Metric Classification

2.1. Attack Graph

Computer attacks have been graphically modeled since the late 1980s by the US DoD as discussed in their paper [16]. Most of the attack modeling performed by analysts was constructed by hand and hence it was a tedious and error-prone process especially if the number of nodes were very large. In 1994 Dacier et al [17] published one of the earliest mathematical models for a security system based on privilege graphs. By the late 1990's a couple of other papers [18, 19] came out which enabled automatic generation of attack graphs using computer aided tools. In [18] the authors describes a method of modeling network risks based on an attack graph where each node in the graph represented an attack state and the edges represented a transition or a change of state caused by an action of the attacker. Since then researchers have proposed a variety of graph-based algorithms to generate attack graphs for security evaluation.

2.2. Classes of Security

There are different classes under which network security metrics fall under. These classes are depicted in Fig 1. Here are some examples of metrics that fall under each category.

2.2.1. Core Metrics

A few examples that fall under this category are Total Vulnerability Measure (TVM) [20] and Langweg Metric (LW) [21]. TVM is the aggregation of two other metrics called the Existing Vulnerabilities Measure (EVM) and the Aggregated Historical Vulnerability Measure (AHVM). CVSS [4-5] is an open standard for scoring IT security vulnerabilities. It was developed to provide organizations with a mechanism to measure vulnerabilities and prioritize their mitigation. For example the US Federal government uses the CVSS standard as the scoring engine for its National Vulnerability database (NVD) [6] which has a repository of over forty-five thousand known vulnerabilities and is updated on an ongoing basis

2.2.2. Structural Metrics

These metrics use the underlying structure of the Attack graph to aggregate the security properties of individual systems in order to quantify network security. The Shortest Path (SP) [18], [7] metric measures the shortest path for an attacker to reach an end goal. The Number of Paths (NP) [7] metric measures the total number of paths for an attacker to reach the final goal. The Mean of Path Lengths (MPL) metric [8] measures the arithmetic mean of the length of all paths to the final goal in an attack graph. The above structural metrics have shortcomings and in [9], Idika et al have proposed a suite of attack graph based security metrics to overcome some of these inherent weaknesses. In [22], Ghosh et al provides an analysis and comparison of all the existing structural metrics.

2.2.3. Probability-Based Metrics

These metrics associate probabilities with individual entities to quantify the aggregated security state of the network. A few examples that fall under this category are Attack Graph-based Probabilistic (AGP) and Bayesian network (BN) based metrics [23-25].

2.2.4. Time-Based Metrics

These metrics quantify how fast a network can be compromised or how quickly a network can take preemptive measures to respond to attacks. Common metric that fall in this category are Mean Time to Breach (MTTB), Mean Time to Recovery (MTTR) [26] and Mean Time to First Failure (MTFF) [27].

The drawback with all these classes of metrics is that they take a more static approach to security analysis and do not leverage the granularity provided by the CVSS metric framework in order to assess overall dynamic security situation and help locate critical nodes for optimization

2.3. Vulnerability Lifecycle Models

Presently, there is research [28-31] on analyzing the evolution of life cycle of different types of vulnerabilities. Frei et al. [31] in particular developed a distribution model to calculate the likelihood of an exploit or patch being available a certain number of days after its disclosure date. To the best of our knowledge, no previous work has been done to analyze overall security of a network, by considering the temporal relationships between all the vulnerabilities that are present in the network, which can be exploited by an attacker.

2.4. Cyber Situation Awareness

Presently, there is research [28-31] on analyzing the evolution of life cycle of different types of vulnerabilities. Frei et al. [31] in particular developed a distribution model to calculate the likelihood of an exploit or patch being available a certain number of days after its disclosure date. To the best of our knowledge, no previous work has been done to analyze overall security of a network, by considering the temporal relationships between all the vulnerabilities that are present in the network, which can be exploited by an attacker.

3. CYBER-SECURITY ANALYTICS FRAMEWORK

In this section, we explore the concept of modeling the Attack graph as a stochastic process. In [40, 41], we established the cyber-security analytics framework (Figure 2) where we have captured all the processes involved in building our security metric framework. In this paper we will extend the model by taking into account the temporal aspects associated with the individual vulnerabilities. By capturing their interrelationship using Attack Graphs, we can predict how the total security of the network changes over time. The fundamental assumption we make in our model is that the time-parameter plays an important role in capturing the progression of the attack process. Markov model is one such modeling technique that has been widely used in a variety of areas such as system performance analysis and dependability analysis [11, 27, 42-43]. While formulating the stochastic model, we need to take into account the behavior of the attacker. In this paper, we assume that the attacker will choose the vulnerability that maximizes his or her probability of succeeding in compromising the security goal.

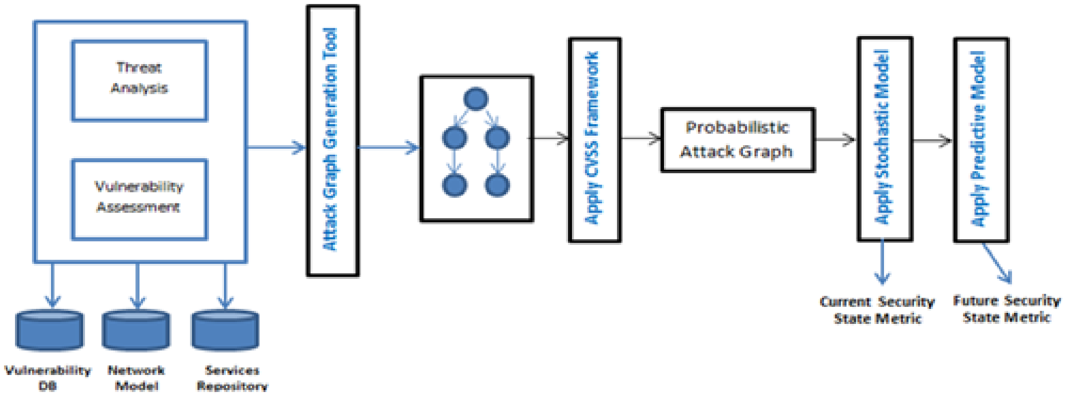

Figure 2. Cyber Security Analytics Framework

3.1. Architecture

Figure 3 shows a high level view of our proposed cyber security analytics architecture which comprises of 4 layers.

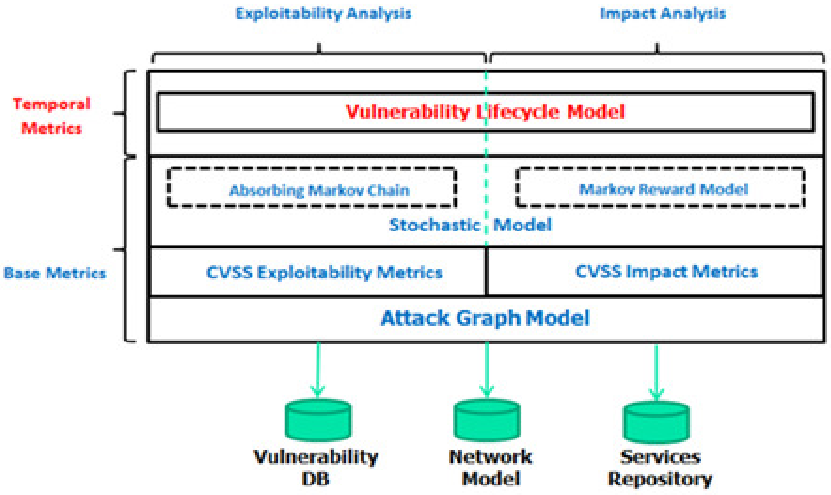

Figure 3. Cyber Security Analytics Architecture

The core component of our architecture is the Attack Graph Model (Layer 1) which is generated using a network model builder by taking as input network topology, services running on each host and a set of attack rules based on the vulnerabilities associated with the different services. The underlying metric domain is provided by the trusted CVSS framework (Layer 2) which quantifies the security attributes of individual vulnerabilities associated with the attack graph. We divide our security analysis by leveraging two CVSS metric domains. One captures the exploitability characteristics of the network and the other analyzes the impact a successful attack can have on a corporations key assets. We believe that both these types of analysis are necessary for a security practitioner to gain a better understanding of the overall security of the network. In layer 3, relevant stochastic processes are applied over the Attack Graph to describe the attacks by taking into account the relationships between the different vulnerabilities in a system. For example, in our approach, we utilize an Absorbing Markov chain for performing exploitability analysis and a Markov Reward Model for Impact analysis. In [40, 41] we discussed how we can model an attack-graph as a discrete time absorbing Markov chain where the absorbing state represents the security goal being compromised.

So far we have been focusing on the security properties that are intrinsic to a particular vulnerability and that doesn't change with time. These measures are calculated from the CVSS Base metric group which aggregates several security properties to formulate the base score for a particular vulnerability. In order to account for the dynamic/temporal security properties of the vulnerability, we apply a Vulnerability Lifecycle model (Layer 4) on the stochastic process to identify trends and understand how the security state of the network will evolve with time. Security teams can thus analyze how availability of exploits and patches can affect the overall network security based on how the vulnerabilities are interconnected and leveraged to compromise the system. We believe that such a framework also facilitates communication between security engineers and business stakeholders and aids in building an effective cyber-security analytics strategy.

3.2. Model Representation

In [40, 41] we have discussed how we can model an attack-graph as a discrete time absorbing Markov chain due to the following two properties.

1. An attack graph has at least one absorbing state or goal state.
2. In an attack graph it is possible to go from every state to an absorbing state.

We also presented a formula for calculating the transition probabilities of the Markov chain by normalizing the CVSS exploitability scores over all the transitions starting from the attacker's source state. In this paper, we will extend the model to analyze and measure two key aspects. First, we take into account both the exploitability as well impact properties associated with a security goal being compromised. By considering both these measures separately, we can derive a complementary suite of metrics to aid the security engineer in optimizing their decisions. Second we combine the temporal trends associated with the individual vulnerabilities into the model to reason about the future security state of the network. In our model we will calculate the daily transition-probability matrices using the well-established Frei's Vulnerability lifecycle model [31].

The security of the network is dependent on the exploitability level of the different vulnerabilities associated with the services running on the machines in the enterprise. In addition the security metrics will dynamically vary based on the temporal aspects of the vulnerabilities taken into consideration. As an example, consider CVE-2014-0416 which is an unspecified vulnerability in Oracle Java SE related to the Java Authentication and Authorization Service (JAAS) component. We define the base exploitability score $e(v)$ as the measure of complexity in exploiting the vulnerability v. The CVSS standard provides a framework for computing these scores using the *access vector* (AV), *access complexity* (AC) and *authentication* (Au) as follows

$$e(v) = 20 \times AV \times AC \times Au \qquad (1)$$

The constant 20 represents the severity factor of the vulnerability. The access vector, authentication and access complexity for this vulnerability CVE-2014-0416 is 1.0, 0.704 and 0.71 respectively. Therefore the base exploitability score of CVE-2014-0416 is 10.0 which indicate that it has very high exploitability. As of this writing the state of exploitability for this vulnerability is documented as "Unproven" which indicate that no exploit code is available. Hence it has a temporal weight score of 0.85. Given the base exploitability score and the temporal weight, the effective temporal exploitability score is as follows

$$e(v_t) = temporal\ weight\ \times e(v) \qquad (2)$$

The temporal exploitability score for CVE-2014-0416 is 8.5. As the vulnerability ages and exploit code become readily availability to exploit the vulnerability, the value of the exploitability score will move closer towards its base value. As a comparison, consider CVE-2012-0551 which is another unspecified vulnerability in Oracle Java SE that has a base exploitability score of 8.6 which is lower than CVE-2014-0416. However the state of exploitability for this vulnerability is documented as "High" which indicates that exploit code is widely available. Hence it has a temporal weight score of 1. Therefore CVE-2012-0551 is considered more exploitable than CVE-2014-0416 even though it has a lower base metric score because we have factored in the lifecycle of the vulnerability.

The transition matrix for an absorbing Markov chain has the following Canonical form**.**

$$P = \begin{bmatrix} Q & R \\ 0 & I \end{bmatrix}$$

Here *P* is the transition matrix, *R* is the matrix of absorbing states, and *Q* is the matrix of transient states. The set of states, *S* in the model represent the different vulnerabilities associated with services running on the nodes that are part of the network. The transition probability matrix P of the Markov chain was estimated using the formula

$$p(i,j) = \frac{e(v_j)}{\sum_{k=1}^{n} e(v_k)} \qquad (3)$$

where p_{ij} is the probability that an attacker currently in state i exploits a vulnerability $e(v_j)$ in state j and $e(v_j)$ is the exploitability score for vulnerability v_j obtained from the CVSS Base Metric group. Further, each row of P is a probability vector, which requires that

$$\sum p(i,j) = 1 \; for \; all \; i \in S$$

In an absorbing Markov chain the probability that the chain will be absorbed is always 1. Hence

$$Q^n \to 0 \; as \; n \; \to \propto$$

where *Q* is the matrix of transient states. Therefore for an absorbing Markov chain $P^{(m)}$, we can derive a matrix $N = (I - Q)^{-1} = I + Q + Q^2 + Q^3 + \cdots$ which is called the *fundamental matrix* for $P^{(m)}$. This matrix N provides considerable insight into the behavior of an attacker who is trying to penetrate the network. The elements of the fundamental matrix n_{ij} describe the expected number of times the chain is in state *j*, given that the chain started in state *i*.

3.3. Non-homogenous model

The temporal weight score that we considered in the example above was a function of the time since the vulnerability was disclosed on a publicly trusted SIP (Security Information Providers). The temporal values recorded by CVSS are discrete and are not suitable for inclusion in a non-homogenous model. It would be more appropriate to use a distribution that would take as input the age of the vulnerability. Therefore we will use the result of Frei's model [31] to calculate the temporal weight score of the vulnerabilities that is part of the Attack graph model. The probability that an exploit is available for a given vulnerability is obtained using a Pareto distribution of the form:

$$F(t) = 1 - \left(\frac{k}{t}\right)^a \qquad (4)$$

a = 0.26, k = 0.00161

where t is the age of vulnerability and the parameter k is called the shape factor. The age t is calculated by taking the difference between the dates the CVSS scoring is conducted and when the vulnerability was first disclosed on an SIP. By combining this distribution in our model, we can get a more realistic estimate of the security of the network based on the age of the different vulnerabilities which are still unpatched in the enterprise.

In the non-homogenous Markov model presented here, we consider the following time dependent covariate which is the age of the vulnerability. In order to have a more realistic model, we update this covariate every day for each of the vulnerabilities present in the network and recalculate the discrete time transition probability matrix P. Given the exploitability scores for each of the vulnerabilities in the Attack Graph, we can estimate the transition probabilities of the Absorbing Markov chain by normalizing the exploitability scores over all the edges starting from the attacker's source state. Let p_{ij} be the probability that an attacker currently in state i exploits a vulnerability in state j. We can then formally define the transition probability below where n is the number of outgoing edges from state i in the attack model and e_j is the temporal exploitability score for the vulnerability in state j.

$$p(i,j) = \frac{e(v_t)_j}{\sum_{l=1}^{n} e(v_t)_l} \qquad (5)$$

$$where\ e(v_t) = \left(1 - \left(\frac{k}{t}\right)^{\alpha}\right) \times e(v) \qquad (6)$$

The matrix $P^{(m)}$ represents the transition probability matrix of the Absorbing Markov chain computed on day m where, $p\ (i,\ j) \geq 0$ for all $i,\ j\ \in S$. In an absorbing Markov chain the probability that the chain will be absorbed is always 1. Further, each row of $P^{(m)}$ is a probability vector, which requires that

$$\sum p(i,j) - 1\ for\ all\ i\ \in S$$

In equation (5), we use the result of Frei's Vulnerability Lifecycle model [31] to calculate the temporal weight score of the vulnerabilities that is part of the Attack graph model. Therefore by calculating the individual temporal scores of the vulnerabilities and by analyzing their causal relationships using an Attack Graph, we can integrate the effect of temporal score to derive the total dynamic security of network.

3.4. Exploitability Analysis

We present quantitative analysis using our cyber security analytics model. The focus of our analysis will on assessing the evolving security state of the network.

3.4.1 Expected Path length (EPL) metric

This metric measures the expected number of steps the attacker will have to take starting from the initial state to compromise the security goal. Using the Fundamental matrix N of the non-homogenous Markov model, we can compute the expected number of steps before the chain goes to the absorbed state. For example let t_i be the expected number of steps before the chain is absorbed, given that the chain starts in state s_i, and let t be the column vector whose i^{th} entry is t_i. Then

$$t = Nc\ where\ for\ all\ j\ c_j\ is\ 1$$

This security metric is analyzing the expected number of steps or the resistance of the network.

3.4.2 Probabilistic Path (PP) metric

This metric measures the likelihood of an attacker to reach the absorbing states of the graph. For this we will calculate the following matrix B where $B = NR$ where N is the fundamental Matrix of the Markov chain and R is obtained from the Canonical form. The element b_{ij} in the matrix measure the probability of reaching the security goal state j given that the attacker started in state

i. The *Probabilistic Path (PP)* metric also aids the security engineer in making decisions on optimizing the network and we will label this as the *Probabilistic Path (PP)* metric.

3.4. Exploitability Analysis

The CVSS standard provides a framework for computing the impact associated with an individual vulnerability v using *confidentiality impact* (C), *integrity impact* (I) and *availability impact* (A) measures as follows

$$Impact(v) = 10.41 * (1 - (1 - C) * (1 - I) * (1 - A)$$

By associating the individual impact/reward scores with each state in our Markov chain, we can extend the underlying stochastic process as a discrete-time Markov reward model (MRM). Given our existing DTMC model, we can represent the Markov Reward process as (ρ, S, P) where (S, P) is a DMTC and ρ is a reward function for each state. Since we are considering only constant rewards or impact scores, the reward function can be represented as a vector $r = [(\rho(s1), \ldots \rho(sn)]$. Hence the expected impact at time t is given as

$$\sum_{i=1}^{n} \rho(s_i).P\{X(t) = s_i\} = r.x(t) = r.P^t.x(0)$$

This value will be termed as the **Expected Impact Metric (EI)**. A non-homogenous MRM can be built by incorporating the temporal trend of individual vulnerabilities given their age. Hence by formulating daily transition probability matrices using Frei's model we can reason about how the expected cost of breaching a security goal can vary over time.

4. ILLUSTRATION

To illustrate the proposed approach in detail, a network similar to [10, 24-25, 44-45] has been considered (refer Figure 4).

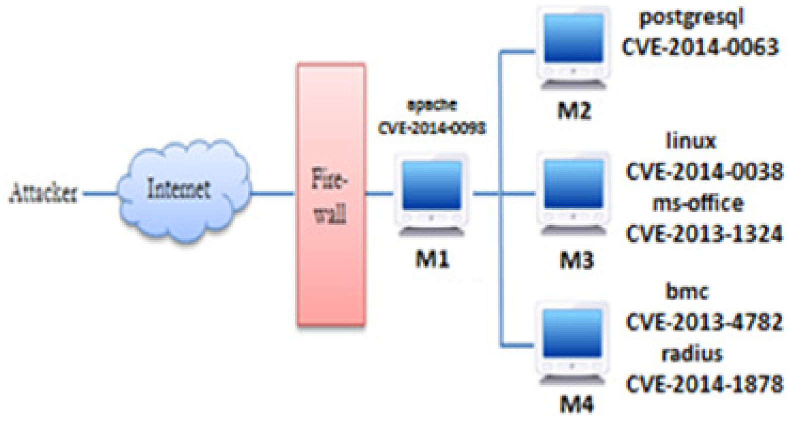

Figure 4. Network Topology

The network is comprised of 4 machines that are interconnected together and operating internally behind a firewall. The machine hosting the web-server M1 is running Apache Webserver. The aim of the attacker is to infiltrate the network and gain root access on M4. In order to accomplish this, the attacker needs to first start with exploiting the apache web-service since that is the only port (80) accessible from the firewall. Once this is exploited, the attacker will then need to slowly work his way through the network to achieve his goal.

4.1. Environment Information

Table 1 contains a list of all the vulnerabilities in the network that can be exploited by an attacker if certain conditions are met.

Table 1. Vulnerability Data.

Service Name	CVE-ID	Exploitability Subscore	Host	Disclosure Date
apache	CVE-2014-0098	10.0	M1	03/18/2014
postgresql	CVE-2014-0063	7.9	M2	02/17/2014
linux	CVE-2014-0038	3.4	M3	02/06/2014
ms-office	CVE-2013-1324	8.6	M3	11/13/2013
bmc	CVE-2013-4782	10	M4	07/08/2013
radius	CVE-2014-1878	10	M4	02/28/2014

Each of the six vulnerabilities is unique and publicly known and is denoted by a CVE (Common Vulnerability and Exposure) identifier. For example Apache web-server was found to have vulnerability CVE-2014-0098 on 03/18/2014 which allows remote attackers to cause segmentation faults. Similarly the postgresql service hosted by M2 had a vulnerability denoted by CVE-2014-0063 which allowed remote attackers to execute arbitrary code.

4.2. Attack Graph Generation

By combining the vulnerabilities present in the network configuration (Figure 4), we can build several scenarios whereby an attacker can reach a goal state. In this particular case, the attacker's goal state would be to obtain root access on Machine M4. Figure 5 depicts the different paths an attacker can take to reach the goal state. By combining these different paths we are able to obtain an Attack Graph. A couple of practical approaches have been proposed [44- 46] to automate generation of attack graphs without the intervention of a red team. In [47] the authors have compared and analyzed several open source AG tools like MulVal, TVA, Attack Graph Toolkit, NetSPA as well as commercial tools from aspects of scalability and degree of attack graph visualization. Table 2 provides an overview of the different available AG toolkits.

In our analysis we have used the MulVAL tool discussed in [45] to generate logical attack graph in polynomial time.

Table 2. Attack Graph Toolkits

Toolkit Name	Complexity	Open Source	Developer
MulVAL	$O(n^2) \sim O(n^3)$	yes	Kansas State University
TVA	$O(n^2)$	no	George Mason University
Cauldron	$O(n^2)$	no	Commercial
NetSPA	O(nlogn)	no	MIT
Firemon	O(nlogn)	no	Commercial

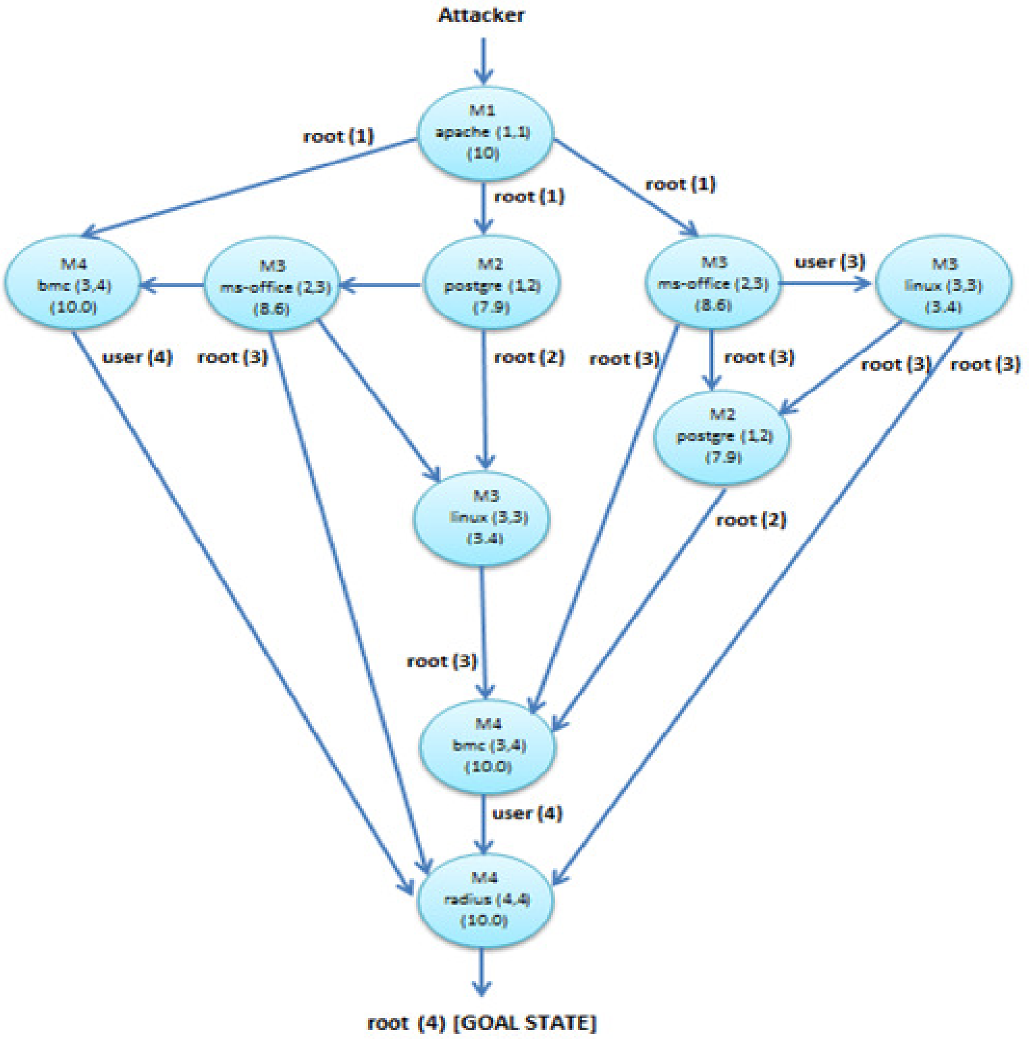

Figure 5. Network Topology

4.3. Security Analysis

In the analysis, we first investigate how the distribution of our proposed attack graph metrics vary over a given time period. In the attack graph model, each node corresponds to a software related vulnerability that exists on a particular machine in the network. The transition probability for a particular edge in the attack graph is calculated by normalizing the CVSS Exploitability scores over all the edges from the attacker's source node. By formulating an Absorbing Markov chain over the Attack graph and applying the Vulnerability lifecycle model to the exploitability scores, we are able to project how these metrics will change in the immediate future.

Figure 6 (a, b, c) depicts the distribution of our proposed attack graph metrics (EPL, Probabilistic Path & Expected Impact) over a period of 150 days. The general trend for the Expected Path Length (EPL) metric (Fig 4.3a) is upward over the next 150 days which signifies that it will take fewer steps (less effort) for an attacker to compromise the security goal as the vulnerabilities in the network age. This visualization graph is very useful for security practitioners for optimizing patch management processes in the organization. By establishing thresholds for these metrics, the security teams can plan in advance as to when to patch a system versus working on an ad-hoc basis. For example, the organization may have a threshold score of 4.86 for the EPL metric. From the graph (Fig 4.3 a), the team can reasonably conclude that the systems in their network are safe from exploits breaching the security goal for the next 50 days as the EPL score is above the threshold value. The thresholds values are typically set by the security team based on how fast they can respond to a breach once it is detected.

The Probability Path (PP) distribution (Fig 4.3b) which signifies the likelihood of an attacker compromising the security goal follows a different trend where it is seen reducing during the first few days and then picks up gradually with time. As vulnerabilities age, exploits become readily available for vulnerabilities which leads to an increase in their CVSS exploitability scores. As a result the transitions probabilities in the model will change likely causing other attack paths in the tree to become more favorable to the attacker. In the figure, we see that the probability of reaching the security goal tapers offafter 50 days. The Expected Impact metric (Fig 4.3c) or cost of an attack to the business reduces with time and this is an indication that the attacker will likely choose a different path due to more exploits being available for other vulnerabilities that have a lower impact score. It is important to note that every organization has a network configuration that is very unique to their operations and therefore the distribution for our proposed attack graph metrics will be different for each of these configurations.

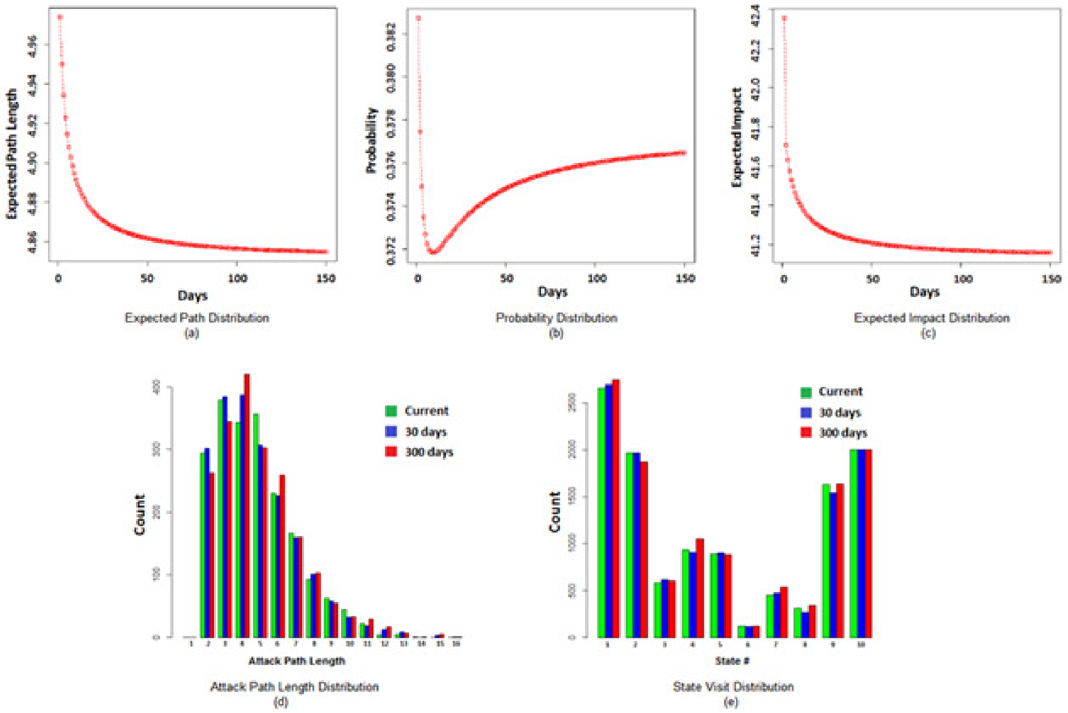

Expected Path Distribution
(a)

Probability Distribution
(b)

Expected Impact Distribution
(c)

Attack Path Length Distribution
(d)

State Visit Distribution
(e)

Figure 6. Network Topology

4.4. Simulation

Based on the Attack Graph generated for the network, a simulation of the Absorbing Markov chain is conducted. In our experiment we model an attacker and simulate over 2000 different instances of attacks over the Attack Graph based on the probability distribution of the nodes. We used the R statistic package [48] to generate the model and run the simulations.

The transition probabilities are formulated from the CVSS scoring framework as described in section 3. Each simulation run uses the transition probability row vector of the Absorbing Markov Chain to move from one state to another until it reaches the final absorbing state. Figure 4.3d depicts a multi-bar graph of the distribution of attack path lengths X_1, X_2 ….. X_{2000} from 2000 simulated attack paths where the security goal was compromised. Each of the colors indicates the trend forecast over different periods of time. For example, in this distribution model, the length of the attack paths with the most frequency is 3, given the current age of all the vulnerabilities (shown in green). However as the vulnerabilities in the network age over a period of 300 days, the length of the paths with most frequency gets updated to 4 (shown in red). We also notice that the frequency of paths of length 3 and 5 decreases gradually over 300 days.

Similarly Figure 4.3e depicts a multi-bar graph of the distribution of the state visits for the Attack Graph for all the 2000 instances of attack paths that were simulated using the non-homogenous Markov chain model. This graph represents the number of times the attacker is likely to visit a particular state/node in the attack graph over those 2000 simulated runs. Based on the simulation results depicted in Fig 4.3e, if we were to exclude the start state (1) and the absorbing state (10), we can find that an attacker is most likely to visit state 2 and least likely to visit state 6. Hence from Table 1, we can conclude that the attacker is most likely to exploit the vulnerability of the bmc service running on M4 (State 2) and least likely to exploit the linux service on M3 (State 6). This information is valuable for a security engineer to prioritize which exploit needs to be patched and how it will affect the strength of the network against attacks. This insight is further enriched when we also consider the trends over a period of 300 days. For example, in Fig 4.3e there is an upward trend in the expected number of times the attacker visits state 4, while there is a downward trend for state 5 during the same time. Hence if the security engineer had to decide whether to patch node 4 or node 5 during this time period, it would make more sense to patch node 4 since it is most susceptible to an outside attack in the future.

One the major challenges when performing patch management is timing when to install patches and which patches have priority. By analyzing the trends over time of how the security state of a network changes, a security engineer can make a more informed and intelligent decision on optimizing the application of patches, thereby strengthening the current as well as the future security state of the enterprise.

5. CONCLUSIONS

In this paper, we presented a non-homogenous Markov model for quantitative assessment of security attributes using Attack graphs. Since existing metrics have potential short-comings for accurately quantifying the security of a system with respect to the age of the vulnerabilities, our framework aids the security engineer to make a more realistic and objective security evaluation of the network. What sets our model apart from the rest is the use of the trusted CVSS framework and the incorporation of a well-established Vulnerability lifecycle framework, to comprehend and analyze both the evolving exploitability and impact trends of a given network using Attack Graphs. We used a realistic network to analyze the merits of our model to capture security properties and optimize the application of patches.

REFERENCES

[1] Secunia Vulnerability Review 2014: Key figures and facts from a global IT-Security perspective, February 2014

[2] INFOSEC Research Council Hard problem List, 2005.

[3] A Crisis of Prioritization, President’s IT Advisory Committee, 2005.

[4] M. Schiffman, “Common Vulnerability Scoring System (CVSS),” http://www.first.org/cvss/

[5] Assad Ali, Pavol Zavarsky, Dale Lindskog, and Ron Ruhl, " A Software Application to Analyze Affects of Temporal and Environmental Metrics on Overall CVSS v2 Score", Concordia University College of Alberta, Edmonton, Canada, October 2010.

[6] National Vulnerability Database 2014.

[7] R. Ortalo, Y. Deswarte, and M. Kaaniche, “Experimenting with quantitative evaluation tools for monitoring operational security,” IEEE Transactions on Software Engineering, vol. 25, pp. 633–650, September 1999.

[8] W. Li and R. Vaughn, “Cluster security research involving the modeling of network exploitations using exploitation graphs,” in Sixth IEEE International Symposium on Cluster Computing and Grid Workshops, May 2006.

[9] N. Idika and B. Bhargava, “Extending attack graph-based security metrics and aggregating their application,” Dependable and Secure Computing, IEEE Transactions on, no. 99, pp. 1–1, 2010.

[10] L. Wang, A. Singhal, and S. Jajodia, "Toward measuring network security using attack graphs," in Proceedings of the 2007 ACM workshop on Quality Protection, pp. 49-54, 2007.

[11] Trivedi KS, Kim DS, Roy A,Medhi D. Dependability and security models. Proc. DRCN, IEEE, 2009; 11–20.

[12] A Roy, D S Kim, and K S. Trivedi. Attack countermeasure trees (ACT): towards unifying the constructs of attack and defense trees.J. of Security and Communication Networks, SI: Insider Threats, 2011.

[13] O. Sheyner, J. W. Haines, S. Jha, R. Lippmann, and J. M. Wing, “Automated generation and analysis of attack graphs,” in IEEE Symposium on Security and Privacy, 2002, pp. 273–284.

[14] Xinming Ou, Sudhakar Govindavajhala, and Andrew W. Appel. MulVAL: A logic-based network security analyzer. In

[15] 14th USENIX Security Symposium, 2005.S. Jajodia and S. Noel, "Advanced Cyber Attack Modeling, Analysis, and Visualization," George Mason University, Fairfax, VA, Technical Report 2010.

[16] S DoD, MIL-STD-1785, “System security engineering program management requirements,” 1988.

[17] M. Dacier, Y. Deswarte, “Privilege Graph: an Extension to the Typed Access Matrix Model,”Proc. ESORICS, 1994.

[18] C. Phillips, L.P. Swiler, “A graph-based system for network-vulnerability analysis,”Proc. WNSP’98, pp.71-79.

[19] L. Swiler, C. Phillips, D. Ellis, S. Chakerian, “Computer-attack graph generation tool,” Proc. DISCEX01, pp.307-321.

[20] M. Abedin, S. Nessa, E. Al-Shaer, and L. Khan, “Vulnerability analysis for evaluating quality of protection of security policies," in Proceedings of Quality of Protection 2006 (QoP '06), October 2006.

[21] H. Langweg, "Framework for malware resistance metrics," in Proceedings of the Quality of Protection 2006 (QoP '06), October 2006.

[22] A. Kundu, N. Ghosh, I. Chokshi and SK. Ghosh, "Analysis of attack graph-based metrics for quantification of network security", India Conference (INDICON), IEEE, pages 530 – 535, 2012.

[23] M.Frigault and L. Wang, "Measuring Network Security Using Bayesian Network-Based Attack Graphs," in Proceedings of the 3rd IEEE International Workshop on Security, Trist and Privacy for Software Applications (STPSA’08), 2008.

[24] L. Wang, T. Islam, T. Long, A. Singhal, and S. Jajodia, "An attack graph-based probabilistic security metric," DAS 2008, LNCS 5094, pp. 283-296, 2008.

[25] L. Wang, A. Singhal, and S. Jajodia, "Measuring overall security of network configurations using attack graphs," Data and Applications Security XXI, vol. 4602, pp. 98-112, August 2007.

[26] A. Jaquith, Security Metrics: Replacing Fear, Uncertainty, and Doubt. Addison-Wesley, Pearson Education, 2007.

[27] K. Sallhammar, B. Helvik, and S. Knapskog, "On stochastic modeling for integrated security and dependability evaluation," Journal of Networks, vol. 1, 2006.

[28] W. Arbaugh, W. Fithen, and J. McHugh, “Windows of vulnerability: a case study analysis,” Computer, vol. 33, no. 12, pp. 52–59, Dec 2000

[29] N. Fischbach, “Le cycle de vie d’une vulnrabilit,” http://www.securite.org, 2003.

[30] J. Jones, “Estimating software vulnerabilities,” Security & Privacy,IEEE, vol. 5, no. 4, pp. 28–32, July-Aug. 2007.

[31] S. Frei, “Security econometrics - the dynamics of (in)security,” ETHZurich, Dissertation 18197, ETH Zurich, 2009.

[32] Tim Bass. “Intrusion Detection System and Multi-sensor Data Fusion”. Communications of the ACM, 43, 4 (2000), pp.99-105.

[33] Huiqiang Wang,etc. “Survey of Network Situation Awareness System”. Computer Science,vol.33,2006,pp.5-10.

[34] Bat sell S G,etc. “Distributed Intrusion Detection and Attack Containment for Organizational Cyber Security”. [Online] http://www.ioc.ornl.gov/projects/documents/containment.pdf, 2005.

[35] Shifflet J. “A Technique Independent Fusion Model For Network Intrusion Detection”. Proceedings of the Midstates Conference on Undergraduate Research in Computer Science and Mat hematics , vol.3,2005,pp.13-19.

[36] Robert Ball, Glenn A. Fink. "Home-centric visualization of network traffic for security administration". Proceedings of the 2004 ACM workshop on Visualization and data mining for computer security. Washington DC, October 2004, 55-64.

[37] Soon Tee Teoh, Kwan-Liu Ma, S.Felix Wu, et al. "Case Study: Interactive Visualization for Internet Security". Proceedings of IEEE VIS. Boson, October 2002, 505-508.

[38] C. Xiuzhen, Z. Qinghua,, G. Xiaohong, L. Chenguang; Quantitative Hierarchical Threat Evaluation Model for Network Security[J]; Journal of Software, Vol.17, No.4, April 2006, pp.885–897

[39] S. Shaoyi and Z. Yongzheng "A Novel Extended Algorithm for Network Security Situation Awareness", International Conference on Computer and Management (CAMAN), pages 1-3 2011

[40] S.Abraham and S.Nair, "Cyber Security Analytics: A stochastic model for Security Quantification using Absorbing Markov Chains" 5th International Conference on Networking and Information Technology, ICNIT 2014

[41] S.Abraham and S.Nair, "A Stochastic Model for Cyber Security Analytics" Tech Report 13-CSE-02 , CSE Dept, Southern Methodist University, Dallas, Texas, 2013.

[42] K. S. Trivedi, Probability and Statistics with Reliability, Queuing, and Computer Science

[43] R.A. Sahner, K. S. Trivedi, and A. Puliafito, Performance and Reliability Analysis of Computer Systems: An Example-Based Approach Using the SHARPE Software Package. Kluwer Academic Publishers,1996.

[44] O. Sheyner, J. W. Haines, S. Jha, R. Lippmann, and J. M. Wing, "Automated generation and analysis of attack graphs," in IEEE Symposium on Security and Privacy, 2002, pp. 273–284.

[45] Xinming Ou, Sudhakar Govindavajhala, and Andrew W. Appel. MulVAL: A logic-based network security analyzer. In

[46] S. Jajodia and S. Noel, "Advanced Cyber Attack Modeling, Analysis, and Visualization," George Mason University, Fairfax, VA, Technical Report 2010.

[47] Shengwei Yi, Yong Peng, Qi Xiong, Ting Wang, Zhonghua Dai, Haihui Gao, Junfeng Xu, Jiteng Wang and Lijuan Xu "Overview on attack graph generation and visualization technology", Anti-Counterfeiting, Security and Identification (ASID), 2013 IEEE International Conference on, Issue Date: Oct. 2013

[48] R statistics tool. http://www.r-project.org/

AUTHORS

Subil Abraham received his B.S. degree in computer engineering from the University of Kerala, India. He obtained his M.S. in Computer Science in 2002 from Southern Methodist University, Dallas, TX. His research interests include vulnerability assessment, network security, and security metrics.

Suku Nair received his B.S. degree in Electronics and Communication Engineering from the University of Kerala. He received his M.S. and Ph.D. in Electrical and Computer Engineering from the University of Illinois at Urbana in 1988 and 1990, respectively. Currently, he is the Chair and Professor in the Computer Science and Engineering Department at the Southern Methodist University at Dallas where he held a J. Lindsay Embrey Trustee Professorship in Engineering. His research interests include Network Security, Software Defined Networks, and Fault-Tolerant Computing. He is the founding director of HACNet (High Assurance Computing and Networking) Labs. He is a member of the IEEE and Upsilon Pi Epsilon..

AUTHOR INDEX